Seismic Behavior and Design of Boundary Frame Members of Steel Plate Shear Walls
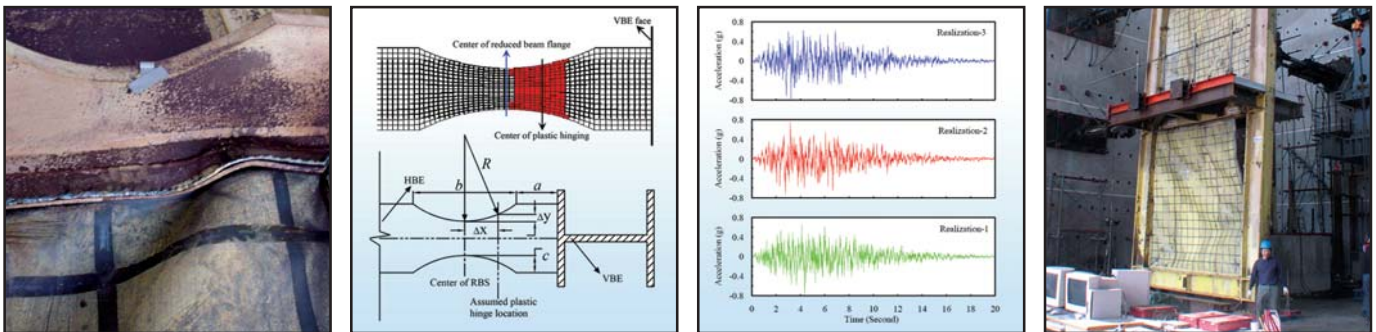
by

Bing Qu and Michel Bruneau

NOTICE

Seismic Behavior and Design of Boundary Frame Members of Steel Plate Shear Walls

by

B. Qu[1] and M. Bruneau[2]

1   Assistant Professor, Department of Civil and Environmental Engineering, California Polytechnic State University; Former Graduate Student, Department of Civil, Structural, and Environmental Engineering, University at Buffalo, State University of New York
2   Professor, Department of Civil, Structural, and Environmental Engineering, University at Buffalo, State University of New York

MCEER
University at Buffalo, State University of New York
Red Jacket Quadrangle, Buffalo, NY 14261
Phone: (716) 645-3391; Fax (716) 645-3399
E-mail: *mceer@buffalo.edu*; WWW Site: *http://mceer.buffalo.edu*

Preface

The Multidisciplinary Center for Earthquake Engineering Research (MCEER) is a national center of excellence in advanced technology applications that is dedicated to the reduction of earthquake losses nationwide. Headquartered at the University at Buffalo, State University of New York, the Center was originally established by the National Science Foundation in 1986, as the National Center for Earthquake Engineering Research (NCEER).

Comprising a consortium of researchers from numerous disciplines and institutions throughout the United States, the Center's mission is to reduce earthquake losses through research and the application of advanced technologies that improve engineering, pre-earthquake planning and post-earthquake recovery strategies. Toward this end, the Center coordinates a nationwide program of multidisciplinary team research, education and outreach activities.

MCEER's research is conducted under the sponsorship of two major federal agencies: the National Science Foundation (NSF) and the Federal Highway Administration (FHWA), and the State of New York. Significant support is derived from the Federal Emergency Management Agency (FEMA), other state governments, academic institutions, foreign governments and private industry.

MCEER's NSF-sponsored research objectives are twofold: to increase resilience by developing seismic evaluation and rehabilitation strategies for the post-disaster facilities and systems (hospitals, electrical and water lifelines, and bridges and highways) that society expects to be operational following an earthquake; and to further enhance resilience by developing improved emergency management capabilities to ensure an effective response and recovery following the earthquake (see the figure below).
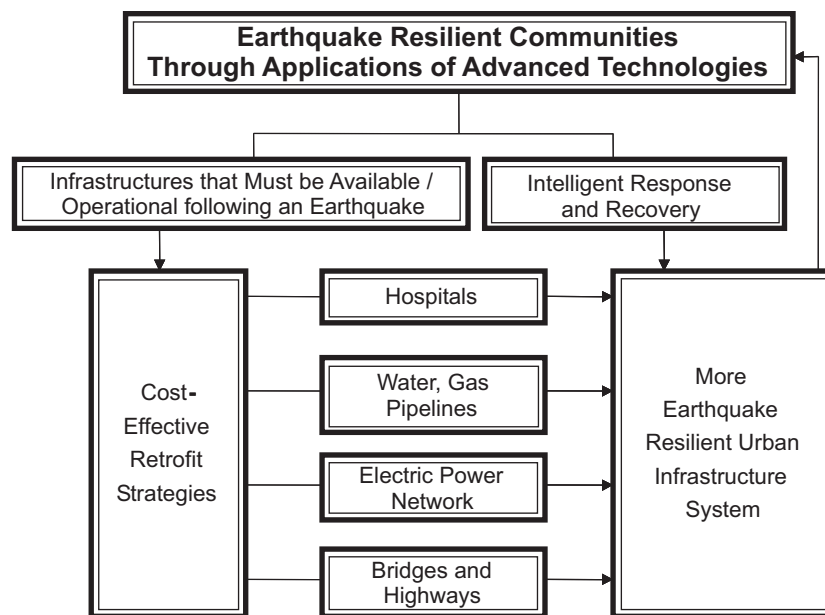
A cross-program activity focuses on the establishment of an effective experimental and analytical network to facilitate the exchange of information between researchers located in various institutions across the country. These are complemented by, and integrated with, other MCEER activities in education, outreach, technology transfer, and industry partnerships.

This report presents the results of an analytical study to investigate the behavior of horizontal and vertical boundary frame members that may impact the performance of Steel Plate Shear Walls (SPSWs). New analytical models were developed for horizontal boundary frame members to calculate the plastic moment and resulting strength reduction caused by biaxial internal stress conditions, and to revisit and develop improved capacity design procedures that account for these reduced plastic moments. The models incorporate observations made in a companion experimental study (see Technical Report MCEER-08-0010). Next, the adequacy of a flexibility limit for the design of vertical boundary frame members specified in current design codes was assessed using the new models. The contribution of the boundary frame moment resisting action and infill panel tension field action to the overall plastic strength of SPSWs was investigated.

ABSTRACT

A Steel Plate Shear Wall (SPSW) consists of infill steel panels surrounded by columns, called Vertical Boundary Elements (VBEs), and beams, called Horizontal Boundary Elements (HBEs). Those infill panels are allowed to buckle in shear and subsequently form diagonal tension field actions to resist the lateral loads applied on the structure. Research conducted since the early 1980s has shown that this type of system can exhibit high initial stiffness, behave in a ductile manner, and dissipate significant amounts of hysteretic energy, which make it a suitable option for the design of new buildings as well as for the retrofit of existing constructions. However, some obstacles still exist impeding more widespread acceptance of this system. For example, there remain uncertainties regarding the seismic behavior and design of boundary frame members of SPSWs. This report presents analytical work conducted to investigate the behavior and design of boundary frame members of SPSWs.

First, analytical models were developed to calculate the HBE plastic moment accounting for the reduction in strength due to the presence of biaxial internal stress conditions followed by development of analytical models, which take into account the reduced plastic moments of HBEs, to estimate the design forces for intermediate HBEs to reliably achieve capacity design. Those models combine the assumed plastic mechanism with a linear beam model of intermediate HBE considering fully yielded infill panels, and are able to prevent in-span plastic hinges. The above advances with regard to HBE behavior make it possible to investigate and explain the observed intermediate HBE failure.

In addition, the work presented in this report assesses the adequacy of a flexibility limit for VBE design specified by the current design codes using new analytical models developed to prevent the undesirable in-plane and out-of-plane performances of VBEs.

Furthermore, this report investigates the relative and respective contributions of boundary frame moment resisting action and infill panel tension field action to the overall plastic strength of SPSWs, followed by a proposed procedure to make use of the strength provided by the boundary frame moment resisting action. Future work needed to provide greater insight on SPSW designs is also identified.

ACKNOWLEDGEMENTS

TABLE OF CONTENTS

TABLE OF CONTENTS (cont'd)

TABLE OF CONTENTS (cont'd)

SECTION	TITLE	PAGE

LIST OF FIGURES

LIST OF FIGURES (cont'd)

LIST OF FIGURES (cont'd)

LIST OF FIGURES (cont'd)

xvi

LIST OF FIGURES (cont'd)

LIST OF FIGURES (cont'd)

LIST OF FIGURES (cont'd)

LIST OF TABLES

NOTATIONS

A_b cross-section area of beam

A_c cross-section area of column

b_f width of beam flange

d_{ci} depth of column at story i

E young's modulus

f_y yield stress of SPSW boundary frame

f_{ypi} yield stress of infill panel at story i

H , h_{si} story height

h_w height of beam web

h_{wci} depth of column web

I_c moment of inertia of column

I_o moment of inertia of top flange of plate girder

I_u moment of inertia of bottom flange of plate girder

I_{yi} moment of inertia of column at story i taken from the weak axis

L bay width

M_{boti} moment developed at the bottom of column at story i

M_{PL} plastic moment at the left end of beam

M_{PR} plastic moment at the right end of beam

M_{topi} moment developed at the top of column at story i

n_s number of SPSW stories

P axial compression in beam

P_{Dli} equivalent earthquake load applied at the left end of beam at story i

P_{Dmi} resultant force from uniform earthquake forces applied along beam at story i

P_{Dri} equivalent earthquake load applied at the right end of beam at story i

R response modification factor

R_y	ratio of expected to nominal yield stress of boundary frame.
R_{yp}	ratio of expected to nominal yield stress of infill panel
t_f	thickness of beam flange
t_w	thickness of beam web
t_{wci}	thickness of column web at story i
t_{wi}	thickness of infill panel of story i
V_{design}	lateral design force applied on SPSW
V_i	shear at story i
V_{ni}	nominal shear strength of infill panel at story i
V_p	plastic strength of SPSW
y_c	compression portion of beam web
y_t	tension portion of beam web
Z	plastic section modulus of beam
α_i	infill tension field inclination angle of story i
β	cross-section plastic moment reduction factor
β_L	cross-section plastic moment reduction factor of the left column face
β_{min}	minimum value of cross-section plastic moment reduction factor
β_R	cross-section plastic moment reduction factor of the right column face
β_S	plastic moment reduction factor at maximum beam interior span moment location
β_w	ratio of the applied axial compression to the nominal axial strength of beam web
δ_i	arbitrarily selected nonzero column deflection factor
Δx	distance between RBS center and assumed plastic hinge
Δy	flange width difference between the RBS center and assumed plastic hinge
η	RBS plastic section modulus reduction ratio
η_o	top flange deflection due to web tension actions in plate girder
η_u	bottom flange deflection due to web tension actions in plate girder

κ	percentage of the total lateral design force assigned to infill panel
ν	Poisson's ratio
σ_c	compression axial yield strength of beam web
$\sigma_{\max}$	maximum of the web tension force components paralleling with the stiffener of plate girder
σ_{mean}	mean of the web tension force components paralleling with the stiffener of plate girder
σ_t	tension axial yield strength of beam web
σ_y	vertical stress in beam web
σ_{y-un}	equivalent constant vertical stress in beam web
τ_{xy}	shear stress in beam web
ω_t	flexibility factor
ω_{xbi}	horizontal component of infill panel yield force along beam
ω_{xci}	horizontal component of infill panel yield force along column
ω_{ybi}	vertical component of infill panel yield force along beam
ω_{yci}	vertical component of infill panel yield force along column

ABBREVIATIONS

AISC	American Institute of Steel Construction
ATC	Applied Technology Council
CSA	Canadian Standards Association
FEMA	Federal Emergency Management Agency
HBE	Horizontal Boundary Element
MCEER	Multidisciplinary Center for Earthquake Engineering Research (Buffalo, NY)
NCREE	National Center for Research on Earthquake Engineering (Taipei, Taiwan)
NEHRP	National Earthquake Hazards Reduction Program
PGA	Peak Ground Acceleration
RBS	Reduced Beam Section
SPSW	Steel Plate Shear Wall
UB	University at Buffalo
UBC	University of British Columbia
VBE	Vertical Boundary Element

SECTION 1

INTRODUCTION

1.1 General

Steel Plate Shear Walls (SPSWs) consist of infill steel panels surrounded by columns, called Vertical Boundary Elements (VBEs), and beams, called Horizontal Boundary Elements (HBEs).These infill panels are allowed to buckle in shear and subsequently form diagonal tension fields when resisting lateral loads. Energy dissipation of SPSWs during seismic events is principally achieved through yielding of the panels along the diagonal tension fields.

Consistent with capacity design principles, the Canadian Standard S16 on Limit State Design of Steel Structures (CSA 2000) and the AISC Seismic Provisions for Structural Steel Buildings (AISC 2005) require the boundary frame members (i.e. HBEs and VBEs) to be designed to be sufficiently rigid to ensure the development of infill tension fields and remain elastic when the infill panels are fully yielded, with exception of plastic hinges at the ends of HBEs and at the VBE bases that are needed to develop the expected plastic mechanism of the wall when rigid HBE-to-VBE and VBE-to-ground connections are used.

However, recent testing on multi-story SPSWs having reduced beam section (RBS) connections by Qu and Bruneau (2008) revealed that the yielding pattern of RBS connections in SPSWs is quite different from that of beams in conventional steel moment frames. Moreover, the intermediate HBEs of their specimen ultimately failed due to fractures at the VBE faces; however, no factures developed in the reduced beam flange regions. Note that intermediate HBEs are those to which are welded steel plates above and below, by opposition to anchor HBEs that have steel plates only below or above. It would be important to investigate the reasons for the difference in observed yielding behavior and to develop an improved capacity design procedure for HBEs to better ensure the ductile performance of SPSWs.

In addition, recent experimental data allow to revisit the effectiveness of equations in current design codes that are derived from plate girder theory and adopted with the intention of ensuring an adequate flexibility for VBE design. Furthermore, additional work is necessary to investigate the relative contribution of boundary frame moment resisting action to the overall strength of SPSWs and possibly achieve an optimum design of SPSWs accounting for that contribution.

1.2   Scope and Objectives

This report presents analytical work conducted to investigate the behavior and design procedure of horizontal and vertical boundary frame members that may impact SPSW performance.

First, new analytical models are developed to calculate the HBE plastic moment accounting for the reduction in strength due to the presence of biaxial internal stress conditions, and to revisit and develop improved capacity design procedure for HBEs taking into account these reduced plastic moments of HBEs. These advances make it possible to investigate and explain the intermediate HBE failure observed in recent tests (Qu and Bruneau, 2008).

Next, the adequacy of a flexibility limit for VBE design specified by the current design codes is assessed using new analytical models developed to prevent the undesirable in-plane and out-of-plane performances of VBEs.

Furthermore, a SPSW design procedure accounting for the contribution of boundary frame moment resisting action is proposed.

1.3   Outline of Report

Section 2 contains a brief overview of past analytical research related to this structural system in applications to provide earthquake resistance.

Section 3 begins with a discussion of HBE plastic moment accounting for the presence of axial force, shear force, and vertical stresses in HBE web due to infill panel yield forces.

Based on the results derived from Section 3, Section 4 develops a revised capacity design procedure for HBEs using enhanced free body diagrams and principle of superposition. The new developed model can be used to explain previously observed undesirable HBE performance.

Section 5 assesses the adequacy of flexibility limit for VBE design specified by the current design codes. Derivation of a flexibility factor in plate girder theory and how that factor was incorporated into current codes are reviewed, followed by the development of analytical models for preventing shear yielding and estimating out-of-plane buckling strength of VBEs of SPSWs.

Building on the knowledge developed in the prior sections for boundary frame member behavior and design, Section 6 investigates the contribution of boundary frame moment resisting action to the overall wall strength. A balanced design procedure is developed to account for this action followed by the derivation of three different procedures for the SPSWs having weak infill panels.

Finally, summary, conclusions, and recommendations for future research in SPSWs are presented in Section 7.

SECTION 2

PAST RESEARCH ON STEEL PLATE SHEAR WALLS

2.1 Introduction

Prior to key research performed in the 1980s (Thorburn *et al.* 1983), designs of SPSW infill panels only allowed for elastic behavior, or shear yielding in the post-elastic range. This design concept typically resulted in selection of relatively thick or heavily-stiffened infill panels. While resulting in a stiffer structure that would reduce displacement demand as compared to the bare steel frame structure during seismic events, these designs would induce relatively large infill panel yield forces on the boundary frame members, resulting in substantial amounts of steel used and expensive detailing. Numerous experimental and analytical investigations conducted since 1980s have demonstrated that a SPSW having unstiffened thin infill panels allowed to buckle in shear and subsequently form a diagonal tension field absorbing input energy, can be an effective and economical option for new buildings as well as for the retrofit of existing constructions in earthquake-prone regions. While extensive reviews of past research can be found in the literature (i.e. Berman and Bruneau 2003, Vian and Bruneau 2005, Sabelli and Bruneau 2007, to name a few), some work relevant to the work presented here is summarized below, with more emphasis on analytical studies using various modeling strategies.

2.2 Thorburn, Kulak, and Montgomery (1983)

Based on the theory of diagonal tension field actions first proposed by Wagner (1931), Thorburn *et al.* (1983) investigated the postbuckling strength of SPSWs and developed two analytical models to represent unstiffened thin infill panels that resist lateral loads by the formation of tension field actions. In both cases, contribution to total lateral strength from the compressive stresses in the infill panels were neglected because it was assumed that plate buckles at a low load and displacement level. In addition, it was assumed that the columns were continuous over the whole height of the wall, to which the beams were connected using simple connections (i.e. "pin" connections).

The first model, an equivalent brace model used to provide the story stiffness of a panel, represents the infill panels as a single diagonal tension brace at each story. Based on elastic strain energy formulation, analytical expressions were provided for the area of this equivalent brace member for two limiting cases of column stiffness, namely, infinitely rigid against bending and completely flexible.

The second model proposed by Thorburn *et al.* (1983) is strip model (also known as a multi-strip model), in which each infill panel is represented by a series of inclined pin-ended only members, as shown in figure 2-1, that have a cross-sectional area equal to strip spacing times the panel thickness.
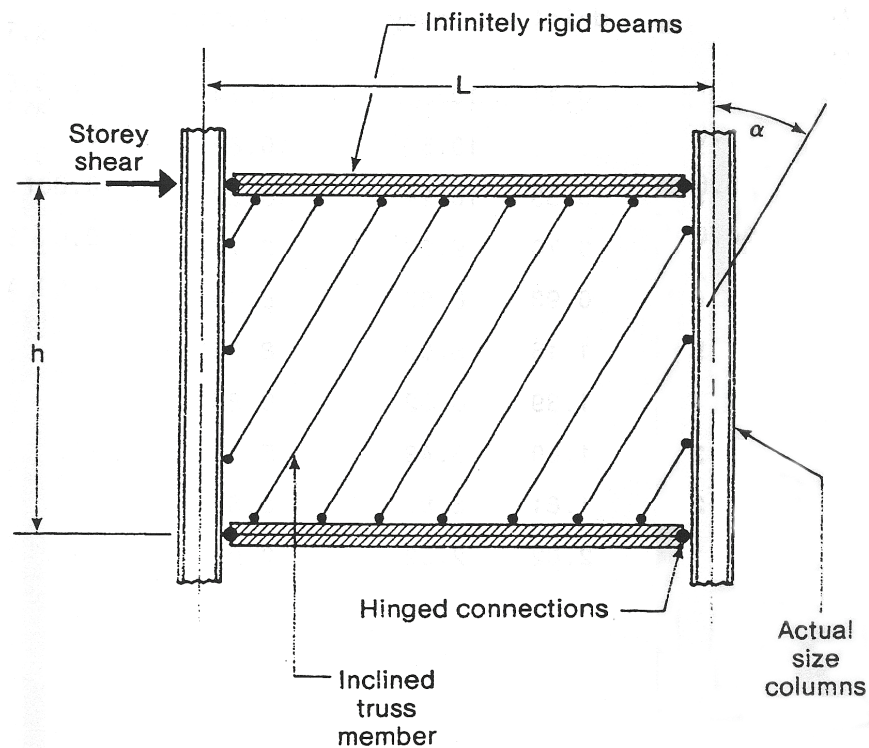
FIGURE 2-1 Schematic of Strip Model (Thorburn *et al.* 1983)

It was found that a minimum of ten strips is required at each story to adequately replicate the behavior of the wall. Using the principle of least work, the inclination angle for the strip, denoted as α, and equal to that of the tension field can be determined for the infinitely rigid column case, as,

$$\tan^4 \alpha = \left[\frac{1 + \dfrac{L \cdot t}{2 \cdot A_c}}{1 + \dfrac{H \cdot t}{A_b}} \right] \qquad (2\text{-}1)$$

where H is the story height; L is the bay width; t is the infill panel thickness; and A_b and A_c are cross section areas of the beam and column, respectively.

2.3 Timler and Kulak (1983)

Based on the work by Thorbrrn *et al.* (1983), Timler and Kulak (1983) considered the effects of column flexibility and revised equation (2-1):

$$\tan^4 \alpha = \left[\frac{1 + \dfrac{L \cdot t}{2 \cdot A_c}}{1 + H \cdot t \cdot \left(\dfrac{1}{A_b} + \dfrac{H^3}{360 \cdot I_c \cdot L} \right)} \right] \qquad (2\text{-}2)$$

where I_c is the moment of inertia of column, and all other terms were defined previously. This equation appears in both the Canadian CSA-S16-01 Standard (CSA 2000) and the 2005 AISC Seismic Provisions (AISC 2005) for design of SPSWs.

2.4 Driver, Kulak, Kennedy and Elwi (1997)

Driver *et al.* modeled their large-scale four-story SPSW specimen tested under cyclic loading, considering both FE model and strip model.

The FE model, as shown in figure 2-2 used quadratic beam elements to represent the beams and columns, and quadratic plate/shell elements to model the infill plates.
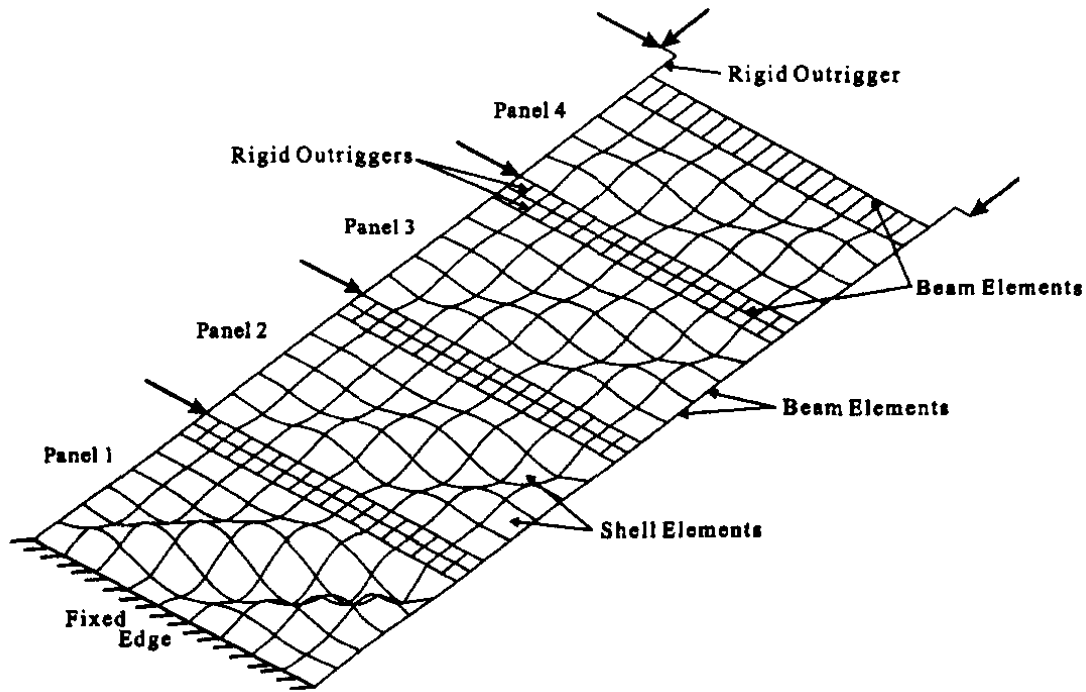
FIGURE 2-2 FE Model of Test Specimen (Driver *et al.* 1997)

As-built dimensions and measured material properties were included into the model. The FE simulation reasonably predicted the ultimate strength for all stories. However, the model overestimated the stiffness of the specimen. It was concluded that this discrepancy was due to the inability to include the geometric nonlinearities.

Using the procedure originally presented by Thorburn *et al.* (1983), Driver *et al.* (1997) also developed the strip model of their specimen, as shown in figure 2-3, and performed a pushover analysis to calculate the envelope of cyclic curves experimentally obtained. Inelastic behavior in the inclined tension field strips and the frame members was modeled. Although the model slightly underestimated the elastic stiffness of the test specimen, excellent agreement was obtained with the experimentally observed ultimate strength.
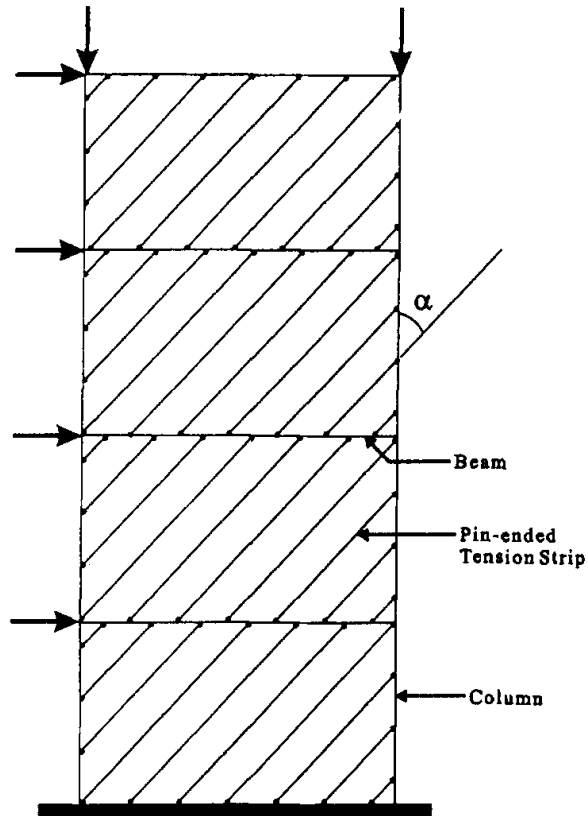
FIGURE 2-3 Strip Model of Driver *et al.* Specimen (Driver *et al.* 1997)

2.5 Berman and Bruneau (2003)

Based on the strip model, Berman and Bruneau (2003) performed plastic analysis to explore the behavior of SPSWs. Fundamental plastic collapse mechanism were described for single story and multistory SPSWs with either simple or rigid beam-to-column connections.

For a single story SPSW with simple beam-to-column connections, as shown in figure 2-4, Berman and Bruneau (2003) demonstrated, using equilibrium and kinematic methods of plastic analysis, that the assumed collapse mechanism for the strip model produces an expression for story shear strength, identical to that of the CAN/CSA S16-01 procedure used in calculating the shear resistance of an SPSW infill panel.

Berman and Bruneau further extended plastic analysis of SPSWs to the multistory cases. They examined two types of plastic mechanisms, namely, a uniform collapse mechanism

9

and a soft-story collapse mechanism which are shown in figure 2-5. These mechanisms and their corresponding ultimate strengths, provide the engineer simple equations for estimating the ultimate capacity of a multistory SPSW and preventing the possible soft story mechanism. The ultimate strengths predicted for these plastic mechanisms were validated by the experimental data from past research.
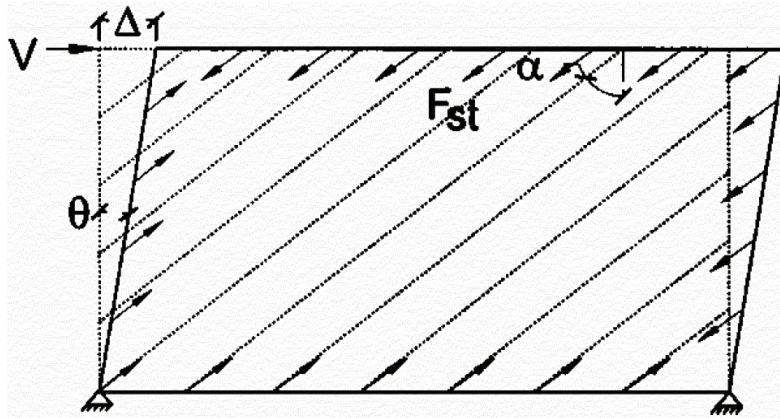
**FIGURE 2-4 Single Story SPSW Collapse Mechanism
(Berman and Bruneau 2003)**
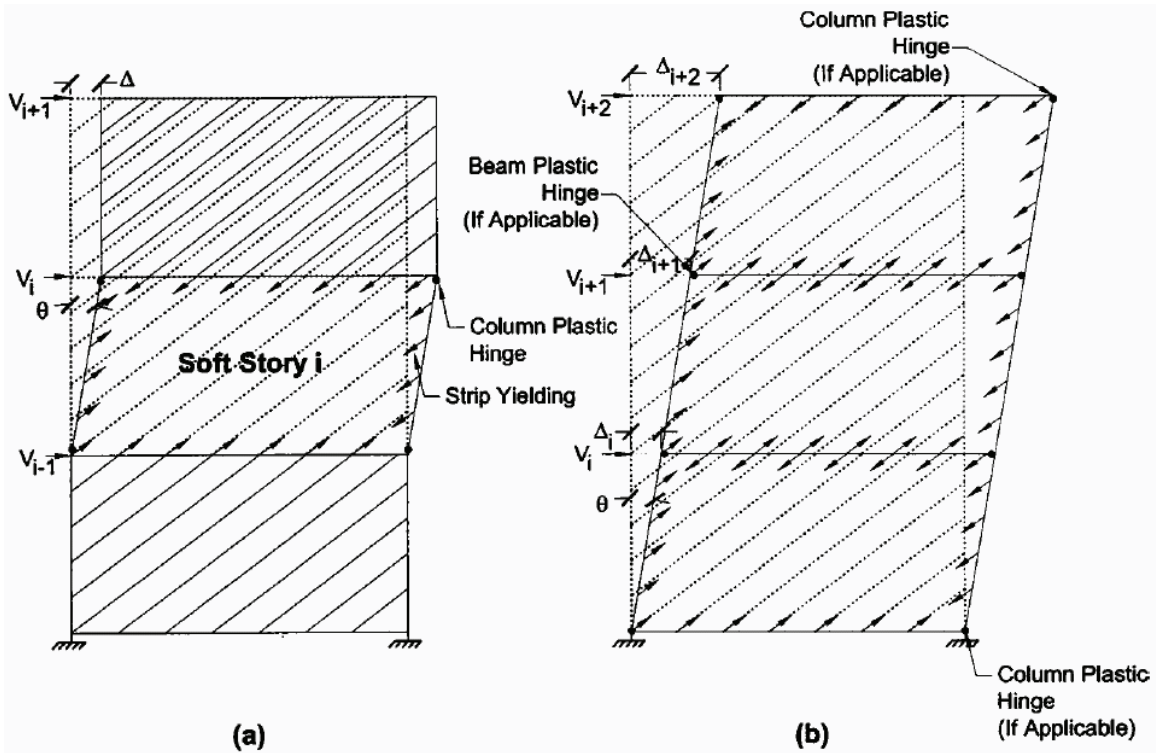
**FIGURE 2-5 Example of Plastic Collapse Mechanism for Multi-story SPSWs
(Berman and Bruneau 2003)**

10

2.6 Behbahanifard, Grondin and Elwi (2003)

Behbahanifard *et al.* (2003) generated a FE model to model their three-story SPSW specimen. Their model, as shown in figure 2-6, was developed based on the nonlinear dynamic explicit formulation, implementing a kinematic hardening material model to simulate the Bauschinger effect, after experiencing convergence problems analyzing the model using the implicit FE model formulation.
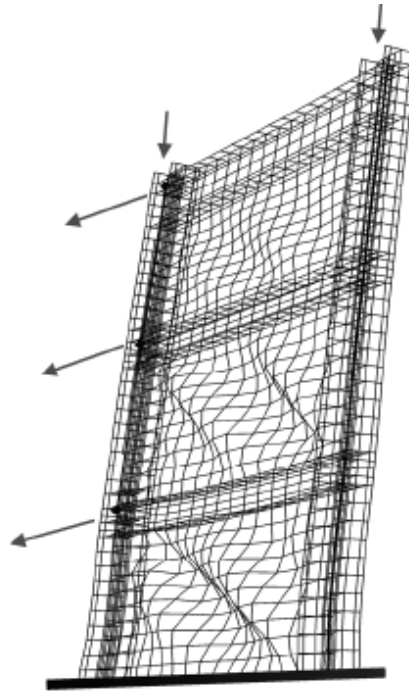
FIGURE 2-6 FE Model of Test Specimen (Behbahanifard *et al.* 2003)

Excellent agreement was observed between the test results and the numerical predictions. Using the validated FE model, parametric studies were conducted to identify and access some of the non-dimensional parameters affecting the behavior of a single panel SPSW with rigid floor beams and subjected to shear force and constant gravity loading.

The researchers found that lower aspect ratio results in greater strength and non-dimensional lateral stiffness for SPSWs. However, this effect is negligible within the aspect ratio range of 1.0 to 2.0, but noticeable for aspect ratio less than 1.0.

In addition, as the column lateral stiffness increased relative to the panel stiffness, the shear wall capacity approached the yield capacity. The stiffer column can more effectively anchor the tension field resulting from infill panel yielding, therefore allowing a more efficient use of the material composing the system.

It was demonstrated that initial out-of-plane imperfections in the infill panel could have a significant influence on the stiffness of the shear panel, while they have no effects on the ultimate shear strength.

Furthermore, the effects of overturning moment and applied gravity load were also investigated using the validated FE model. It was found that increasing either gravity load or the overturning moment reduces the elastic stiffness of the shear wall panel in an almost linear manner and also significantly reduces the normalized capacity and ductility.

2.7 Kharrazi, Ventura, Prion, and Sabouri-Ghomi (2004)

Kharrazi *et al.* (2004) proposed a numerical model referred to as the Modified Plate-Frame Interaction (M-PFI) model to analyze the shear and bending of ductile SPSW. The objective was to describe the interaction between those components and characterize the respective contribution to deformation and strength at whole structure level. Thus, the M-PFI model separates the behavior of ductile SPSW into three parts: elastic buckling, post-buckling, and yielding. Several steps were involved in developing these equations. First, a shear analysis was conducted that looked at the behavior of the infill panels and frames respectively and then the shear-displacement relationships for each were superimposed to obtain the shear behavior of the ductile SPSW. Second, a bending analysis was conducted assuming that the frame and plate act as wide flange shape. Equations were proposed to obtain certain points on a shear-displacement relationship that can be used for analyzing the behavior of the wall.

Kharrazi *et al.* (2004) used test data from Driver *et al.* (1997) to evaluate the M-PFI model using an assumed tension field inclination of 45 degree. The model overestimated the initial stiffness by 5% and underestimated the ultimate capacity of the specimen by about 10%, although it overestimated the specimen capacity slightly at initial yielding. It

should be mentioned that the model does not describe the ductility of the SPSW specimen or the actual mechanism, nor does it provide a means of determining the frame forces for use in design.

2.8   Vian and Bruneau (2005)

Vian and Bruneau (2005) investigated some new methods for the design of SPSW anchor beams. Based on simple free body diagrams as shown in figure 2-7, and the principle of superposition, they proposed a procedure to ensure that frame plastic hinging occurs in the beams and not in columns. Limits were proposed to estimate the drift of a frame with and without SPSW panels at yielding, so that the system may be assessed in the context of the structural "fuse" concept, and considered to dissipate input energy through SPSW panel yielding at a drift level less than that causing the frame members to yield.
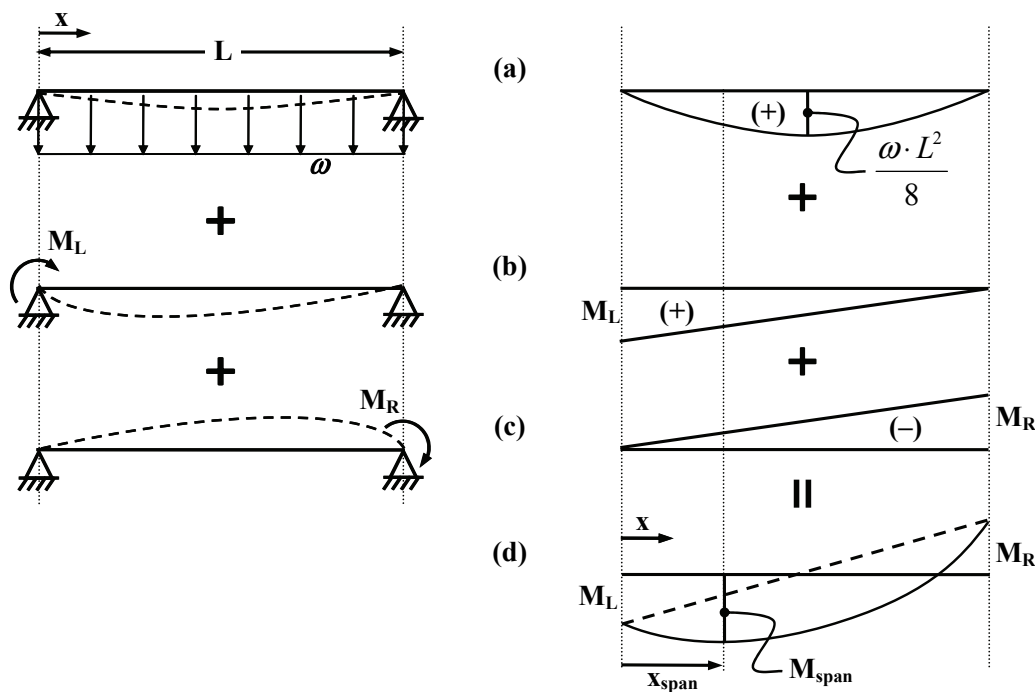
FIGURE 2-7 Free Body Diagram of Anchor HBE

13

2.9   Lopez-Garcia and Bruneau (2006)

Lopez-Garcia and Bruneau (2006) performed some preliminary investigation on the seismic behavior of intermediate beams in SPSWs using strip model. Of primary interest was the determination of the strength level needed to avoid the formation of in-span plastic hinges. To attain this objective, the seismic response of several SPSW models designed according to the FEMA/AISC regulations and the Canadian standard CAN/CSA S16-01 were analyzed by performing linear and nonlinear analysis. The SPSW models considered in this research were designed as an alternative to provide the lateral load resisting system to the four-story MCEER Demonstration Hospital, a reference building model used as part of a broader MCEER research project. The intermediate beams of the FEMA/AISC models were designed according to three different criteria: (I) for gravity loads only; (II) for the ASCE 7 load combinations: (III) for the forces generated by fully yielded webs.

In all cases, the thickness of the thinnest hot-rolled plate available turned out to be larger than the minimum thickness required by the FEMA/AISC guidelines, which resulted in SPSW models having the same plate thickness at all stores (constant plate thickness case). In order to obtain insight into the behavior of intermediate beams of SPSWs having different plate thickness at different stories, models whose plates have the minimum thickness required were also considered for each of the abovementioned design criteria (variable plate thickness case).

Seismic loads were calculated per FEMA 450 assuming that the structure was located in Northridge, California ($S_S = 1.75g$ and $S_S = 0.75g$). The SPSWs were analyzed using the commercial computer program SAP-2000 version 8.3.3. Each infill panel was modeled by a set of 10 parallel, uniformly spaced tension-only strips pinned at both ends (i.e. elements capable of resisting tension axial force only), while the beams and columns were modeled by conventional frame elements.

Forces imposed by the ASCE 7 load combination were assessed through FEMA 450's Equivalent Lateral Force Procedure (linear static analysis). The inelastic behavior of the SPSW models under seismic loading was analyzed by performing FEMA 450's Nonlinear

Static procedure (Pushover analysis). For this, P-M plastic hinges were modeled at the ends of the beams and columns. The strain hardening ratio was set equal to 0.5%. Axial plastic hinges having an elastic-perfectly plastic force-deformation relationship were modeled at the middle of each strip. As indicated by FEMA 450, a set of gravity loads equal to $D+0.25L$ was applied to the models prior to the incremental application of earthquake loads. The pattern of seismic forces was set equal to that indicated by the Equivalent Lateral Force Procedure.

It was found that the FEMA/AISC models designed according to criteria I and II developed in-span plastic hinges in intermediate beams, which is not allowed by the FEMA/AISC regulations. Models designed according to criteria III exhibited the desired behavior (i.e. inelastic deformations occur only at the ends of the beams and in the webs) even when a global collapse mechanism developed. The behavior of CAN/CSA S16-01 models was found to be satisfactory at the response level corresponding to the design basic earthquake, but the global mechanism of these models included in-span plastic hinges in the anchor beams. All these observations were found to apply regardless of whether the SPSW systems have constant or variable plate thickness.

2.10 Shishkin, Driver and Grondin (2005)

Shishkin *et al.* (2005) proposed refinements to the strip model, as described by Thorburn *et al.* (1983), to obtain a more accurate prediction of the inelastic behavior of SPSW using a conventional structural engineering software package. The refinements were based on observations from laboratory tests on SPSW specimens. Modeling efficiency was also evaluated against accuracy of the solution. A modified version of the strip model was proposed as pictured in figure 2-8, which was shown to be efficient while maintaining a high degree of accuracy. In this model, a pin-ended compression strut was used to account for the small contribution of the stiffness and the strength of the infill panel from compressive resistance, which may be significant in the corner regions where effective length of the plate under compression is small.
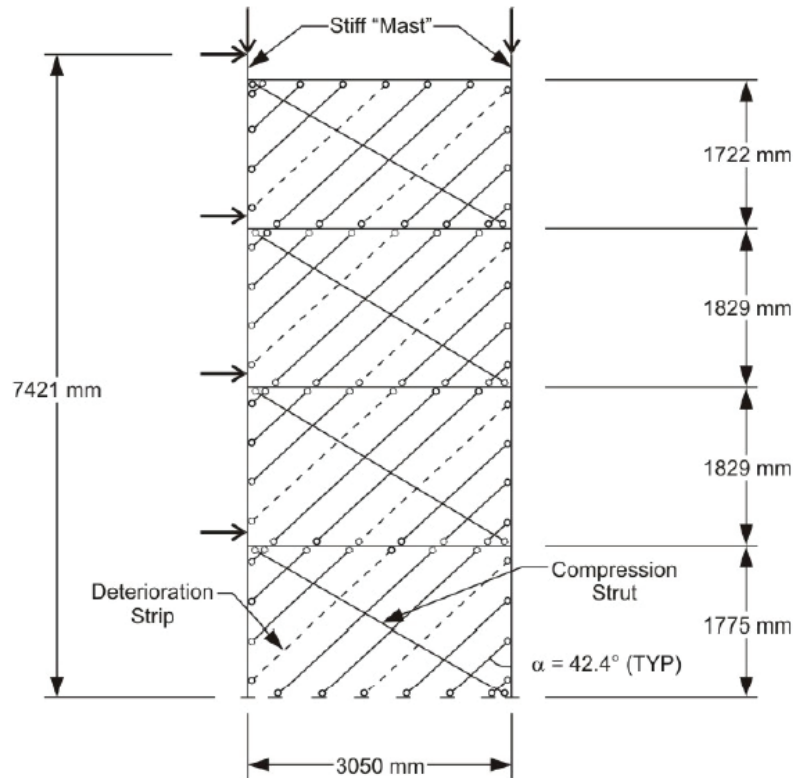
FIGURE 2-8 Schematic of the Modified Strip Model (Shishkin *et al.* 2005)

The parameters of the proposed model are generic and can be implemented into structural analysis program with pushover analysis capacities. A parametric study was also performed to determine the sensitivity of the predicted nonlinear behavior to variations in the angle of inclination of the infill panel tension field.

2.11 Purba and Bruneau (2006)

As part of the further investigations on some concerns reported by Vian and Bruneau (2005), Purba and Bruneau (2006) performed some analytical study on the behavior of unstiffened thin SPSW having openings on the infill plate under monotonic pushover displacement. Two SPSW systems with openings proposed by Vian and Bruneau (2005), namely the perforated and the cutout corner SPSW, were discussed.

The researchers first studied individual perforated strips, which may play an important role in the behavior of perforated SPSW. The effect of mesh refinement on the

16

convergence of solutions was investigated before evaluating various perforated strip models with different perforation diameters, boundary conditions, and material idealizations. The results were presented in terms of stress-strain distribution throughout the strip section as well as in terms of global deformations. Then, a series of one-story SPSWs having multiple perforations on panels were considered, with variation in perforation diameter, boundary conditions, infill plate thickness, material properties idealization, and element definition. The objective of this analysis was to verify the accuracy of the results obtained from FE analysis of individual perforated strips to predict the SPSW strength by summing the strength of "simpler" individual strips. Shell elements were used to model the infill plates as well as the boundary frame member webs and flanges. Good agreement in overall behavior between the models considered and individual perforated strip model was observed. The applicability of the equation proposed by previous researchers to approximate the strength of a perforated panel was also re-assessed.

In addition, two cutout corner SPSW models were also investigated. The first model replicated the cutout corner SPSW specimen tested by Vian and Bruneau (2005) in which a flat-plate reinforcement was introduced along the cutout edges. The second model considered had a T-section reinforcement along the cutout edges; this model was built by adding a new plate perpendicularly to the previous flat-plate reinforcement. No significant difference between the two models was observed in terms of frame deformations and stress distributions along the cutout corner SPSW. However, some local effects were observed adjacent to the cutout corner, in terms of diagonal displacement of the cutout reinforcement plate and stress distribution along the length of the plates.

2.12 Berman and Bruneau (2008)

Berman and Bruneau (2008) performed research on developing capacity procedure for VBEs in SPSWs. They reviewed the current approaches provided in the AISC Seismic Provisions (AISC 2005) for determination of capacity design loads for VBEs of SPSWs and identified the deficiency of these procedures. Then, a new procedure was proposed

that based on a fundamental plastic collapse mechanism and linear beam analysis to approximate the design actions for VBEs for the given infill panels and HBEs. The VBE free body diagrams they used were shown in figure 2-9. Their procedure does not involve nonlinear analysis, making it practical for use in design. VBE design loads were estimated using the proposed procedure for two example SPSW configurations. It is found that VBE design forces predicted from the proposed procedure agree well with those from the nonlinear pushover analysis.
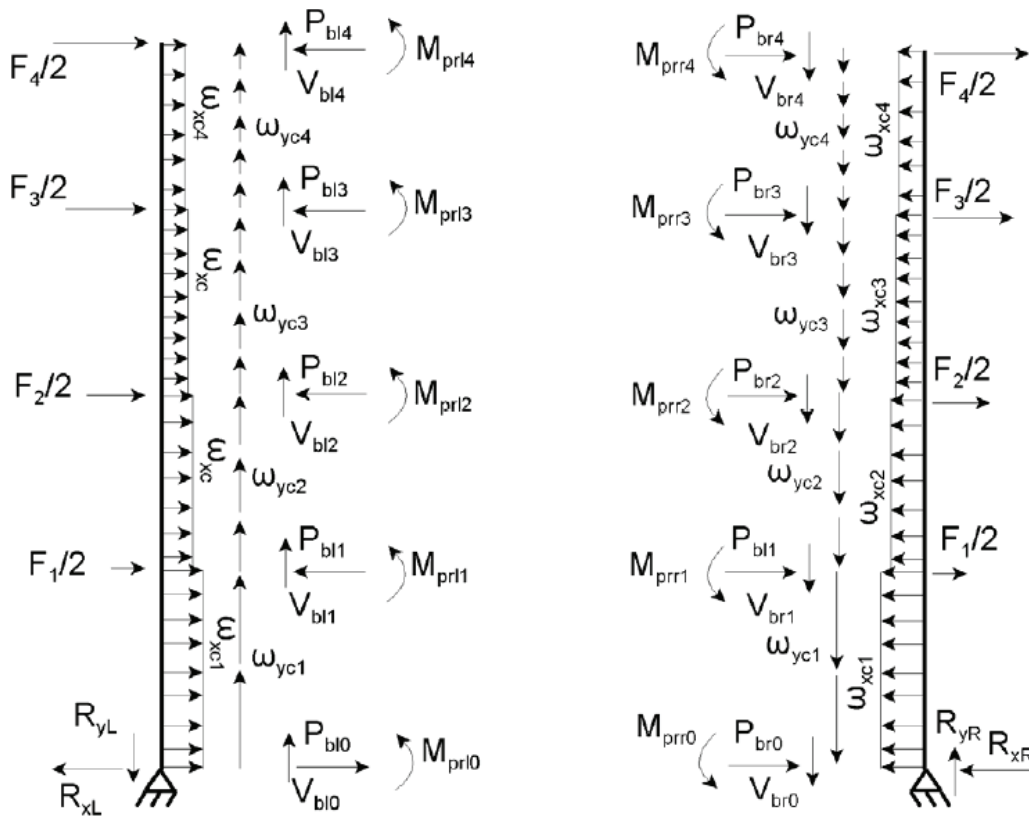
FIGURE 2-9 VBE Free Body Diagrams (Berman and Bruneau 2008)

SECTION 3

PLASTIC MOMENT OF HORIZONTAL BOUNDARY ELEMENTS

3.1 Introduction

The HBE yield patterns observed in the recent tests on SPSWs by Qu *et al*. (2008) indicate that the stress distribution at the HBE plastic hinges is more complex than accounted by simple analysis methods. Therefore, if one wishes to understand how to design an HBE, the first step is to correctly quantify the strength of HBE plastic hinges accounting for this condition.

Conventional plastic analysis procedures for determining the plastic moment of wide flange member in a moment frame can not be applied to HBEs of SPSWs because the HBE web is under large bi-axial stress condition. To account for this effect, analytical procedures to estimate the plastic moment resistance of HBEs subjected to axial force, shear force, and vertical stresses due to infill panel forces, are needed to ensure predictable and ductile behavior of HBEs.

This section first discusses the loading characteristics of HBE cross-sections. Following a review of the conventional procedure to calculate the plastic moment of wide flange members in a conventional steel moment frame, the reduced yield strength of HBE web under shear and vertical stresses is studied using the von Mises yield criterion. Analytical procedures for estimating the plastic moment of intermediate HBEs and anchor HBEs are then developed, respectively. Note that intermediate HBEs are those to which are welded steel plates above and below, by opposition to anchor HBEs that have steel plates only below or above. Procedures for calculating plastic moment of intermediate HBEs under equal and unequal top and bottom tension fields are first investigated. Those procedures are verified by FE examples and are simplified for practical purpose. Next, additional numerical examples are developed to confirm that those procedures proposed for intermediate HBEs can also apply to anchor HBEs. Note that the analytical procedures to estimate HBE plastic moment developed in this section will be used in Section 4 for capacity design of HBEs.

3.2 Loading Characteristics of HBE Cross-Sections

In any multistory SPSW such as the one shown in figure 3-1, the HBEs can be differentiated as anchor HBEs and intermediate HBEs. Anchor HBEs are the top and bottom ends of a SPSW and that anchor the SPSW infill panel yield forces. Since they are loaded by infill tension field forces only on one side (either above or below), they are typically of substantial size. Intermediate HBEs are the beams at all other levels. The variation between the top and bottom infill panel stresses acting on the HBE can sometimes be small or null when the top and bottom infill panels of identical (or near identical) thicknesses are both yielding. Comparing with the sizes of anchor HBEs, intermediate HBEs are often relatively small.
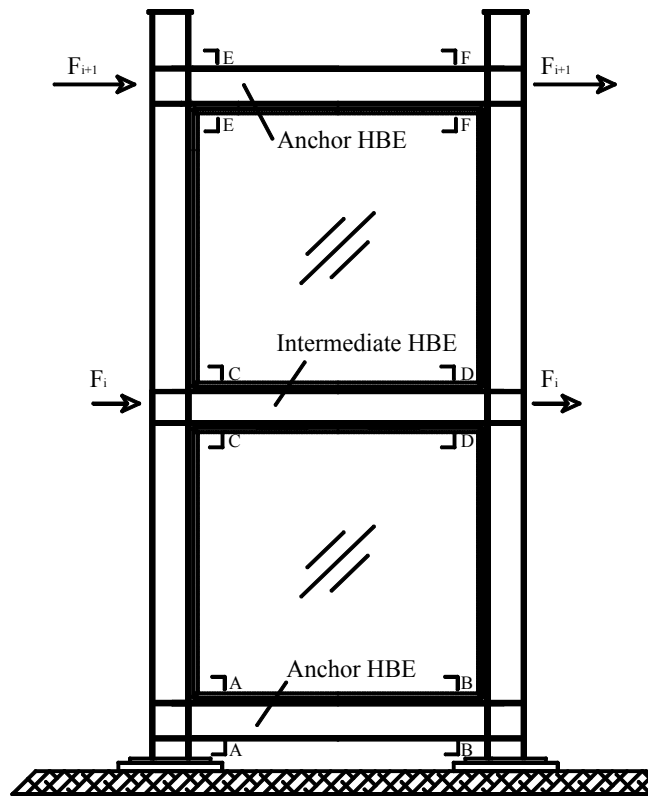
FIGURE 3-1 Typical Multistory SPSW

To understand the infill panel effects on HBE behaviors, consider the aforementioned SPSW with rigid HBE-to-VBE connections. The shear stress and external loading at the HBE ends are schematically shown in figure 3-2, where τ represents the shear stress in HBE web; and P and M represent the axial force and moment acting at HBE ends,

respectively; when the expected plastic collapse mechanism of the SPSW develops. In this figure, ω_{ybi+1} and ω_{ybi} represent the vertical components of the top and bottom infill tension fields, respectively. Mathematical expressions for ω_{ybi+1} and ω_{ybi} will be given in the Section 4.
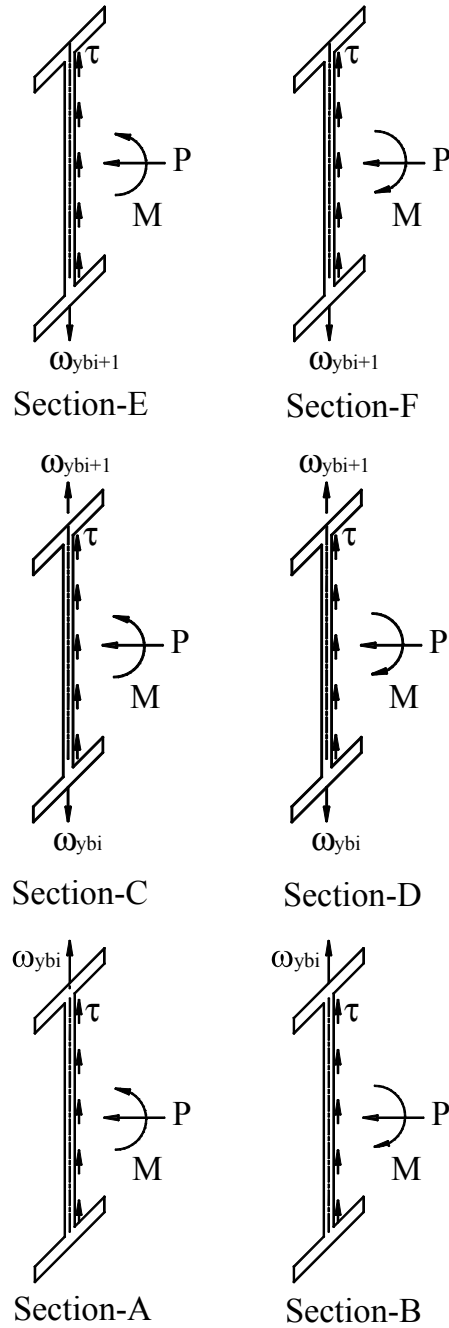
FIGURE 3-2 Shear Stress and Loading at HBE Ends

Note that an HBE is typically in compression which will be demonstrated in Section 4. The magnitudes of τ, P, and M vary at different locations along an HBE. Although the direction of shear stress, τ, depends on the resulting shear effects due to tension field forces and HBE flexural actions, it has no effect on HBE plastic moment resistance as demonstrated in Section 3.5.3. Accordingly, the loading characteristics of HBE cross-sections are summarized in table 3-1. Note that for the purpose of the present discussion, flexure designated as "+"or "-" respectively refers to the bending action producing tension or compression in the flange on which the greater tension field force is applied. For intermediate HBEs with equal top and bottom tension fields, the acting direction of flexure has no impact on the plastic moment resistance as demonstrated in Section 3.5.1.

TABLE 3-1 Summary of Loading Characteristics of HBE Cross-Section

HBE type	Corresponding section on figure 3-2	Flexure		Tension field ratio $\left(\omega_{yi}/\omega_{yi+1}\right)$
		+	-	
Intermediate	C/D			1
Intermediate	C	√		>1
Intermediate	D		√	>1
Anchor	A		√	0 [-a]
Anchor	B	√		0 [-a]
Anchor	E	√		∞ [-b]
Anchor	F		√	∞ [-b]

[-a] when $\omega_{yi} = 0$.

[-b] when $\omega_{yi+1} = 0$.

3.3 Plastic Moment of Wide Flange Members in Moment Frame

A well-known lower bound approach to estimate plastic moment for wide flange members in steel moment frame, based on stress diagrams, and classic plastic analysis can be used to account for the combined interaction of flexure, axial and shear forces (Bruneau *et al.* 1998). Using this procedure, the uniform shear stress, τ_w, assumed to act on the web of the cross-section as a result of the applied shear force, V, is calculated as:

$$\tau_w = \frac{V}{h_w t_w} \tag{3-1}$$

22

where h_w and t_w are the web depth and thickness of the cross-section, respectively.

Then, the von Mises yield criterion is used to calculate the maximum axial stress, σ_w, that can be applied on the web (i.e., the remaining axial yield strength):

$$\sigma_w = \sqrt{f_y^2 - 3\tau_w^2} \qquad (3\text{-}2)$$

where f_y is the yield strength of steel.

Strength of the flanges remains f_y. In the case that the neutral axis remains in the web; as shown in figure 3-3, location of the neutral axis, y_o, is given by:

$$y_o = \frac{P}{\sigma_w t_w} \qquad (3\text{-}3)$$

where P is the applied axial compression.

Neglecting strain hardening, the plastic axial stress diagram of a typical wide flange section can be divided into pure flexural and axial contributions as shown in figure 3-3. The contributions of the web and flanges to the plastic moment resistance can be calculated based on the flexural stress diagrams shown in figure 3-3, as:

$$M_{pr-web}^{P,V} = \frac{t_w \left(d - 2t_f\right)^2}{4}\sigma_w - \frac{t_w \left(2y_o\right)^2}{4}\sigma_w \qquad (3\text{-}4)$$

$$M_{pr-flange}^{P,V} = b_f t_f \left(d - t_f\right) f_y \qquad (3\text{-}5)$$

$$M_{pr}^{P,V} = M_{pr-web}^{P,V} + M_{pr-flange}^{P,V} \qquad (3\text{-}6)$$

where the superscript (P, V) indicates that the plastic moment is reduced taking into account the applied axial and shear forces, and where b_f and t_f are the flange width and thickness of the cross-section, respectively.
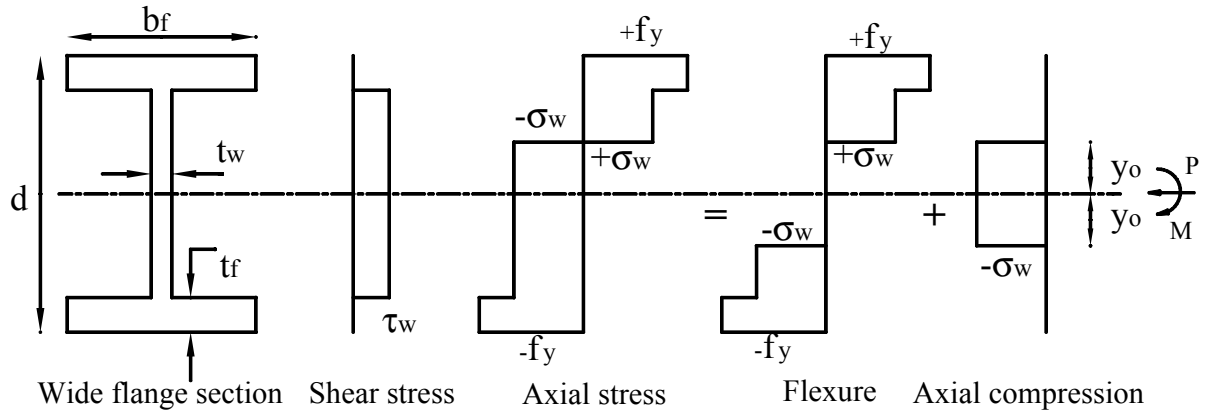
FIGURE 3-3 Example of Plastic Resistance of a Wide Flange Structural Shape Subjected to Flexure, Axial, and Shear Forces

The above lower bound approach, which provides acceptable results, has been used for steel moment frame design. However, for SPSW, the experimental results described in Qu *et al*. (2008) provide evidence that a more sophisticated procedure is warranted. To do so, a review of the von Mises criterion in plane stress condition is necessary and done in the following section.

3.4 Reduced Yield Strength in HBE Web

To better understand the reduced axial yield strength in HBE web accounting for the shear stress and vertical stresses due to infill panel forces, two elements are arbitrarily selected from the axial tension and compression zones in the web of a typical intermediate HBE segment as shown in figure 3-4. These elements are in plane stress condition. The free body diagrams, stress diagrams and Mohr's circles are also schematically shown in figure 3-4. Note that the exact Mohr's circles of elements A and B depend on the magnitudes of the vertical components of the tension fields, i.e. ω_{ybi+1} and ω_{ybi}, applied above and below the intermediate HBE segment.
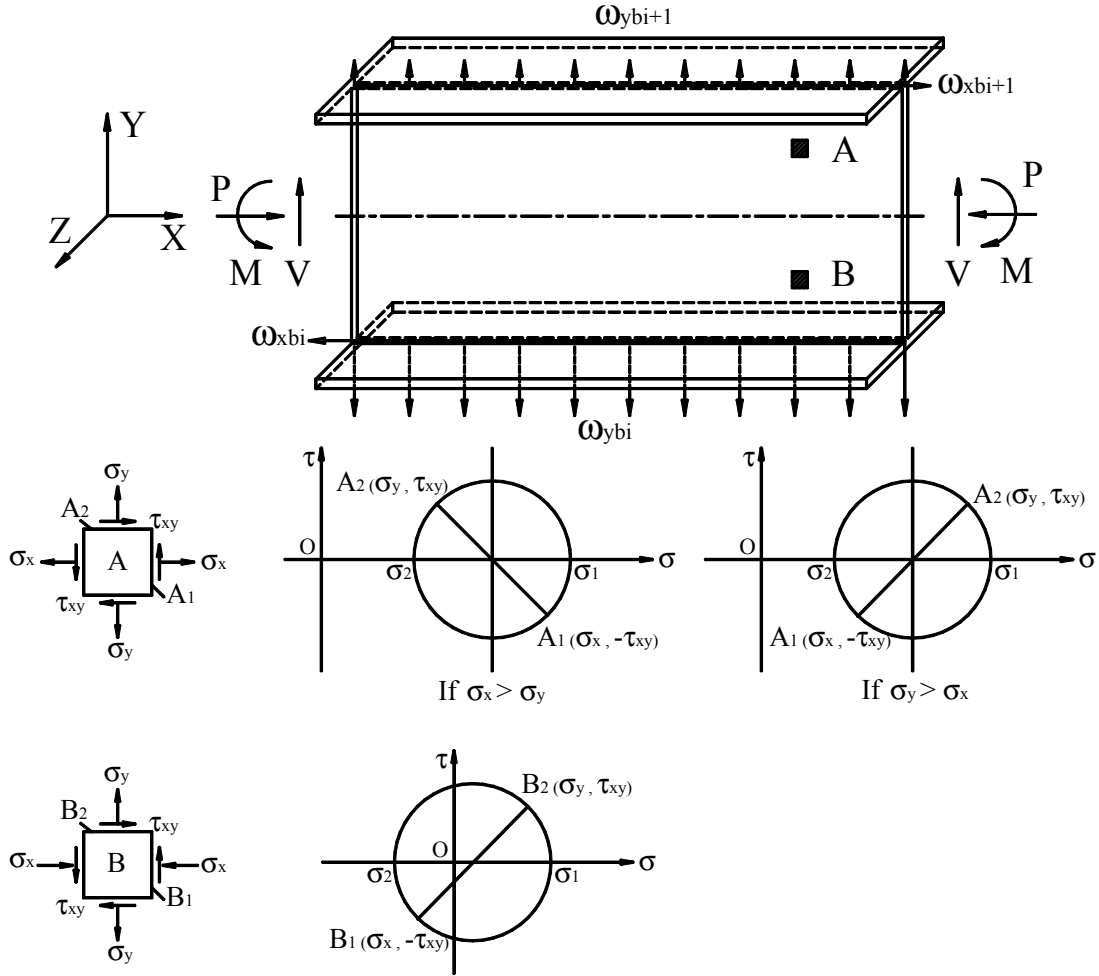
**FIGURE 3-4 Loading of Intermediate HBE Segment and
Mohr's Circles of the Elements on the Web**

The results of classic mechanics of materials show that the radius of the Mohr's circle
can be determined as:

$$R^2 = \left(\frac{\sigma_x - \sigma_y}{2}\right)^2 + \tau_{xy}^2 \tag{3-7}$$

Graphically, the maximum and minimum in-plane principal stresses, σ_1 and σ_2, can be
calculated as:

$$\sigma_1 = \frac{\sigma_x + \sigma_y}{2} + R \tag{3-8}$$

$$\sigma_2 = \frac{\sigma_x + \sigma_y}{2} - R \tag{3-9}$$

In addition, for steel subjected to multi-axial plane-stress conditions and having a uniaxial elasto-perfectly plastic behavior, steel can be modeled using the von Mises yield criterion and expressed as:

$$\frac{1}{2}\left[\left(\sigma_1 - \sigma_2\right)^2 + \sigma_1^2 + \sigma_2^2\right] = f_y^2 \tag{3-10}$$

Substituting(3-7), (3-8) and (3-9) into (3-10) and normalizing the resulting equation, the von Mises yield criterion can be rewritten as:

$$\left(\frac{\sigma_x}{f_y}\right)^2 - \left(\frac{\sigma_x}{f_y}\right)\left(\frac{\sigma_y}{f_y}\right) + \left(\frac{\sigma_y}{f_y}\right)^2 + 3\left(\frac{\tau_{xy}}{f_y}\right)^2 = 1 \tag{3-11}$$

Equation (3-11) can be reorganized as a quadratic equation in terms of σ_x/f_y or τ_{xy}/f_y and solved to respectively give the reduced axial and shear yield strengths for given values of the other terms:

$$\left(\frac{\sigma_x}{f_y}\right) = \frac{1}{2}\left(\frac{\sigma_y}{f_y}\right) \pm \frac{1}{2}\sqrt{4 - 3\left(\frac{\sigma_y}{f_y}\right)^2 - 12\left(\frac{\tau_{xy}}{f_y}\right)^2} \tag{3-12}$$

$$\left(\frac{\tau_{xy}}{f_y}\right) = \pm\frac{1}{\sqrt{3}}\sqrt{1 - \left(\frac{\sigma_x}{f_y}\right)^2 + \left(\frac{\sigma_x}{f_y}\right)\left(\frac{\sigma_y}{f_y}\right) - \left(\frac{\sigma_y}{f_y}\right)^2} \tag{3-13}$$

Note that the reduced tension and compression axial yield strength can be obtained by considering the "+" and "-" cases in (3-12) respectively.

Equations (3-12) and (3-13), can be simplified as shown in (3-14) and (3-15) for cases of uniaxial stress and pure shear respectively.

$$\left(\frac{\sigma_x}{f_y}\right) = \pm\sqrt{1-3\left(\frac{\tau_{xy}}{f_y}\right)^2} \quad \text{if } \sigma_y = 0 \tag{3-14}$$

$$\tau_{xy} = \frac{f_y}{\sqrt{3}} \quad \text{if } \sigma_x = \sigma_y = 0 \tag{3-15}$$

Note that (3-14) is equivalent to (3-2) which is used for estimating the plastic moment resistance of wide flange members in steel moment frame. The von Mises yield criterion, in the σ_x/f_y and τ_{xy}/f_y space, for given values of σ_y/f_y are shown in figure 3-5 as a graphical representation of (3-12) .
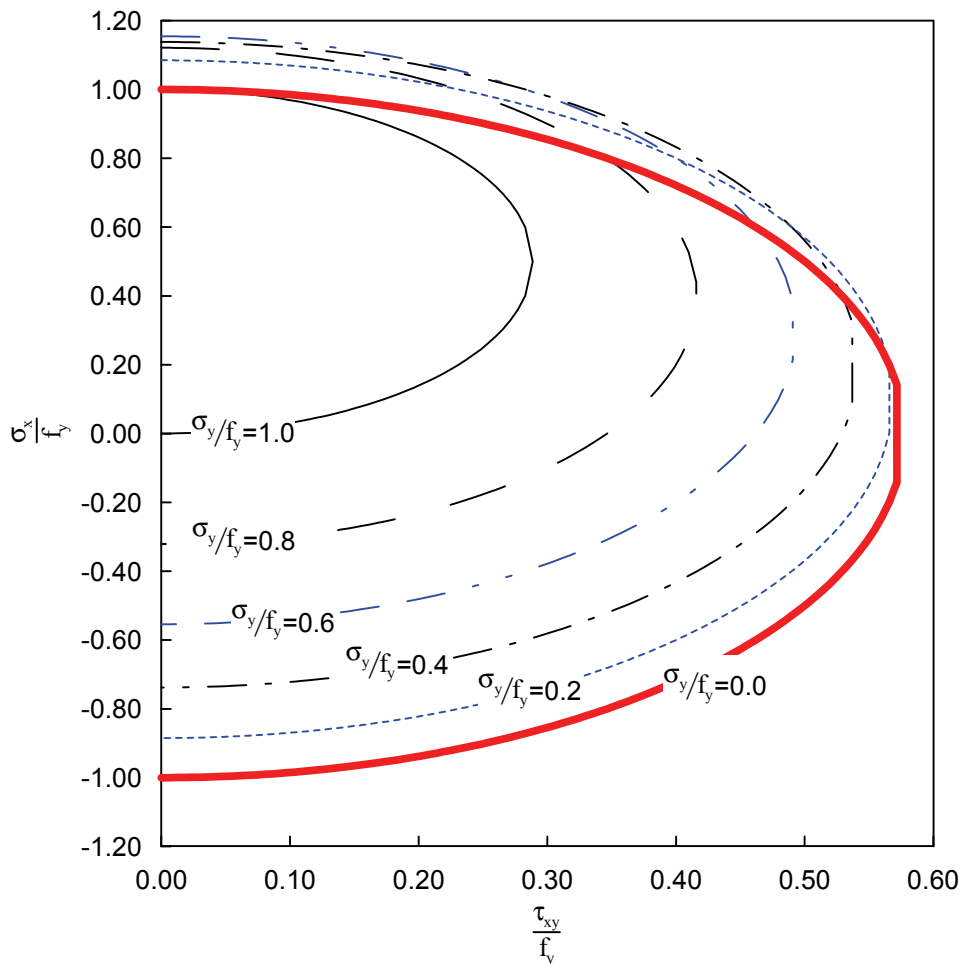
FIGURE 3-5 Reduced Yield Strength per the Von Mises Criterion in Plane Stress

As observed in (3-12), the reduced axial yield strength is a function of shear stress τ_{xy} and vertical stress σ_y . In the absence of vertical axial stresses (i.e. $\sigma_y = 0$), the compression and tension axial yield strengths are of the same magnitude. This is the case illustrated in figure 3-3 , for a wide flange member in conventional moment frame. However, as shown in figure 3-5, the presence of vertical stresses results in unequal tension and compression axial yield strengths. This is the stress condition found in an HBE cross-section. Note from figure 3-5 that the compression axial yield strength is significantly reduced, and can even become null under the combined action of shear and vertical stresses. The tension axial yield strength is also affected by the shear and vertical stresses, but to a lesser degree. Reading the figure differently, due to the presence of given vertical and axial compression/tension stresses, the shear yield strength is also reduced. Given that the vertical stresses in the whole HBE web may not be constant, figure 3-6 is helpful to compare the compression and tension axial yield strengths for a wide range of vertical stress ratio (i.e. σ_y / f_y). Note from figure 3-6 that the maximum value of σ_y / f_y can be reached is less than 1.0 in some cases (e.g. for the case of $\tau_{xy} / f_y = 0.40$). It is because the maximum allowable vertical stress is reduced due to the presences of the axial stress in horizontal direction (i.e. σ_x) and the shear stress (i.e. τ_{xy}) as shown in figure 3-5.
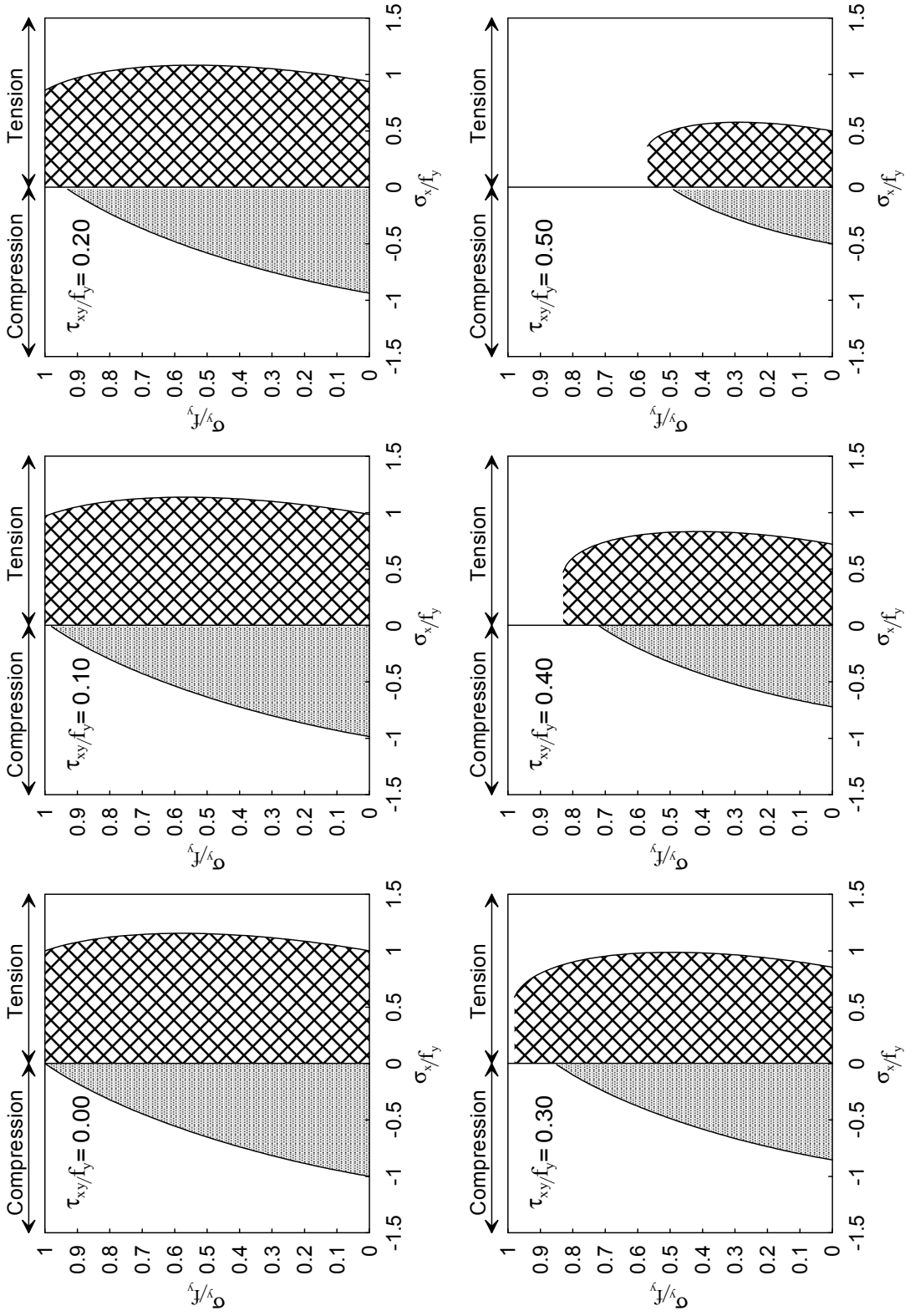
FIGURE 3-6 Axial Yield Strength under Combinations of Shear and Vertical Stresses per the Von Mises Yield Criterion

29

3.5   Intermediate HBE under Equal Top and Bottom Tension Fields

The plastic moment resistance of intermediate HBE under constant vertical stresses, resulting from equal top and bottom tension fields, is first discussed because this case provides some of the building blocks necessary to understand the more complex scenarios presented later in this section.

3.5.1   Derivation of Plastic Moment

In the spirit of classic plastic cross-section analysis and following a procedure similar to that presented in Section 3.3, also using reduced axial yield strength obtained from the von Mises yield criterion accounting for the vertical and shear stresses as presented in Section 3.4, one can generate the stress diagrams for a fully plastified wide flange section under uniform vertical tension fields as shown in figure 3-7. Note that this case corresponds to the stress conditions generated in an intermediate HBE when the infill panels above and below the HBE are of equal thicknesses and fully yielded (i.e. $\omega_{ybi} = \omega_{ybi+1}$). Also note that all the equations derived in this section remain valid for case of opposite flexure case (i.e. the top and bottom parts of figure 3-7 show the stress diagrams corresponding to both flexure cases.).

As traditionally done in structural steel for wide flange sections, uniform shear stress is assumed to act on the HBE web. In addition, a constant vertical tension stress is assumed in the HBE web as a result of the identical top and bottom tension fields. The shear stress is calculated according to (3-1). The uniform vertical stress is given by:

$$\sigma_y = \frac{\omega_{ybi}}{t_w} \tag{3-16}$$

Consistent with (3-12), the tension and compression axial yield strengths, σ_t and σ_c, can be respectively calculated as:

$$\left(\frac{\sigma_t}{f_y}\right) = \frac{1}{2}\left(\frac{\sigma_y}{f_y}\right) + \frac{1}{2}\sqrt{4 - 3\left(\frac{\sigma_y}{f_y}\right)^2 - 12\left(\frac{\tau_w}{f_y}\right)^2} \tag{3-17}$$

$$\left(\frac{\sigma_c}{f_y}\right) = \frac{1}{2}\left(\frac{\sigma_y}{f_y}\right) - \frac{1}{2}\sqrt{4 - 3\left(\frac{\sigma_y}{f_y}\right)^2 - 12\left(\frac{\tau_w}{f_y}\right)^2} \qquad (3\text{-}18)$$

FIGURE 3-7 Stress Diagrams of Intermediate HBE Cross-Section under Flexure, Axial Compression, Shear Force, and Vertical Stresses due to Equal Top and Bottom Tension Fields

From the geometry in figure 3-7,

$$y_t = h_w - y_c \qquad (3\text{-}19)$$

where y_c and y_t represent compression and tension portion of the web ,respectively.

For the most common case that the neutral axis remains in the web, the governing equation of axial force equilibrium can be given as

$$\sigma_c y_c t_w + \sigma_t y_t t_w = P \qquad (3\text{-}20)$$

where P is the applied axial compression.

The contribution of the flanges to axial compression is null since the resultant axial forces of each flange have the same magnitude but opposite signs (and thus cancel each other).

Substituting (3-19) into (3-20) and solving for y_c gives,

$$y_c = \frac{\left(\dfrac{\sigma_t}{f_y}\right) + \beta_w}{\left(\dfrac{\sigma_t}{f_y}\right) - \left(\dfrac{\sigma_c}{f_y}\right)} \cdot h_w \tag{3-21}$$

where β_w is the ratio of the applied axial compression to the nominal axial strength of the web, which is given by:

$$\beta_w = \frac{-P}{f_y h_w t_w} \tag{3-22}$$

The contributions of the web and flanges to the plastic moment resistance, M_{pr-web} and $M_{pr-flange}$, can be respectively determined as:

$$M_{pr-web} = \sigma_t t_w y_t \left(\frac{h_w}{2} - \frac{y_t}{2}\right) - \sigma_c t_w y_c \left(\frac{h_w}{2} - \frac{y_c}{2}\right) \tag{3-23}$$

$$M_{pr-flange} = f_y b_f t_f \left(d - t_f\right) \tag{3-24}$$

A cross-section plastic moment reduction factor, β, is defined to quantify the loss in plastic strength attributable to the combined effects of the applied axial compression, shear force, and vertical stresses due to the infill panels forces acting on the HBE. This factor, β, can be determined as:

$$\beta = \frac{M_{pr-web} + M_{pr-flange}}{f_y Z} \tag{3-25}$$

where Z is the HBE plastic section modulus.

For the extreme case for which the web of the cross-section makes no contribution to the flexure, the minimum value of the reduction factor, β_{min}, is obtained, and is given as:

$$\beta_{min} = \frac{M_{pr-flange}}{f_y Z} \tag{3-26}$$

This will happen when the entire web is under uniform compression.

3.5.2 FE Verification

To validate the approach developed in Section 3.5.1 to calculate the cross-section plastic moment reduction factor of the intermediate HBE under equal top and bottom tension fields, a series of FE analyses were performed on a segment of HBE. The FE model is shown in figure 3-8.

**FIGURE 3-8 FE Model of Intermediate HBE Segment
under Flexure, Axial Compression, Shear Force, and Vertical
Stresses due to Equal Top and Bottom Tension Fields**

In this case, a W21x73 member was modeled in ABAQUS/Standard. The length of the member was twice the cross-section depth. Material was assumed to be A572 Grade 50 steel with elasto-perfectly plastic constitutive behavior. Shell element (ABAQUS element S4R) was employed for the web and flanges. A fine mesh with 9,000 elements (2,000 elements per flange and 5,000 elements for the web) was used in this model.

As shown in figure 3-8, uniformly distributed loads, ω_{ybi+1} and ω_{ybi}, of identical magnitude but applied in opposite directions at the top and bottom edges of the HBE web represented the vertical components of the top and bottom tension fields. Uniform shear stresses, τ_{xy}, were applied along the HBE web edges. Axial forces applied at the ends of the member represented the axial compression in the HBE.

The FE analysis was conducted in two stages to correctly replicate boundary conditions and to achieve the desired load scenario while keeping the whole model in self-equilibrium. In the first stage, the aforementioned tension field forces, shear stresses and axial forces were applied on the FE model. In the next stage, a displacement controlled analysis procedure was used to obtain the plastic moment resistance of the cross-section, in which the rotations at the end of the HBE segment were proportionally increased up to a magnitude of 0.035 rad, but in opposite directions.

A series of analyses were conducted on the FE model to assess the accuracy of the analytical procedure. Results are shown in figure 3-9. In these analyses, for the given axial compression and shear, the magnitudes of the identical tension fields were increased from null to the maximum allowable value in the HBE web. To capture the entire range of the solutions developed analytically, for each case of β_w, five different vertical stress conditions (approximately equally spaced in the allowable range of σ_y/f_y) were considered in the FE models. Note that the combined axial compression, shear and vertical stresses selected for these analyses may not necessarily develop in a real intermediate HBE. Also, note that the plastic moment reduction factor shown in figure 3-9 for the intermediate HBE cross-section reduces to that which corresponds to values for the ordinary beam action in the absence of tension fields from the SPSW infill panels.

As shown in figure 3-9, the cross-section plastic moment reduction factors obtained from the FE analysis agree very well with those predicted using the approach presented in Section 3.5.1. One can also observe the cross section plastic moment reduction factor varies from unity to a minimum when increasing the axial force, shear, and vertical stress.

FIGURE 3-9 Plastic Moment Reduction Factor of Intermediate HBE Cross-Section under Axial Compression, Shear Force, and Uniform Vertical Stresses: Analytical Predictions versus FE Results

3.5.3 Effects of Shear Direction

Though (3-17) and (3-18) show that the acting direction of shear stresses has no effects on the resulting compression/tension axial yield strength, and consequently make no difference in the calculated cross-section plastic moment reduction factor, numerical examples were conducted to confirm this point. Directions of the edge shear shown in figure 3-8 were switched and the FE model was reanalyzed for the cases shown in figure 3-9 case (b). The results from this new model (i.e.FE^2) are plotted in figure 3-10 together with those from the original model (i.e.FE^1) and from the approach proposed in Section 3.5.1. As shown, the direction of shear stresses has no impact on the cross-section plastic moment reduction factor.
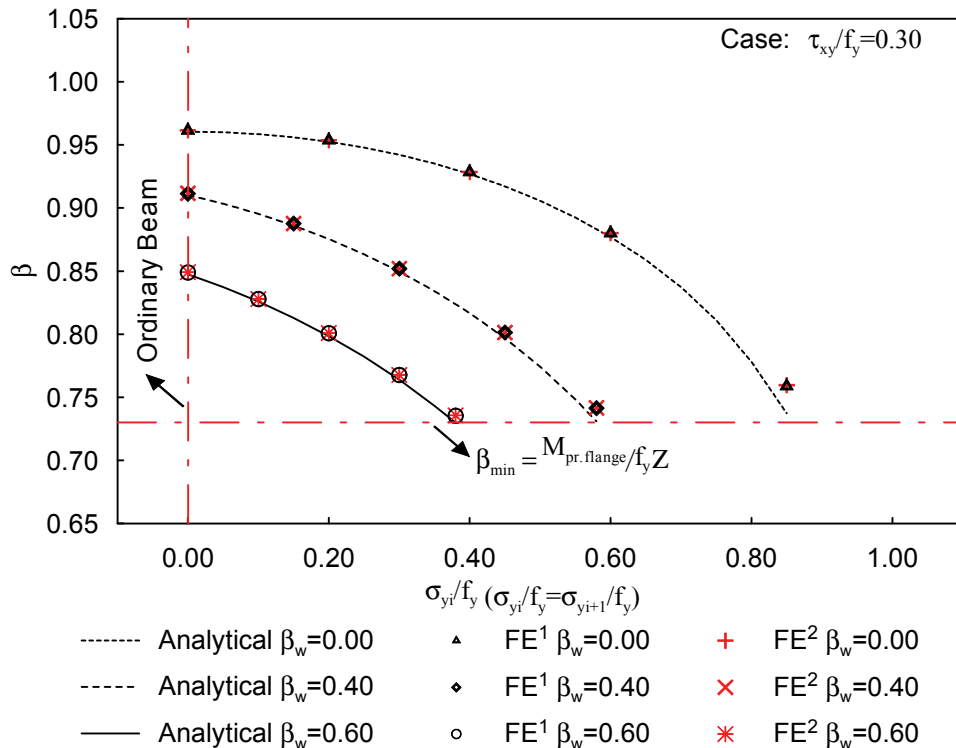
FIGURE 3-10 Effects of Shear Direction on Cross-Section Plastic Moment Reduction Factor of Intermediate HBE

3.6 Intermediate HBE under Unequal Top and Bottom Tension Fields

In Section 3.5, it was assumed that identical tension fields were acting above and below the intermediate HBE. However, in many instances this is not the case and it is necessary

to investigate how the HBE plastic moment resistance would be affected by the unequal top and bottom tension fields. As listed in table 3-1, both positive and negative flexure cases are considered. The same fundamental concepts and modeling assumptions previously presented still apply, except that a linear variation of vertical stresses is assumed instead of the prior constant vertical stresses.

3.6.1 Derivation of Plastic Moment under Positive Flexure

One can generate the stress diagrams shown in figure 3-11 for a fully plastified HBE cross-section of elasto-perfectly plastic steel subjected to axial compression, shear, vertical stresses due to unequal top and bottom tension fields, and positive flexure.
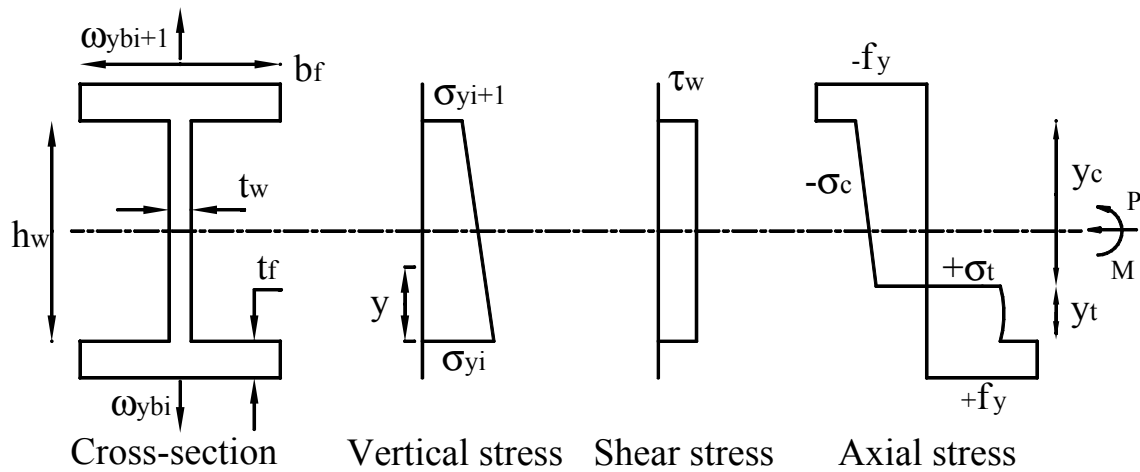
FIGURE 3-11 Stress Diagrams of Intermediate HBE Cross-Section under Positive Flexure, Axial Compression, Shear Force, and Vertical Stresses due to Unequal Top and Bottom Tension Fields

As a reasonable approximation, linearly varying vertical stresses are assumed to act on the HBE web. Mathematically, this assumption is expressed as:

$$\frac{\sigma_y(y)}{f_y} = \left(\frac{\sigma_{yi}}{f_y}\right) \cdot \left(1 - \frac{y}{h_w}\right) + \left(\frac{\sigma_{yi+1}}{f_y}\right) \cdot \left(\frac{y}{h_w}\right) \tag{3-27}$$

where the vertical stresses at the top and bottom edges of the HBE web, σ_{yi+1} and σ_{yi}, can be calculated based on the tension field information respectively as:

$$\sigma_{yi+1} = \frac{\omega_{ybi+1}}{t_w} \tag{3-28}$$

$$\sigma_{yi} = \frac{\omega_{ybi}}{t_w} \tag{3-29}$$

In accordance with (3-12), the tension and compression axial yield strengths at any location in the web can be determined respectively as:

$$\frac{\sigma_t(y)}{f_y} = \frac{1}{2}\frac{\sigma_y(y)}{f_y} + \frac{1}{2}\sqrt{4 - 3\left[\frac{\sigma_y(y)}{f_y}\right]^2 - 12\left(\frac{\tau_w}{f_y}\right)^2} \tag{3-30}$$

$$\frac{\sigma_c(y)}{f_y} = \frac{1}{2}\frac{\sigma_y(y)}{f_y} - \frac{1}{2}\sqrt{4 - 3\left[\frac{\sigma_y(y)}{f_y}\right]^2 - 12\left(\frac{\tau_w}{f_y}\right)^2} \tag{3-31}$$

Substituting (3-27) into (3-30) and (3-31), one obtains:

$$\frac{\sigma_t(y)}{f_y} = \frac{1}{2}\left[\left(\frac{\sigma_{yi}}{f_y}\right)\cdot\left(1 - \frac{y}{h_w}\right) + \left(\frac{\sigma_{yi+1}}{f_y}\right)\cdot\left(\frac{y}{h_w}\right)\right]$$
$$+ \frac{1}{2}\sqrt{4 - 3\left[\left(\frac{\sigma_{yi}}{f_y}\right)\cdot\left(1 - \frac{y}{h_w}\right) + \left(\frac{\sigma_{yi+1}}{f_y}\right)\cdot\left(\frac{y}{h_w}\right)\right]^2 - 12\left(\frac{\tau_w}{f_y}\right)^2} \tag{3-32}$$

$$\frac{\sigma_c(y)}{f_y} = \frac{1}{2}\left[\left(\frac{\sigma_{yi}}{f_y}\right)\cdot\left(1 - \frac{y}{h_w}\right) + \left(\frac{\sigma_{yi+1}}{f_y}\right)\cdot\left(\frac{y}{h_w}\right)\right]$$
$$- \frac{1}{2}\sqrt{4 - 3\left[\left(\frac{\sigma_{yi}}{f_y}\right)\cdot\left(1 - \frac{y}{h_w}\right) + \left(\frac{\sigma_{yi+1}}{f_y}\right)\cdot\left(\frac{y}{h_w}\right)\right]^2 - 12\left(\frac{\tau_w}{f_y}\right)^2} \tag{3-33}$$

From the geometry in figure 3-11, again:

$$y_t = h_w - y_c \tag{3-34}$$

For the case when the neutral axis remains in the HBE web, the contribution of the top and bottom flanges to axial fore is null since the resultant axial forces in each flange have the same magnitude but opposite signs. Therefore, cross-section axial force equilibrium is given as:

$$\int_0^{y_t} \sigma_t(y) t_w \, dy + \int_{y_t}^{h_w} \sigma_c(y) t_w \, dy = P \tag{3-35}$$

Substituting (3-32), (3-33) and (3-34) into (3-35), gives the following equation:

$$\int_0^{h_w-y_c} \left\{ \frac{\dfrac{1}{2}\left[\left(\dfrac{\sigma_{yi}}{f_y}\right)\cdot\left(1-\dfrac{y}{h_w}\right)+\left(\dfrac{\sigma_{yi+1}}{f_y}\right)\cdot\left(\dfrac{y}{h_w}\right)\right]}{+\dfrac{1}{2}\sqrt{4-3\left[\left(\dfrac{\sigma_{yi}}{f_y}\right)\cdot\left(1-\dfrac{y}{h_w}\right)+\left(\dfrac{\sigma_{yi+1}}{f_y}\right)\cdot\left(\dfrac{y}{h_w}\right)\right]^2-12\left(\dfrac{\tau_{xy}}{f_y}\right)^2}} \right\} t_w \, dy$$

$$+\int_{h_w-y_c}^{h_w} \left\{ \frac{\dfrac{1}{2}\left[\left(\dfrac{\sigma_{yi}}{f_y}\right)\cdot\left(1-\dfrac{y}{h_w}\right)+\left(\dfrac{\sigma_{yi+1}}{f_y}\right)\cdot\left(\dfrac{y}{h_w}\right)\right]}{-\dfrac{1}{2}\sqrt{4-3\left[\left(\dfrac{\sigma_{yi}}{f_y}\right)\cdot\left(1-\dfrac{y}{h_w}\right)+\left(\dfrac{\sigma_{yi+1}}{f_y}\right)\cdot\left(\dfrac{y}{h_w}\right)\right]^2-12\left(\dfrac{\tau_{xy}}{f_y}\right)^2}} \right\} t_w \, dy = P \tag{3-36}$$

The above equation includes the integral of $\int \sqrt{ax^2+bx+c}\, dx$, of which the solution is

$$\int \sqrt{ax^2+bx+c}\, dx = \frac{b+2ax}{4a}\sqrt{ax^2+bx+c} + \frac{4ac-b^2}{8a^{3/2}}\ln\left|2ax+b+2\sqrt{ax^2+bx+c}\right| + C \tag{3-37}$$

However solving for the closed-form solution of y_c from the resulting equation is not possible. One can use some software packages such as Mathcad to solve for y_c. Then, knowing y_c, the contribution of the web to the moment resistance can be determined as:

$$M_{pr-web} = \int_0^{h_w-y_c} \sigma_t(y)\left(\frac{h_w}{2}-y\right)t_w \, dy + \int_{h_w-y_c}^{h_w} \sigma_c(y)\left(\frac{h_w}{2}-y\right)t_w \, dy \tag{3-38}$$

For the contribution of the flanges, $M_{pr-flange}$, and cross-section plastic moment reduction factor, β, (3-24) and (3-25) still apply.

3.6.2 Derivation of Plastic Moment under Negative Flexure

Results can also be generated following the same procedure for the case of negative flexure, i.e. for flexural moment acting in a direction opposite to what was considered in the Section 3.6.1. The resulting stress diagrams are shown in figure 3-12 for a fully plastified HBE cross-section of elasto-perfectly plastic steel subjected to axial compression, shear, vertical stresses due to unequal top and bottom tension fields, and negative flexure.
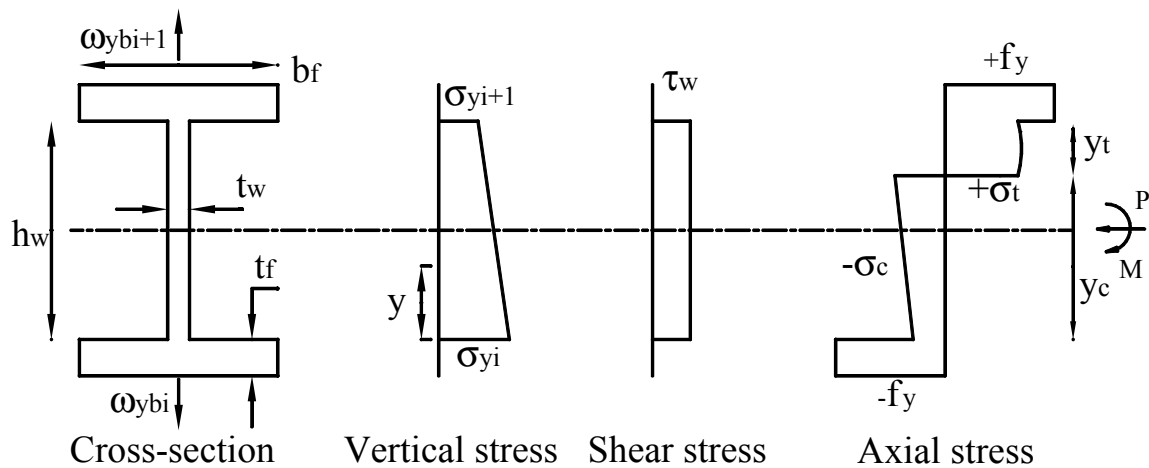
FIGURE 3-12 Stress Diagrams of Intermediate HBE Cross-Section under Negative Flexure, Axial Compression, Shear Force, and Vertical Stresses due to Unequal Top and Bottom Tension Fields

All the equations developed to locate the neutral axis in Section 3.6.1 remain valid except that the integral limits of (3-36) need to be modified as shown below according to the stress diagrams shown in figure 3-12.

$$
\int_{y_c}^{h_w} \left\{ \frac{\dfrac{1}{2}\left[\left(\dfrac{\sigma_{yi}}{f_y}\right)\cdot\left(1-\dfrac{y}{h_w}\right)+\left(\dfrac{\sigma_{yi+1}}{f_y}\right)\cdot\left(\dfrac{y}{h_w}\right)\right]}{+\dfrac{1}{2}\sqrt{4-3\left[\left(\dfrac{\sigma_{yi}}{f_y}\right)\cdot\left(1-\dfrac{y}{h_w}\right)+\left(\dfrac{\sigma_{yi+1}}{f_y}\right)\cdot\left(\dfrac{y}{h_w}\right)\right]^2-12\left(\dfrac{\tau_{xy}}{f_y}\right)^2}} \right\} t_w dy
$$

$$
+\int_{0}^{y_c} \left\{ \frac{\dfrac{1}{2}\left[\left(\dfrac{\sigma_{yi}}{f_y}\right)\cdot\left(1-\dfrac{y}{h_w}\right)+\left(\dfrac{\sigma_{yi+1}}{f_y}\right)\cdot\left(\dfrac{y}{h_w}\right)\right]}{-\dfrac{1}{2}\sqrt{4-3\left[\left(\dfrac{\sigma_{yi}}{f_y}\right)\cdot\left(1-\dfrac{y}{h_w}\right)+\left(\dfrac{\sigma_{yi+1}}{f_y}\right)\cdot\left(\dfrac{y}{h_w}\right)\right]^2-12\left(\dfrac{\tau_{xy}}{f_y}\right)^2}} \right\} t_w dy = P
$$

(3-39)

Solving for y_c from (3-39), one can obtain the contribution of the web to the cross-section plastic moment resistance as:

$$
M_{pr-web} = \int_{y_c}^{h_w} \sigma_t(y)\left(y-\frac{h_w}{2}\right)t_w dy + \int_{0}^{y_c} \sigma_c(y)\left(y-\frac{h_w}{2}\right)t_w dy \tag{3-40}
$$

For the contribution of the flanges to the moment resistance, $M_{pr-flange}$, and cross-section plastic moment reduction factor , β, (3-24) and (3-25) still apply.

3.6.3 FE Verification

To validate the approach developed in Sections 3.6.1 and 3.6.2 for the plastic moment resistance of intermediate HBE under axial compression, shear force and vertical stresses due to unequal top and bottom tension fields, a series of FE analyses were performed. The FE models for positive and negative flexure cases are shown in figures 3-13 and 3-14 respectively.
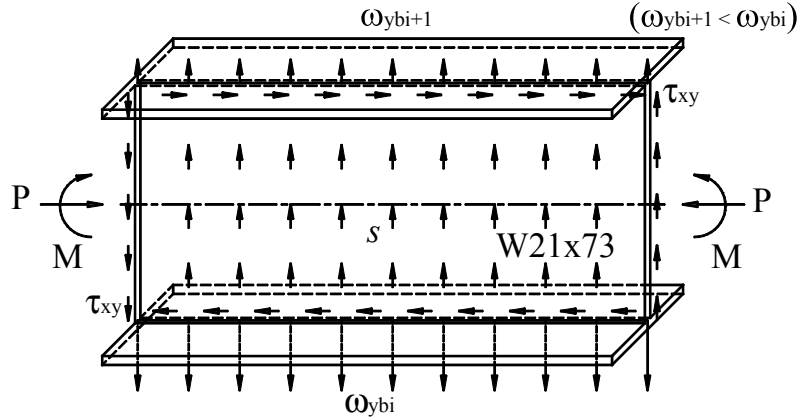
FIGURE 3-13 FE Model of Intermediate HBE under Positive Flexure, Axial Compression, Shear Force, and Vertical Stresses due to Unequal Top and Bottom Tension Fields
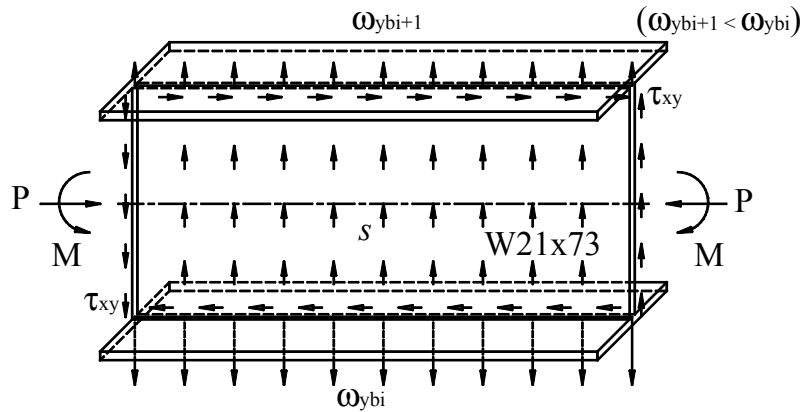
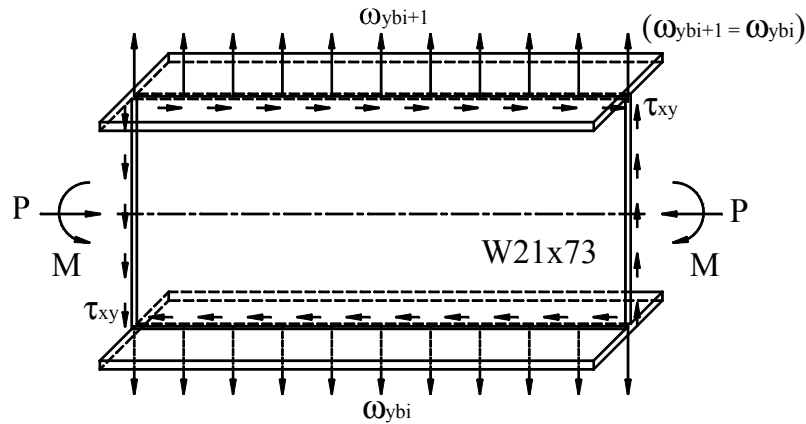**FIGURE 3-14 FE Model of Intermediate HBE under Negative Flexure, Axial Compression, Shear Force, and Vertical Stresses due to Unequal Top and Bottom Tension Fields**

The material, element, mesh, boundary condition, and loading condition are the same as those used in Section 3.5.2 except that a surface traction was applied on the HBE web to achieve the transition between the unbalanced infill panel forces and satisfy vertical force equilibrium, and opposite end rotations were applied in the negative flexure case. The surface traction can be calculated as:

$$S = \frac{\omega_{ybi} - \omega_{ybi+1}}{h_w} \tag{3-41}$$

42

Note that, in reality, no such traction force is applied on the HBE web, as the unbalanced infill panel forces are equilibrated similarly to a uniformly distributed load on a beam. However, in modeling only a small beam segment as done above, application of the traction keeps the segment in self-equilibrium and guarantee linear distribution of vertical stresses in the HBE web in accordance with the assumption used for the analytical procedure presented in Sections 3.6.1 and 3.6.2.

A series of analyses were conducted using the FE models described above to assess the accuracy of the analytical procedure, and the effectiveness of the proposed model. In these analyses, for the given axial compression and shear force, the vertical component of the bottom tension field was kept constant and various magnitudes of the vertical component of the top tension field were considered, from zero up to a value equal to that of the bottom tension field. This range of infill panel forces acting on the top tension field starts from an intermediate HBE section equivalent to an anchor HBE section in the absence of the top tension field, and ends with the previously considered case of an intermediate HBE section under equal top and bottom tension fields.

Comparisons between the results obtained from the FE analysis and those obtained by the procedure proposed in Sections 3.6.1 and 3.6.2 for the positive and negative flexure cases are shown in figures 3-15 and 3-16, respectively. It is shown that the plastic moment resistance of intermediate HBE can be accurately estimated using the proposed procedure. The cross-section plastic moment reduction factor varies from unity to the minimum determined by (3-26) as a result of the increasing shear force, axial force and vertical stresses.

Comparing the results shown in figures 3-15 and 3-16, it is also possible to observe that, for the same combination of axial compression, shear and vertical stresses, the positive plastic moment resistance is greater than the negative one. For example, according to case (a) shown in figure 3-15, the plastic moment reduction factor is 0.97 for an intermediate HBE under positive flexure for which $\tau_{xy}/f_y = 0.00$, $\beta_w = 0.00$, $\sigma_{yi}/f_y = 1.00$, and $\sigma_{yi+1}/f_y = 0.20$; however, a smaller value of 0.86 is obtained for plastic moment reduction factor in the negative flexure case in case (a) shown in figure 3-16

assuming the same loading combination. This can be explained on the basis that higher vertical stresses are acting at the bottom of the beam segment, which is also in axial compression in the negative flexure case. Recall from figure 3-6 that shows yielding under biaxial loading conditions, per the von Mises criterion, that the compression axial yield strength is more reduced by the presence of vertical stresses than the tension axial yield strength. Therefore, the plastic moment is reduced more in the negative flexure case than the positive flexure case.
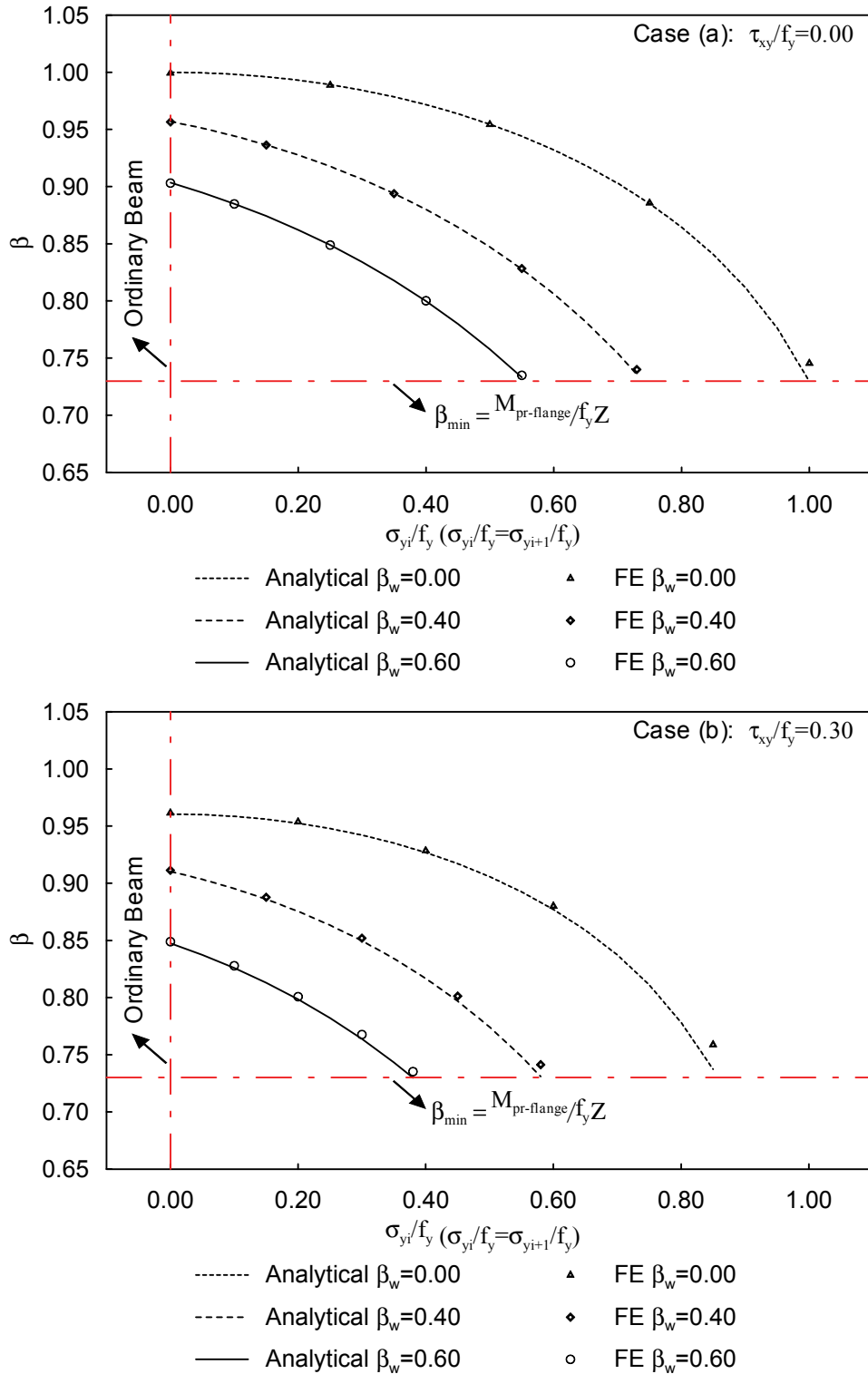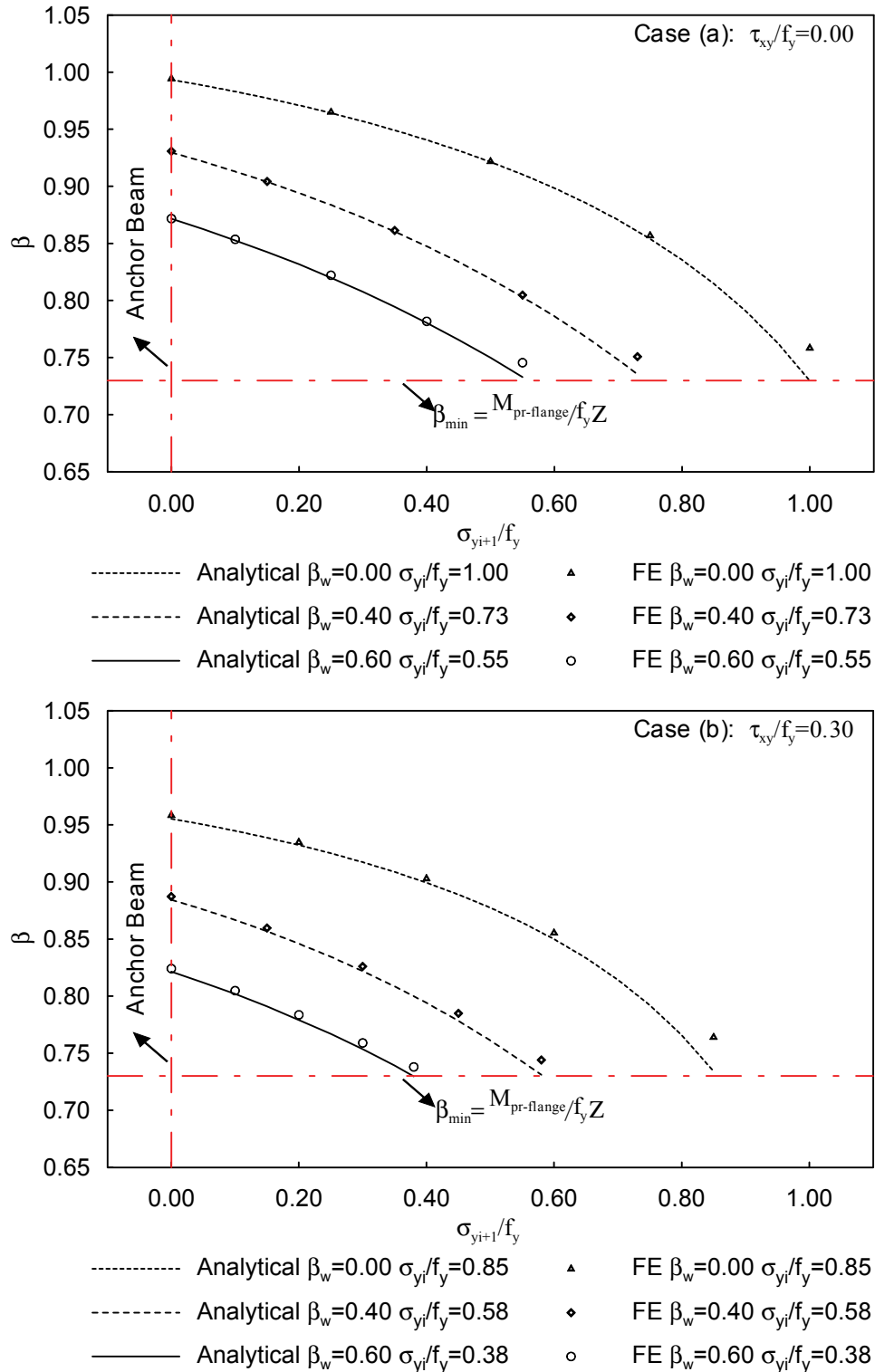
FIGURE 3-15 Plastic Moment Reduction Factor of Intermediate HBE Cross-Section under Positive Flexure, Axial Compression, Shear Force, and Linear Vertical Stresses: Analytical Predictions versus FE Results
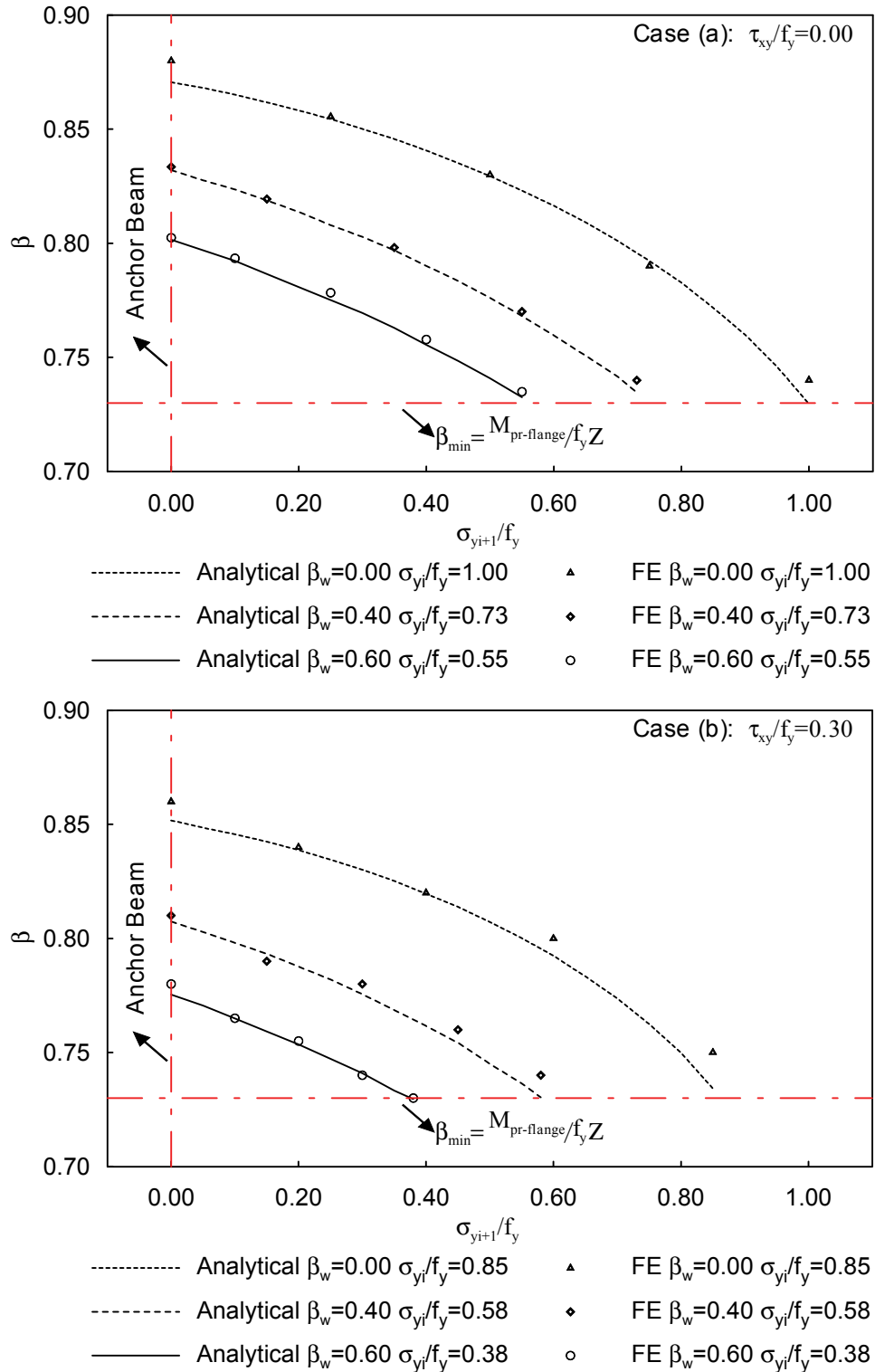
FIGURE 3-16 Plastic Moment Reduction Factor of Intermediate HBE Cross-Section under Negative Flexure, Axial Compression, Shear Force, and Linear Vertical Stress: Analytical Predictions versus FE Results

46

3.6.4 Simplification of Analytical Procedures

Though the analytical procedures to estimate the plastic moment resistance of intermediate HBE under unequal top and bottom tension fields were developed in Sections 3.6.1 and 3.6.2 and verified by the FE results in Section 3.6.3, impediments exists that may limit the wide acceptance of this approach in design. For example, there are challenges in solving for y_c from (3-36) and (3-39). The mathematic difficulty results from the presence of non-uniform vertical stresses.

Aiming at the kind of simple equations derived to calculate plastic moment of the intermediate HBE under equal top and bottom tension fields, for which a constant vertical stress is assumed, it would be expedient to replace the linearly varying vertical stresses in the case at hand by an equivalent constant vertical stress. However, it would not be appropriate to use a constant vertical stress of magnitude equal to the average stress of the linearly varying vertical stresses as an approximation, because such a unique approximate constant vertical stress would result in identical positive and negative cross-section plastic moments. This is inconsistent with the prior observations on plastic moment resistances of intermediate HBEs under positive and negative flexures as shown in figures 3-15 and 3-16, respectively.

As a compromise between simplicity and accuracy, to consider the different effects of vertical stresses on positive and negative cross-section plastic moments, the magnitudes of those stresses at the three-fourth and one-fourth points of the linearly varying stress diagram, as shown in figure 3-17 (i.e. mean of the average and the minimum, and mean of the average and the maximum, respectively), are taken as the magnitudes of the approximate constant vertical stresses for the positive and negative flexure cases, respectively. Mathematically, the magnitudes of these equivalent constant vertical stress distributions can be expressed as:

$$\sigma_{y-un} = \frac{1}{2}\left(\sigma_{yi} + \sigma_{yi+1}\right) \pm \frac{1}{4}\left(\sigma_{yi} - \sigma_{yi+1}\right) \qquad (3\text{-}42)$$

"-" and "+" are employed in (3-42) for positive and negative flexure cases respectively. Then, the procedures to determine the plastic moment of intermediate HBE under equal top and bottom tension fields (as presented in Section 3.5.1) can be used.
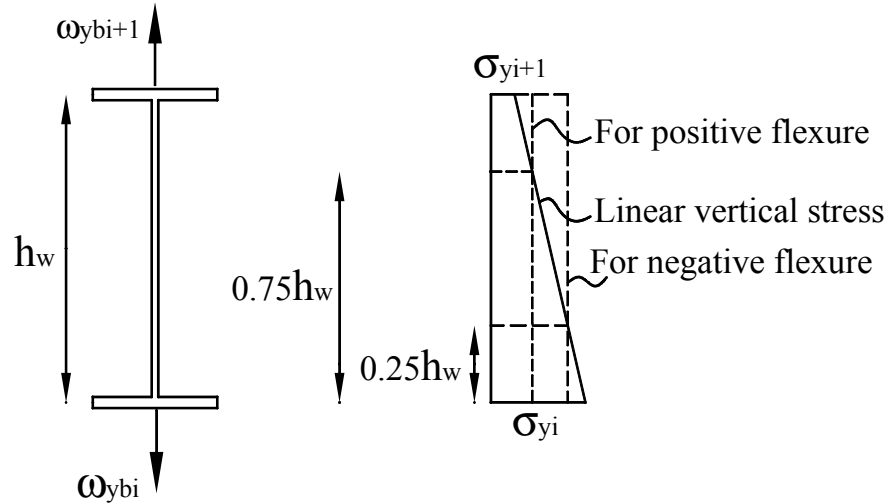
FIGURE 3-17 Simplification of Vertical Stress Distribution

To check the adequacy of this model, the results obtained using the above simplified procedure are compared with those using the more rigorous approach developed earlier (Sections 3.6.1 and 3.6.2 for positive and negative flexure cases respectively) in figures 3-18 and 3-19, respectively. It is found that the simplified procedure provides reasonable and relatively efficient estimates for the cross-section plastic moment reduction factor, although slightly less accurate results are observed in the negative flexure case.
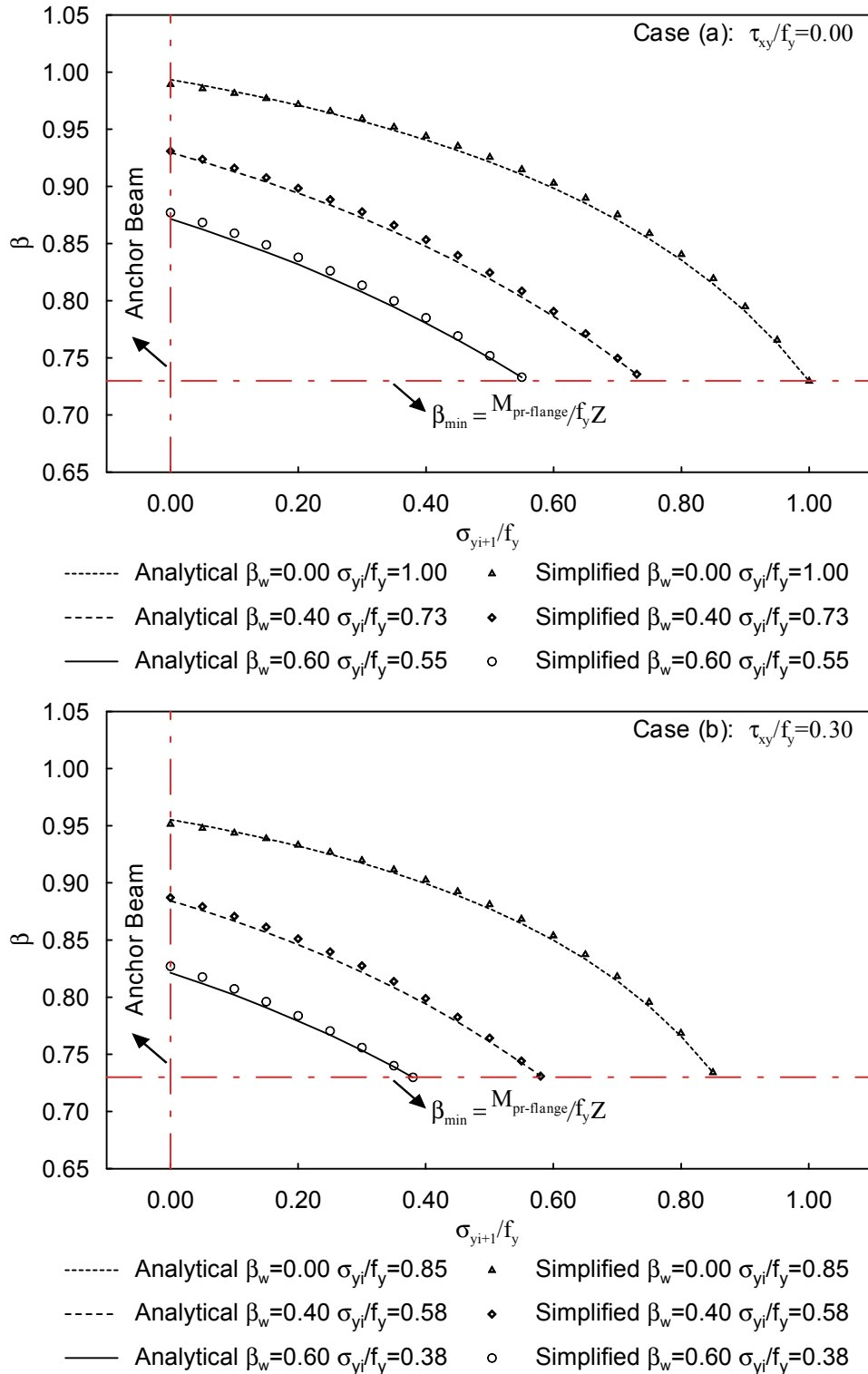
FIGURE 3-18 Plastic Moment Reduction Factor of Intermediate HBE Cross-Section under Positive Flexure, Axial Compression, Shear Force, and Linear Vertical Stresses: Analytical Predictions versus Simplified Approach
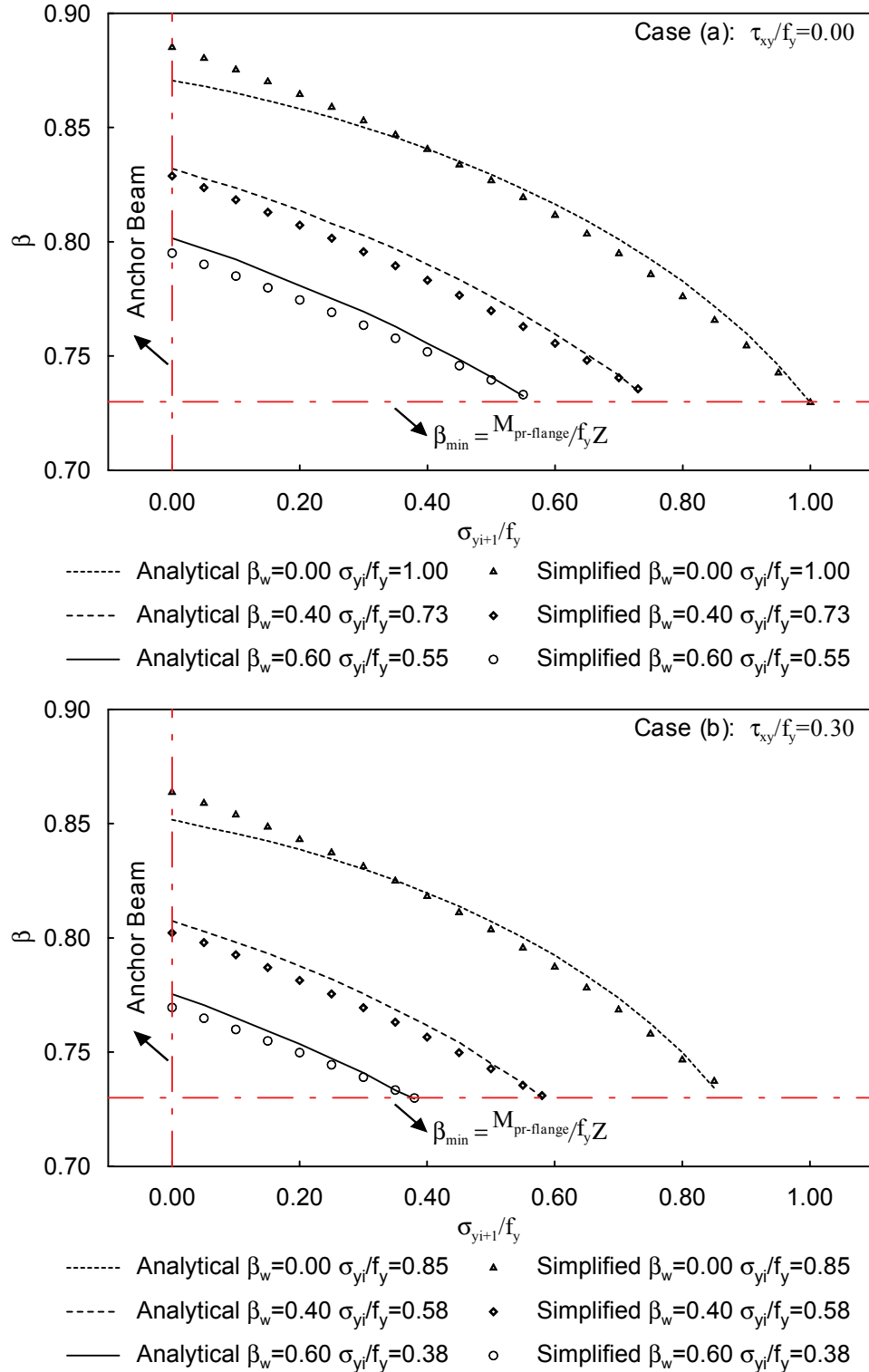
FIGURE 3-19 Plastic Moment Reduction Factor of Intermediate HBE Cross-Section under Negative Flexure, Axial Compression, Shear Force, and Linear Vertical Stresses: Analytical Predictions versus Simplified Approach

3.7 Additional Discussions on Anchor HBEs

The procedure developed in Section 3.6 to calculate plastic moment of intermediate HBE can also be applied for anchor HBE, since an anchor HBE is only a special case of an intermediate HBE for which the tension field is only applied on one side. However, anchor HBEs deserve further treatment here since the analytical, FE, and simplified results shown in figures 3-15, 3-16, 3-18 and 3-19 respectively, only provide results for anchor HBE in limited scenarios (i.e. only loading scenarios corresponding to the left ends of those curves shown in figures 3-15, 3-16, 3-18 and 3-19). Additional examples are provided in this section to further confirm that the procedures proposed in Section 3.6 for estimating the plastic moment of intermediate HBEs remain valid for anchor HBEs.

For anchor HBEs, the vertical stress distribution can be expressed as:

$$\frac{\sigma_y(y)}{f_y} = \left(\frac{\sigma_{yi}}{f_y}\right) \cdot \left(1 - \frac{y}{h_w}\right) \tag{3-43}$$

which is obtained by setting $\sigma_{yi+1} = 0$ in (3-27).

Accordingly, the analytical procedures presented in Sections 3.6.1 and 3.6.2, and simplified approach presented in Section 3.6.4 still apply by setting σ_{yi+1} equal to zero in all equations.

A series of analyses were conducted using the same FE models described earlier (as shown in figures 3-13 and 3-14) to investigate the plastic moment of anchor HBEs. For the given shear and axial compression, ω_{ybi+1} shown in figures 3-13 and 3-14 was set equal to zero, and ω_{ybi} was varied from zero up to the maximum allowable value that can be applied in the web of the anchor HBE. Note that the anchor HBE becomes an ordinary beam in the absence of the infill panel forces (i.e. $\omega_{ybi} = 0$). The results using the analytical procedures proposed in Sections 3.6.1 and 3.6.2 are compared with those from FE analyses in figures 3-20 and 3-21 for the positive and negative flexure cases, respectively. The analytical procedure is shown to accurately predict the plastic moment

reduction factor for anchor HBEs. Also, for the same reason as described in detail in Section 3.6.3 for intermediate HBEs, the anchor HBE plastic moment reduces more when the beam segment is subjected to negative flexure than the positive flexure case as shown in figures 3-20 and 3-21.

In one significant departure from the trends shown in figures 3-15 and 3-16, the anchor HBE plastic moment reduction factor, β, does not reduce to β_{min} even when the maximum allowable tension field is applied. For example, according to case (a) shown in figure 3-15, the intermediate HBE plastic moment reduction factor reduces to a β_{min} of 0.73 when $\tau_{xy}/f_y = 0.00$ and $\beta_w = 0.40$. This value of β_{min} is reached for any value of σ_{yi}/f_y. However, the lowest value of β reached for the corresponding case (a) in figure 3-20 is 0.83 (greater than the β_{min} of 0.73). It is obtained when the tension field force increases to the maximum allowable value (i.e. $\sigma_{yi}/f_y = 1.00$), assuming the same shear and axial compression. This is because, for the intermediate HBE examples shown in figures 3-15 and 3-16, the factor β reduce to β_{min} only when the magnitude of the top tension field becomes equal to that of the bottom tension field, resulting in constant vertical stresses in the intermediate HBE web. Here, in the absence of infill panel forces on one side of the anchor HBE, β can not reduce to β_{min} even when the maximum permitted tension field is applied on the other side.

Results obtained using the simplified approach described in Section 3.6.4 are also compared with those obtained from the analytical procedure described in Sections 3.6.1 and 3.6.2 for the positive and negative flexure cases in figures 3-22 and 3-23, respectively. Reasonable agreements are observed through the comparisons.
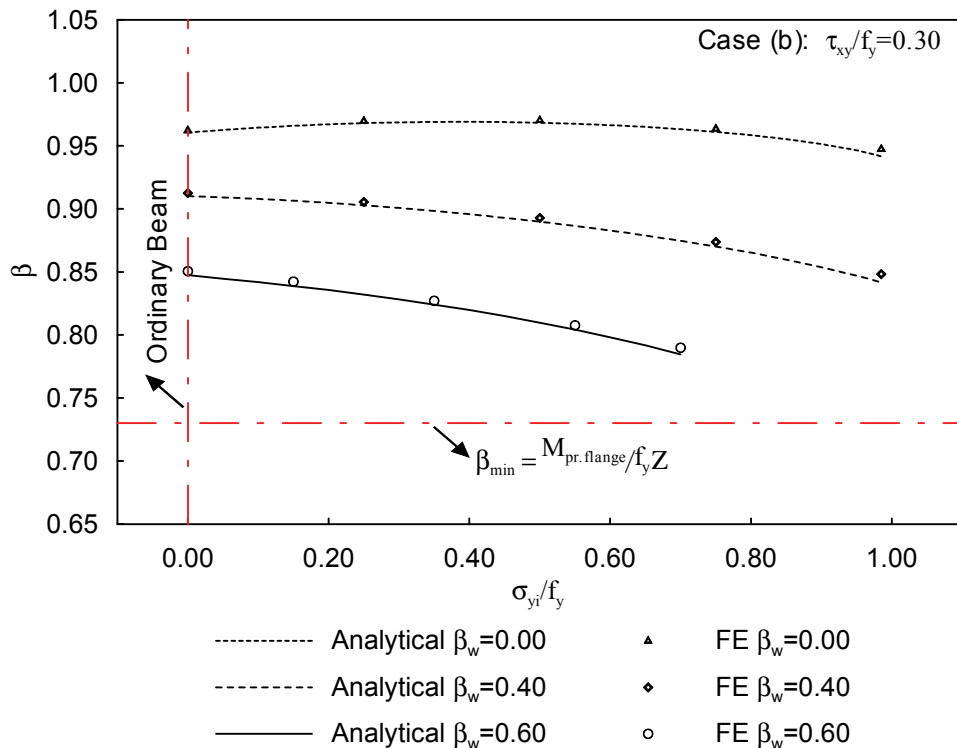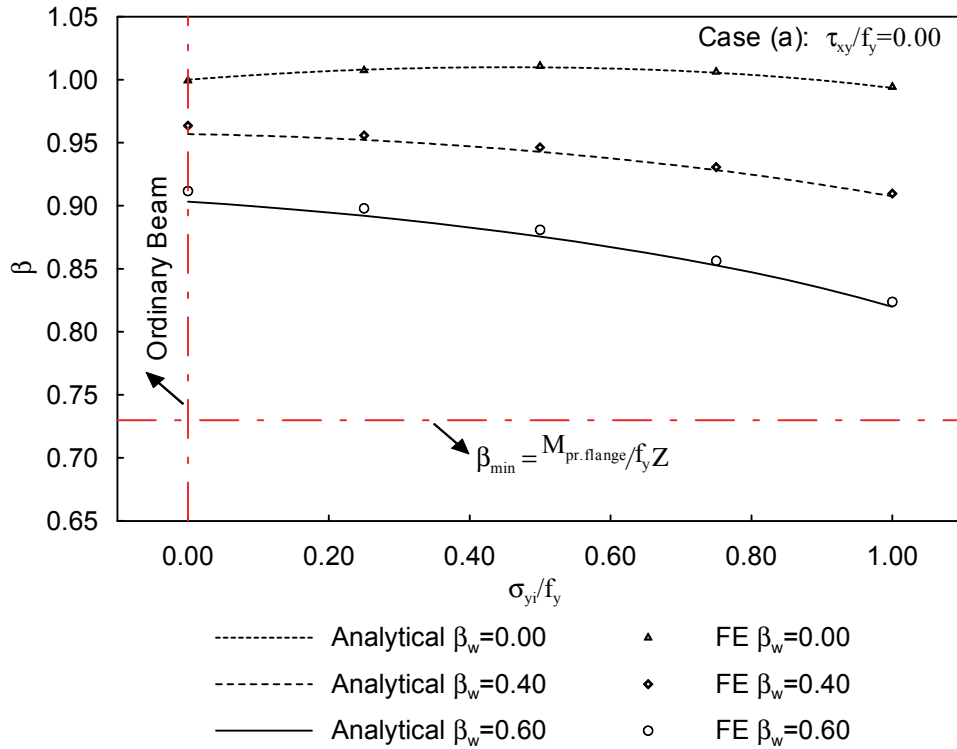
FIGURE 3-20 Plastic Moment Reduction Factor of Anchor HBE Cross-Section under Positive Flexure, Axial Compression, Shear Force, and Linear Vertical Stresses: Analytical Predictions versus FE Results

53
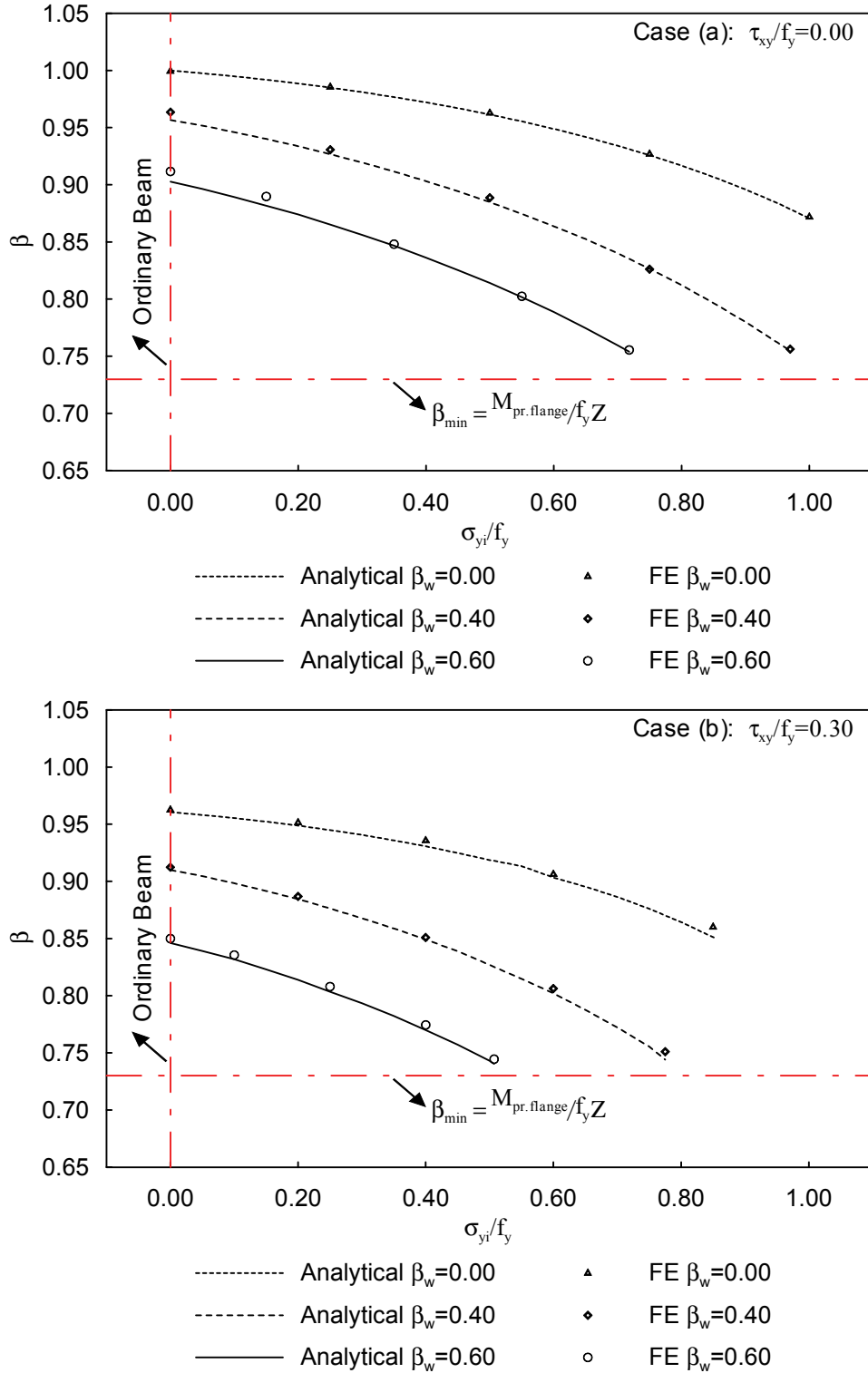
FIGURE 3-21 Plastic Moment Reduction Factor of Anchor HBE Cross-Section under Negative Flexure, Axial Compression, Shear Force, and Linear Vertical Stresses: Analytical Predictions versus FE Results
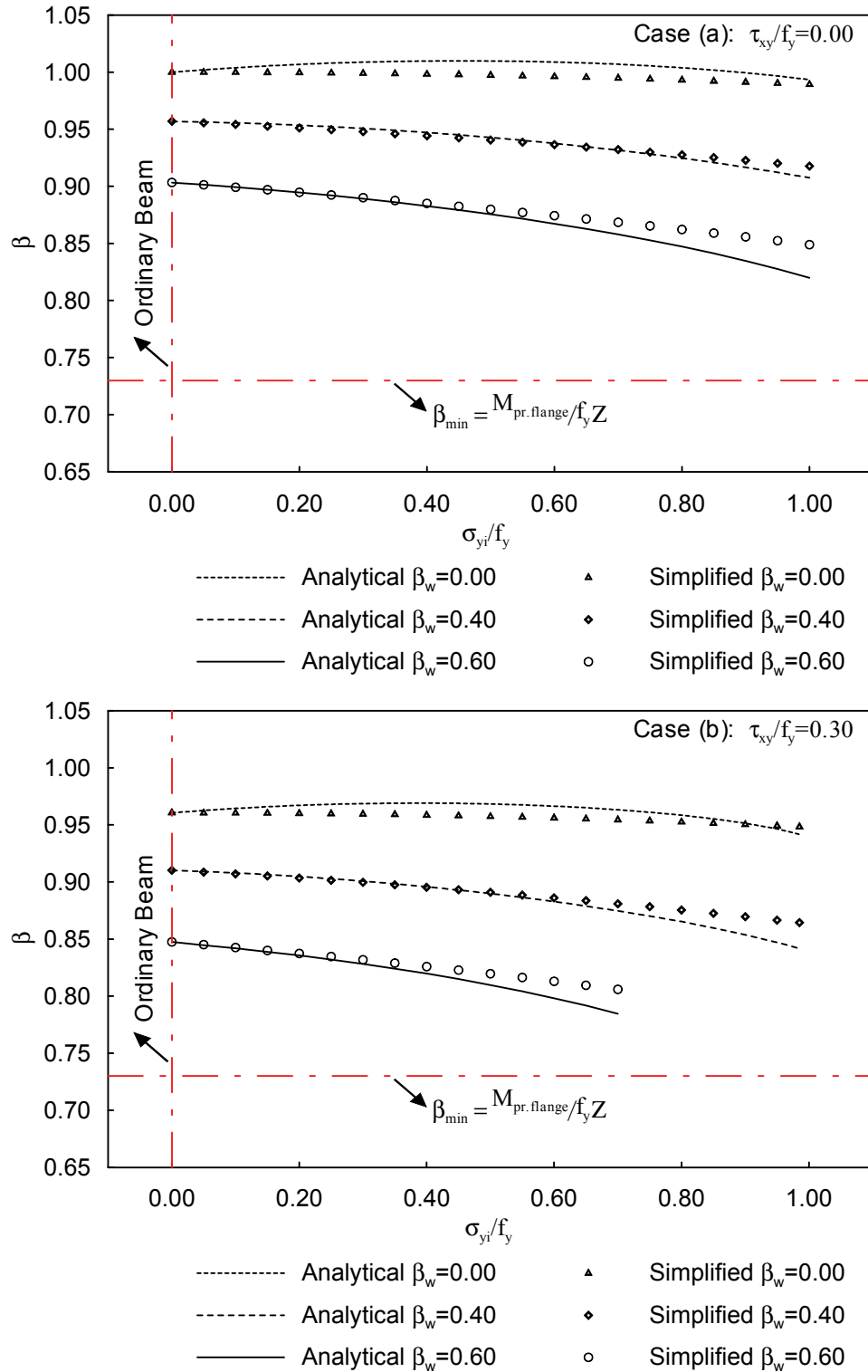
FIGURE 3-22 Plastic Moment Reduction Factor of Anchor HBE Cross-Section under Positive Flexure, Axial Compression, Shear Force, and Linear Vertical Stresses: Analytical Predictions versus Simplified Approach

55
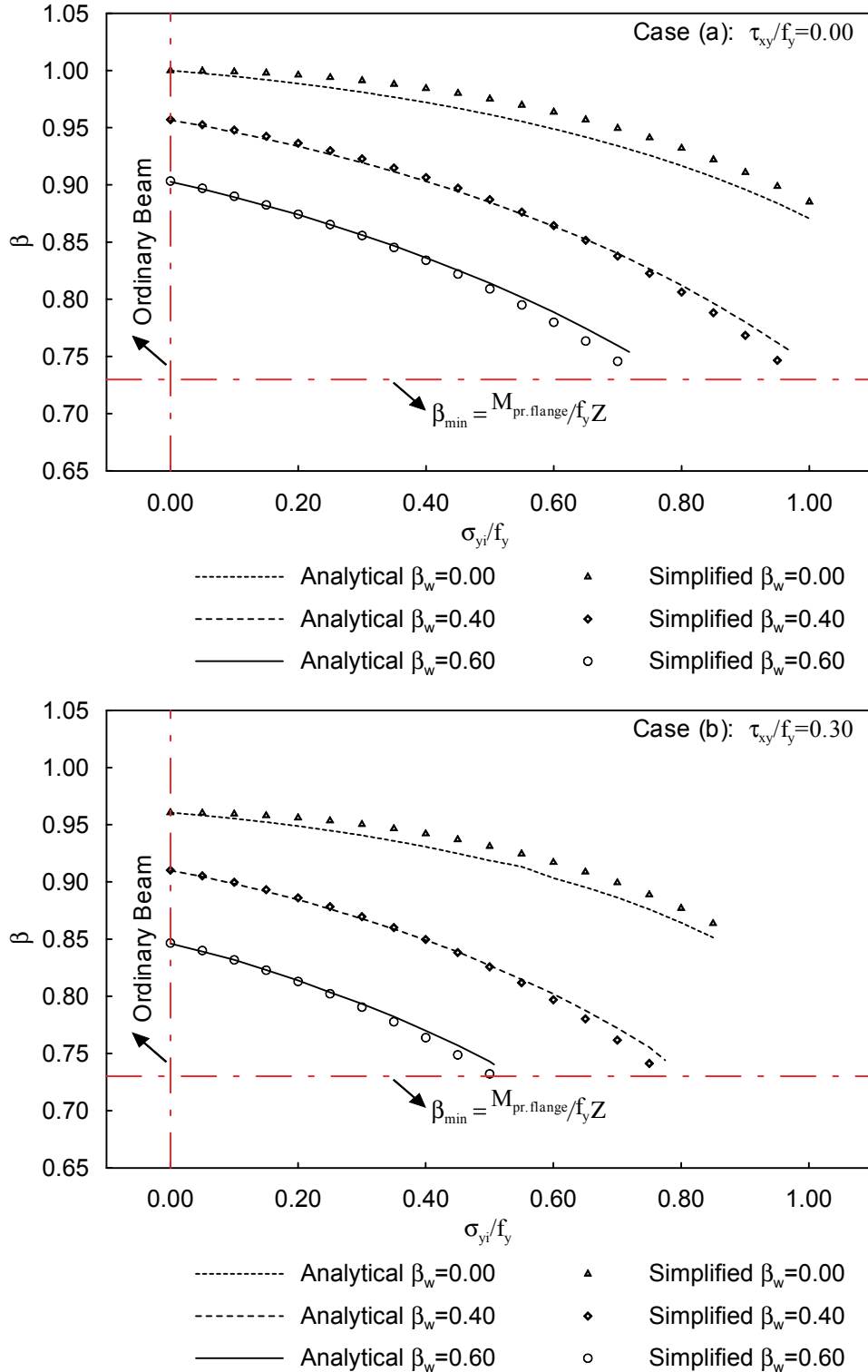
FIGURE 3-23 Plastic Moment Reduction Factor of Anchor HBE Cross-Section under Negative Flexure, Axial Compression, Shear Force, and Linear Vertical Stresses: Analytical Predictions versus Simplified Approach

3.8 Summary

Analytical procedures for estimating the plastic moments of HBEs in SPSWs have been proposed in this section. Those procedures are based on classic plastic analysis and rely on calculation of the reduced axial yield strength of the HBE web accounting for the presence of shear and vertical stresses due to infill panel forces. Results from these procedures were shown to agree well with the results from FE analysis. Simplified models developed for practical purposes were shown to be accurate

.

SECTION 4

CAPACITY DESIGN OF HORIZONTAL BOUNDARY ELEMENTS

4.1 Introduction

Design procedures for SPSWs (CSA 2000 and AISC 2005), per capacity design principles, require that the HBEs of SPSWs be designed to resist the maximum forces developed by infill panel yielding. With the exception of plastic hinges at its ends, an HBE are expected to remain essentially elastic when the SPSW develops the expected plastic mechanism.

As mentioned previously, work presented in Section 3 shows the importance of using proper procedure to calculate the HBE plastic moment. However, as demonstrated in the tests on a full-scale two-story SPSW specimen by Qu *et al*. (2008), current design approaches do not necessarily lead to intermediate HBEs that meet the requirements of ductile behavior under the forces generated by the fully yielded infill panels and the SPSW sway. This was notably observed by the unexpected failures at the ends of the intermediate HBE of the MCEER/NCREE specimen (Qu *et al*. 2008).

Simple models using line elements for boundary frame members (e.g. models conventionally used in SAP2000) are not capable of producing satisfactory results of design forces for intermediate HBEs due to the intrinsic complexity in modeling the strength of HBE plastic hinges, and consequently fail to explain the observed failure in the intermediate HBE of the MCEER/NCREE specimen (Qu *et al*. 2008). Nonlinear FE analysis using 3D shell elements can be used to provide more accurate estimates of design forces for intermediate HBEs, but is too tedious for broad use for this simple design purpose. Therefore, there is a need to develop a reasonably accurate and more efficient method to estimate the design loads for HBEs when the SPSW develops the expected plastic mechanism.

Such an approach is developed and proposed below. Based on the expected plastic mechanism and infill panel yield forces, which are first reviewed in this section, the axial

and shear forces used for sizing intermediate HBEs are determined using free body diagrams with close attention paid to local effects at the ends of intermediate HBEs. Ways to avoid in-span plastic hinges in intermediate HBEs are addressed followed by a simple free body diagram to determine the moment demands at VBE faces. Then those procedures are verified by the nonlinear FE analysis results and a design approach is proposed for capacity design of intermediate HBEs. Finally, the intermediate HBE of the tested SPSW specimen is examined using the proposed models to explain the unexpected failure observed.

4.2 Expected Mechanism of SPSW and Infill Panel Yield Force

Plastic mechanisms of a multistory SPSW subject to lateral loads have been studied by Berman and Bruneau (2003) and the corresponding procedures for estimating SPSW plastic strength have been validated by a series of experimental results. Based on their study, the expected plastic mechanism for a ductile multistory SPSW of the type considered here is taken to be the one that develops when the infill fully yields at all levels as shown in figure 4-1.
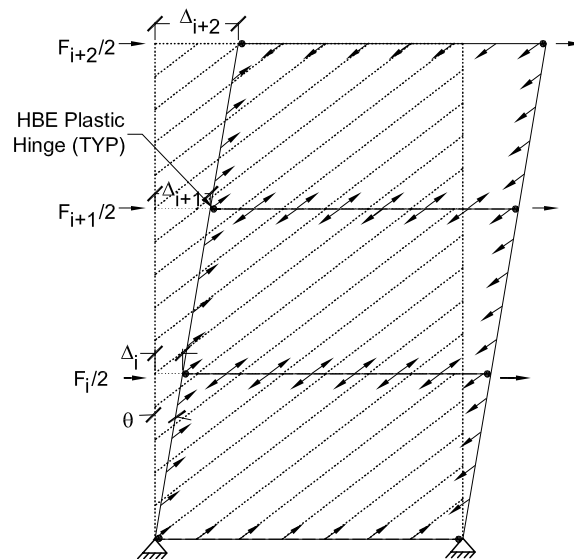
FIGURE 4-1 Uniform Yielding Mechanism of a Multistory SPSW
(adapted from Berman and Bruneau 2003)

60

Assuming a multistory SPSW designed according to the 2005 AISC Seismic Provisions and that satisfactorily develops the above plastic mechanism under seismic forces, the distributed loads to be applied along the VBEs (ω_{xci} and ω_{yci}) and HBEs (ω_{xbi} and ω_{ybi}) from infill panel yielding at the ith story can be determined as:

$$\omega_{yci} = R_{yp}f_{yp}t_{wi}\sin 2\alpha/2 \tag{4-1}$$

$$\omega_{xci} = R_{yp}f_{yp}t_{wi}\left(\sin\alpha\right)^2 \tag{4-2}$$

$$\omega_{ybi} = R_{yp}f_{yp}t_{wi}\left(\cos\alpha\right)^2 \tag{4-3}$$

$$\omega_{xbi} = R_{yp}f_{yp}t_{wi}\sin 2\alpha/2 \tag{4-4}$$

These are obtained by resolving the infill panel yield forces, occurring at an angle α from the vertical, into horizontal and vertical components acting along the VBEs and HBEs. Such components of yield forces per unit lengths are a function of infill panel thickness, t_{wi}, yield strength of infill panels f_{yp}, and the ratio of expected to nominal yield stress R_{yp} (Berman and Bruneau, 2008).

4.3 Axial Force in Intermediate HBE

To understand the nature of the axial effects in intermediate HBEs, consider the single-bay multistory SPSW with rigid HBE-to-VBE and VBE-to-foundation connections shown in figure 4-2a. This SPSW (labeled frame A) can be decomposed into two lateral force resisting systems for analysis purpose, as shown in figures 4-2b and 4-2c, namely: (i) frame B consisting of infill panels, which resists the lateral loads (i.e. F_{Si} and F_{Si+1}) entirely through infill tension field actions together with a boundary frame without moment resisting connections; and (ii) frame C as a frame without infill panels, which resists lateral loads (i.e. F_{Mi} and F_{Mi+1}) only through moment frame actions up to the development of plastic moments at the HBE-to-VBE and VBE-to-foundation connections. Note that the HBE end fixities and the VBE fixities at the base are removed in frame B, since the contribution to lateral force resistance due to those fixities is taken into account in frame C. The summation of lateral force resistances of the above two systems is equal to the overall lateral strength of the SPSW, which is necessary to develop the desired plastic collapse mechanism.

The tension field forces applied on frame B can be further broken into three components for analysis purpose, namely: (i) horizontal components of infill tension fields applied on VBEs, as shown in figure 4-2d; (ii) vertical components of infill tension fields applied on HBEs, as shown in figure 4-2e; and (iii) horizontal and vertical components applied on HBEs and VBEs respectively, as shown in figure 4-2f. Note that frames D and E shown in figures 4-2 are in self-equilibrium and the lateral force resisted by frame B is applied on frame F.

According to figure 4-2, using the principle of superstition, the resulting axial force in the intermediate HBE of frame A can be obtained by adding up the axial effects in the intermediate HBEs of frames C, D, E and F, which are presented in the following parts of this section. Note that compatibility of deformations is not enforced by this procedure, but this simplifying assumption has been found to have negligible impacts on the results.
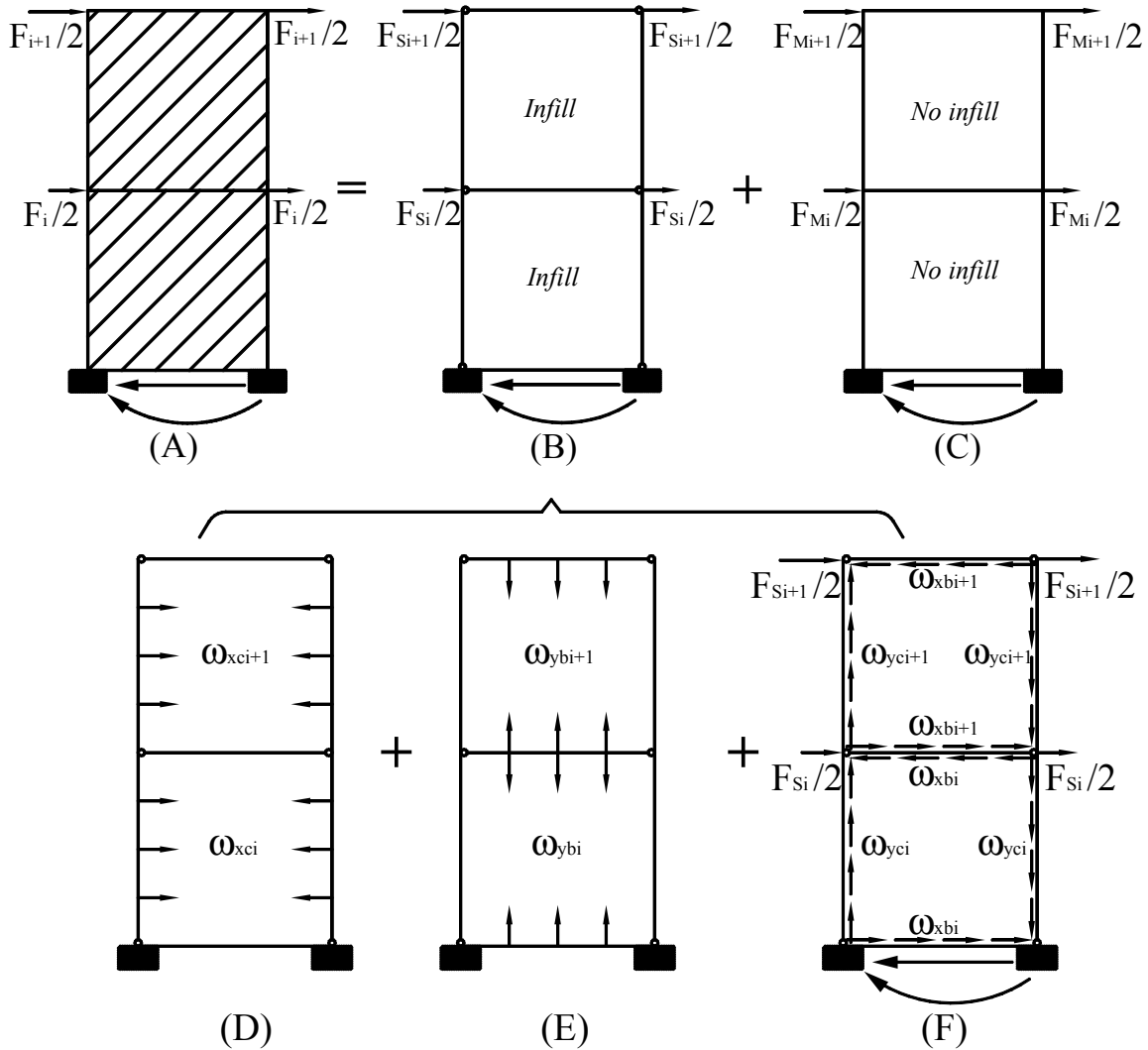
FIGURE 4-2 Decomposition of SPSW Free Body Diagrams: (a) Typical SPSW; (b) Boundary Frame with Infill Panels; (c) Boundary Frame without Infill Panels; (d) Boundary Frame with Horizontal Components of Infill Panel Yield Forces on VBEs; (e) Boundary Frame with Vertical Components of Infill Panel Yield Forces on HBEs; (f) Boundary Frame with Horizontal and Vertical Components of Infill Panel Yield Forces on HBEs and VBEs Respectively.

4.3.1 Axial Effects Due to Boundary Moment Frame Sway

The behavior of frame C shown in figure 4-2 is similar to that of a typical steel moment frame. All HBEs are connected to the VBEs with moment resisting connections able to develop plastic moments when the expected mechanism develops. For the case shown in figure 4-2c, where equal equivalent seismic lateral loads are applied on both sides of the frame, no axial forces develop in the HBEs.

63

4.3.2 Axial Effects of Horizontal Tension Field Components on VBEs

To estimate the axial force caused by horizontal components of infill panel yield forces on VBE as shown in figure 4-2d, Berman and Bruneau (2008) proposed a simple analytical model consisting of a continuous beam element representing the VBE supported by elastic springs at the HBE locations. Based on this model, the spring force, P_{Ci}, corresponding to compression axial force in HBE , which is typically of significant magnitude, can be estimated from the horizontal components of the tension fields on the VBEs considering VBE lengths tributary to each HBE, i.e.:

$$P_{Ci} = \omega_{xci}\left(\frac{h_{si}}{2} - \frac{d_i}{2}\right) + \omega_{xci+1}\left(\frac{h_{si+1}}{2} - \frac{d_i}{2}\right) \tag{4-5}$$

where h_{si} is the ith story height; d_i is the depth of the HBE considered.

4.3.3 Axial Effects of Vertical Tension Field Components on HBE

Another (and often neglected) potential source of axial force in HBE is due to deformation compatibility of the HBE web. Axial restraint of an HBE, if present, can lead to axial forces in that HBE when its web is subjected to the vertical components of infill panel yield forces, as shown in figure 4-2e. To illustrate this, consider an element located within the web of an intermediate HBE, as shown in figure 4-3.
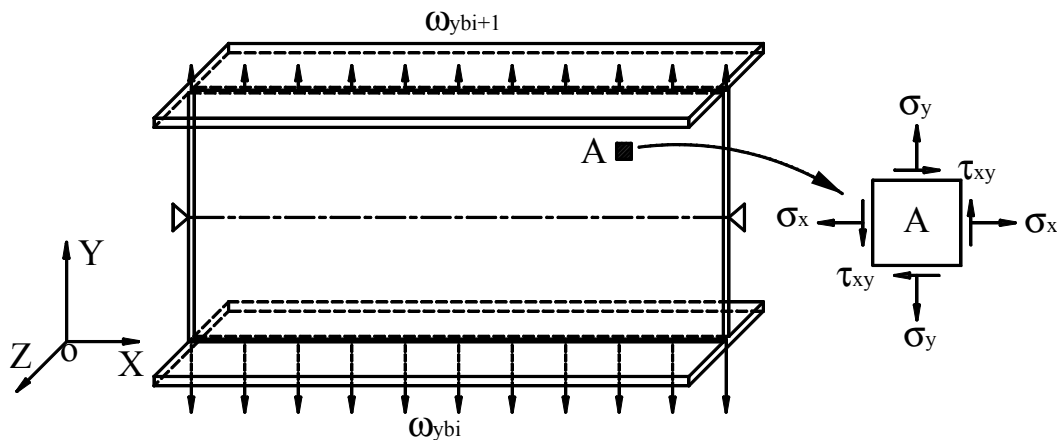
FIGURE 4-3 Intermediate HBE under Vertical Components of Infill Panel Yield Forces

Note that the web of the HBE is in plane-stress condition. The axial strain, $\varepsilon_x(y)$, of the considered element can be obtained according to Hook's law:

$$\varepsilon_x(y) = \frac{\sigma_x(y) - v\sigma_y(y)}{E} \qquad (4\text{-}6)$$

where v is Poisson's ratio and E is Young's modulus. Stresses $\sigma_x(y)$ and $\sigma_y(y)$ are in-plane stress components in the coordinate system shown in figure 4-3.

For an HBE with ideally rigid axial restraints, the web of that HBE is unable to elongate along the member's longitudinal axis, which is mathematically expressed as:

$$\varepsilon_x(y) = 0 \qquad (4\text{-}7)$$

Substituting (4-7) into (4-6), one can obtain the relationship between vertical and axial stresses:

$$\sigma_x(y) = v\sigma_y(y) \qquad (4\text{-}8)$$

The axial tension due to this Poisson's effect can be obtained by integrating the axial stress along depth of the HBE web:

$$P_{Di} = \int_0^{h_w} \sigma_x(y) t_w dy \qquad (4\text{-}9)$$

where t_w and h_w are thickness and depth of the HBE web, respectively.

Assuming a linear distribution of vertical stresses from the bottom to the top of the HBE web as used in Section 3, such that:

$$\sigma_y(y) = \frac{\omega_{ybi}}{t_w}\left(1 - \frac{y}{h_w}\right) + \frac{\omega_{ybi+1}}{t_w}\left(\frac{y}{h_w}\right) \qquad (4\text{-}10)$$

and substituting (4-10) into (4-9) and integrating, the axial tension in the axially restrained HBE is obtained as:

$$P_{Di} = \frac{\nu\left(\omega_{ybi} + \omega_{ybi+1}\right)}{2} h_w \qquad (4\text{-}11)$$

Although the potential for the above axial force theoretically exists, the magnitude of the contribution of this axial effect to the total axial force in HBEs typically would be on the order of 5% if the VBEs were able to fully restrain the HBEs against axial deformation. Results reported in the literature have not commented on this effect at the time of this writing, and it is difficult to identify whether this effect has been occurring in prior tests since it is only a small contribution. Furthermore, whether or not the HBEs can effectively be restrained axially varies from wall to wall, depending on the fixity at the ends of the HBE and the relative stiffness of HBEs and VBEs along the height of the SPSW. It would be interesting in future research to monitor to what extent this effect contributes to structural behavior. However, the FE models presented in Section 4.7 include this effect. For consistency, wherever the boundary conditions used in finite element studies prevent axial elongation, this effect has to be taken into account to assess the accuracy of proposed simplified approach against such finite element benchmark results as done later in this section.

4.3.4 Axial Effects of Horizontal Tension Field Components on HBE

As shown in figure 4-2f, for lateral loads equally applied on both sides of the frame, the axial force resulting from the horizontal components of the infill panel yield forces acting along the HBE varies as shown in figure 4-4.
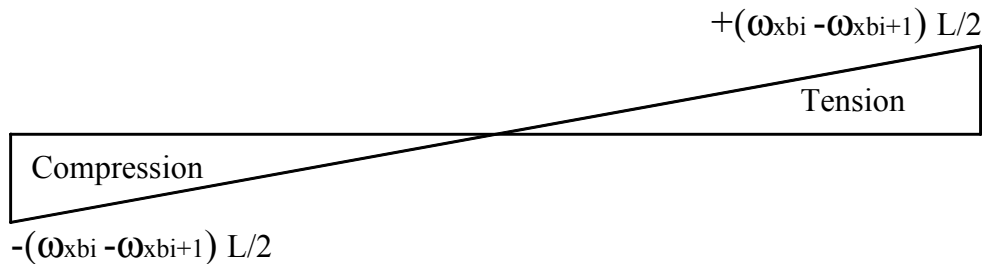
FIGURE 4-4 Assumed HBE Axial Force Distribution Due to Horizontal Components of Infill Panel Yield Forces on HBE

For some regular SPSWs, this assumption is proper. However, for more general applications, the axial force distribution in HBE depends on the distribution of the equivalent earthquake loads applied at floor levels. To better understand this, consider the two SPSWs shown in figure 4-5. These two structures have identical mass distributions and column layout, but the steel plate shear walls are implemented at two different locations. The free body diagram of the intermediate HBE is also provided in figure 4-5 assuming that the two SPSWs with simple HBE-to-VBE and VBE-to-ground connections are subjected to rightward sway.

Plan view (SPSW-A)   Plan view (SPSW-B)

Elevation view (SPSW-A)   Elevation view (SPSW-B)

Free body diagram of intermediate HBE
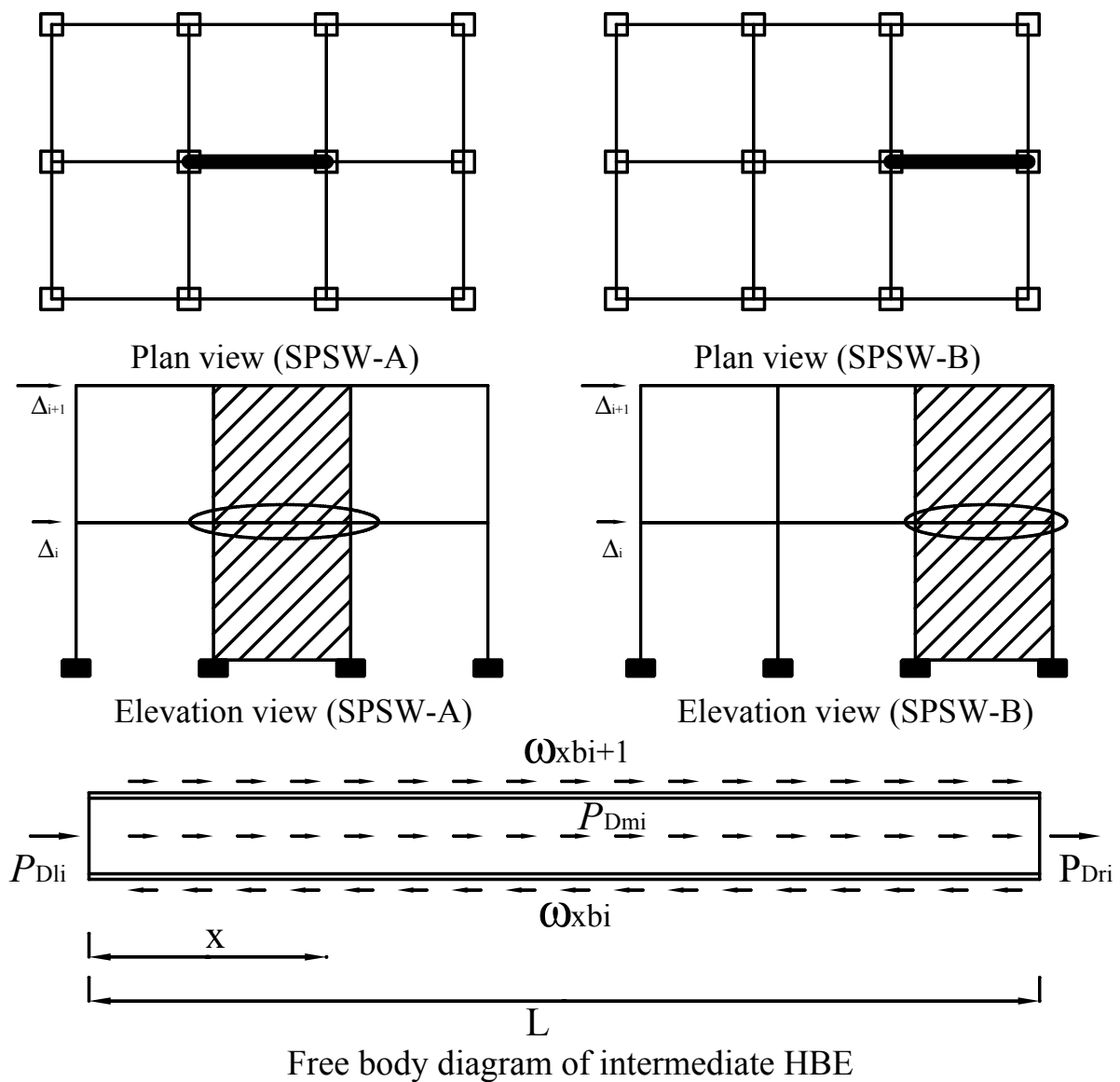
FIGURE 4-5 Structures with SPSW Implemented at Different Locations

The HBE axial force equilibrium gives:

$$P_{Dli} + P_{Dmi} + P_{Dri} = \left(\omega_{xbi} - \omega_{xbi+1} \right) \cdot L \tag{4-12}$$

where P_{Dli} and P_{Dri} are the equivalent earthquake loads applied at the left and right ends of the intermediate HBE, respectively; and P_{Dmi} is the resultant force from a uniform earthquake force applied along the intermediate HBE, if any are acting there (loads transferred by the concrete slab for example). Accounting for those forces, earthquake load application factors can be defined as:

$$\gamma_{li} = \frac{P_{Dli}}{\left(\omega_{xbi} - \omega_{xbi+1} \right) \cdot L} \tag{4-13}$$

$$\gamma_{mi} = \frac{P_{Dmi}}{\left(\omega_{xbi} - \omega_{xbi+1} \right) \cdot L} \tag{4-14}$$

$$\gamma_{ri} = 1 - \gamma_{li} - \gamma_{mi} \tag{4-15}$$

where γ_{li}, γ_{ri} and γ_{mi} are the percentages of the seismic loads at the ith floor applied at the left and right sides, and within the bay of the wall respectively. For example, for SPSW-B shown in figure 4-5, γ_{li} and γ_{ri} are 100% and 0% respectively, assuming no loads are transferred within the bay of the wall.

Referring again to the example buildings in figure 4-5, the earthquake loads, (which are essentially inertia forces depending on structure configuration and mass distribution), are different in SPSW-A and SPSW-B: no inertia force develops on the right side of infill panels in SPSW-B, unlike SPSW-A in which identical inertia forces develop on both sides of the frame. Thus, for the given earthquake loads, the axial force at location x along an HBE can be determined as

$$P_{Di}(x) = \left[-\gamma_{li} - \gamma_{mi} \frac{x}{L} + \frac{x}{L} \right] \left(\omega_{xbi} - \omega_{xbi+1} \right) \cdot L \tag{4-16}$$

Figure 4-6 shows the distributions of the axial force normalized by the magnitude of the resulting force of the horizontal components of infill panel yield forces along the HBE, for different earthquake load application factors. The assumed axial force distribution shown in figure 4-4 corresponds to the typical case that $\gamma_{li} = \gamma_{ri} = 0.5$ and $\gamma_{mi} = 0$.
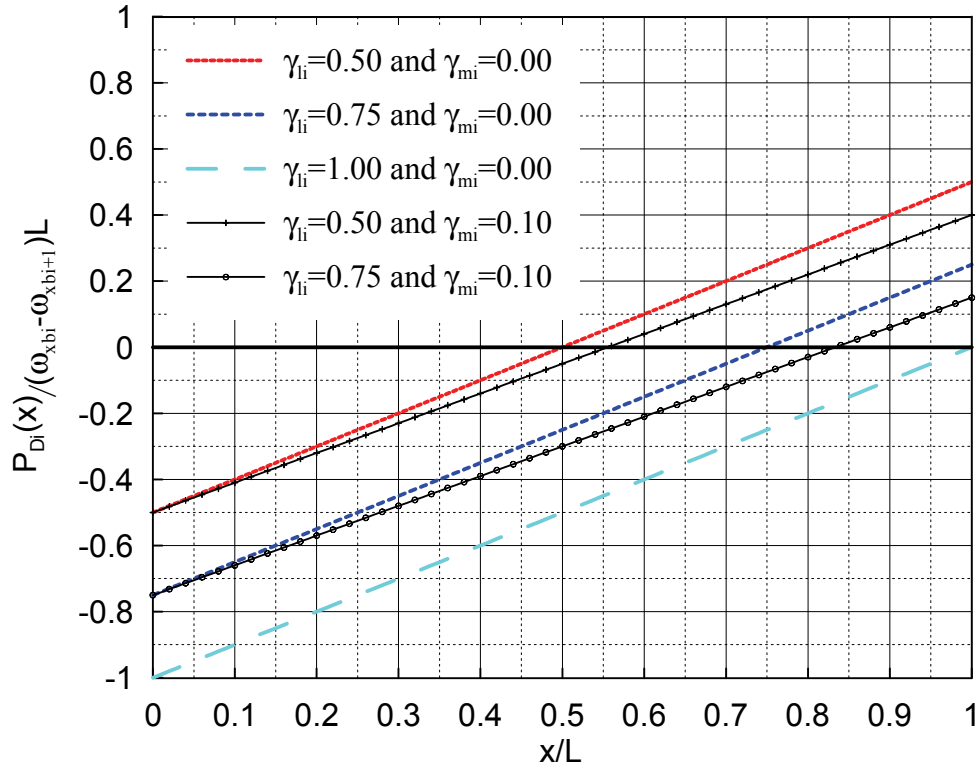
FIGURE 4-6 Normalized Axial Force Distribution in Intermediate HBE Due to Horizontal Components of Infill Panel Yield Forces on HBE

4.3.5 Resulting Axial Force in HBE

The analytical procedures to estimate the magnitude and distribution of axial forces in intermediate HBE have been developed for each sub-system shown in figure 4-2. These axial effects are then combined, considering an arbitrary sign convention (i.e. "-" and "+" for compression and tension respectively), resulting in the following equation for the axial force at any location, x, of the HBE:

$$P_{bi}(x) = \underbrace{-\omega_{xci}\left(\frac{h_{si}}{2} - \frac{d_i}{2}\right) - \omega_{xci+1}\left(\frac{h_{si+1}}{2} - \frac{d_i}{2}\right)}_{\text{Axial effect in intermediate HBE of frame D}}$$

$$+ \underbrace{\frac{v\left(\omega_{ybi} + \omega_{ybi+1}\right)}{2} h_w}_{\text{Axial effect in intermediate HBE of frame E}} + \underbrace{\left[-\gamma_{li} - \gamma_{mi}\frac{x}{L} + \frac{x}{L}\right]\left(\omega_{xbi} - \omega_{xbi+1}\right)\cdot L}_{\text{Axial effect in intermediate HBE of frame F}} \tag{4-17}$$

4.4 Shear Force in Intermediate HBE

Shear force in an intermediate HBE comes from two sources: tension fields and boundary frame sway. To better understand this, following the same logic adopted in Section 4.3 to account for the contributions of various effects on axial force, the free body diagram of a typical intermediate HBE (figure 4-7A), when the SPSW develops the expected plastic mechanism, can be decomposed into two sub-systems, as shown in figures 4-7b and 4-7c respectively, namely: (i) Beam B, a simply supported beam subjected to top and bottom infill tension fields, which will be investigated in Section 4.4.1 to determine the shear effects only resulting from infill panel yield forces (i.e ω_{bi} and ω_{bi+1}); and (ii) Beam C, also a simply supported beam subjected to plastic end moments, which will be investigated in Section 4.4.2 to take into account the shear effects only due to boundary frame sway.

For calculating the shear effects only due to top and bottom tension fields (i.e. shear force in Beam B shown in figure 4-7), two analytical models based on different free body diagrams will be developed in Sections 4.4.1.1 and 4.4.1.2 respectively. FE analysis will be used in Section 4.4.1.3 to verify those two analytical models. The shear force in HBE only due to frame sway (i.e. shear effects in Beam C) is a well-known and validated effect. The corresponding results for HBEs with and without RBS at the ends will be presented in Section 4.4.2 for convenience. The total effects of infill panel yield forces and boundary frame sway will be provided in Section 4.4.3.

For simplicity, the tension field orientation angle, α, typically close to 45° from the vertical, is assumed to be identical above and below the considered HBE. Note that, in

design, one may alternatively use the average orientation angle of the top and bottom tension fields.
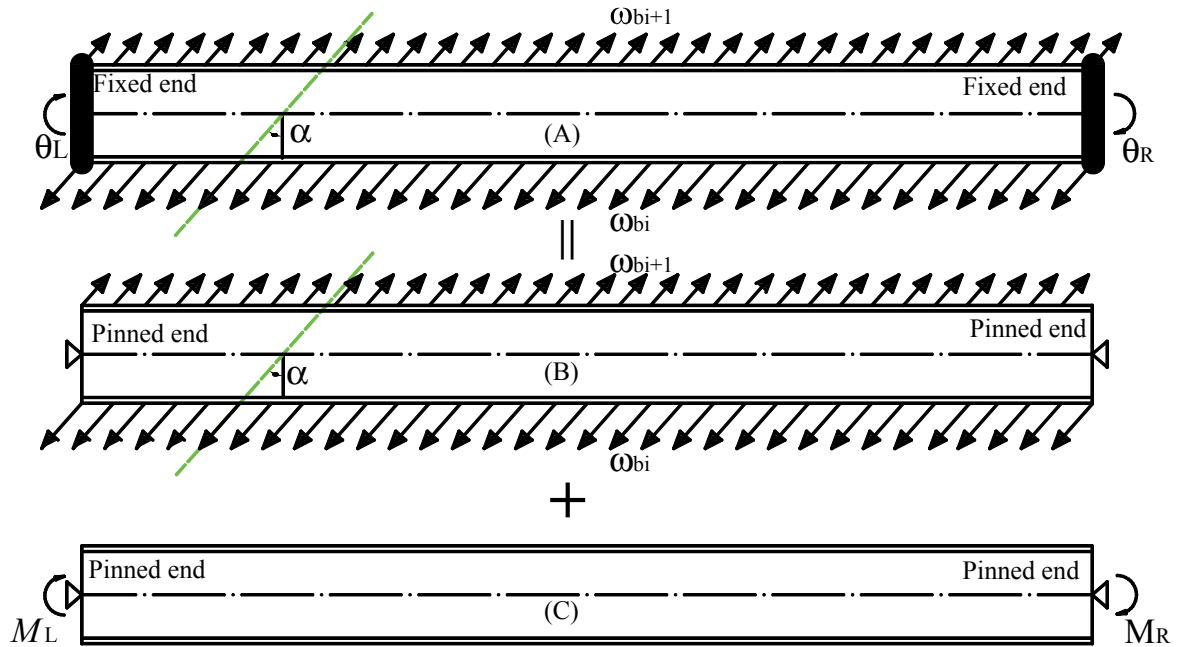
FIGURE 4-7 Decomposition of Loading on Intermediate HBE: (A) Typical Intermediate HBE; (B) Intermediate HBE Subjected to Infill Panel Yield Forces; (C) Intermediate HBE Subjected to Plastic End Moments

4.4.1 Shear Effects Only Due to Infill Panel Yield Forces

Beam B shown in figure 4-7 is studied in this section. Two analytical models, using different free body diagrams to calculate the shear effects only due to top and bottom tension fields, are developed in Sections 4.4.1.1 and 4.4.1.2 respectively. The first model divides the tension fields into three sub-tension fields, and obtains the shear forces by superposing the shear effects caused by each sub-tension field. The second model decomposes the tension fields into horizontal and vertical components, and estimates the shear force by combining the shear effects resulting from each component of the tension fields. These two models are validated by FE results in Section 4.4.1.3.

4.4.1.1 Superposing Shear Effects from Sub-Tension Fields

The tension fields on both sides of an intermediate HBE labeled B, shown in figure 4-8, can be divided into three sub-tension fields in accordance with boundaries determined by

two parallel lines at inclination angle of α. Those boundaries pass through the top right and bottom left corners of the top and bottom fish plates, respectively. Accordingly, the infill panel yield force are divided into 3 free body diagrams labeled B1, B2 and B3 respectively as shown in figure 4-8. In free-body-diagram B1, both top and bottom tension field forces are uniformly distributed in the middle part of the HBE. In free-body-diagrams B2 and B3, bottom and top tension field forces act on the right and left ends of the HBE, respectively.
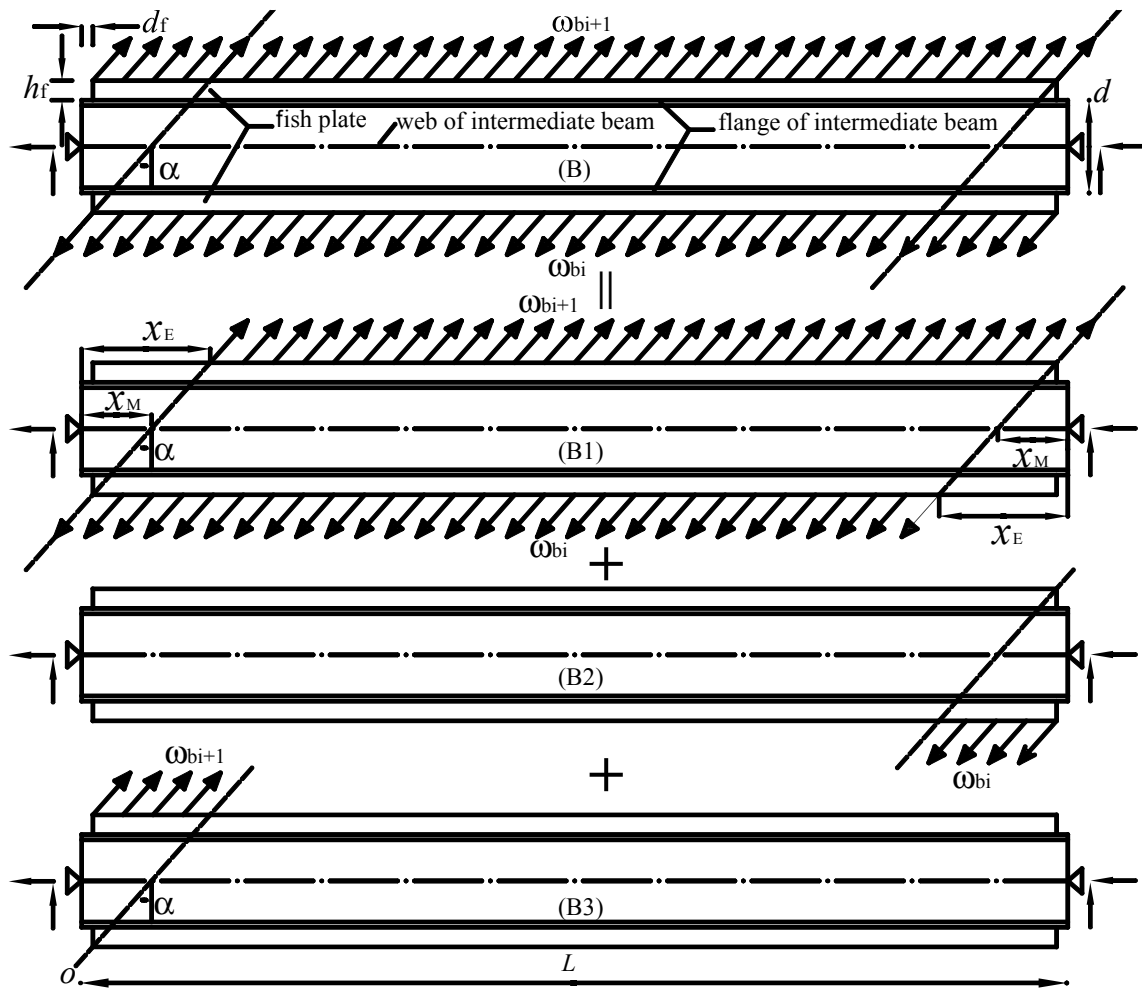
FIGURE 4-8 Infill Panel Yield Forces on Simply Supported Intermediate HBE

From the principle of superposition, the resulting shear action can be determined by combining the shear effects in free-body-diagrams B1, B2 and B3 (i.e. shear effects due to each sub-tension field).

Fish plates, which are used to connect infill panels and HBEs, are included in the free body diagrams since they have an impact on shear estimation as demonstrated later. In figure 4-8, d_f is the distance between the fish plate end to the VBE face, and h_f is the distance between the HBE flange and the welds connecting the infill panel to the fish plate. The terms, x_E and x_M, define the distances from the VBE face to the parallel line boundaries, respectively measured from the weld of the infill panels to the fish plates or the centerline of the HBE as shown in figure 4-9 . The corresponding equations for x_E and x_M are:

$$x_E = d_f + (d + 2h_f) \tan \alpha \tag{4-18}$$

$$x_M = d_f + \left(\frac{d}{2} + h_f\right) \tan \alpha \tag{4-19}$$
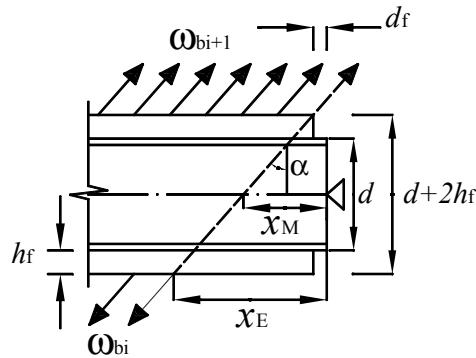
FIGURE 4-9 Intermediate HBE End

To understand the shear effects caused by the top and bottom infill panel yield forces in free-body-diagram B1 shown in figure 4-8, consider a small segment of the HBE as shown on the left-hand side of figure 4-10a.

73
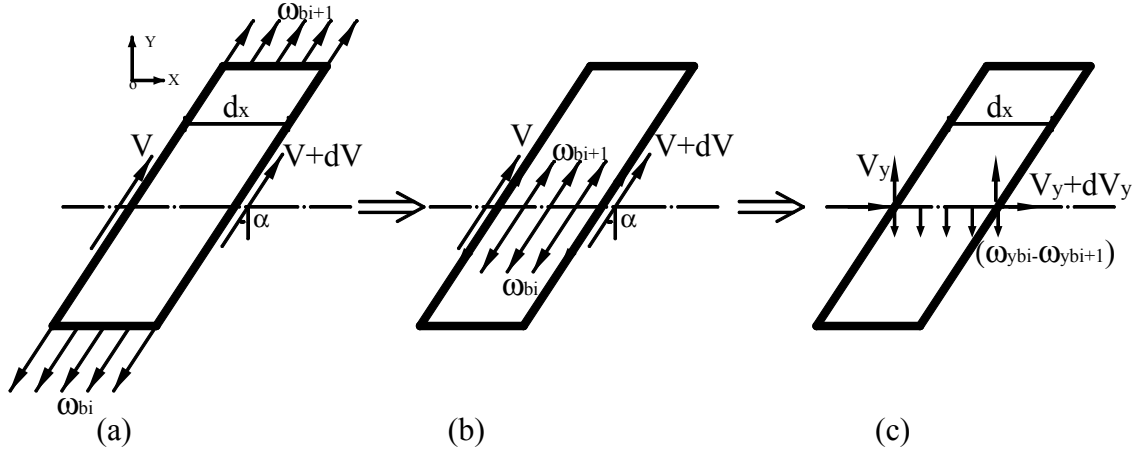
FIGURE 4-10 Simplification of Infill Panel Forces on HBE Segment

The equilibrium equation of that segment along the acting direction of infill panel yield force gives:

$$dV = \left(\omega_{bi} - \omega_{bi+1} \right) dx \qquad (4\text{-}20)$$

Multiplying by $\cos\alpha$ on both sides of (4-20), and recalling $dV_y = dV \cdot \cos\alpha$, $\omega_{byi} = \omega_{bi} \cdot \cos\alpha$ and $\omega_{byi+1} = \omega_{bi+1} \cdot \cos\alpha$, one can obtain equilibrium in the vertical direction as:

$$dV_y = \left(\omega_{ybi} - \omega_{ybi+1} \right) \cdot dx \qquad (4\text{-}21)$$

The vertical shear force in free-body-diagram B1 shown in figure 4-8 can be similarly determined through a free body diagram in which the resulting vertical infill panel yield forces are applied on the centerline of B1 as shown in figure 4-11. However, for free-body-diagrams B2 and B3 shown in figure 4-8, in which infill panel yield forces are applied on only one side (either top or bottom), the above logic can not be followed due to the absence of infill panel yield forces on the other side.

The shear force from the free-body-diagram B2 shown in figure 4-8 is obtained by breaking that free body diagram into two sub-systems: namely (i) free-body-diagram B21 shown in figure 4-11, in which the vertical components of the infill panel yield forces is applied on the centerline, and (ii) free-body-diagram B22 shown in figure 4-11, in which

74

a uniformly distributed moment equal to the magnitude of the horizontal components of the infill panel yield force times the distance between its line of action and the beam centerline is applied. From the above two sub-systems, the shear effects resulting from the horizontal and vertical components of the infill panel yield forces in free-body-diagram B2 shown in figure 4-8 can be taken into account respectively. Similarly, free-body-diagram B3 shown in figure 4-8 is divided into free-body-diagrams B31 and B32 as shown in figure 4-11.
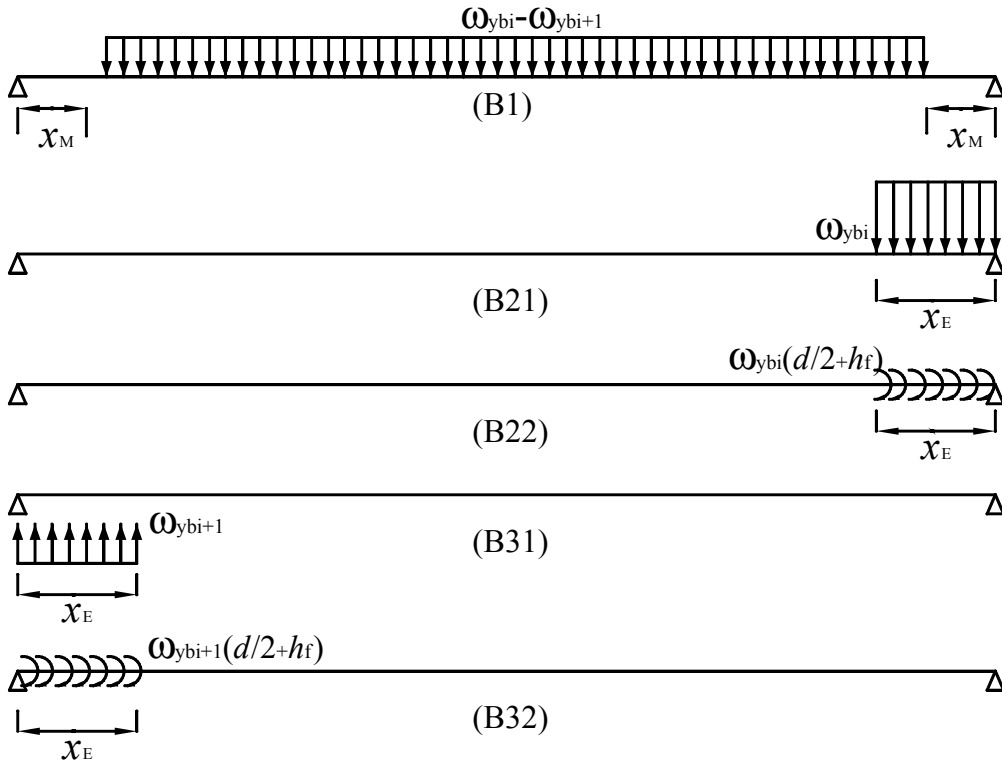
FIGURE 4-11 Free Body Diagrams of Simply Supported HBE under Fundamental Loading Due to Sub-Tension Fields

Based on the loading characteristics, the free body diagrams shown in 4-11 are differentiated into the following two categories: (i) simply supported beams under partial uniform loads (i.e. B1, B21 and B31), and (ii) simply supported beams under partial uniform moments (i.e. B22 and B32). Shear diagrams for the above two general cases are derived below, from which the shear force corresponding to each free body diagram can be obtained.

First consider the effect of a uniform load over part of the HBE length as shown in figure 4-12. The parameters, a, c and d, describe the location of loads applied to the HBE, and. ω and W are the magnitudes of the uniform load and its resultant action, respectively.
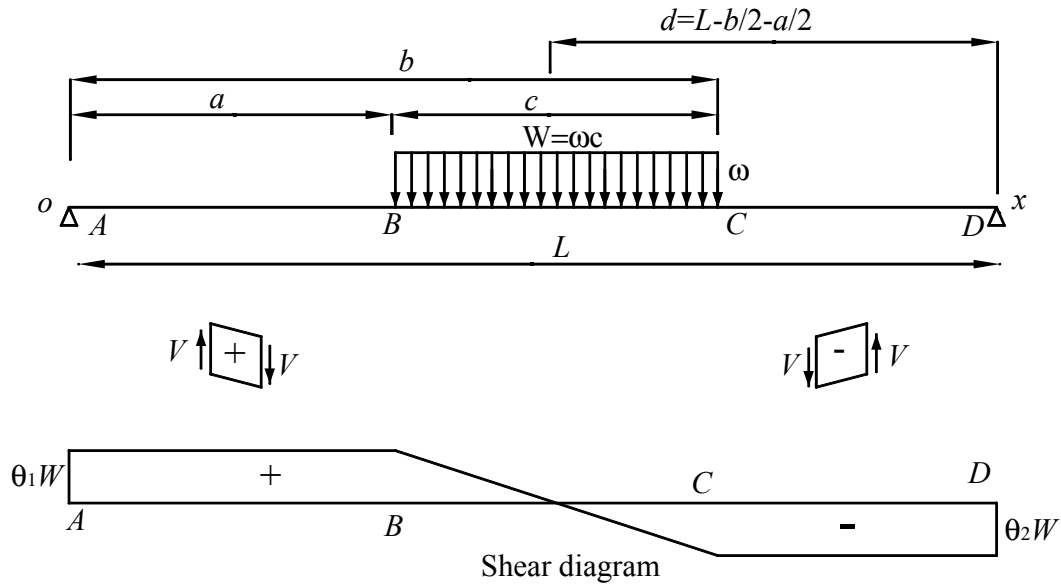
FIGURE 4-12 Free Body Diagram and Shear Diagram of Simply Supported Beam under Partial Uniform Load

For the sign convention shown in the above figure, the shear along the beam is given as:

$$V(x) = \begin{cases} \theta_1 \cdot W & \text{if} \quad 0 \leq x < a \\ \left[\theta_1 - \dfrac{x-a}{c}\right] W & \text{if} \quad a \leq x < b \\ -\theta_2 \cdot W & \text{if} \quad b \leq x < l \end{cases} \quad (4\text{-}22)$$

where θ_1 and θ_2 are two factors for calculating the shear forces at the left and right ends respectively, equal to

$$\theta_1 = d/L \quad (4\text{-}23)$$

$$\theta_2 = 1 - \theta_1 \quad (4\text{-}24)$$

76

Shear forces in free-body-diagrams B1, B21 and B31 shown in figure 4-11 can be derived from the general results presented in (4-22) and parameters used in (4-22) for each free body diagram are summarized in table 4-1.

TABLE 4-1 Parameters for Determining Shear Forces

FBD	a	b	ω	θ_1	θ_2
B1	x_M	$L-x_M$	$\omega_{ybi}-\omega_{ybi+1}$	0.5	0.5
B21	$L-x_E$	$L-d_f$	ω_{ybi}	$0.5\left(x_E+d_f\right)/L$	$1-0.5\left(x_E+d_f\right)/L$
B31	d_f	x_E	$-\omega_{ybi+1}$	$1-0.5\left(x_E+d_f\right)/L$	$0.5\left(x_E+d_f\right)/L$

Then, consider the shear effect of uniform moment over part of the HBE length as shown in figure 4-13. The parameter, c, is used to describe the effective length along which m is acting, where m and M are the magnitudes of the uniform moment and its resultant action, respectively.
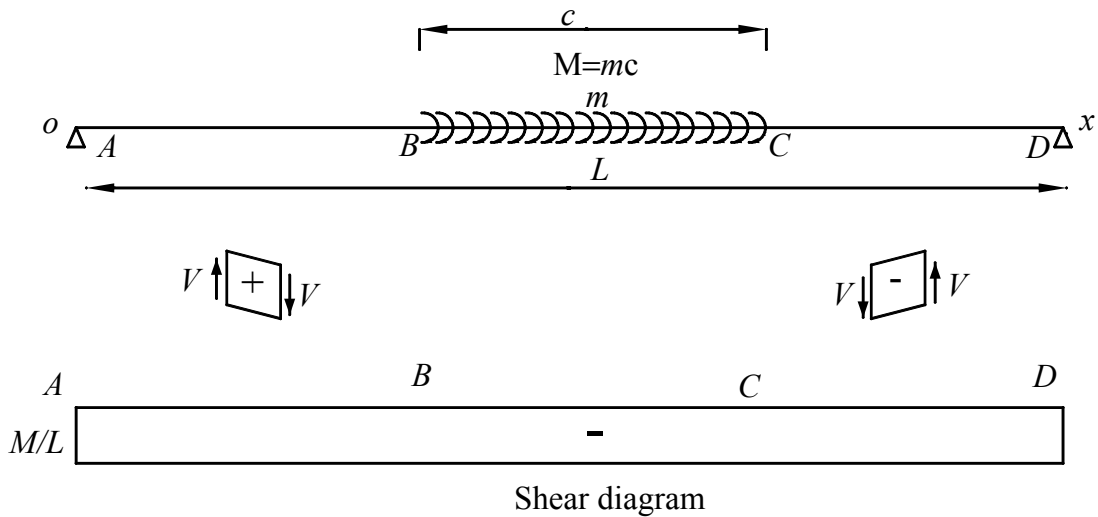
Shear diagram

FIGURE 4-13 Free Body Diagram and Shear Diagram of Simply Supported Beam under Partial Uniform Moment

For the sign convention shown in the above figure, the shear along the beam is given as:

$$V(x)=mc/L=M/L \tag{4-25}$$

Shear forces in free-body-diagrams B22 and B32 shown in 4-11 can be determined by using the same general results presented in (4-25) by substituting the resulting moment calculated below:

$$
M = \begin{cases} \omega_{ybi}\left(\dfrac{d}{2}+h_f\right)\left(x_E - d_f\right) & \text{for } B21 \\[3mm] \omega_{ybi+1}\left(\dfrac{d}{2}+h_f\right)\left(x_E - d_f\right) & \text{for } B22 \end{cases}
\tag{4-26}
$$

The shear forces in free-body-diagrams B1, B21, B22, B31 and B32 shown in figure 4-11 have been determined from the above derivations. One can obtain the resulting shear forces in an HBE subjected to infill panel yield forces by superposing the effect from each aforementioned free body diagram. The shear force at the right and left ends of the HBE, V_{SR} and V_{SL}, caused only by the infill panel yield forces are provided below:

$$
V_{SR} = \underbrace{\frac{\left(\omega_{ybi} - \omega_{ybi}\right)\left(L - 2x_M\right)}{2}}_{\text{Shear effect from B1}} + \underbrace{\theta\omega_{ybi}\left(x_E - d_f\right)}_{\text{Shear effect from B21}}
$$
$$
\underbrace{-(1-\theta)\omega_{ybi+1}\left(x_E - d_f\right)}_{\text{Shear effect from B31}} + \underbrace{\frac{\left(\omega_{xbi} + \omega_{xbi+1}\right)\left(x_E - d_f\right)\left(\dfrac{d}{2}+h_f\right)}{L}}_{\text{Shear effects from B22 and B32}}
\tag{4-27}
$$

$$
V_{SL} = \underbrace{\frac{\left(\omega_{ybi} - \omega_{ybi}\right)\left(L - 2x_M\right)}{2}}_{\text{Shear effect from B1}} + \underbrace{(1-\theta)\omega_{ybi}\left(x_E - d_f\right)}_{\text{Shear effect from B21}}
$$
$$
\underbrace{-\theta\omega_{ybi+1}\left(x_E - d_f\right)}_{\text{Shear effect from B31}} - \underbrace{\frac{\left(\omega_{xbi} + \omega_{xbi+1}\right)\left(x_E - d_f\right)\left(\dfrac{d}{2}+h_f\right)}{L}}_{\text{Shear effects from B22 and B32}}
\tag{4-28}
$$

where θ is the load distribution factor

$$
\theta = 1 - x_M/L
\tag{4-29}
$$

Results from (4-27) and (4-28) are compared with the FE results for assessing their accuracy in Section 4.4.1.3.

4.4.1.2 Combining Shear Effects from Tension Field Components

For determination of the shear effects in an intermediate HBE from infill panel yield forces only, the second model decomposes the top and bottom tension fields on an intermediate HBE into horizontal and vertical components as shown in figure 4-14. Accordingly, the total shear in the HBE can be obtained by combining the shear effects due to horizontal and vertical components of the tension fields.
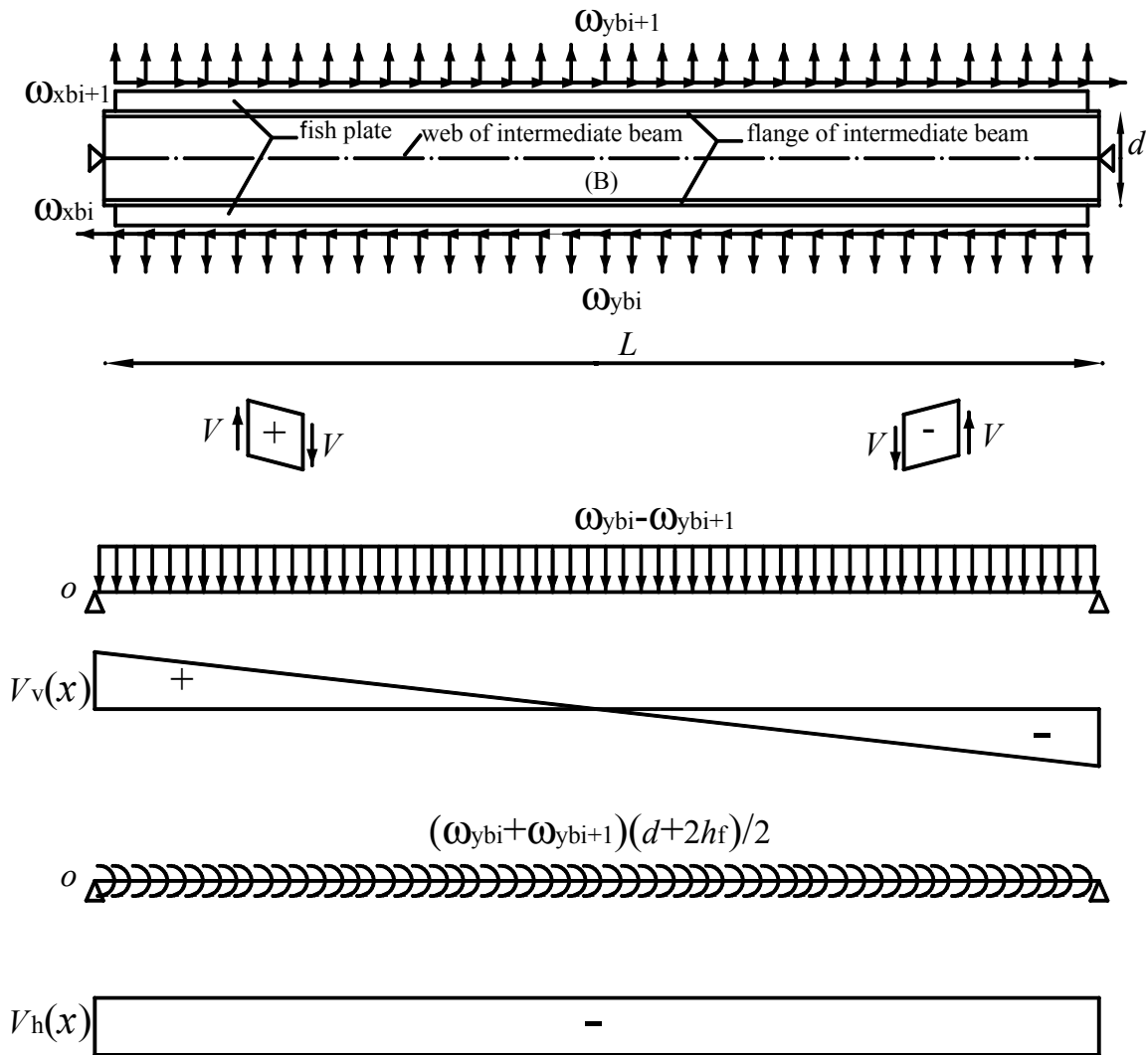
FIGURE 4-14 Decomposition of Infill Panel Yield Forces on the Simply Supported Beam and the Corresponding Shear Diagrams

To account for the shear effect caused by the vertical components of the top and bottom tension fields (i.e. ω_{ybi+1} and ω_{ybi}), the resulting vertical infill panel yield forces (i.e.

$\left(\omega_{ybi} - \omega_{ybi+1} \right))$ are applied at the beam centerline as shown in the middle part of figure 4-14. By setting $a = d_f$, $b = L - d_f$ and $\omega = \omega_{ybi} - \omega_{ybi+1}$ in (4-22), (4-23) and (4-24), which are the general results for shear force in a simply supported beam subjected a uniform load over part of its length , one can obtain the corresponding shear as:

$$
V_V(x) = \begin{cases} \dfrac{\left(\omega_{ybi} - \omega_{ybi+1} \right)\left(L - 2d_f \right)}{2} & \text{if} \quad 0 \le x < d_f \\[4mm] \dfrac{\left(\omega_{ybi} - \omega_{ybi+1} \right)\left(L - 2x \right)}{2} & \text{if} \quad d_f \le x < L - d_f \\[4mm] -\dfrac{\left(\omega_{ybi} - \omega_{ybi+1} \right)\left(L - 2d_f \right)}{2} & \text{if} \quad L - d_f \le x < L \end{cases} \qquad (4\text{-}30)
$$

To account for the shear effects generated by the horizontal components of the top and bottom tension fields, a free body diagram is shown in the bottom of figure 4-14, in which the horizontal components of the tension fields acting in opposite directions at the top and bottom edges of the HBE web (i.e. ω_{xbi+1} and ω_{xbi}) are equivalently replaced by uniformly distributed moments of magnitude equal to the horizontal components of the tension fields times the distance from the acting line to the beam centerline. By setting $c = L - 2d_f$ and $m = \left(\omega_{xbi} + \omega_{xbi+1} \right) \cdot \left(\dfrac{d}{2} + h_f \right)$ in (4-25), which is the general result for shear force in a simply supported beam subjected to a uniform moment over part of the length, one can obtain the corresponding shear as:

$$
V_h(x) = -\frac{\left(\omega_{xbi} + \omega_{xbi+1} \right)\left(d + 2h_f \right)\left(L - 2d_f \right)}{2L} \qquad (4\text{-}31)
$$

By combining the shear force predicted by (4-30) and (4-31), i.e. shear effects caused by vertical and horizontal components of the infill panel yield forces respectively, one can obtain the total shear forces in an HBE due to the top and bottom tension fields. Correspondingly, the shear forces at the right and left ends of the HBE, V_{SR} and V_{SL}, are obtained by setting $x = 0$ and $x = L$ in the expression for the total shear forces:

80

$$V_{SR} = -\frac{\left(\omega_{ybi} - \omega_{ybi+1}\right)\left(L - 2d_f\right)}{2} - \frac{\left(\omega_{xbi} + \omega_{xbi+1}\right)\left(d + 2h_f\right)\left(L - 2d_f\right)}{2L} \qquad (4\text{-}32)$$

Shear effects due to vertical components of the tension fields   Shear effects due to horizontal components of the tension fields

$$V_{SL} = \frac{\left(\omega_{ybi} - \omega_{ybi+1}\right)\left(L - 2d_f\right)}{2} - \frac{\left(\omega_{xbi} + \omega_{xbi+1}\right)\left(d + 2h_f\right)\left(L - 2d_f\right)}{2L} \qquad (4\text{-}33)$$

Shear effects due to vertical components of the tension fields   Shear effects due to horizontal components of the tension fields

Indeed, results obtained from (4-32) and (4-33) are equivalent to (4-27) and (4-28), respectively, although they have different expressions derived using different free body diagrams. Detailed mathematical proof is presented in Appendix A.

4.4.1.3 FE Verification of Shear Effects due to Tension Fields

In Sections 4.4.1.1 and 4.4.1.2, two approaches for estimating the shear forces in intermediate HBEs only due to tension fields are presented based on different free body diagrams. To assess the adequacy of those approaches, four different HBEs were investigated using the FE methods. Those four examples considered intermediate HBEs under either equal or unequal top and bottom tension fields, and with or without fish plates.

All HBEs modeled consisted of a 3508 mm long W24x76 beam. An orientation angle of $\alpha = 45°$ was assumed for the top and bottom tension fields in all cases. Material was assumed to be A572 Grade 50 steel with isotropic and elasto-perfectly plastic constitutive behavior. The considered magnitudes of top and bottom tension fields and the defining parameters of fish plates for the models are summarized in table 4-2.

<div style="text-align:center">

TABLE 4-2 Magnitudes of Top and Bottom Tension Fields and Defining Parameters of Fish Plates

</div>

HBE ID	ω_{xbi} (N/mm)	ω_{ybi} (N/mm)	ω_{xbi+1} (N/mm)	ω_{ybi+1} (N/mm)	d_f (mm)	h_f (mm)
1	496	496	496	496	0	0
2	496	496	496	496	40	35
3	496	496	357	357	0	0
4	496	496	357	357	40	35

The corresponding FE models were analyzed in ABAQUS/Standard. Shell element (ABAQUS element S4R) was used for the webs and flanges. A total number of 18,660 and 17,280 elements were used for the HBEs with and without fish plates, respectively. The top and bottom tension field forces were applied on the FE models. The ends of the beams were simply supported to be consistent with the boundary conditions used in the free body diagrams. The shear reaction forces at the beam ends obtained from FE analyses are presented in table 4-3 along with those predicted using the approaches proposed in Sections 4.4.1.1 and 4.4.1.2 for comparison purpose. Also compared are the results from the following equation which was assumed, prior to this study, to be the correct acting shear on the basis of HBE free body diagrams, in which the HBE depth was neglected and the vertical resultant force of the tension fields was assumed to be equally transferred to both ends of HBE, namely:

$$V_S = \frac{\left(\omega_{ybi} - \omega_{ybi+1}\right)\left(L - 2d_f\right)}{2} \tag{4-34}$$

TABLE 4-3 Magnitudes of HBE End Shears from Different Models

HBE ID	V_{SL} (kN)			V_{SR} (kN)			V_S (kN)
	FE	Eq.(4-33)	Eq.(4-28)	FE	Eq.(4-32)	Eq.(4-27)	Eq.(4-34)
1	292.5	292.5	292.5	-292.5	-292.5	-292.5	0
2	319.8	319.8	319.8	-319.8	-319.8	-319.8	0
3	6.7	6.7	6.7	-496.1	-496.1	-496.1	244.7
4	35.7	35.7	35.7	-513.9	-513.9	-513.9	239.1

As shown in the above table, the estimates on HBE end shears using the approaches presented in Sections 4.4.1.1 and 4.4.1.2 agree well with the FE results. However, equation (4-34), which was previously used for the design of HBEs, fails to capture the important variation of shear forces at the ends of the intermediate HBE that occurs because the resultant action of the vertical tension field components is not equally resisted by each end of the HBE. Also found in the above table, the end shears increase slightly due to the presence of fish plates.

4.4.2 Shear Effects Due to Boundary Frame Sway Action Alone

Shear effects in HBEs due to boundary frame sway action alone (i.e. shear in Beam C shown in figure 4-7) is straightforward and a well known result. In this section, RBS connections at the HBE ends are taken into account to calculate the shear effects for the following two reasons: (i) HBEs without RBS connections at the ends are only a special case of the HBEs with RBS connections at the ends (i.e. reduction in flange is zero), and correspondingly the shear force in the HBE without RBS connections can be obtained from the general results of the HBE with RBS connections as demonstrated later, and; (ii) it is helpful to investigate the case with RBS connections for the later examination on the failed intermediate HBE of the MCEER/NCREE specimen described in Qu *et al.* (2008), in which RBS connections were used.

The free body diagram, corresponding moment diagram and shear diagram of an HBE with RBS connections are shown in figure 4-15. Parameter e is the distance from plastic hinge to VBE face, which can be calculated according to flange reduction geometry, as described in FEMA 350 (FEMA, 2000).
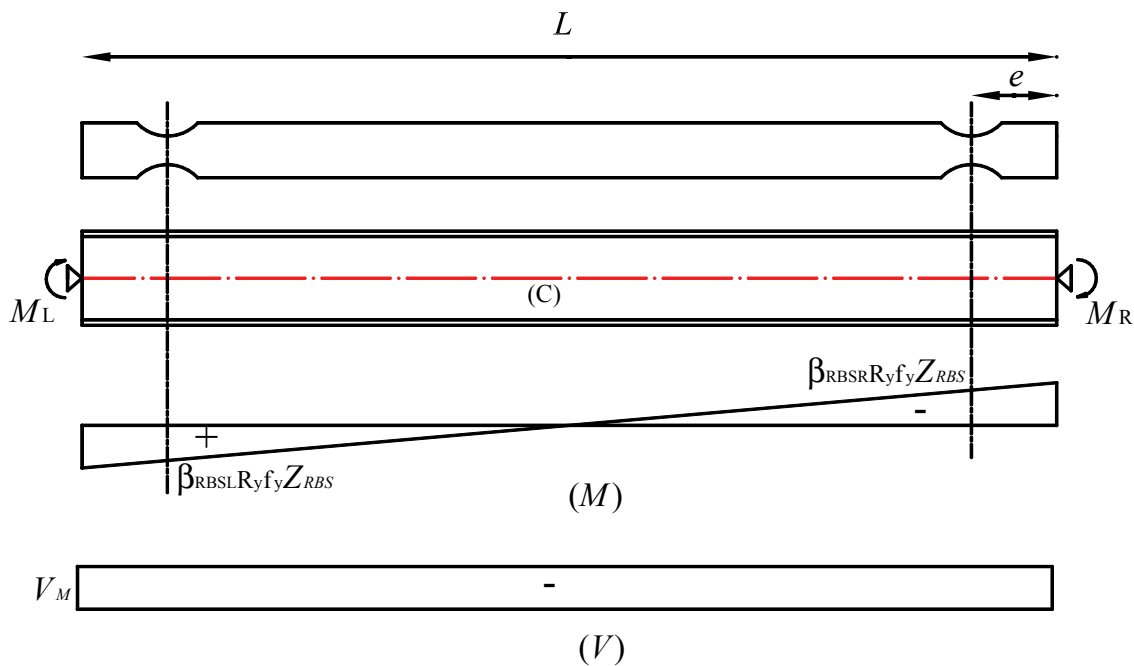
FIGURE 4-15 Free Body Diagram, Moment Diagram and Shear Diagram of an HBE with RBS Connections under Plastic End Moments Due to Frame Sway

Note that the nominal plastic moment at the center of the RBS is reduced to account for the presence of axial load, shear force and vertical stresses in the HBE web due to the infill panel yield forces. Using the cross-section plastic moment reduction factors of the left and right plastic hinges, β_{RBSL} and β_{RBSR}, per the procedures proposed in Section 3, the uniform shear in the HBE only due to boundary frame sway, can be expressed as:

$$V_M = -\frac{(\beta_{RBSL} + \beta_{RBSR}) R_y f_y Z_{RBS}}{L - 2e} \qquad (4\text{-}35)$$

where Z_{RBS} is the plastic section modulus of the HBE plastic hinge, and R_y is the ratio of expected to nominal yield stress of the HBE.

Also note that iteration may be necessary in design since the plastic moment reduction factors, β_{RBSL} and β_{RBSR}, depend on the total shear forces acting at the HBE plastic hinges and that these must be assumed at the beginning of the design process.

For HBEs without RBS connections, the shear effects due to boundary frame sway can be obtained by setting $e = 0$, and replacing Z_{RBS}, β_{RBSL} and β_{RBSR} in (4-35) with Z, β_L and β_R, respectively:

$$V_M = -\frac{(\beta_L + \beta_R) R_y f_y Z}{L} \qquad (4\text{-}36)$$

where Z is the plastic section modulus of the unreduced HBE cross-section; β_L and β_R are the cross-section plastic moment reduction factors of the left and right ends of the HBE, respectively, which can be determined using the procedures proposed in Section 3.

4.4.3 Resulting Shear Force in HBE

The analytical procedures to estimate the shear force in Beams B and C shown in figure 4-7 have been developed in Sections 4.4.1 and 4.4.2 respectively. These shear effects are then combined to obtain the total shears in HBEs. For use in calculating plastic moment reduction factors at VBE face, the resulting shear forces at VBE faces obtained combining all effects considered above are provided below.

For HBEs having RBS connections, the shear at the left and right VBE faces (i.e. V_L and V_R) can be obtained by adding up (4-33) and (4-35), and (4-32) and (4-35) respectively.

$$V_L = \underbrace{\frac{\left(\omega_{ybi} - \omega_{ybi+1}\right)\left(L - 2d_f\right)}{2}}_{\text{due to vertical components of the tension fields}} - \underbrace{\frac{\left(\omega_{xbi} + \omega_{xbi+1}\right)\left(d + 2h_f\right)\left(L - 2d_f\right)}{2L}}_{\text{due to horizontal components of the tension fields}}$$
$$-\underbrace{\frac{\left(\beta_{RBSL} + \beta_{RBSR}\right)R_y f_y Z_{RBS}}{L - 2e}}_{\text{due to boundary frame sway}} \tag{4-37}$$

$$V_R = \underbrace{-\frac{\left(\omega_{ybi} - \omega_{ybi+1}\right)\left(L - 2d_f\right)}{2}}_{\text{due to vertical components of the tension fields}} - \underbrace{\frac{\left(\omega_{xbi} + \omega_{xbi+1}\right)\left(d + 2h_f\right)\left(L - 2d_f\right)}{2L}}_{\text{due to horizontal components of the tension fields}}$$
$$-\underbrace{\frac{\left(\beta_{RBSL} + \beta_{RBSR}\right)R_y f_y Z_{RBS}}{L - 2e}}_{\text{due to boundary frame sway}} \tag{4-38}$$

Similarly, for HBEs without RBS connections, the shear at the left and right VBE faces can be obtained by adding up (4-33) and (4-36), and (4-32) and (4-36) respectively:

$$V_L = \underbrace{\frac{\left(\omega_{ybi} - \omega_{ybi+1}\right)\left(L - 2d_f\right)}{2}}_{\text{due to vertical components of the tension fields}} - \underbrace{\frac{\left(\omega_{xbi} + \omega_{xbi+1}\right)\left(d + 2h_f\right)\left(L - 2d_f\right)}{2L}}_{\text{due to horizontal components of the tension fields}} - \underbrace{\frac{\left(\beta_L + \beta_R\right)R_y f_y Z}{L}}_{\text{due to boundary frame sway}} \tag{4-39}$$

$$V_R = \underbrace{-\frac{\left(\omega_{ybi} - \omega_{ybi+1}\right)\left(L - 2d_f\right)}{2}}_{\text{due to vertical components of the tension fields}} - \underbrace{\frac{\left(\omega_{xbi} + \omega_{xbi+1}\right)\left(d + 2h_f\right)\left(L - 2d_f\right)}{2L}}_{\text{due to horizontal components of the tension fields}} - \underbrace{\frac{\left(\beta_L + \beta_R\right)R_y f_y Z}{L}}_{\text{due to boundary frame sway}} \tag{4-40}$$

4.5 Prevention of In-Span HBE Plastic Hinge

The AISC Seismic Provisions (AISC 2005) specifies that with the exception of plastic hinges at their ends, HBEs must be designed to remain elastic when the plastic mechanism of the SPSW is fully developed. In-span HBE plastic hinge, however, could partly prevent yielding of the infill panels and is deemed to be undesirable.

Vian and Bruneau (2005) proposed a procedure to prevent in-span plastic hinges in an anchor HBE. Here, the moment diagram used in their procedure is reviewed in Section 4.5.1 and applied to intermediate HBEs by considering the net resulting distributed forces from the top and bottom infill panel tension fields. In Section 4.5.2, that procedure is extended to account for the reduced HBE plastic moment due to the presence of axial compression, shear force and vertical stresses in the HBE.

4.5.1 Moment Diagram of Intermediate HBE

Vian and Bruneau (2005) obtained the moment diagram for an anchor HBE by superposing plastic HBE end moments due to the boundary frame sway action and a quadratic "hanging" moment due to the vertical components of the infill panel yield forces. Following this logic, the moment diagram of an intermediate HBE can be obtained as shown in figure 4-16.

The equation for the resulting moment diagram, $M(x)$, using the sign convention shown in the figure, is

$$M(x) = \frac{\left(\omega_{ybi} - \omega_{ybi+1}\right) \cdot x}{2}(l-x) - M_{PR} \cdot \frac{x}{l} + M_{PL}\left(1 - \frac{x}{l}\right) \qquad (4\text{-}41)$$

where M_{PL} and M_{PR} are plastic moments at the left and right ends, respectively; and l is the distance between the left and right plastic hinges. For HBEs with and without RBS, l can be taken as $L - 2e$ and L respectively, where L is the distance between VBE faces.

The location of the maximum moment, x_{span}, is calculated by differentiating $M(x)$ with respect to x, setting the result equal to zero, and solving:

$$x_{span} = \frac{l}{2} - \left[\frac{M_{PL} + M_{PR}}{\left(\omega_{ybi} - \omega_{ybi+1}\right) \cdot l} \right]$$

(4-42)

The location of the maximum moment will be out of the span if the value of x_{span}, which theoretically can be anywhere from negative infinity to $l/2$, is less than zero. This case implies plastic hinges can only form at the HBE ends.

Substituting (4-42) into (4-41) and simplifying:

$$M_{span} = \frac{\left(\omega_{ybi} - \omega_{ybi+1}\right) \cdot l^2}{8} + \frac{\left(M_{PL} + M_{PR}\right)^2}{2 \cdot \left(\omega_{ybi} - \omega_{ybi+1}\right) \cdot l^2} + \frac{M_{PL} - M_{PR}}{2}$$

(4-43)
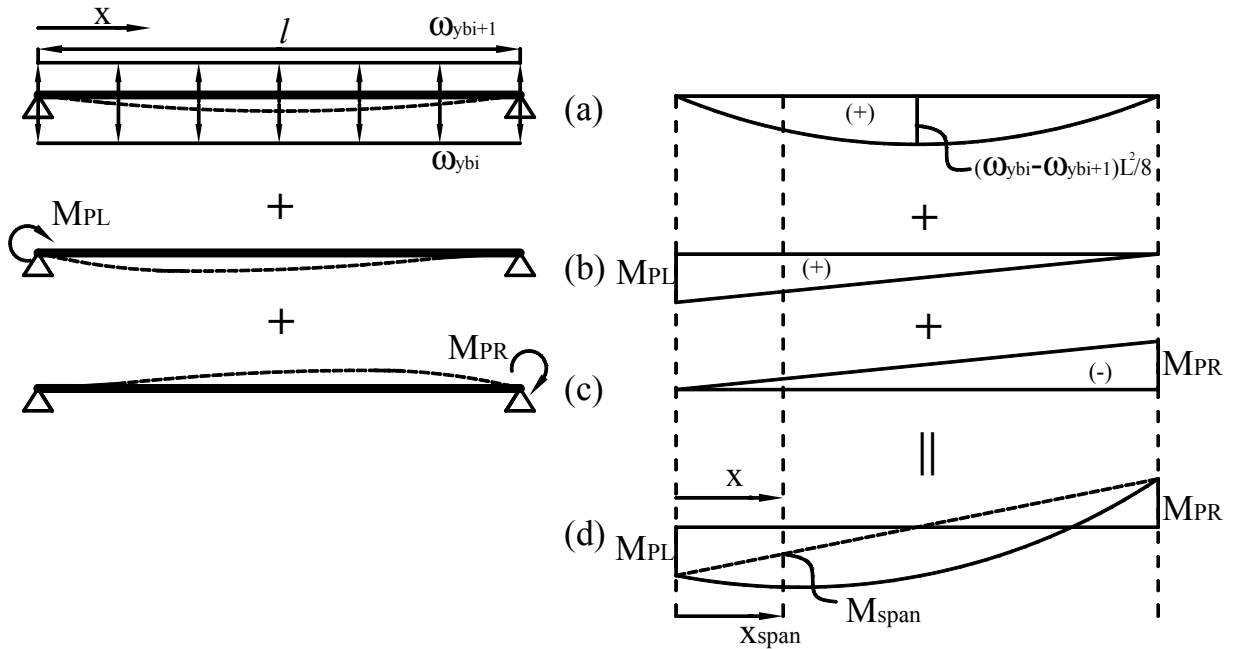
FIGURE 4-16 Deformed Shape, Loading and Moment Diagrams for Calculating Intermediate HBE Collapse Mechanisms Using Equilibrium Methods for: (a) Vertical Components of Infill Panel Yield Forces; (b) Left End Redundant Moment; (c) Right End Redundant Moment; (d) Combined Moment Diagram

4.5.2 Procedure to Avoid In-Span Plastic Hinge

For an HBE with RBS connections at its ends, the plastic section modulus at the RBS center, Z_{RBS}, can be obtained by reducing the plastic section modulus of the unreduced HBE cross-section, Z, to the fraction, η:

$$Z_{RBS} = \eta \cdot Z \tag{4-44}$$

where, η, referred to here as the "RBS plastic section modulus reduction ratio", may vary from unity and the minimum value of RBS flange reduction permitted by design specifications and guidelines such as FEMA 350 (FEMA 2000).

Considering that the plastic moment resistance of HBE is reduced by the axial force, shear force and vertical stresses acting in the HBE web, as shown in Section 3, the plastic moment at the ends of an HBE can be determined by incorporating the cross-section plastic moment reduced factors that account for these effects into calculations:

$$M_{RBSL} = \beta_{RBSL} \cdot \eta \cdot R_y \cdot f_y \cdot Z \tag{4-45}$$

$$M_{RBSR} = \beta_{RBSR} \cdot \eta \cdot R_y \cdot f_y \cdot Z \tag{4-46}$$

To prevent development of an in-span plastic hinge, the maximum flexural demand on an HBE should therefore be smaller than the available plastic strength within the span:

$$M_{span} \leq \beta_S R_y f_y Z \tag{4-47}$$

where β_S is the plastic moment reduction factor at the location of the maximum moment.

Therefore, replacing M_{PL}, M_{PR} and l in (4-43) by M_{RBSL}, M_{RBSR} and $L - 2e$ respectively, and considering (4-47), the following requirement for avoidance of in-span plastic hinge is obtained:

$$\frac{\left(\omega_{ybi} - \omega_{ybi+1}\right) \cdot \left(L - 2e\right)^2}{8} + \frac{\left[\left(\beta_{RBSL} + \beta_{RBSR}\right)\eta R_y f_y Z\right]^2}{2 \cdot \left(\omega_{ybi} - \omega_{ybi+1}\right) \cdot \left(L - 2e\right)^2} + \frac{\left(\beta_{RBSL} - \beta_{RBSR}\right)\eta R_y f_y Z}{2} \quad (4\text{-}48)$$

$$\leq \beta_S R_y f_y Z$$

This expression can be reorganized as a quadratic inequality and solved for Z, obtaining the lower bound of plastic section modulus:

$$Z_{min} = \frac{\left(\omega_{ybi} - \omega_{ybi+1}\right)\left(L - 2e\right)^2}{4R_y f_y} \cdot \frac{1}{\beta_{1R} + \sqrt{\beta_{1R}^2 - \beta_{2R}^2}} \quad (4\text{-}49)$$

where

$$\beta_{1R} = \beta_S + \frac{\left(\beta_{RBSR} - \beta_{RBSL}\right) \cdot \eta}{2} \quad (4\text{-}50)$$

$$\beta_{2R} = \frac{\left(\beta_{RBSR} + \beta_{RBSL}\right) \cdot \eta}{2} \quad (4\text{-}51)$$

Mathematically, as part of the solution to the quadratic inequality (4-48), an upper bound for the plastic section modulus also exists:

$$Z_{max} = \frac{\left(\omega_{ybi} - \omega_{ybi+1}\right)\left(L - 2e\right)^2}{4R_y f_y} \cdot \frac{1}{\beta_{1R} - \sqrt{\beta_{1R}^2 - \beta_{2R}^2}} \quad (4\text{-}52)$$

However, one can neglect this upper bound for the HBE design. As determined in (4-42), the maximum moment location will be outside of the span (i.e. $x_{span} < 0$) if the plastic moment of HBE is of significant magnitude (e.g. when Z is greater than Z_{max}), which implies that no plastic hinges will form except those at the ends of the HBE.

For the HBE without RBS connections, the lower bound plastic section modulus to prevent the in-span HBE plastic hinge is obtained by replacing β_{RBSL} and β_{RBSR} by β_L and β_R respectively, and setting $\eta = 1$ and $e = 0$ in (4-49):

$$Z_{min} = \frac{\left(\omega_{ybi} - \omega_{ybi+1}\right)L^2}{4R_y f_y} \cdot \frac{1}{\beta_1 + \sqrt{\beta_1^2 - \beta_2^2}} \qquad (4\text{-}53)$$

where

$$\beta_1 = \beta_S + \frac{\left(\beta_R - \beta_L\right)}{2} \qquad (4\text{-}54)$$

$$\beta_2 = \frac{\left(\beta_R + \beta_L\right)}{2} \qquad (4\text{-}55)$$

4.6 Moment Demand at VBE Faces

For design of an HBE having RBS connections at its ends, it is also necessary to check the adequacy of flexural strength at the VBE face to ensure satisfactory behavior of the HBE. For determining moment demand at VBE faces, a simple free body diagram is developed in figure 4-17, in which all inelastic beam action is assumed to concentrate at RBS centers.

In the figure, distributed loads (i.e. ω_{ybi}, ω_{xbi}, ω_{ybi+1} and ω_{xbi+1}) represent the infill panel yield forces; P_R and P_L respectively represent axial forces at the right and left HBE ends; M_R and M_L respectively represent moment demands at the right and left HBE ends; V_R and V_L respectively represent shear forces at the right and left HBE ends; P_{RBSR} and P_{RBSL} respectively represent axial forces at the right and left plastic hinges; V_{RBSR} and V_{RBSL} respectively represent shear forces at the right and left plastic hinges; and $\beta_{RBSR} R_y f_y Z_{RBS}$ and $\beta_{RBSL} R_y f_y Z_{RBS}$ respectively represent the reduced plastic moments at the right and left plastic hinges. For analysis purpose, the beam is divided into three segments, the middle segment between two plastic hinges, and the right and left segments outside of the plastic hinges.
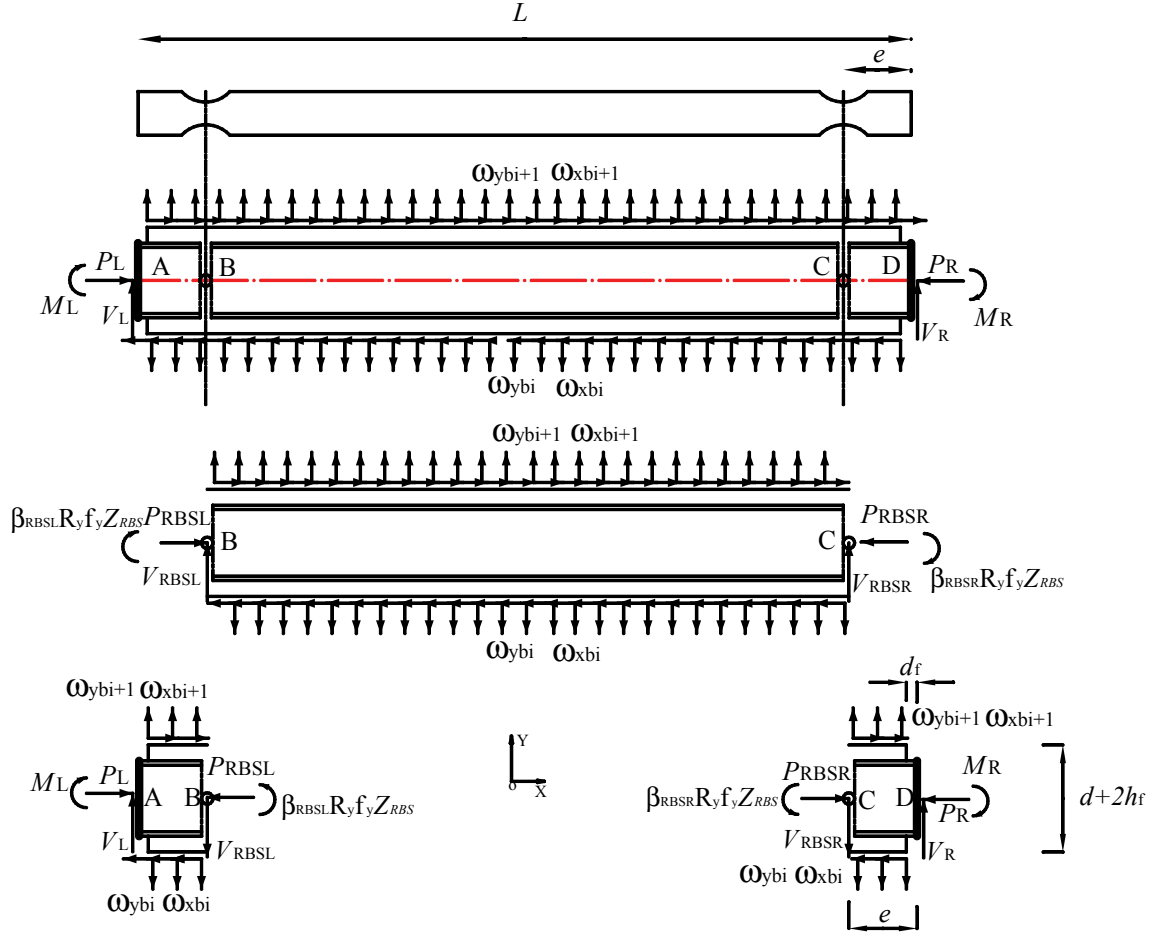
FIGURE 4-17 Free Body Diagrams of Intermediate HBE for Calculation of Moment Demand at VBE face

For the middle segment of the beam (i.e. segment BC shown in figure 4-17), the moment equilibrium to the left plastic hinge (i.e. point B) gives

$$\left(\beta_{RBSR}+\beta_{RBSL}\right)R_y f_y Z_{RBS}+\left(\omega_{ybi}-\omega_{ybi+1}\right)\left(L-2e\right)^2\big/2$$
$$+\left(\omega_{xbi}+\omega_{xbi+1}\right)\left(L-2e\right)\left(d+2h_f\right)\big/2-V_{RBSR}\left(L-2e\right)=0 \tag{4-56}$$

Solving for V_{RBSR}:

$$V_{RBSR}=\left(\beta_{RBSR}+\beta_{RBSL}\right)R_y f_y Z_{RBS}\big/\left(L-2e\right)+\left(\omega_{ybi}-\omega_{ybi+1}\right)\left(L-2e\right)\big/2$$
$$+\left(\omega_{xbi}+\omega_{xbi+1}\right)\left(d+2h_f\right)/2 \tag{4-57}$$

Similarly, based on the moment equilibrium to the right plastic hinge (i.e. point C), one can obtain

$$V_{RBSL} = \left(\omega_{ybi} - \omega_{ybi+1}\right)\left(L - 2e\right)\big/2 - \left(\beta_{RBSR} + \beta_{RBSL}\right)R_y f_y Z_{RBS}\big/\left(L - 2e\right)$$
$$- \left(\omega_{xbi} + \omega_{xbi+1}\right)\left(d + 2h_f\right)/2 \tag{4-58}$$

For the right segment of the HBE (i.e. beam segment CD shown in figure 4-17), the moment equilibrium to the right VBE face (i.e. point D) gives

$$M_R + \left(\omega_{xbi} + \omega_{xbi+1}\right)\left(d + 2h_f\right)\left(e - d_f\right)\big/2$$
$$- V_{RBSR}e - \left(\omega_{ybi} - \omega_{ybi+1}\right)\left(e - d_f\right)\left(e/2 + d_f/2\right) - \beta_{RBSR}R_y f_y Z_{RBS} = 0 \tag{4-59}$$

Solving for M_R:

$$M_R = \beta_{RBSR}R_y f_y Z_{RBS} + V_{RBSR}e$$
$$+ \left(\omega_{ybi} - \omega_{ybi+1}\right)\left(e - d_f\right)\left(e/2 + d_f/2\right) \tag{4-60}$$
$$- \left(\omega_{xbi} + \omega_{xbi+1}\right)\left(d + 2h_f\right)\left(e - d_f\right)\big/2$$

For the left segment of the HBE (i.e. beam segment AB shown in figure 4-17), the moment equilibrium to the left VBE face (i.e. point A) gives

$$M_L = \beta_{RBSL}R_y f_y Z_{RBS} - V_{RBSL}e$$
$$- \left(\omega_{ybi} - \omega_{ybi+1}\right)\left(e - d_f\right)\left(e/2 + d_f/2\right) \tag{4-61}$$
$$- \left(\omega_{xbi} + \omega_{xbi+1}\right)\left(d + 2h_f\right)\left(e - d_f\right)\big/2$$

Note that the moment demands at VBE faces determined from (4-60) and (4-61) should compare with the available plastic moment resistance of those cross-sections using the procedures proposed in Section 3. As a result, the flexural strengths at the left and right VBE faces can be obtained respectively:

$$M_{L.Strength} = \beta_L R_y f_y Z \tag{4-62}$$

$$M_{R.Strength} = \beta_R R_y f_y Z \tag{4-63}$$

92

where β_L and β_R are the cross-section plastic moment reduction factors of the left and right VBE faces, respectively.

4.7 FE Verification and Design Recommendations

To check the adequacy of the analytical models proposed in Sections 4.3 to 4.6 for determining the axial force, shear forces and moment demand at VBE faces, and to prevent of in-span HBE plastic hinge, FE analyses on an intermediate HBE having RBS connections were conducted. Using the MCEER/NCREE specimen described in Qu *et al.* (2008) as a prototype SPSW, the intermediate HBE was redesigned using the design demands per the developed analytical models.

This section first describes the FE model of the redesigned intermediate HBE. Then, axial forces, shear forces and moments at VBE faces of the redesigned HBE obtained from the FE analysis were compared with those predicted using the analytical models proposed in Sections 4.3 to 4.6. Finally, additional recommendations to use the proposed analytical models in design practices are also presented.

The resulting new intermediate HBE is a W24x76 member, replacing the original H350x252x11x19 member. RBS connections were also used in the new HBE. The cross-section properties and flange reduction geometries of the redesigned and original members are summarized in table 4-4.

**TABLE 4-4 Summary of Cross-Section Properties and
Flange Reduction Geometries**

HBE	d (mm)	b_f (mm)	t_f (mm)	t_w (mm)	a^{*} (mm)	b^{*} (mm)	c^{*} (mm)
Original	350	252	19	11	135	230	48
Redesigned	607	228	17.3	11.2	160	486	57

* flange reduction geometry parameters described in figure 4-19

The redesigned intermediate HBE was modeled in ABAQUS/Standard. Shell elements (ABAQUS element, S4R) were used for the web and flanges. A total of 17,280 elements were used in the model. Material was assumed to have a yield strength of 346MPa with isotropic and elasto-perfectly plastic constitutive behavior. The beam flanges were reduced according to the geometries presented in table 4-4.

93

The FE analysis was conducted in two stages. In the first stage, the uniformly distributed loads, ω_{yb1}, ω_{xb1}, ω_{yb2} and ω_{xb2}, which were respectively determined to be 557 N/mm, 492 N/mm, 400 N/mm, and 353 N/mm, using the actual thicknesses, yield strengths, and inclination angles of the infill panels at the first and second story of the MCEER/NCREE specimen, were applied along the top and bottom edges of the HBE web to represent the infill panel yield forces. At the same time, both ends of the beam were fully fixed except that the axial restraint at the right end was released and an axial load (P_R) was applied to replicate the axial force in the HBE. Magnitude of that axial load was determined by setting $x = L$ in (4-17). In the second stage, a displacement controlled method of analysis was used. HBE end rotations with identical magnitude up to 0.035 rad, which corresponded to rightward sway of the SPSW, were applied at the ends of the HBE to obtain the shear and moment demands at VBE faces.

In the FE analysis, no in-span plastic hinge developed in the redesigned HBE. The axial forces, shear forces and moment demands at the left and right VBE faces obtained from the FE analysis are shown in table 4-5, together with those predicted using the approaches proposed in Sections 4.3 to 4.5.

TABLE 4-5 Design Forces at VBE face

VBE Face	Design forces	Finite element analysis	Plastic analysis based on free body diagrams with plastic hinge location taken as			
			Center of RBS		Proposed for design	
			Value	Error (%)	Value	Error (%)
Left	Axial Force (kN)	1426	1426	-*	1426	-*
	Shear Force (kN)	432	395	-8.6	455	5.3
	Moment (kNm)	729	632	-13	809	11
Right**	Axial Force (kN)	941	941	-*	941	-*
	Shear Force (kN)	981	945	-3.7	1005	2.4
	Moment (kNm)	875	842	-3.8	876	0.1

-* not applicable.
-** control the design.

As shown in the table, the predictions agree reasonably well with the FE results. The difference between those predictions and FE results mainly comes from the simplification of plastic hinge location in the free body diagrams shown in figures 4-15 and 4-17, in which the plastic hinges are assumed to form ideally at the center of the RBS (i.e. where

the beam flange is reduced most severely). However, it is not the actual case due to the presence of variable axial force, shear force, and vertical stresses in the HBE.

To illustrate the actual location of plastic hinging in an HBE, the yielding pattern of the bottom flange at the right RBS connection at the onset of inelastic behavior obtained from the FE analysis is shown in figure 4-18a. Note that the yielding zones are represented by the shaded areas. This shows that the center of the yielding zone and thus the location of the lumped plastic hinge moves towards the near VBE face. At the time of this writing, no experiments have been conducted on the redesigned HBE to confirm the above observations from FE analysis. However, similar yielding patterns in the HBEs were consistently observed during the MCEER/NCREE tests and the recent NCREE tests on SPSWs (Lee and Tsai, 2008) as shown in figures 4-18b, c and d, respectively. Note that the yielding parts in the specimens are represented by the flaked whitewash. For comparison purpose, the yielding pattern of RBS in steel moment frame observed from previous tests (Zhang and Ricles, 2006) is presented in figures 4-18e. As shown, the plastic hinge forms at the center of the RBS in steel moment frame, which is different from the plastic hinge location observed in the HBE.

The yielding pattern in the web of the redesigned HBE is presented in figure 4-18f. As shown, the yielding zones spread over a large area in the HBE web due to the presence of significant bi-axial and shear stresses as discussed in detail in Section 3. Similar yielding behavior was also consistently observed during the MCEER/NCREE tests as shown in figure 4-18g. For comparison purpose, the yielding pattern in the beam web observed from the prior tests on the beam having RBS in steel moment frame (Jones *et al.* 2002) is presented in figure 4-18h. As shown, the yielding zones concentrated around the RBS center line in steel moment frame, which is different from the yielding pattern of HBE web described above.
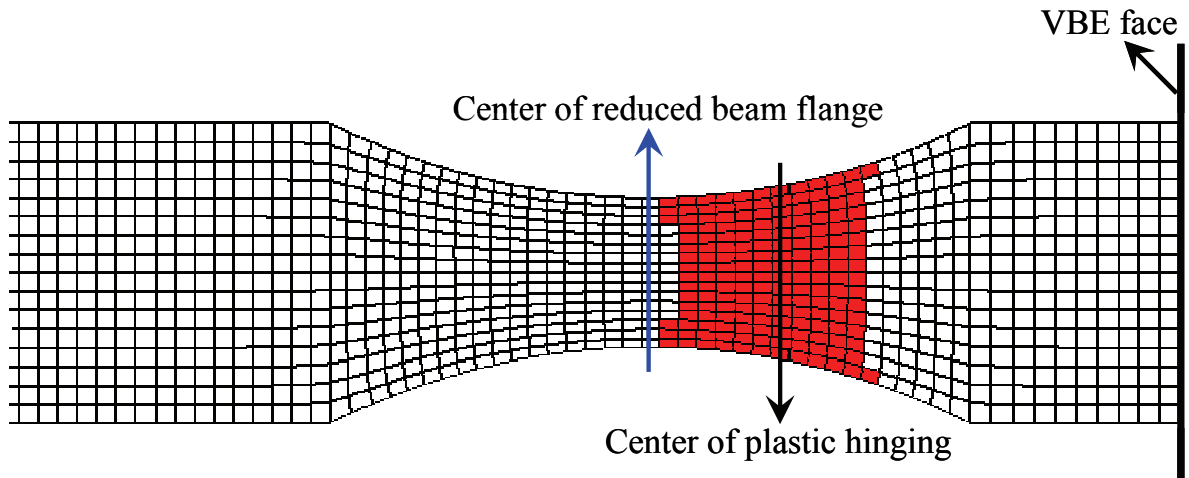
(a) Flange of the redesigned intermediate HBE-FE model
(at the onset of inelastic behavior)
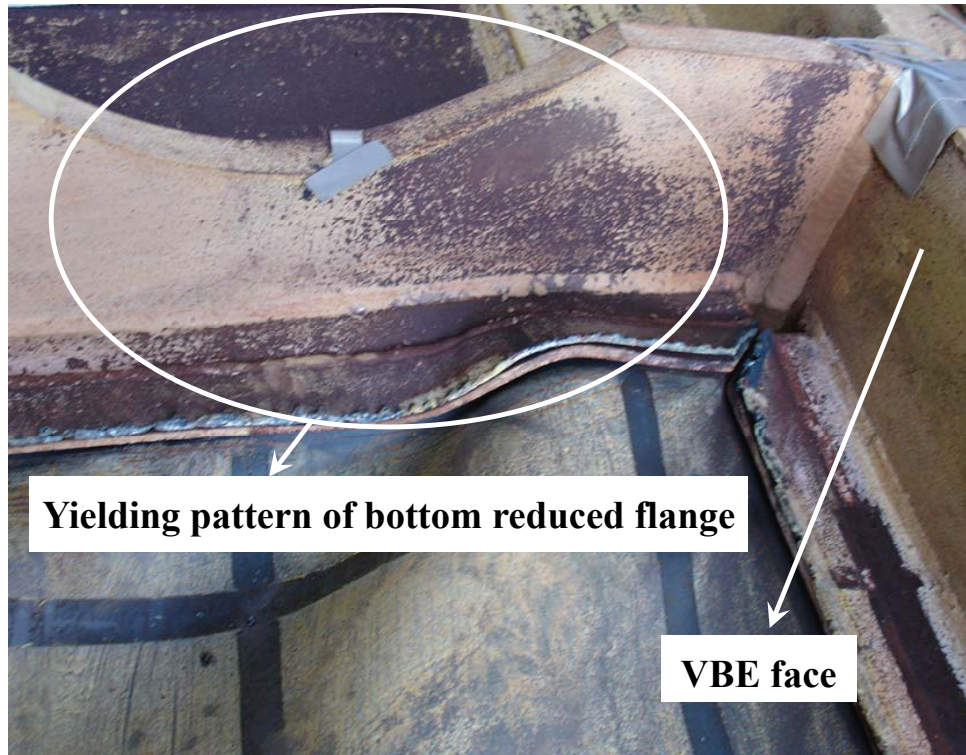
(b) Flange of the intermediate HBE-MCEER/NCREE SPSW
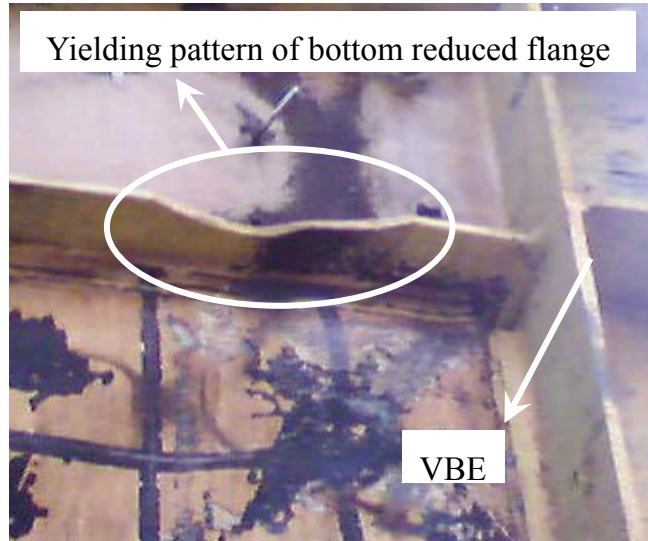
**(c) Flange of the intermediate HBE in recent NCREE testing
(K.C. Tsai, NCREE, 2007, personal communication, Photo by M. Bruneau)**
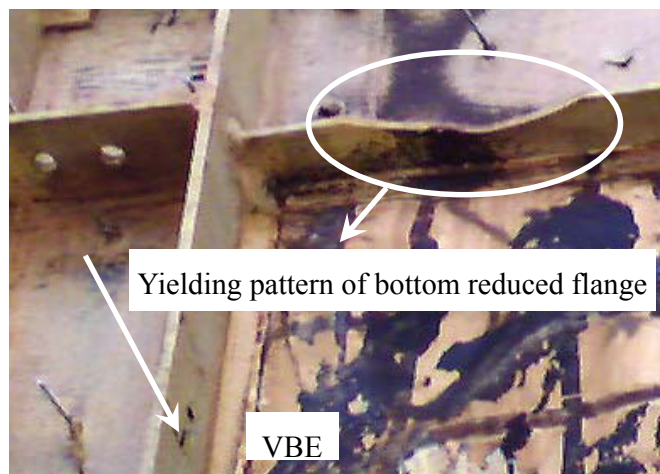
**(d) Flange of the intermediate HBE in recent NCREE testing (K.C. Tsai, NCREE,
2007, personal communication, Photo by M. Bruneau)**
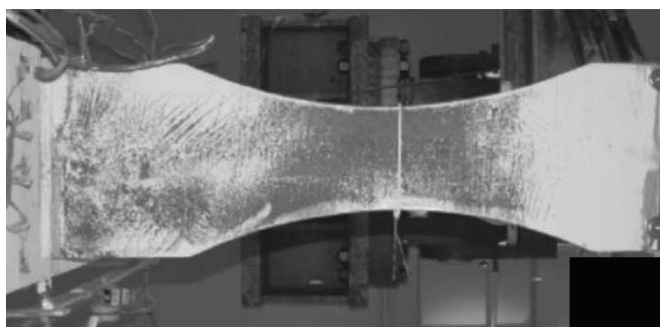
(e) Flange of the beam with RBS in moment frame (from Zhang and Ricles, 2006)
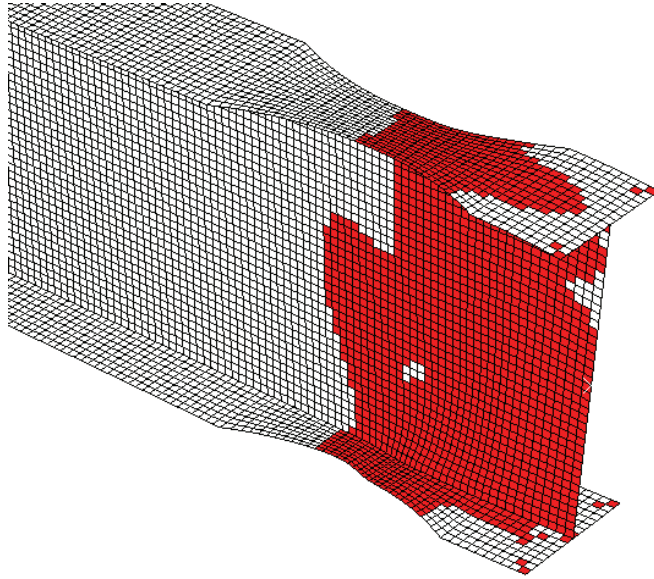
(f) Web of the redesigned intermediate HBE at the end of the FE analysis

(g) Web of the intermediate HBE at the end of MCEER/NCREE testing

(h) Web of the beam with RBS in moment frame (from Jones *et al.* 2002)

FIGURE 4-18 Yielding Patterns at RBS

For design purposes, for greater accuracy, it is possible to account for the actual location of plastic hinge. Calculation of the distance from the center of the reduced beam flange to the actual plastic hinge location toward the VBE face can be simplified by assuming that the plastic section modulus of the actual plastic hinge is equal to the average of the plastic section moduli of the unreduced part of the HBE and that at the RBS center, which is

$$Z_{RBS} = \frac{(1+\eta)}{2} Z \tag{4-64}$$

Accordingly, the distance, e, as shown in figures 4-15 and 4-17, can be calculated as

$$e = a + \frac{b}{2} - \Delta x \tag{4-65}$$

where Δx is the distance between RBS center and the assumed plastic hinge as shown in figure 4-19:

$$\Delta x = \sqrt{2 \cdot \Delta y \cdot R - \Delta y^2} \tag{4-66}$$

99

where Δy is the flange width difference between the RBS center and the assumed plastic hinge, and R is the radius of the arc cutout of reduced beam flange as shown in figure 4-19:

$$\Delta y = \frac{(1-\eta)Z}{4t_f\left(d-t_f\right)}$$ (4-67)

$$R = \frac{4c^2 + b^2}{8c}$$ (4-68)
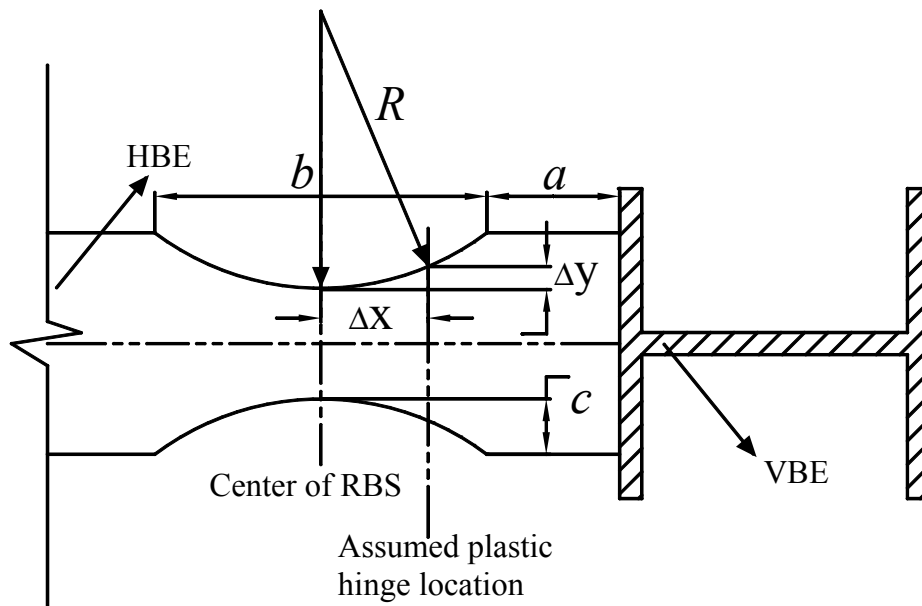
FIGURE 4-19 Geometries of RBS Connections

Beyond this difference, the rest of the procedure established on the basis of free body diagrams in figures 4-15 and 4-17 remain valid. Results obtained using this modified approach are presented in table 4-5. It is observed that this modified approach provides more accurate estimate for moment at the side governing the design (i.e. right VBE face). For shear, the accuracy is not significantly improved, however; at least, the modified approach provides conservative estimate by 2.4% as supposed to be unconservative by 3.7% from the model assuming plastic hinge developed at the RBS center.

Detailed calculation for the results for estimating HBE design forces using each assumed plastic hinge location are provided in Appendixes B, and C.

4.8 Capacity Design Procedure for Intermediate HBEs

Based on the concepts presented in Sections 4.2 to 4.7, a capacity design procedure is proposed for intermediate HBEs. It differs from the current design approach in that it: (i) considers the reduced plastic moment strength of HBE to account for the presence of axial load, shear force and vertical stresses in HBE web due to infill panel yield forces; (ii) is able to capture the fact that resultant action of the vertical tension field components is not equally resisted by each end of the HBE; and (iii) accounts for the variation of plastic hinge location in HBE when RBS connections are used.

The proposed procedure for capacity design of an intermediate HBE having RBS connections is illustrated in figure 4-20. Design steps of this procedure are outlined below:

Step 1. Assume an intermediate HBE cross-section;

Step 2. Calculate infill panel yield forces following the approach presented in Section 4.2;

Step 3. Determine the axial force in HBE per (4-17), and the vertical stresses in HBE web (per (3-28) and (3-29) proposed in Section 3);

Step 4. Select the flange reduction geometries in compliance with the design specifications and guidelines such as FEMA 350. Determine the location and plastic section modulus of plastic hinge in accordance with figure 4-19. Assume plastic moment reduction factors of the plastic hinges (i.e. β_{RBSR} and β_{RBSL}) for the initial iteration of the design process;

Step 5. Determine the shear forces at plastic hinges per (4-57) and (4-58);

Step 6. Based on the approaches proposed in Section 3, calculate the plastic moment reduction factors of plastic hinges. If the calculated factors are close enough to those assumed in step 4, continue the design. Otherwise, return to step 4 and modify the assumed plastic moment reduction factors;

Step 7. Calculate the maximum moment location in the HBE per (4-42). If the obtained result is negative, which means the maximum moment develops out-of-span, go to step 8. Otherwise, calculate the plastic moment reduction factor at the maximum moment location and check (4-49). If (4-49) is not satisfied, return to step 1 and modify the assumed HBE cross-section.

Step 8. Calculate the shear forces at VBE faces per (4-37) and (4-38). Determine the plastic moment reduction factors at VBE faces based on the approaches proposed in Section 3. Obtain the moment strengths at VBE faces per (4-62) and (4-63).

Step 9. Calculate moment demands at VBE faces per (4-60) and (4-61). If the strengths are greater than the demands obtained in step 8, design is acceptable. Otherwise, return to step 1 and modify the assumed HBE cross-section.
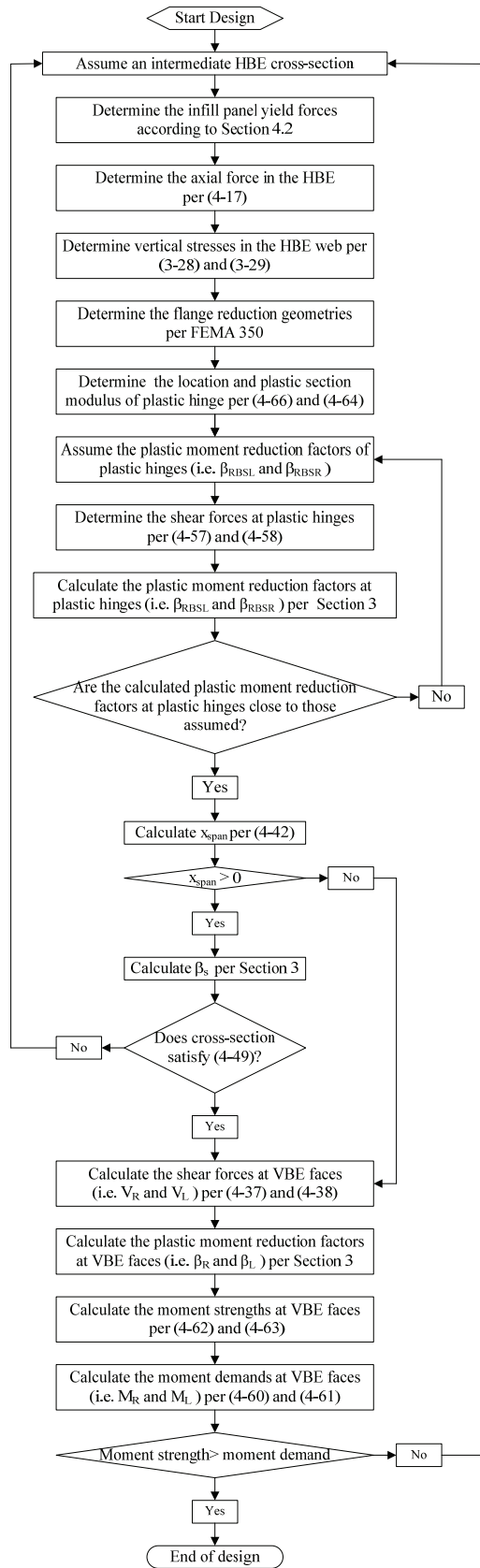
FIGURE 4-20 Design Procedure of Intermediate HBEs Having RBS Connections

For capacity design of an intermediate HBE without RBS connections, the proposed procedure is illustrated in figure 4-21. Design steps of this procedure are summarized below:

Step 1. Assume an intermediate HBE cross-section;

Step 2. Calculate infill panel yield forces according to the approach presented in Section 4.2;

Step 3. Determine the axial force per (4-17);

Step 4. Determine the vertical stresses in HBE web per equation (3-28) and (3-29);

Step 5. Assume the plastic moment reduction factors at the HBE ends (i.e. β_R and β_L)

Step 6. Determine the shear forces at the HBE ends per (4-39) and (4-40)

Step 7. Based on the approaches proposed in Section 3, calculate the plastic moment reduction factors at the HBE ends. If the calculated factors are close enough to those assumed in step 5, continue the design. Otherwise, return to step 5 and modify the assumed plastic moment reduction factors;

Step 8. Calculate the maximum moment location of the HBE per (4-42).If the obtained result is negative, which means the maximum moment develops out-of-span, accomplish the design. Otherwise, calculate the plastic moment reduction factor at the maximum moment location and check (4-49). If (4-49) is satisfied, design is acceptable. Otherwise, return to step 1 and modify the assumed HBE cross-section.

Start Design

Assume an intermediate HBE cross-section

Determine the infill panel yield forces according to Section 4.2

Determine axial force in the HBE per (4-17)

Determine vertical stresses in the HBE web per (3-28) and (3-29)

Assume plastic moment reduction factors of HBE ends (i.e. β_R and β_L) per Section 3

Determine the shear forces at HBE ends per (4-39) and (4-40)

Calculate plastic moment reduction factors at HBE ends (i.e. β_L and β_R) per Section 3

Are the calculated plastic moment reduction factors at plastic hinges close to those assumed? — No

Yes

Calculate x_{span} per (4-42)

$x_{span} > 0$ — No

Yes

Calculate β_s per Section 3

Does cross-section satisfy (4-49)? — No

Yes

End of design

FIGURE 4-21 Design Procedure of Intermediate HBEs without RBS Connections

105

It should be noted that gravity loads have not been considered in the free body diagrams of this section, as they will usually be relatively small in SPSWs. However if so desired, they can be considered by adding them to the vertical components of the infill panel yield forces that are applied to the intermediate HBE. Additionally, derivations in this paper neglect strain hardening since steel in the verification FE example was assumed to have an elasto-perfectly plastic constitutive behavior. However, to achieve capacity design, the factor, C_{pr}, to account for strain hardening as per FEMA 350 (FEMA 2000) should be incorporated into determination of the plastic hinge strength in RBS. Furthermore, anchor HBEs, as a special case of intermediate HBEs, may be also considered by the proposed procedure with a tension field acting on only one side.

4.9 Examination of Intermediate HBE Fractures in Tests

As described in Qu *et al.* (2008), during the tests of the MCEER/NCREE SPSW specimen, the intermediate HBE, which used RBS connections, developed complete fractures at the ends of its flanges, but, no fractures in the reduced beam flange regions. This section examines behavior of the intermediate HBE of the MCEER/NCREE SPSW specimen in light of the knowledge developed in Sections 3 and 4.

Although many effects may have contributed to the unexpected failure in the intermediate HBE of the MCEER/NCREE SPSW specimen, flexural strength deficiency at VBE faces is a factor worthy of investigation. A preliminary assessment can be made by comparing the design moment demands and available flexural strengths at the VBE faces. Based on the intermediate HBE design procedure proposed in Section 4.8, the flexural demands and strengths of the original HBE are obtained and presented in table 4-6.

Effects of material strain hardening, composite floor, ancillary floor truss and fish plates in the MCEER/NCREE SPSW specimen are neglected here for simplicity. Note that these effects result in higher plastic hinge moments and higher design demands at VBE faces. For comparison purpose, the design moments and strengths of a redesigned HBE are also provided in table 4-6. The redesigned HBE is a W24x76 member, as mentioned in Section 4.7.

106

TABLE 4-6 Design Demands and Available Strengths at VBE Faces

HBE	Left VBE face		Right VBE face	
	$M_{L.Demand}$ $(kN \cdot m)$	$M_{L.Strength}$ $(kN \cdot m)$	$M_{R.Demand}$ $(kN \cdot m)$	$M_{R.Strength}$ $(kN \cdot m)$
Original	660	774	748	571
Redesigned	809	951	876	897

As shown in the above table, at the right VBE face, the flexural strength of the original HBE is smaller than the demand. This would explain the unexpected failure (i.e. fractures at the HBE ends) observed during the tests. By comparison, the redesigned HBE strengths are greater than demands, suggesting it would not have likely suffered from the observed premature failure.

4.10 Summary

The effects of axial and shear forces in intermediate HBEs have been studied in this section using plastic mechanisms and simple free body diagrams. A design procedure to achieve capacity design of intermediate HBEs has also been proposed. This procedure prevents the HBE in-span plastic hinge and ensures adequate moment capacity at the VBE faces when RBS connections are used. FE analyses were used to validate the proposed approach. Finally, behavior of the intermediate HBE of the tested SPSW specimen was examined and explained using the knowledge and methodologies developed in Sections 3 and 4.

SECTION 5

BEHAVIOR OF VERTICAL BOUNDARY ELEMENTS

5.1 Introduction

Building on the knowledge developed in the prior sections for the capacity design of HBEs, it would be interesting and apropos to investigate the current design approach of VBEs. The early Canadian provisions for SPSW (i.e. CSA S16-95, CSA 1994) required the VBEs to be designed as beam-column using a conventional strength-based approach. This approach was challenged by the results of tests on quarter-scale SPSW specimens conducted at the University of British Columbia (UBC), Canada (Lubell *et al.* 2000), in which the VBEs designed using the strength-based approach exhibited undesirable premature out-of-plane buckling or significant "pull-in" deformations in VBEs. Members of the CSA S16 committee ascribed these observed failures to the insufficient VBE stiffness. If VBEs deform excessively, they may be unable to anchor the infill panel yield forces. A non-uniform diagonal tension field may then develop and solicit the VBEs inconsistently to the design assumptions.

To ensure adequately stiff VBEs, CSA S16-01 (CSA 2000) introduced the flexibility factor, ω_t, proposed in the previous analytical work and development of plate girder theory, as an index of VBE flexibility. Noting that the Lubell *et al.* specimens had a flexibility factor of 3.35, and that all other known tested specimens that behaved in a ductile manner had a flexibility factor of 2.5 or less (e.g. Driver's specimen had a flexibility factor of 1.73, Driver *et al.* 1997), CSA S16-01 empirically specified an upper bound of 2.5 on the flexibility factor. Note that this requirement can be converted into the flexibility requirement for VBE design presented in the current design codes as demonstrated later.

In design, the intent is that the aforementioned flexibility limit prevents the excessively slender VBE. However, beyond the empirical observations and analogy to plate girder theory, no work has investigated whether the significant inward inelastic deformations of VBEs observed in some past tests were directly caused by the excessive VBE flexibilities

109

or due to other causes, such as shear yielding at the ends of VBEs. In addition, no theoretical research has established a relationship between the flexibility factor, ω_t, and the out-of-plane buckling strength of VBE as part of SPSW behavior.

To better understand the above issues, the derivation of flexibility factor developed in plate girder theory is first reviewed in this section, followed by the description of how that factor was incorporated into the current design codes. Then, analytical models for preventing the shear yielding and estimating the out-of-plane buckling strength of VBEs are developed. Finally, results for some previously tested SPSWs are revisited and assessed to validate the proposed analytical models.

5.2 Review of Flexibility Factor in Plate Girder Theory

A typical SPSW, as the one shown in figure 5-1, consists of boundary frame members (i.e. HBEs and VBEs) and infill panels. In the SPSW literature, the analogy that the behavior of a SPSW is similar to that of a cantilever vertical plate girder has often been made. Using this analogy, the story height and bay width of a SPSW are analogous to the stiffener spacing and depth of a plate girder, respectively. Note that this analogy has only qualitative merits in providing a conceptual understanding of the VBE behavior in a SPSW. Berman and Bruneau (2004) has identified that many significant differences exist in the strengths and behavior of these two systems.
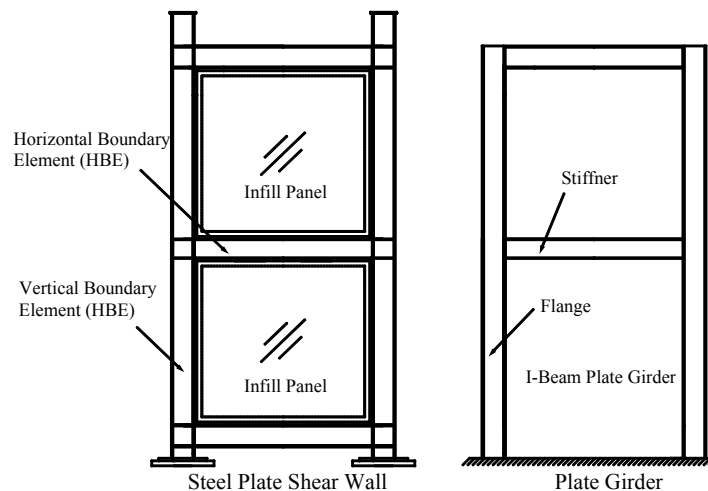
**FIGURE 5-1 Typical Steel Plate Shear Wall and
Analogous Vertical Cantilever Plate Girder**

110

Nonetheless, plate girder studies provided the theoretical framework from which equation (5-1) that will be introduced in detail later was originally derived. The current design specifications (the 2005 AISC Seismic Provisions and CSA S16-01) reference Wagner's analytical studies (Wagner 1931) on elastic behavior of the girders with thin metal webs (referred to as "flat sheet girder" in the literature of those days) subjected to transverse shear, where a method for determining the minimum moments of inertia of flanges to ensure a sufficiently uniform tension field across the web plate has been developed. Since that method is the one underlying the current flexibility limit for VBE design, a brief review of that study is presented here. The symbols used in the original work have been changed to fit the nomenclatures used for SPSW designs (i.e. consistent with the notation used in previous sections).

Wagner's analysis postulated that the deformation of a cantilever plate girder under transverse load can be schematically shown as in figure 5-2. The subscripts "o" and "u" are assigned to the variables corresponding to the top and bottom flanges, respectively.
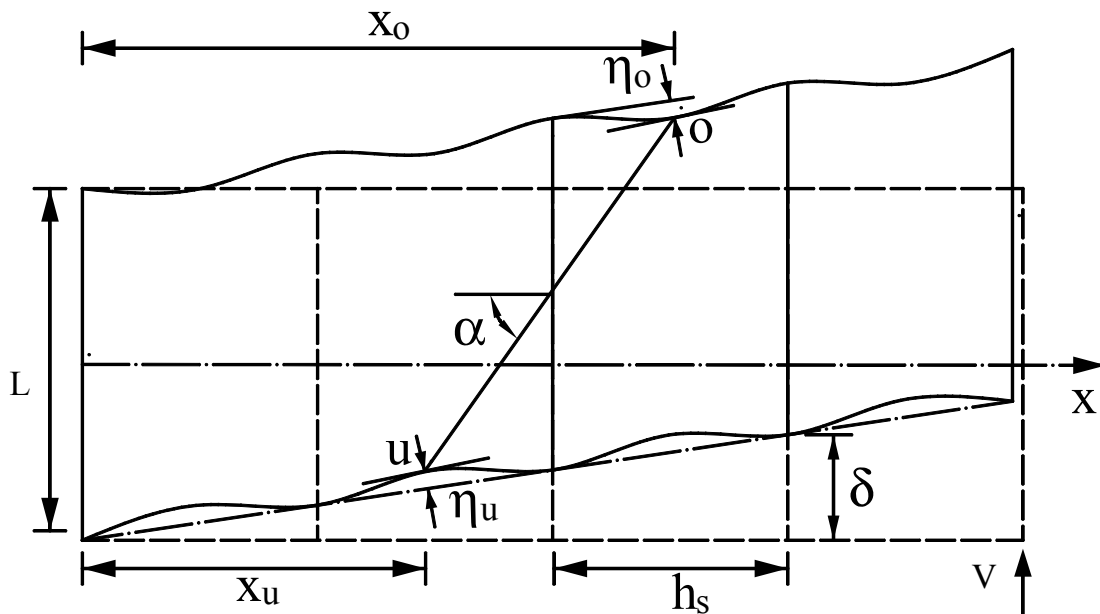
**FIGURE 5-2 Deformation of a Cantilever Plate Girder under Transverse Load
(Adapted from Wagner 1931)**

As shown in figure 5-2, plate girder flange deformation is obtained by the superposition of two effects, namely: global deflection of the plate girder due to transverse load,

111

represented by δ, and local deflections of the flanges between neighbouring stiffeners due to web tension actions, represented by η_u and η_o. In figure 5-2, L is the depth of the plate girder; and α is the inclination of infill web tension actions.

Uniformity of the tension field across web plate of the girder depends on the flexibility of flanges. To better understand this, consider the effect of a single tension diagonal, which is denoted by line "*uo*" in figure 5-2. When the flanges are flexible and develop inward deflections (i.e. η_u and η_o shown in figure 5-2) under the web plate forces, the elongation of *uo* decreases, compared to the case when rigid flanges would be present, as a result of deformation compatibility. Note that this effect varies along the flanges (i.e. the elongations of tension diagonals at different locations are different), resulting in uneven tension fields across the web plate. For flanges infinitely rigid in bending, there would be no local deflections of flanges between neighbouring stiffeners, resulting in a uniform tension field across the web plate.

Modeling each flange of the plate girder as a continuous beam on elastic foundations, and accounting for the real load distribution along each flange, which can be determined by superposing the uniform load obtained assuming that the flanges are infinitely rigid and the loss of this uniform load due to flange flexibility, Wagner (1931) derived the following governing equation for the local flange deflections:

$$\frac{d^4\left(\eta_u-\eta_o\right)}{dx^4}=\left(\frac{1}{I_u}+\frac{1}{I_o}\right)t_{wi}\sin^2\alpha\varepsilon_g-\left(\frac{1}{I_u}+\frac{1}{I_o}\right)\frac{t_{wi}\sin^4\alpha}{L}\left(\eta_u-\eta_o\right) \qquad (5\text{-}1)$$

where η_u and η_o are the deflections of the bottom and top flanges due to web tension actions respectively;

I_u and I_o are moments of inertia of the bottom and top flanges respectively;

α is the inclination angle of the web plate tension action;

t_{wi} is the web plate thickness;

L is the depth of the plate girder which corresponds by analogy to the width of a SPSW;

and ε_g is the strain in the tension diagonals assuming that the flanges are rigid.

Equation (5-1) is a fourth order ordinary differential equation and can be solved for $(\eta_u - \eta_o)$ using classic procedures. The maximum value of $(\eta_u - \eta_o)$, which corresponds to the maximum loss of the elongation of tension diagonal (i.e. an index of the maximum loss of the uniform load along the flanges), is:

$$(\eta_u - \eta_o)_{max} = \frac{\varepsilon_g L}{\sin^2 \alpha}\left(1 - \frac{\sin\left(\frac{\omega_t}{2}\right)\cosh\left(\frac{\omega_t}{2}\right) + \cos\left(\frac{\omega_t}{2}\right)\sinh\left(\frac{\omega_t}{2}\right)}{\sin\left(\frac{\omega_t}{2}\right)\cos\left(\frac{\omega_t}{2}\right) + \sinh\left(\frac{\omega_t}{2}\right)\cosh\left(\frac{\omega_t}{2}\right)}\right) \qquad (5\text{-}2)$$

where ω_t is a flexibility factor, defined as:

$$\omega_t = h_{si} \sin \alpha \sqrt[4]{\left(\frac{1}{I_u} + \frac{1}{I_o}\right)\frac{t_{wi}}{4L}} \qquad (5\text{-}3)$$

where h_{si} is the spacing between neighbouring stiffeners in a plate girder (which corresponds by analogy to story height of a SPSW).

As explicitly expressed in (5-3), when increasing the stiffness of flanges of a SPSW (i.e. increasing I_u and I_o), the corresponding flexibility factor would decrease for given values of the other terms.

To assess the uniformity of the web tension field, a stress uniformity ratio, $\sigma_{mean}/\sigma_{max}$, was proposed and calculated as:

$$\frac{\sigma_{mean}}{\sigma_{max}} = \frac{2}{\omega_t} \cdot \frac{\cosh(\omega_t) - \cos(\omega_t)}{\sinh(\omega_t) + \sin(\omega_t)} \qquad (5\text{-}4)$$

where σ_{mean} is the mean of the web tension force components paralleling with the stiffener; σ_{max} is the maximum of the web tension force components paralleling with the stiffener.
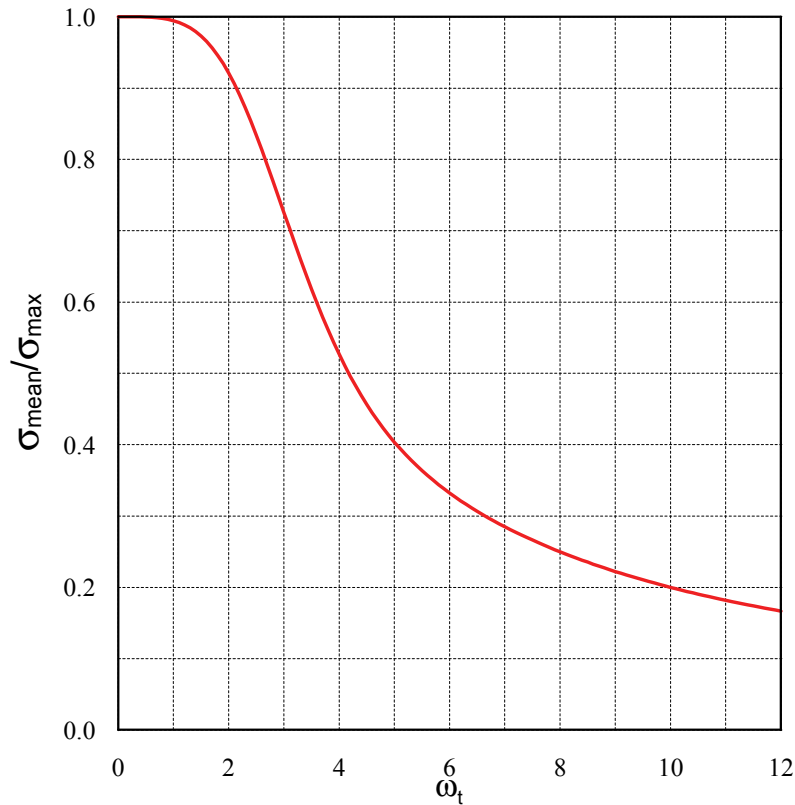
FIGURE 5-3 Relationship between the Flexibility Factor and the Stress Uniformity Ratio

The relationship between the stress uniformity ratio (i.e. $\sigma_{mean}/\sigma_{max}$) and the flexibility factor (i.e. ω_t) is shown in figure 5-3. As shown on that curve, for smaller values of ω_t (e.g. in the range $0 \leq \omega_t \leq 1$), for which the plate girder has relatively stiff flanges, the stress uniformity ratio approximately equals one (which physically means that the maximum stress is close to the average stress), indicating development of a uniform web tension field. However, with increases in the flexibility factor, the stress uniformity ratio decreases, indicating formation of a less uniform web tension field in plate girders having more flexible flanges.

For simplicity, Kuhn *et al.* (1952) simplified equation (5-3), by assuming $\alpha = 45°$, for which $\sin\alpha = 0.7$, and by substituting the algebraic equivalency $\left(\dfrac{1}{I_u} + \dfrac{1}{I_o} \right) = \dfrac{4}{\left(I_u + I_o \right)}$, to obtain:

$$\omega_t \approx 0.7 h_s \sqrt[4]{\frac{t_{wi}}{\left(I_u + I_o \right) L}} \tag{5-5}$$

Kuhn *et al.* (1952) proposed the stress amplification factor, C_2, which can be determined from the following equation, to characterize the uniformity of web tension field:

$$\sigma_{\max} = (1 + C_2)\sigma_{\text{mean}} \tag{5-6}$$

As expressed in (5-6), the stress amplification factor, C_2, captures the difference between $\sigma_{\max}$ and σ_{mean}. Large value of the stress amplification factor corresponds to a significant difference between $\sigma_{\max}$ and σ_{mean}, indicating the formation of a less uniform web tension field. Solving for C_2 with respect to the stress uniformity ratio (i.e. $\sigma_{\text{mean}}/\sigma_{\max}$) from (5-6) and recalling (5-4), the relationship between C_2 and ω_t can be obtained and is illustrated in figure 5-4.

Consistent with figure 5-3, the curve shown in figure 5-4 indicates that a less uniform tension field (which corresponds to a greater value of C_2) will develop in a plate girder with more flexible flanges (which corresponds to a greater value of ω_t).
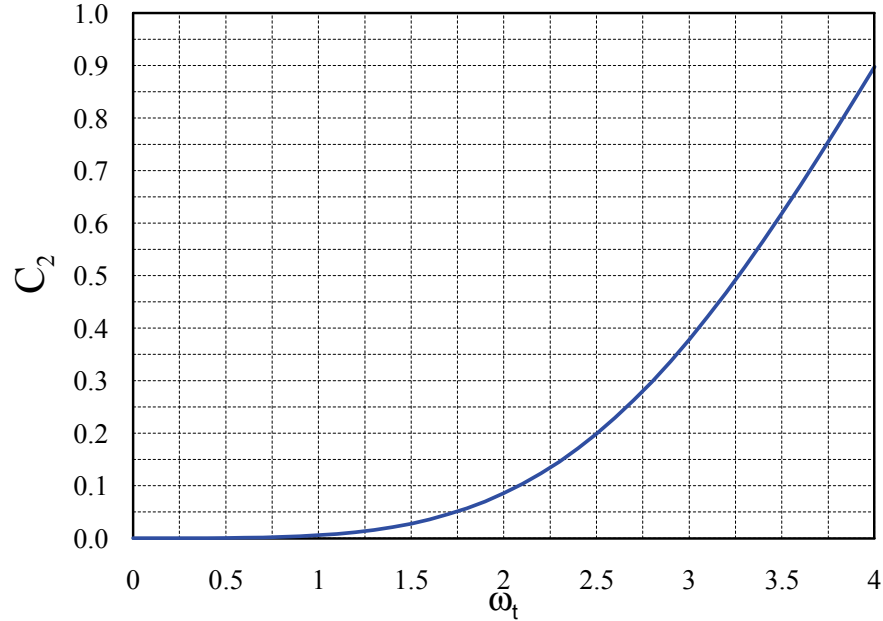
**FIGURE 5-4 Relationship between the Flexibility Factor and
the Stress Amplification Factor**

5.3 Flexibility Limit for VBE Design

To quantify the minimum VBE flexural stiffness needed to ensure uniformity of elastic infill tension fields in SPSWs and avoid the undesirable behavior of VBEs described previously, CSA S16-01 adopted (5-5). Provided that each VBE has the same moment of inertia, I_c, as normally the case in SPSWs, (5-5) becomes:

$$\omega_t = 0.7 h_{si} \sqrt[4]{\frac{t_{wi}}{2 I_c L}}$$ (5-7)

For reasons described earlier, the CSA S16 committee elected to limit this factor to a maximum value of 2.5 in SPSWs. This limit of 2.5 was agreed to be desirable on the assumption that tension fields should be sufficiently uniform for ductile behavior to develop. This limit was also selected on the assumption that tension fields should be sufficiently uniform for ductile behavior to develop. In figure 5-4, limiting the flexibility factor to a value of 2.5 is shown to correspond to a maximum stress not exceeding by more than 20% the average stress of the web tension field. Mathematically, imposing this limit on (5-7), gives:

116

$$\omega_t = 0.7 h_{si} \sqrt[4]{\frac{t_{wi}}{2 I_c L}} \leq 2.5 \qquad (5\text{-}8)$$

Solving for I_c leads to the following flexibility requirement, first implemented in CSA S16-01.

$$I_c \geq \frac{0.00307 t_{wi} h_{si}^{4}}{L} \qquad (5\text{-}9)$$

This requirement was subsequently adopted in the NEHRP Provisions (National Earthquake Hazards Reduction Program Provisions for Seismic Regulations for New Buildings and Other Structures, also known as FEMA 450, FEMA, 2004), and then the 2005 AISC Seismic Provisions (AISC, 2005)

Note that the analytical work by Wagner (1931) and Kuhn *et al.* (1952) for plate girders, from which the aforementioned empirically based flexibility limit of SPSWs was determined, assumed elastic behavior. Although at the onset of the tension field action, the maximum stress in an infill panel may be significantly greater than the average due to VBE deflections, this difference could decrease upon greater story drifts, provided that the boundary frame members are able to allow infill panel stress redistribution after the first yielding of tension diagonals. To better understand this, stress distributions across the first-story web plates (i.e. along the direction perpendicular to the tension diagonals) are shown in figure 5-5 for two tested specimens, namely, the specimen tested by Driver (1997) and the specimen, SPSW S, tested by Lee and Tsai (2008). Note that these two specimens have different flexibility factors and will be introduced in further details in a later section. Figure 5-5 shows that, as drift levels progressively increase, both specimens will ultimately develop uniform tension fields, although the specimen tested by Lee and Tsai (which had more flexible VBEs) develops less uniform tension fields at lower drift levels. This observation of identical uniform stress distribution in the panels of SPSW raises questions on the relevance of the flexibility factor, ω_t, in SPSW design. For that reason, different models are investigated in the next sections to rationalize desirable and undesirable VBE behaviors.
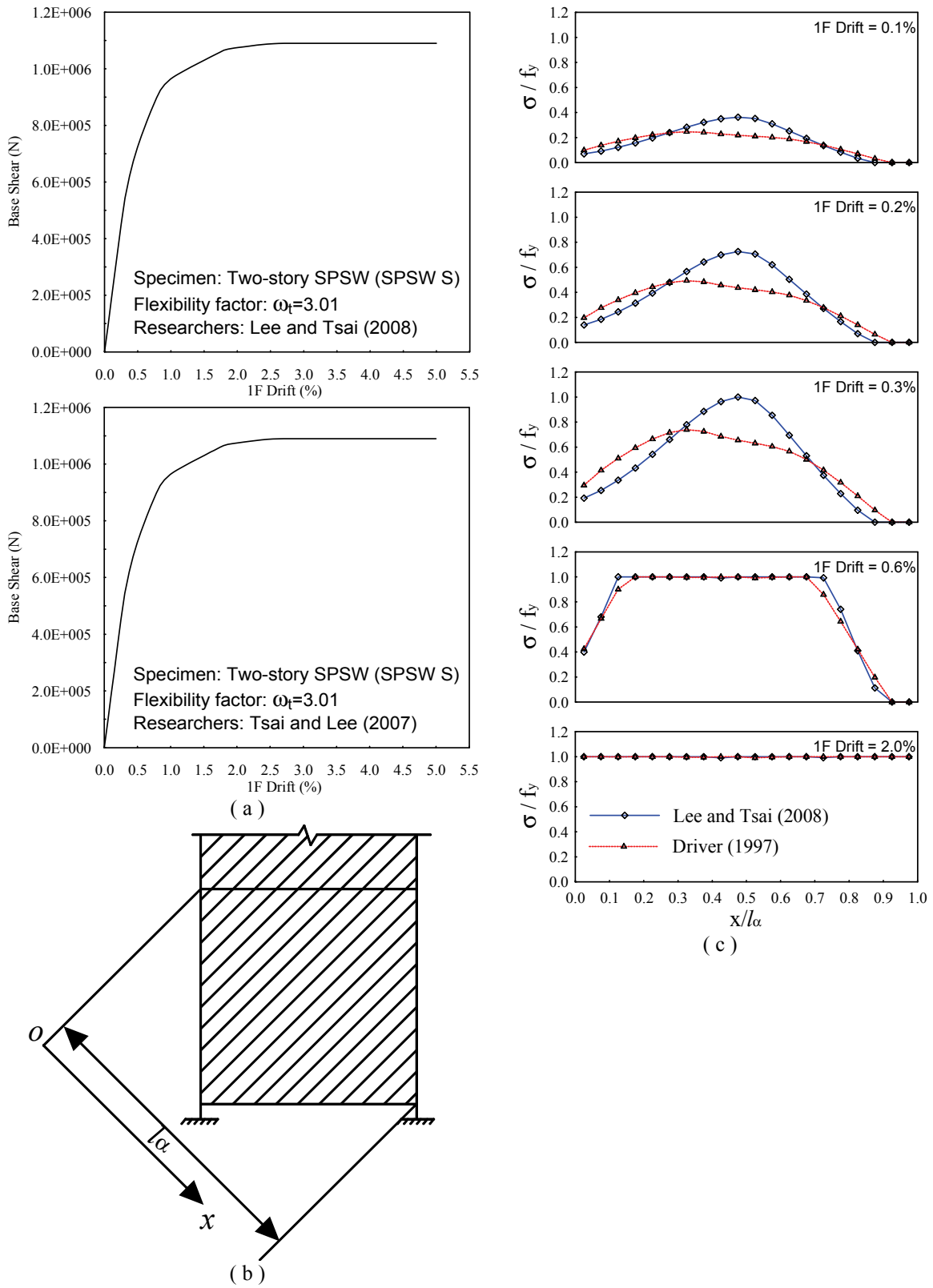
FIGURE 5-5 Uniformity of Tension Fields (a) Pushover Curves, (b) Schematic of Tension Fields, (c) Uniformity of Panel Stresses

5.4 Prevention of VBE In-Plane Shear Yielding

As mentioned earlier, the significant "pull-in" deformation of VBEs observed during the tests on single-story SPSWs by Lubell *et al.* (2000) as shown in figure 5-7 was a milestone event that led to the current limit specified for the VBE flexibility (AISC 2005 and CSA 2000). This undesirable performance was ascribed to the insufficient VBE stiffness. However, VBE shear yielding is another important factor that may result in significant inelastic VBE deflections. At the time of this writing, no literature has reported or checked whether the previously tested specimens have encountered VBE shear yielding.

To have a better understanding of the observed significant pull-in deformations in VBEs, an analytical model for estimating VBE shear demand is proposed in Section 5.4.1. Then, previously tested SPSWs are assessed in Section 5.4.2 using the proposed analytical model. For comparison purpose, results from pushover analysis on strip models of those tested SPSWs are presented. Predictions are compared with the observed behavior.

5.4.1 Shear Demand and Strength of VBE

The AISC Seismic Provisions requires that the VBEs of a SPSW be designed to remain elastic when the webs are fully yielded, with exception of plastic hinges at the VBE bases (when columns are fixed to ground) which are needed to develop the uniform yielding plastic mechanism. Although not explicitly stated, those plastic hinges should be flexural-plastic hinges (i.e. as opposed to shear-yielding hinges) for the infill panels to be effectively anchored and consequently allow development of the expected tension fields.

As shown in figure 5-6, the free body diagram of the right-hand side VBE at the ith story is used to determine the maximum VBE shear demand in a uniformly yielded SPSW under rightward lateral forces. From equilibrium, the shear forces at the top and bottom ends of the member can be respectively obtained as:

$$V_{topi} = \frac{M_{topi} + M_{boti}}{h_{si}} + \frac{\omega_{xci} h_{si}}{2} + \frac{\omega_{yci} d_{ci}}{2} \qquad (5\text{-}10)$$

$$V_{boti} = \frac{M_{topi} + M_{boti}}{h_{si}} - \frac{\omega_{xci}h_{si}}{2} + \frac{\omega_{yci}d_{ci}}{2} \qquad (5\text{-}11)$$

where d_{ci} is the depth of the VBE; M_{topi} and M_{boti} are the moments developed at the top and bottom ends of the VBE.
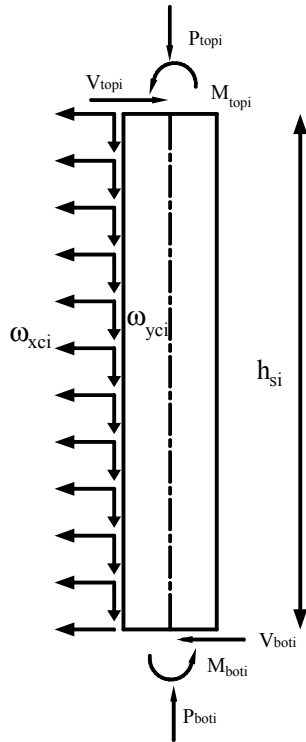
FIGURE 5-6 In-plane Free Body Diagram of the VBE at the ith story for Determination of Shear Demand

Conservatively, assuming that the moments applied at the top and bottom ends of the VBE are equal to the expected nominal plastic moments, one can obtain the following estimate of VBE shear demand:

$$V_{u-design} = \frac{2R_y f_y Z_c}{h_{si}} + \frac{\omega_{xci}h_{si}}{2} + \frac{\omega_{yci}d_{ci}}{2} \qquad (5\text{-}12)$$

It is recognized that (5-12) overestimate the VBE shear design force for two reasons, namely, (i): the plastic moments at the VBE ends may be reduced due to the presence of axial force, shear force, and vertical stresses in the VBE. (i.e. similar to the reduction of HBE plastic moments presented in Section 3); and (ii) plastic hinges in properly designed

SPSWs may develop in the HBEs, not in the VBEs. However, for expediency and design purpose, it is conservative to calculate the shear force predicted using (5-12) to size the columns. Note that the same design shear force can be obtained at the bottom end of the left-hand side VBE based on the corresponding free body diagram and assumptions.

In design, the shear demand obtained from (5-12) should be compared to the VBE shear strength, V_n , which, when the web of the VBE cross-section is compact (i.e. $h_{wci}/t_{wci} \leq 2.45\sqrt{E/f_y}$), is calculated as:

$$V_n = 0.6 f_y d_{ci} t_{wci} \tag{5-13}$$

where h_{wci} is the web depth of the VBE cross-section; t_{wci} is the web thickness of the VBE cross-section, and other terms have been defined previously.

5.4.2 Observation of VBE Shear Yielding in Past Testing

To check whether shear yielding had occurred in the VBEs of previously tested SPSWs, a sample of SPSWs for which the experimental data are available are assessed in table 5-1. Those examples include both single-story and multi-story SPSWs. Using the analytical model proposed in Section 5.4.1, the shear demands (i.e. $V_{u-design}$) and strengths (i.e. V_n) respectively calculated using (5-12) and (5-13) are presented in table 5-1. Additionally, using published information on SPSW geometries and member sizes, strip models for those considered SPSWs were developed and the corresponding maximum VBE shears obtained from the pushover analysis using SAP2000 (i.e. $V_{sap2000}$) are provided in table 5-1. Note that 20 strips were used for the infill plates at each story in all specimens. Steel was modeled as an elasto-perfectly plastic material using the yield strength provided in each relevant reference. Plastic hinges accounting for the interaction of axial force and flexure were defined at the ends of HBEs and the VBE bases. The vertical distributions of lateral forces used in the pushover analyses were determined according to the loading conditions reported for each actual test. For comparison purpose, specimen scale, aspect ratio and tension field inclination angle of those considered SPSWs are also provided in table 5-1.

TABLE 5-1 Evaluation of VBE Shear Demand and Strength[-a]

Case	Researcher	Specimen identification	Number of stories	Scale	Aspect ratio[-c] (L/h)	α (°)	ω_t	V_n (kN)	$V_{sap2000}$ (kN)	$V_{u-design}$ (kN)	Shear Yielding
					(i) single-story specimen						
1	Lubell et al. (2000)	SPSW2	1	1:4	1.00	37.4	3.35	75	108	113	Yes
2	Berman and Bruneau (2005)	F2	1	1:2	2.00	44.8	1.01	932	259	261[-d]	No
					(ii) multi-story specimen[-a]						
3	Driver et al. (1998)	–[b]	4	1:2	1.58	43.4	1.73	766	1361	1458	Yes
4	Park et al. (2007)	SC2T	3	1:3	1.46	44.4	1.24	999	676	1064	No
5		SC4T	3	1:3	1.46	44.1	1.44	999	984	1383	No
6		SC6T	3	1:3	1.46	43.9	1.58	999	1218	1622	Yes
7		WC4T	3	1:3	1.46	45.0	1.62	560	920	1210	Yes
8		WC6T	3	1:3	1.46	45.0	1.77	560	1151	1461	Yes
9	Qu et al. (2008)	–[b]	2	1:1	1.00	41.3	1.95	2881	1591	2341	No
10	Lee and Tsai (2008)	SPSW N	2	1:1	0.66	38.8	2.53	968	776	955	No
11		SPSW S	2	1:1	0.66	36.5	3.01	752	675	705	No

[a] For multi-story specimens, VBEs at the first story are evaluated.
[b] Not applicable.
[c] Using the first story height
[d] The plastic moments applied at the VBE ends are equal to the strength of web-angle beam-to-column flexible connections

Comparing $V_{sap2000}$ to $V_{u-design}$, table 5-1 confirms that equation (5-12) proposed in Section 5.4.1 gives conservative VBE design shear forces (as expected since it assumes plastic hinges at both ends of the VBE). The level of conservatism varies from 0.7% and 57%, and is on average 25% for the cases considered.

On the other hand, comparing V_n to $V_{sap2000}$ reveals that the VBEs in Cases 1, 3, 6, 7, and 8 should have experienced shear yielding during their tests while the VBEs in other cases would not. This prediction is consistent with experimental observations. For a better understanding, the following will focus on the observed VBE behaviors in Cases 1, 3, 6, 7, and 8.

For the SPSW of Case 1 (i.e. the single-story SPSW, SPSW2, tested by Lubell *et al.* 2000), significant inward deformations were observed in the VBEs as shown in figure 5-7. Montgomery and Medhekar (2001) ascribed this undesirable VBE behavior to: (i) the small infill panel width-to-height aspect ratio compared to those of other specimens for which the VBEs exhibited desirable behavior, (ii) relative small tension field inclination angle calculated per the equation provided in the AISC Seismic Provisions and CSA S16-01, and (iii) inadequate VBE flexibility per (5-8).

The fact that the single-story specimen had a width-to-height infill panel aspect ratio of approximately 1.0, by itself, should not be a concern contrary to the claim by Montgomery and Medhekar (2001). This value is within the permissible range of 0.8 and 2.5 specified by the AISC Seismic Provisions and CAN/CSA S16-01. More importantly, the VBEs of the MCEER/NCREE SPSW specimen described in Qu *et al.* (2008), which had the same width-to-height aspect ratio of 1.0, exhibited desirable ductile performance.

In addition, the tension field inclination angle of the single-story specimen calculated per the AISC Seismic Provisions and CSA S16-01 is 37.4º. That, by itself, should not be a reason for the observed undesirable VBE behavior. As presented in table 5-1, the two-story SPSW (specimen SPSW S) recently tested by Lee and Tsai (2008) had an even smaller inclination angle of 36.5º and exhibited satisfactory VBE performance up to story drifts greater than 5%, as described later.

As to whether the undesirable VBE inward deformation observed in the single-story specimen can be attributed to excessive VBE flexibility, even though this specimen had a flexibility factor of 3.35 (i.e. greater than the code specified limit of 2.5), the results in table 5-1 demonstrate that VBE shear yielding occurred in that specimen during the tests, resulting in the significant in-plane VBE deflections due to inelastic shear deformations. Yielding pattern of the VBE webs further confirms this point. As indicated by the flaked whitewash shown in figure 5-7, the VBE web yielded uniformly at the VBE ends as opposed to the yielding pattern usually observed in flexural plastic hinges, indicating significant inelastic shear deformations. Note that the axial force in the VBEs can also affect the yielding pattern of VBE webs. However, the axial force developed in the VBEs is insignificant in this single-story case.
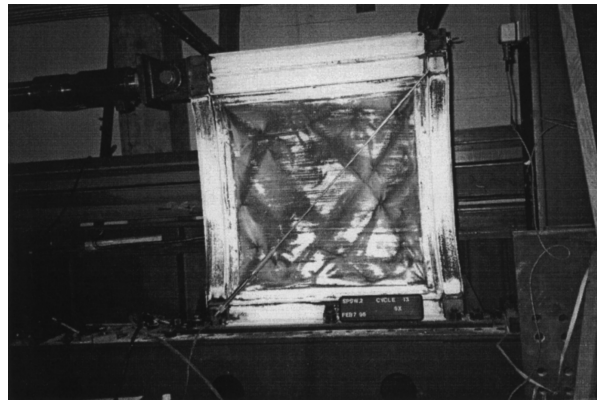
FIGURE 5-7 Deformation and Yield Patterns of SPSW2 after $6\times\delta_y$
(from Lubell *et al.* 2000)

For the SPSW of case 3 (i.e. the four-story SPSW tested by Driver *et al.* 1997), deformations at the first story of the wall are shown in figure 5-8. Note that this specimen had a code-compliant flexibility factor of 1.73. Incidentally, the plastic strength of the wall predicted using the procedure proposed by Berman and Bruneau (2003), which has been verified by numerous other experimental results, is substantially greater than the strength obtained during the test. Sabouri-Ghomi (2005) alleged that the plastic strength of the wall could be reduced due to overall bending effects. However, results shown in table 5-1 unequivocally show that shear yielding occurred in the first-story VBEs of Driver's specimen. This may have resulted in incomplete development of the expected

VBE plastic moments and infill tension field at the first story, and thus the lower ultimate base shear compared to predictions from plastic analysis. Interestingly, fractures were observed to penetrate into the VBE web at the column bases during that test, which may also be related to the significant shear force acting there.
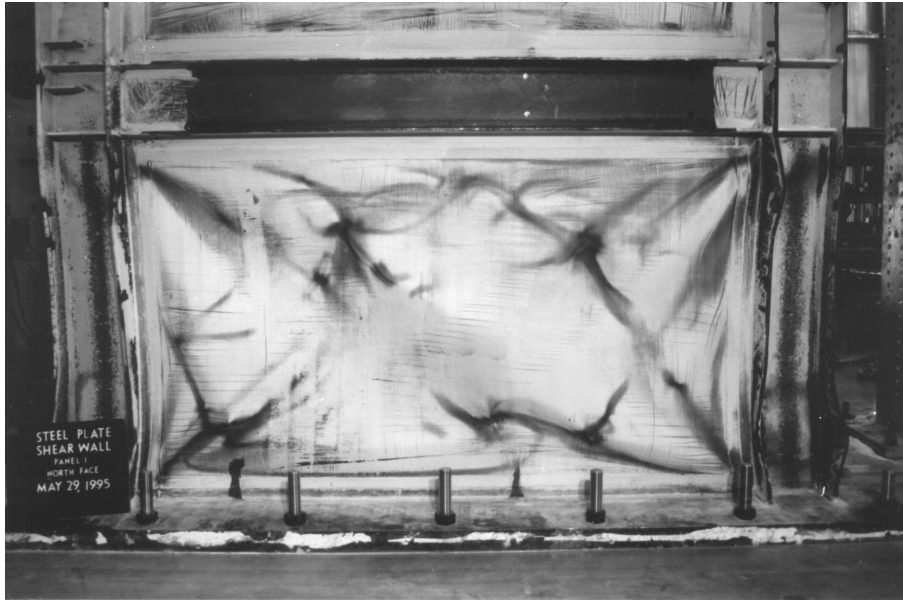
FIGURE 5-8 First-Story of Driver's SPSW
(Photo: Courtesy of Driver. R.G.)

Cases 6, 7 and 8 are three-story specimens from a series of tests on SPSWs by Park *et al.* (2007). For comparison purpose, case 6 is first compared against cases 4 and 5. Specimens of cases 4, 5 and 6 (i.e. SC2T, SC4T and SC6T respectively in Park *et al.* 2007) have flexibility factors of 1.24, 1.44 and 1.58 respectively, which all satisfied the code-specified limit of 2.5. These specimens had identical boundary frame members and constant infill panels along the height of each wall (with thicknesses of 2mm, 4mm, and 6mm in SC2T, SC4T and SC6T, respectively). Per (5-13), these specimens had the same VBE members and thus the same VBE shear strength. However the shear demands on the first-story VBEs of SC2T, SC4T and SC6T increased directly as a function of the infill panel yield forces (which are determined from the infill panel thicknesses). As shown from the results in table 5-1, the VBEs of specimen SC6T are expected to yield in shear while those of SC2T and SC4T would not. This prediction agrees with the observed yielding patterns at the first-story VBEs as shown in figure 5-9.

125

(a) SC2T   (b) SC4T   (c) SC6T
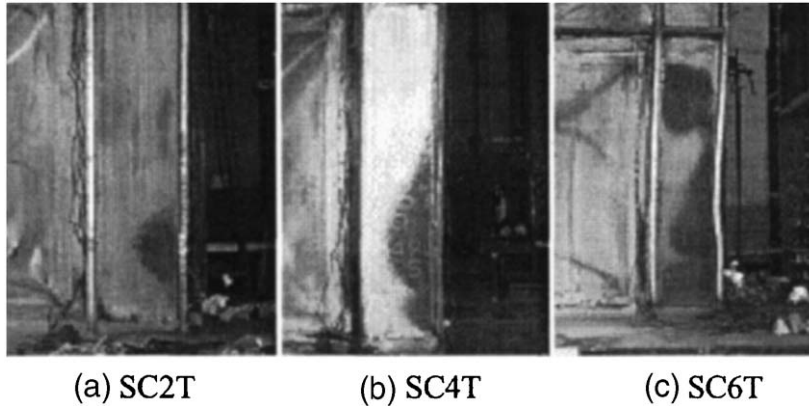
FIGURE 5-9 Yield Zone of VBE in SC Specimens (from Park *et al.* 2007)

For the specimens in cases 7 and 8 (i.e. WC4T and WC6T in Park *et al.* 2007 respectively), the VBEs were wide flange members with noncompact flanges with code-compliant flexibility factors of 1.62 and 1.77 respectively. However, significant pull-in deformations were observed in the VBEs of these two specimens. Local buckling due to flange noncompactness is an important factor that contributed to the VBE deflections during these tests, but the results in table 5-1 indicate that shear yielding also developed in those VBEs. The observed VBE yielding patterns and deformations further confirm this point. As shown in figure 5-10, yield lines gradually developed in the VBE web of WC4T with increasing story drift indirectly expressed by greater load cycle numbers in figure 5-11, indicating the development of VBE shear yielding, which finally resulted in significant inward deflections in the VBEs shown in figure 5-11.

(a) Cycle 19   (b) Cycle 23   (c) Cycle 30
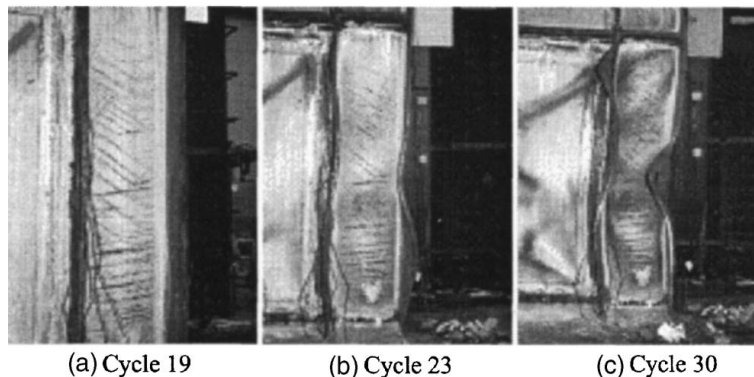
FIGURE 5-10 Yield Zone of VBE in WC4T (from Park *et al.* 2007)

126
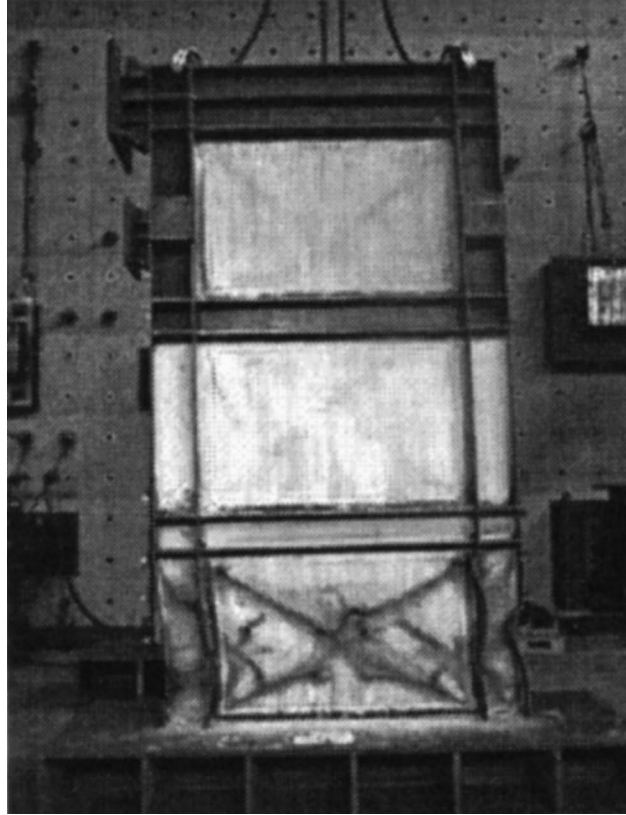
FIGURE 5-11 WC4T at the End of Test (from Park *et al.* 2007)

Note that Park *et al.* (2007) proposed a free body diagram for calculating the shear demands in VBE, in which the shear effects due to the moment resisting actions at the VBE ends and the vertical components of infill panel yield forces were neglected. According to their free body diagram, no shear yielding would have occurred in the VBEs of SC6T. However, that prediction is inconsistent with the observed behavior shown in figure 5-9, invalidating their proposed free body diagram.

As discussed above, undesirable inward VBE deflections were observed in SPSW specimens with and without code-compliant and non-compliant flexibility factors. There is no correlation between flexibility factor and significant VBE pull-in deformations. Instead, the analytical work presented in this section demonstrates that the observed undesirable VBE deflections were caused by VBE shear yielding.

5.5 VBE Out-of-Plane Buckling Strength

Besides the aforementioned excessive pull-in deformations, another undesirable behavior of VBE is out-of-plane buckling, which has been observed during the tests on a quarter-scale four-story SPSW specimen by Lubell *et al.* (2000). This undesirable performance was also ascribed to the insufficient VBE stiffness. However, no theoretical work has been conducted to establish the correlation between ω_t and out-of-plane buckling strength of VBEs.

This section will investigate whether or not the available database of test results sustain the use of flexibility limit for VBE design to successfully prevent the out-of-plane buckling of VBE, or whether different methods are necessary for that purpose. To be able to do such comparisons, analytical models for estimating the out-of-plane buckling strength of VBEs are derived in Section 5.5.1 based on simple free body diagrams and the energy method taking into account representative boundary conditions of VBEs. Using the proposed analytical models, the out-of-plane behaviors of VBEs in a few representative SPSW specimens that have various values of flexibility factors are reviewed in Section 5.5.2.

5.5.1 Analytical Models for Out-of-plane Buckling Strength of VBEs

5.5.1.1 Free Body Diagrams of VBEs

The expected plastic mechanism of a multistory SPSW subjected to lateral loads described in Section 4.2 is considered here. This expected mechanism gives the free body diagrams of the left and right VBEs in a typical single-bay multistory SPSW under the rightward lateral forces as shown in figure 5-5.

In the free body diagrams, ω_{xci} and ω_{yci} represent horizontal and vertical components of the infill plate yield force along the VBE at the ith story, P_{bli} and P_{bri} represent the axial forces at the left and right ends of HBE, V_{li} and V_{ri} represent the shear forces at the left and right VBE faces, M_{li} and M_{ri} represent the moments at the left and right VBE faces,

R_{xl}, R_{xr}, R_{yl}, R_{yr}, M_{cl} and M_{cr} represent the reaction forces at VBE bases, and F_i represents the applied lateral forces needed to develop the expected plastic mechanism.
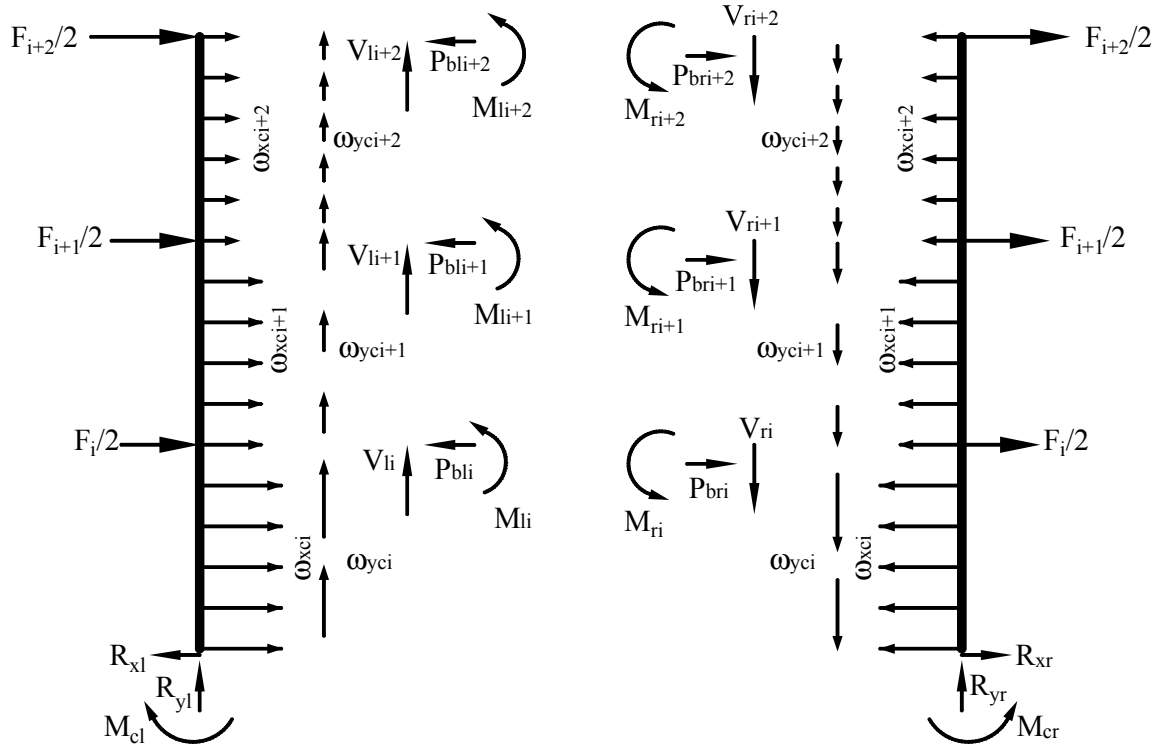
FIGURE 5-12 VBE Free Body Diagrams

Free body diagram of the VBE on the right-hand side is chosen for derivation of the out-of-plane buckling strength of VBE for analysis purpose, since the compression effect in that VBE resulting from the HBE end shears is additive to that from the vertical component of the infill panel yield forces along that VBE. The compressions at the top and bottom ends of the considered VBE, P_{topi} and $P_{bottomi}$, can be obtained as:

$$P_{topi} = \sum_{j=i}^{n_s} V_{rj} + \sum_{j=i+1}^{n_s} \omega_{ycj} \cdot h_{sj} \tag{5-14}$$

$$P_{bottomi} = P_{topi} + \omega_{yci} \cdot h_{si} \tag{5-15}$$

where n_s is the number of SPSW stories, and all other terms have been defined previously.

129

To ensure the desirable behavior of VBE, it is recommended, although slightly conservative, to neglect the reduction effects on HBE plastic moments accounting for the presence of axial force, shear force, and vertical stresses in HBEs. Note that the plastic section modulus of a plastic hinge in an HBE should be determined according to equation (4-64) to account for the variation of plastic hinge location when RBS connections are used in HBE. Accordingly, the right end shears of HBEs with and without RBS connections are obtained based on a modified version of equations (4-38) and (4-40) respectively, namely:

$$V_{ri} = \frac{\left(\omega_{ybi} - \omega_{ybi+1}\right)L}{2} + \frac{\left(\omega_{xbi} + \omega_{xbi+1}\right)d}{2} + \frac{2R_y f_y Z_{RBS}}{L - 2e} \tag{5-16}$$

$$V_{ri} = \frac{\left(\omega_{ybi} - \omega_{ybi+1}\right)L}{2} + \frac{\left(\omega_{xbi} + \omega_{xbi+1}\right)d}{2} + \frac{2R_y f_y Z}{L} \tag{5-17}$$

where all terms have been defined previously.

5.5.1.2 Energy Method and Boundary Conditions

Although modeling the considered VBE in some FE software packages such as ABAQUS is always possible, at the cost of computational efforts, it is relatively expedient and efficient using the energy method to develop approximate calculations of the critical buckling strength of VBE (i.e. the Euler buckling strength assuming elastic behavior and no initial imperfection in the member - it is recognized that the actual buckling strength of the member considering the above effects could be lower and that the buckling strength calculated by this approach is an optimistic assessment. It should be therefore not used for design, but will be useful to illustrate key points in later sections.).

The energy method is used in buckling problems to determine approximate values of the critical buckling strength when an exact solution of the differential equation of the deflection curve is either unknown or too complicated. In such cases, solution proceeds by assuming a reasonable shape for the deflection curve. While it is not essential for an approximate solution that the assumed curve perfectly match the deflected shape, it should satisfy the boundary conditions at the ends of the member. Using a reasonable

assumed shape for the deflection curve, the energy method can give an approximate out-of-plane buckling strength of VBE, within the previously enunciated constraints (Timoshenko and Gere 1961).

In a typical SPSW, the ends of VBEs are laterally supported by the floor system and the first-story VBE is either fixed or pinned to ground. Under those conditions, the out-of-plane translations at the VBE ends are restrained. However, the out-of-plane rotational restraints due to the beams framing into the VBEs can vary from fully free to fully fixed and would have to be assessed on a case by case basis. The VBE end conditions considered in the following sections are presented in table 5-2 and correspond to ideal cases.

TABLE 5-2 Summary of VBE End Conditions

VBE ends	Case A	Case B	Case C	Case D
Top	Pin	Fixed	Pin	Fixed
Bottom	Pin	Fixed	Fixed	Pin

In Sections 5.5.1.3 to 5.5.1.6, the out-of-plane buckling strength of VBE is derived successively for each of these boundary conditions respectively.

5.5.1.3 Out-of-Plane Buckling Strength of VBE - Case A

Figure 5-13 illustrates the typical orientations of the VBE weak and strong axes in a SPSW, for which the smaller and greater moments of inertia of the VBE cross-section can be obtained. Note that VBE deflections due to out-of-plane buckling develop in the plane perpendicular to the weak axis.

The out-of-plane buckling of the VBE at the ith story under Case A boundary conditions is schematically shown in figure 5-14. Note that both the top and bottom ends are hinged in this case (i.e. only translations are restrained).
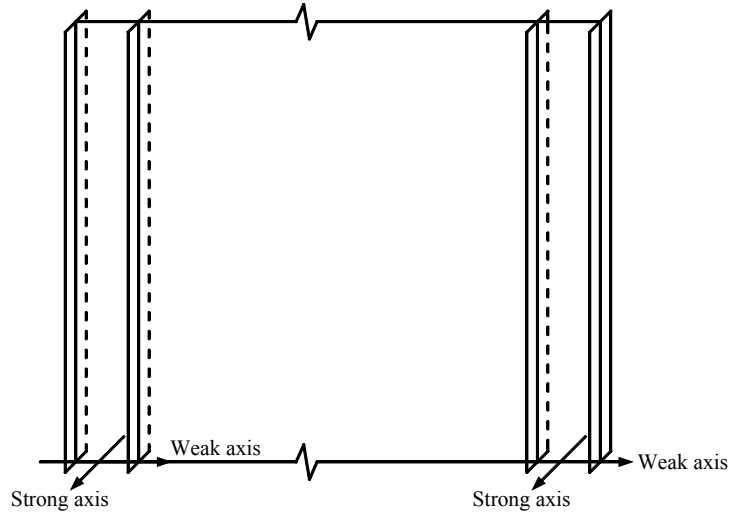
FIGURE 5-13 Strong and Weak Axes of VBEs
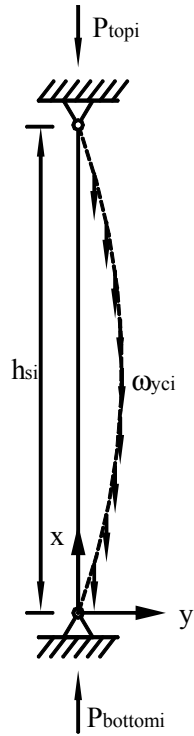
FIGURE 5-14 Free Body Diagram of the VBE at the ith Story: Case A Boundary Conditions

Assume that the deflection curve of the VBE is a sine curve in the coordinate system shown in figure 5-14, which is

$$y = \delta_i \sin\left(\frac{\pi x}{h_{si}}\right) \tag{5-18}$$

where δ_i is an arbitrarily selected nonzero deflection factor. Note that the magnitude of δ_i will not have any impacts on the buckling strength as demonstrated later.

Then, by differentiation, one can obtain

$$\frac{dy}{dx} = \frac{\pi \delta_i}{h_{si}} \cos\left(\frac{\pi x}{h_{si}}\right) \tag{5-19}$$

$$\frac{d^2 y}{dx^2} = -\frac{\pi^2 \delta_i}{h_{si}^2} \sin\left(\frac{\pi x}{h_{si}}\right) \tag{5-20}$$

Consistent with the boundary conditions shown in figure 5-14, the following requirements are satisfied by the deflection curve determined from (5-18).

$$y\big|_{x=0,h_{si}} = 0 \tag{5-21}$$

$$\frac{d^2 y}{dx^2}\bigg|_{x=0,h_{si}} = 0 \tag{5-22}$$

Physically, (5-21) and (5-22) indicate that no translations and no moments occur at the VBE ends.

Owing to the inclination of an element ds of the deflection curve as shown in figure 5-15, the upper part of the load undergoes a downward displacement equal to

$$ds - dx \approx \frac{1}{2}\left(\frac{dy}{dx}\right)^2 dx \tag{5-23}$$

and the corresponding work done by the uniform load from that element to the top end of the VBE is

133

$$\underbrace{\omega_{yci}\left(h_{si}-x\right)}_{\text{resultant foce}} \cdot \underbrace{\frac{1}{2}\left(\frac{dy}{dx}\right)^2 dx}_{\text{downward displacement}} \tag{5-24}$$
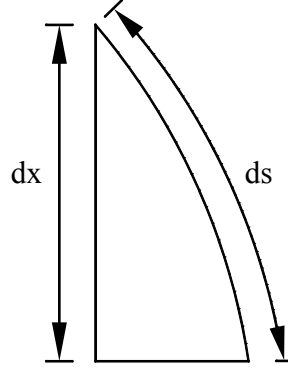
FIGURE 5-15 Deflection of VBE at Element Level

Therefore, the total work produced by the infill panel yield force along that VBE during buckling is

$$\Delta T_1 = \int_0^{h_{si}} \frac{1}{2}\omega_{yci}\left(h_{si}-x\right)\left(\frac{dy}{dx}\right)^2 dx \tag{5-25}$$

Similarly, the work done by the concentrated load at the top of the VBE can be determined as

$$\Delta T_2 = \int_0^{h_{si}} \frac{P_{topi}}{2}\left(\frac{dy}{dx}\right)^2 dx \tag{5-26}$$

By summation, the total work done by external forces is

$$\Delta T = \Delta T_1 + \Delta T_2 = \int_0^{h_{si}} \frac{1}{2}\omega_{yci}\left(h_{si}-x\right)\left(\frac{dy}{dx}\right)^2 dx + \int_0^{h_{si}} \frac{P_{topi}}{2}\left(\frac{dy}{dx}\right)^2 dx \tag{5-27}$$

Substituting (5-19) into (5-27) and integrating, one can determine the total work as:

$$\Delta T = \frac{\pi^4 \delta_i^2 EI_{yi}}{4h_{si}^3}\left(m+\frac{n}{2}\right) \tag{5-28}$$

134

where I_{yi} is moment of inertia of the VBE taken from the weak axis; m and n are the generalized external forces, which can be respectively obtained by normalizing the concentrated force applied at the top of the VBE (i.e. P_{topi}) and the resultant infill panel yield force along the VBE (i.e. $\omega_{yci}h_{si}$), by the Euler buckling load of a simply supported VBE without any intermediate loads along its height. Namely, m and n can be determined from the following two equations

$$m = \frac{P_{topi}}{\left[\dfrac{\pi^2 EI_{yi}}{h_{si}^2}\right]} \tag{5-29}$$

$$n = \frac{\omega_{yci}h_{si}}{\left[\dfrac{\pi^2 EI_{yi}}{h_{si}^2}\right]} \tag{5-30}$$

The strain energy due to bending of the buckled VBE is

$$\Delta U = \int_0^{h_{si}} \frac{EI_{yi}}{2}\left(\frac{d^2y}{dx^2}\right)^2 dx \tag{5-31}$$

Substituting (5-20) into (5-31) and integrating,

$$\Delta U = \frac{\pi^4 \delta_i^2 EI_{yi}}{4h_{si}^3} \tag{5-32}$$

The critical buckling strength can be found from the following equation

$$\Delta U = \Delta T \tag{5-33}$$

Substituting (5-28) and (5-32) into (5-33), the critical combination of m and n for case A can be expressed as

$$m + \frac{n}{2} = 1 \tag{5-34}$$

Note that (5-27), (5-31) and (5-33) remain valid for derivations of other boundary conditions (i.e. Cases B, C and D).

A graphical version of (5-34) is shown in figure 5-16. For a given load combination (i.e. a pair of m and n), if the left-hand side of (5-34) is greater than 1, the VBE is expected to encounter out-of-plane buckling failure. Those combinations for which buckling failure occurs are represented by the shaded area in figure 5-16.

Incidentally, Timoshenko and Gere (1961) provided the critical buckling strength of the column shown in figure 5-14 for a few selected individual cases. Their results are also presented in figure 5-16. As expected, a good agreement is observed through comparisons.
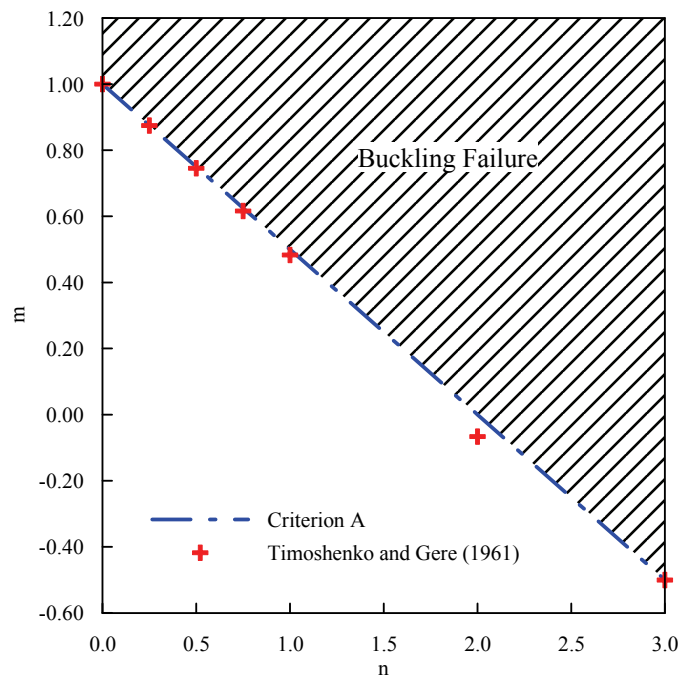
FIGURE 5-16 Interaction of Critical Loads for Out-of-Plane Buckling of VBE: Case A Boundary Conditions

Interestingly, figure 5-16 shows that for large value of n, which corresponds to large infill panel yield force applied along the column, the required value of m to avoid the out-of-plane buckling failure could be negative (i.e. corresponding to tension force applied at the top end of the member). However, such a theoretical case, in which the concentrated

force applied at the top of the bar needs to act upward instead of downward to counteract the axial effect resulting from the distributed force to prevent buckling, is not practical.

5.5.1.4 Out-of-Plane Buckling Strength of VBE - Case B

The out-of-plane buckling of the VBE at the ith story under Case B boundary conditions is schematically shown in figure 5-17. Note that both ends of the VBE are fixed in this case (i.e. both translations and rotations are restrained).
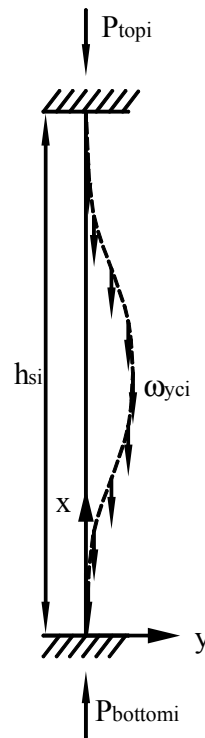
FIGURE 5-17 Free Body Diagram of the VBE at the ith Story: Case B Boundary Conditions

Assuming that the deflection curve of the VBE is a cosine curve in the coordinate system shown in figure 5-17, which is

$$y = \delta_i \left[1 - \cos\left(\frac{2\pi x}{h_{si}} \right) \right] \tag{5-35}$$

then, by differentiation, one can obtain

$$\frac{dy}{dx} = \frac{2\pi\delta_i}{h_{si}}\sin\left(\frac{2\pi x}{h_{si}}\right) \qquad (5\text{-}36)$$

$$\frac{d^2y}{dx^2} = \frac{4\pi^2\delta_i}{h_{si}^2}\cos\left(\frac{\pi x}{h_{si}}\right) \qquad (5\text{-}37)$$

In this case, the following boundary conditions are satisfied:

$$y\big|_{x=0,h_{si}} = 0 \qquad (5\text{-}38)$$

$$\frac{dy}{dx}\bigg|_{x=0,h_{si}} = 0 \qquad (5\text{-}39)$$

where (5-38) and (5-39) respectively correspond to no translations and no rotations at the VBE ends.

Following a procedure similar to that described earlier for Case A, one can obtain the out-of-plane buckling strength of the VBE with Case B boundary conditions. Note that all terms have been defined previously.

Substituting (5-36) into (5-27) and integrating, one can determine the total work as:

$$\Delta T = \frac{\pi^4\delta_i^2 EI_{yi}}{h_{si}^3}\left(m + \frac{n}{2}\right) \qquad (5\text{-}40)$$

Substituting (5-37) into (5-31) and doing the integration,

$$\Delta U = \frac{4\pi^4\delta_i^2 EI_{yi}}{h_{si}^3} \qquad (5\text{-}41)$$

Thus, in accordance with (5-33), the critical combination of m and n for case B can be mathematically stated as

$$\frac{m}{4} + \frac{n}{8} = 1 \qquad (5\text{-}42)$$

Graphically, (5-42) is shown in figure 5-18.
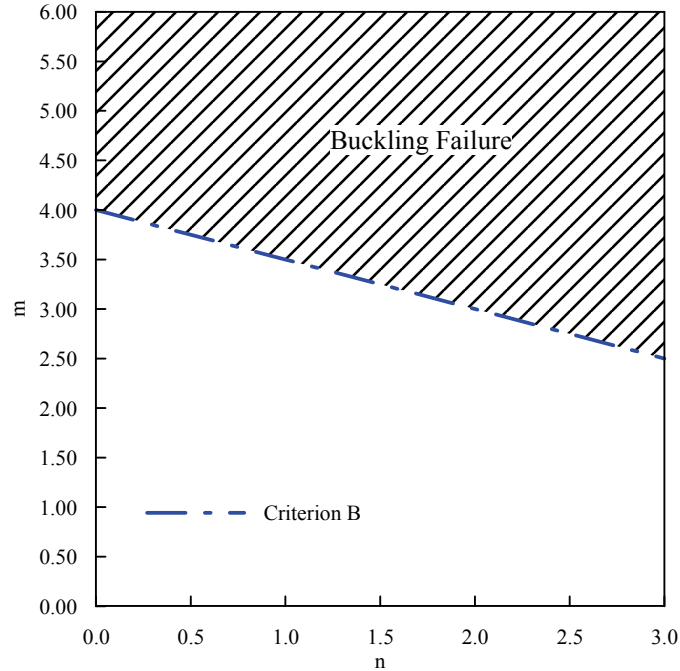
FIGURE 5-18 Interaction of Critical Loads for Out-of-Plane Buckling of VBE: Case B Boundary Conditions

As determined from (5-42), at the limit when no infill panel yield forces are applied (i.e. when $n = 0$), the VBE is a fix-fix column and has a buckling strength four times that of a simply supported column (i.e. corresponding to $m = 4$), as expected. Based on the criterion shown in figure 5-18, the value of m decreases when the value of n increases, which physically means that lower concentrated force can be applied at the top of the column to avoid column buckling when higher infill panel yield forces are applied along the column.

5.5.1.5 Out-of-Plane Buckling Strength of VBE - Case C

The out-of-plane buckling of the VBE at the ith story under Case C boundary conditions is schematically shown in figure 5-19. Note that the bottom and top ends are fixed and hinged respectively (i.e. both translations and rotations at the bottom end are restrained, but only translations at the top end are restrained.). This case is useful to consider here because the top end of the VBE in a SPSW may be typically free to rotate on account of how the framing system connects to the SPSW at that location.
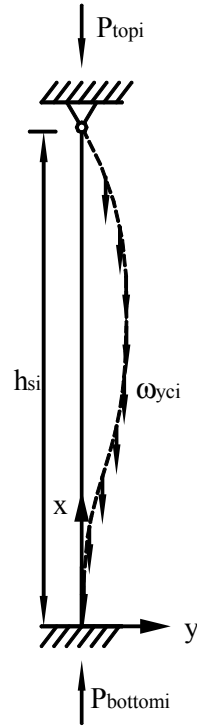
FIGURE 5-19 Free Body Diagram of the VBE at the ith Story: Case C Boundary Conditions

Assuming that the deflection curve of the considered VBE is determined by the following polynomial in the coordinate system shown in figure 5-19,

$$y = \delta_i \left[2x^4 + 3x^2 h_{si}^2 - 5x^3 h_{si} \right] \tag{5-43}$$

then, by differentiation, one can obtain

$$\frac{dy}{dx} = \delta_i \left[8x^3 + 6x h_{si}^2 - 15x^2 h_{si} \right] \tag{5-44}$$

$$\frac{d^2 y}{dx^2} = \delta_i \left[24x^2 + 6h_{si}^2 - 30x h_{si} \right] \tag{5-45}$$

For this case, the following boundary conditions are satisfied:

$$y \big|_{x=0, h_{si}} = 0 \tag{5-46}$$

140

$$\left. \frac{dy}{dx} \right|_{x=0} = 0 \tag{5-47}$$

$$\left. \frac{d^2 y}{dx^2} \right|_{x=h_{si}} = 0 \tag{5-48}$$

where (5-46) indicates no translation at both ends, and (5-47) and (5-48) respectively indicate zero rotation and zero moment at the bottom and top ends.

Following the procedure described earlier, one can obtain the out-of-plane buckling strength of the VBE for Case C boundary conditions, again using the terms defined previously.

Substituting (5-44) into (5-27) and integrating, one can determine the total work as:

$$\Delta T = \frac{6\pi^2 \delta_i^2 EI_{yi} h_{si}^5}{35} \left(m + \frac{3n}{8} \right) \tag{5-49}$$

Substituting (5-45) into (5-31) and integrating,

$$\Delta U = \frac{18 \delta_i^2 EI_{yi} h_{si}^5}{5} \tag{5-50}$$

In accordance with (5-33), the critical combination of m and n for case C can be mathematically stated as

$$\frac{\pi^2}{21} m + \frac{\pi^2}{56} n = 1 \tag{5-51}$$

A graphical version of (5-51) is shown in figure 5-20.
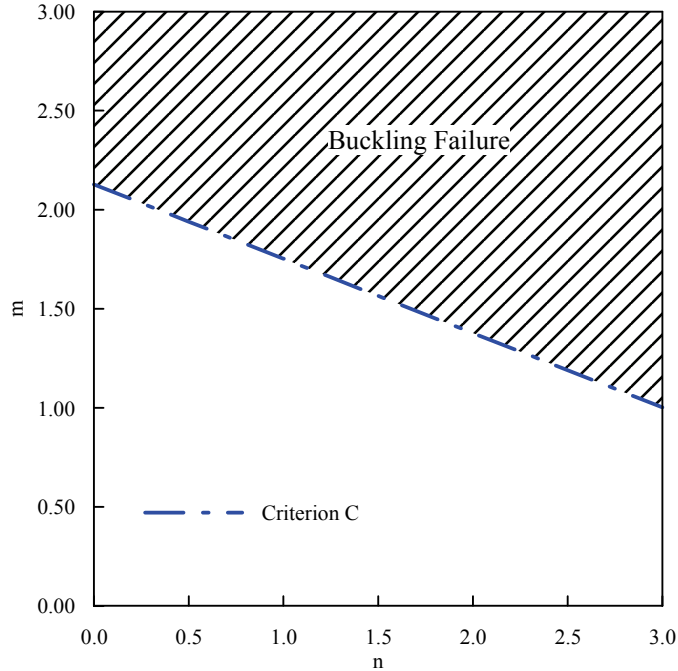
FIGURE 5-20 Interaction of Critical Loads for Out-of-Plane Buckling of VBE: Case C Boundary Conditions

At the limit when no infill panel yield forces are applied (i.e. $n = 0$), the VBE is simply a column with one end fixed and the other end hinged. As shown in the figure, the proposed criterion predicts $m = 2.12$, which physically means that critical buckling strength of that member is 2.12 times that of the corresponding simply supported column. Incidentally, for this case, Timoshenko and Gere (1961), obtained a value of 2.05 using an alternative approach based on the differential equations of beam-column theory. This small difference of 3.4% provides confidence in the accuracy of the proposed solution for VBEs.

5.5.1.6 Out-of-Plane Buckling Strength of VBE - Case D

The out-of-plane buckling of the VBE at the ith story under Case D boundary conditions is schematically shown in figure 5-21. Note that the top and bottom ends are fixed and pinned respectively (i.e. both translations and rotations at the top end are restrained, but, only translations at the bottom end are restrained.). Although this case is less likely to exist in SPSWs, it is discussed here for completeness of the derivations.
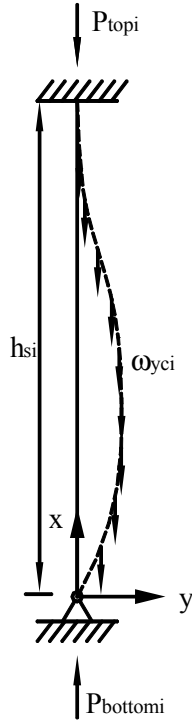
FIGURE 5-21 Free Body Diagram of the VBE at the ith Story: Case D Boundary Conditions

Assuming that the deflection curve of the considered VBE is a curve determined by the following polynomial in the coordinate system shown in figure 5-21,

$$y = \delta_i \left[2x^4 - 3x^3 h_{si} + x h_{si}^3 \right] \tag{5-52}$$

then, by differentiation, one can obtain

$$\frac{dy}{dx} = \delta_i \left[8x^3 - 9x^2 h_{si} + h_{si}^3 \right] \tag{5-53}$$

$$\frac{d^2 y}{dx^2} = \delta_i \left[24x^2 - 18x h_{si} \right] \tag{5-54}$$

For this case, the following boundary conditions are satisfied:

$$y\big|_{x=0,h_{si}} = 0 \tag{5-55}$$

143

$$\left.\frac{dy}{dx}\right|_{x=h_{si}} = 0 \tag{5-56}$$

$$\left.\frac{d^2y}{dx^2}\right|_{x=0} = 0 \tag{5-57}$$

where (5-55) indicates no translation at both ends, and (5-56) and (5-57) respectively indicate zero rotation and zero moment at the top and bottom ends.

Following the procedure described earlier, one can obtain out-of-plane buckling strength of the VBE for Case D boundary conditions, where all terms are defined previously.

Substituting (5-53) into (5-27) and doing the integrations, one can determine the total work as:

$$\Delta T = \frac{6\pi^2 \delta_i^2 EI_{yi} h_{si}^5}{35}\left(m + \frac{5n}{8}\right) \tag{5-58}$$

Substituting (5-54) into (5-31) and integrating,

$$\Delta U = \frac{18\delta_i^2 EI_{yi} h_{si}^5}{5} \tag{5-59}$$

In accordance with (5-33), the critical combination of m and n for case D can be stated as

$$\frac{\pi^2}{21}m + \frac{5\pi^2}{168}n = 1 \tag{5-60}$$

A graphical version of (5-60) is shown in figure 5-22.

At the limit case when no infill panel yield forces are applied (i.e. $n = 0$), Criterion D predicts the same magnitude of m as Criterion C (i.e. $m = 2.12$ as shown in figure 5-22). This is because the VBEs under the case C and case D boundary conditions are

equivalent when the infill panel yield forces are absent. The two cases (i.e. cases C and D) significantly differ for all other cases (i.e. when $n \neq 0$).
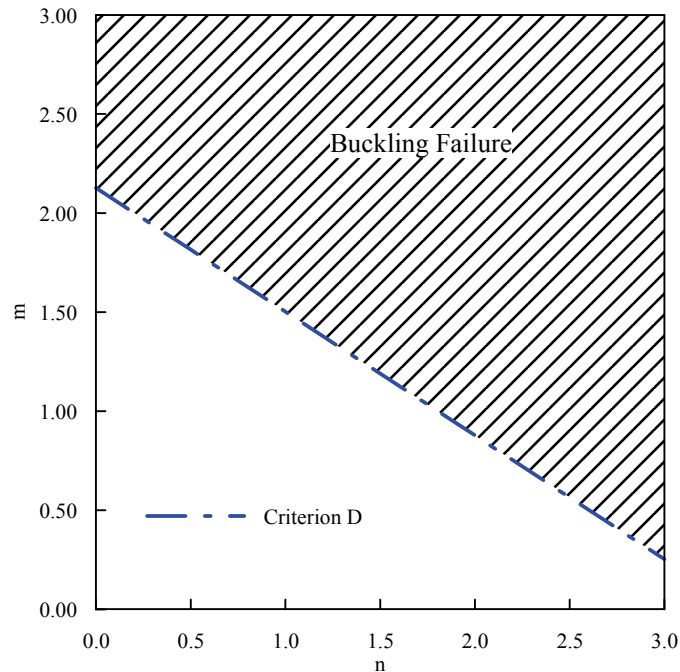
FIGURE 5-22 Interaction of Critical Loads for Out-of-Plane Buckling of VBE: Case D Boundary Condition

5.5.2 Review of Out-of-Plane Buckling of VBEs in Past Tests

To better understand the VBE out-of-plane buckling behavior, performance of the VBEs in previously tested SPSWs are revisited in perspective of the criteria derived in the previous section to see whether the proposed alternative approach can shed additional light on the behavior of VBEs.

The considered SPSW specimens are assessed using the criteria developed for all the four boundary conditions considered since the out-of-plane restraints at the ends of the VBEs of some specimens are not provided in the available references. As shown by the results presented in table 5-3, no matter what boundary conditions were applied, VBE out-of-plane buckling would not be predicted to occur in any of the SPSWs except for the Lubell *et al.* quarter-scale four-story SPSW. This prediction is consistent with the observations on those SPSWs obtained during tests as described below, validating to some degree the proposed analytical models for calculating VBE out-of-plane buckling strength.

The Lubell *et al.* specimen, schematically shown in figure 5-23, had 1.5mm (16 gauge) unstiffened hot-rolled infill panels with aspect ratio of 1.0. The VBEs and HBEs were sized to be S75x8 except that a S200x34 HBE was used at the roof level. All the HBE-to-VBE connections were rigid. The material yield strengths for the boundary frame and infill panels were determined to be 380 MPa and 320 MPa respectively from the tension coupon tests. Hysteresis loops obtained from the test are presented in figure 5-24, showing that insignificant amounts of hysteretic energy were dissipated before instability of VBE precipitated the system failure, when the specimen achieved a maximum displacement of $1.5\delta_y$, where δ_y is a global yield displacement.

A closer look at the Lubell *et al.* specimen reveals that Case C boundary conditions were applied to the buckled VBE (i.e. bottom end of the VBE was fixed to the ground while the top end was pinned in the out-of-plane direction). To better understand this, the VBE deflection traced from the specimen is superposed to those corresponding to Case B and Case C boundary conditions in figure 5-25. Comparison of deflection shapes confirms that the VBE end conditions are similar to those of Case C. Accordingly, applying Criterion C provides a value of 1.066 greater than 1.0 as shown in table 5-3, indicating the occurrence of VBE out-of-plane buckling failure. Therefore, failure of the Lubell *et al.* specimen was caused by the insufficient out-of-plane buckling strength of VBE rather than excessive column flexibilities.
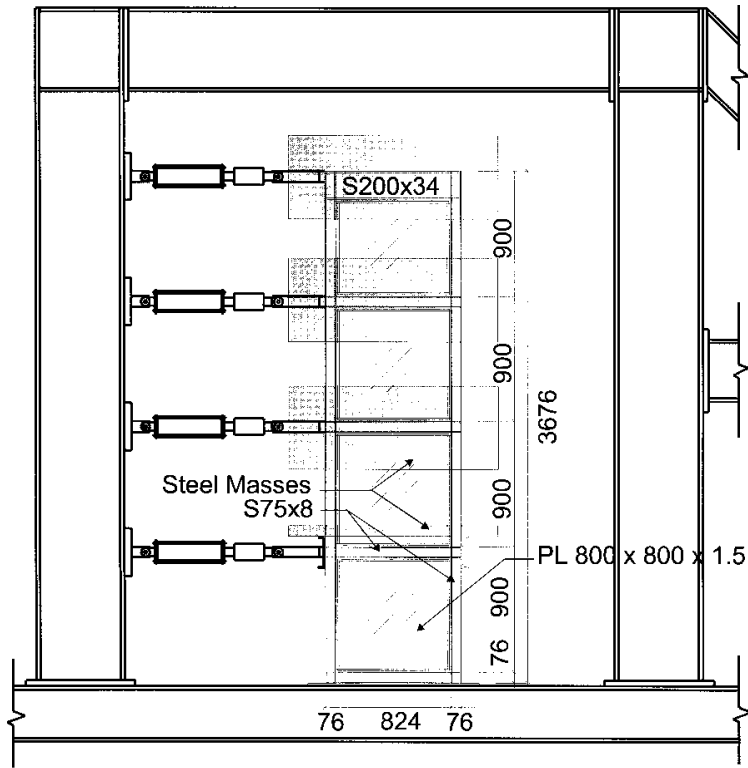
FIGURE 5-23 Test Setup-UBC Test (from Lubell *et al.* 2000)

(a)

(b)
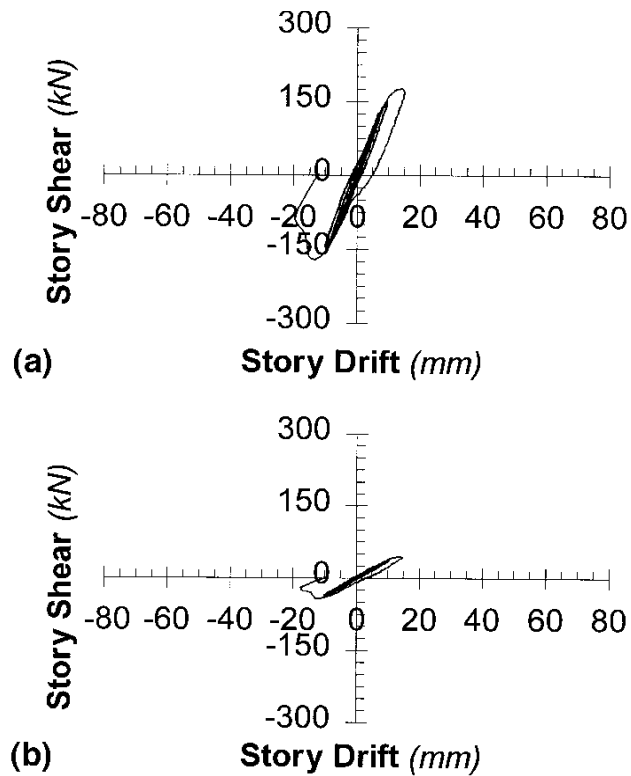
FIGURE 5-24 Load Deformation Curves for SPSW4:
(a) First Story; (b) Fourth Story (from Lubell *et al.* 2000)

147
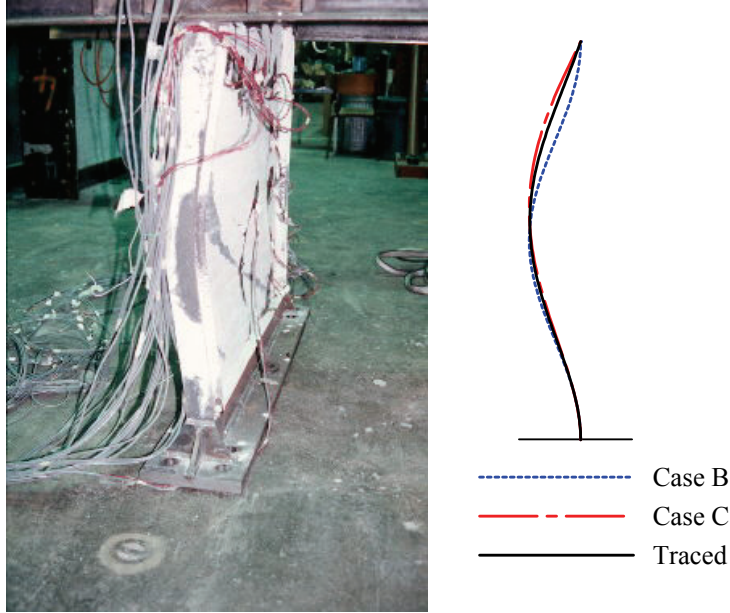
FIGURE 5-25 Out-of-Plane Buckling of Bottom VBE
(Photo: Courtesy of Ventura. C.E.)

Two other interesting and noteworthy cases in table 5-3 are the two specimens (i.e. SPSW N and SPSW S) tested by Lee and Tsai (2008). SPSW N and SPSW S respectively had flexibility factors of 2.53 and 3.01, which are greater than the limit of 2.5 specified in the AISC Seismic Provision and the CSA S16-01 Standard. Yet, based on the proposed analytical models, the VBEs in these two specimens are not expected to undergo out-of-plane buckling. This prediction is consistent with the experimental observations. The VBEs of these two specimens exhibited ductile behavior up to story drifts greater than 5% as shown figures 5-26 and 5-27. The above assessment on SPSW N and SPSW S further confirms that there is no correlation between the flexibility factor, ω_t, and VBE out-of-plane buckling strength.
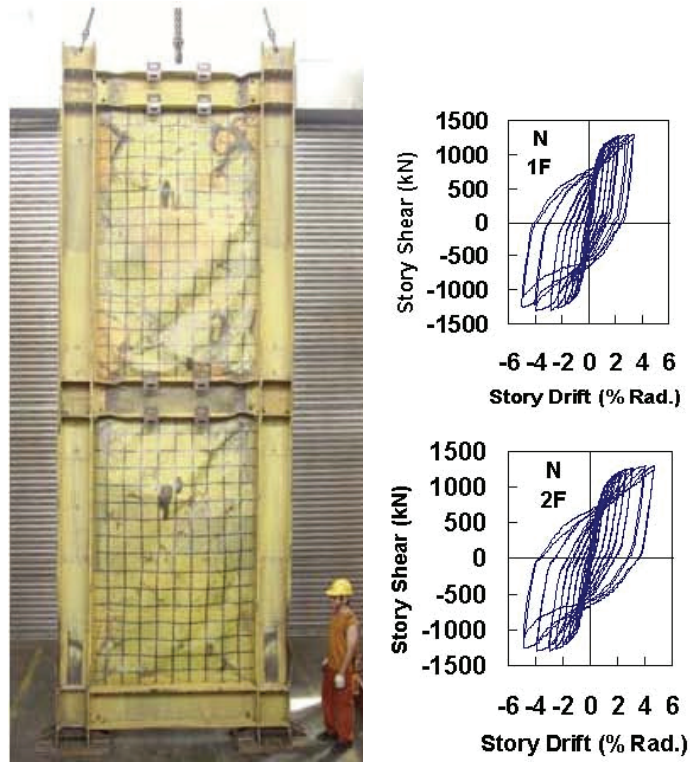
FIGURE 5-26 SPSW N at the End of the Tests and Hysteretic Curves
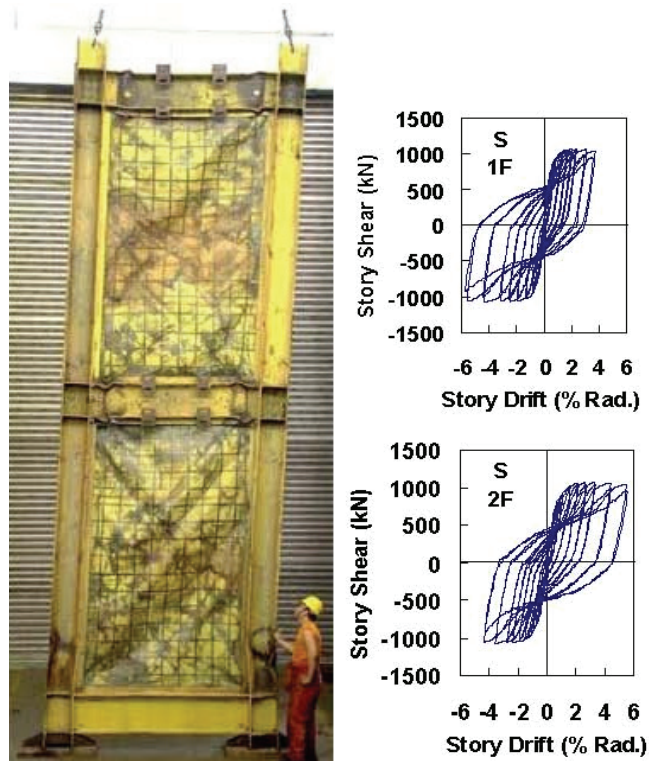
FIGURE 5-27 SPSW S at the End of the Tests and Hysteretic Curves

149

TABLE 5-3 Evaluation of VBE Out-of-Plane Buckling[a]

Case	Researcher	Specimen identification	Number of stories	ω_t	Criterion A	Criterion B	Criterion C	Criterion D
			(i) single-story specimens					
1	Lubell *et al.* (2000)	SPSW2	1	3.35	0.609	0.152	0.260	0.313
2	Berman and Bruneau (2005)	F2	1	1.01	0.006	0.001	0.002	0.003
			(ii) multi-story specimens					
3	Driver *et al.* (1998)	_[b]	4	1.73	0.159	0.040	0.073	0.077
4	Lubell *et al.* (2000)	SPSW4	4	3.35	2.325	0.581	1.066	1.119
5	Park *et al.* (2007)	SC2T	3	1.24	0.051	0.013	0.024	0.024
6		SC4T	3	1.44	0.087	0.022	0.040	0.042
7		SC6T	3	1.58	0.115	0.029	0.053	0.055
8		WC4T	3	1.62	0.142	0.036	0.065	0.068
9		WC6T	3	1.77	0.188	0.047	0.086	0.090
10	Qu *et al.* (2008)	_[b]	2	1.95	0.238	0.060	0.107	0.116
11	Lee and Tsai (2008)	SPSW N	2	2.53	0.111	0.028	0.050	0.054
12		SPSW S	2	3.01	0.199	0.050	0.090	0.097

[a] For multi-story specimens, VBEs at the first story are evaluated.
[b] Not applicable.

150

5.6 Summary

In this section, analytical work was conducted to assess the adequacy of the existing limit on the flexibility factor, ω_t, specified for VBE design by the AISC Seismic Provisions and the CSA S16-01 Standard. Review of the derivation of this flexibility factor from plate girder theory, and of how that factor was incorporated into current design codes was followed by the development of analytical models for preventing shear yielding and for estimating out-of-plane buckling strength of VBEs in SPSWs.

It is shown that putting the existing limit on ω_t is uncorrelated to ensure satisfactory in-plane/out-of-plane VBE performance. Alternatively, the proposed analytical models for in-plane shear demands, for which predicted performance correlates well with past experimental results, can be used in design to ensure desirable VBE behavior.

Future analytical and experimental research should investigate whether in-plane buckling equations similar to those used for out-of-plane buckling are necessary for use in the interaction equations to calculate the beam-column strength of VBEs, and whether other concerns may justify retaining the use of ω_t factor to achieve satisfactory seismic performance of VBEs in SPSWs.

SECTION 6

DESIGN OF STEEL PLATE SHEAR WALLS CONSIDERING BOUNDARY FRAME MOMENT RESISTING ACTION

6.1 Introduction

Building on the knowledge presented in the prior sections for the behavior and design of boundary frame members of SPSWs, it would be interesting and apropos to investigate the effects of boundary frame relative strength on global behavior and overall strength of SPSWs. Previous tests and analytical studies on single-story and multistory SPSWs (e.g. Berman and Bruneau 2003, Berman and Bruneau 2005, and Driver *et al.* 1997) recognized that a SPSW's ultimate strength combines the contributions of both the moment resisting boundary frame and the infill panels. However, strength of the wall due to the moment resisting action of boundary frame is not explicitly taken into account in the design of SPSWs by codes (i.e. the AISC Seismic Provisions and the CSA S16 Standard), typically resulting in a conservative but possibly more expensive SPSW design.

To investigate the relative contribution of boundary frames to the overall strength of SPSWs and possibly achieve an optimum design of SPSWs accounting for that contribution, this section reviews knowledge on the plastic strength of SPSWs, and summarizes some design assumption in current design codes. Then, design procedures considering boundary frame moment resisting actions are derived followed by a case study developed to compare the performance of SPSWs designed using various assumptions on the relative strength and design of boundary frames. A final section discusses the future work needed to further investigate the effectiveness of the proposed models.

6.2 Plastic Strength of Steel Plate Shear Walls

Plastic collapse mechanisms for SPSWs subjected to lateral loads have been investigated by Berman and Bruneau (2003). From that work, equations for the ultimate strength of

SPSWs have been shown to agree well with the results obtained from tests of single and multistory SPSWs. They examined two types of plastic mechanisms for multistory SPSW, namely, a uniform collapse mechanism and a soft-story collapse mechanism which are shown schematically in figure 6-1a and 6-1b, respectively.
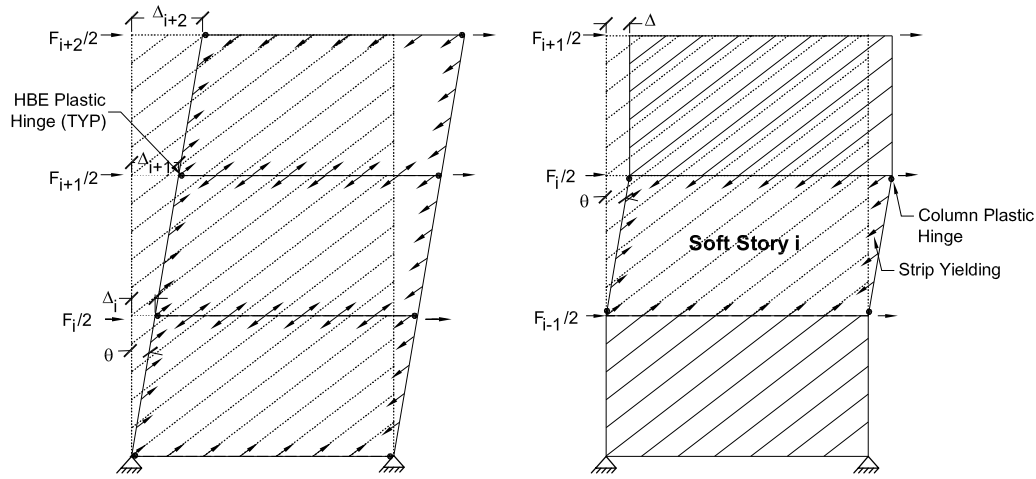
(a) Uniform Collapse Mechanism　　　**(b) Soft-Story Collapse Mechanism**
FIGURE 6-1 Plastic Mechanism of SPSWs (From Berman and Bruneau 2003)

The soft-story mechanism should be avoided in design. In the desired plastic mechanism, all the infill panels over the height of the wall must be fully yielded. This can be achieved, even for web plates of equal thickness over the height, by adjusting the sizes and moments of inertia of the surrounding HBEs and VBEs. Therefore, the uniform collapse mechanism shown in figure 6-1a is selected as the desired design objective for SPSWs and will be used in the derivations presented in the following sections.

For the uniform collapse mechanism, by equating the internal and external work, Berman and Bruneau (2003) derived the following general equation for the overall plastic strength of a SPSW with moment resisting HBE-to-VBE connections:

$$\sum_{i=1}^{n_s} F_i h_i = \underbrace{\sum_{i=1}^{n_s}\left(M_{pl_i} + M_{pr_i}\right)}_{\text{Contribution of boundary frame}} + \underbrace{\sum_{i=1}^{n_s}\frac{1}{2}R_{yp}f_{yp}Lh_i\left(t_{wi} - t_{wi+1}\right)\sin(2\alpha_i)}_{\text{Contribution of infill panels}} \qquad (6\text{-}1)$$

where F_i is the equivalent earthquake force applied on the wall; h_i is the ith story elevation; M_{pl_i} and M_{pr_i} are the expected plastic moments at the left and right ends of

154

the ith HBE respectively, t_{wi} is the thickness of the infill panel at the ith story; R_{yp} is the ratio of expected to nominal yield strength of infill panel; f_{yp} is the nominal yield strength of infill panel; L is the SPSW bay width; n_s is the total number of stories; and α_i is the tension field inclination angle at the ith story. Note that it is assumed here that VBEs of the wall are pinned to the ground and HBE hinges will form instead of VBE hinges at the roof level.

While the above provides the analytical expression that separates clearly the contribution of boundary frame and the contribution of infill panel to the total lateral strength of the SPSW, further experimental results in the literature explicitly quantify the contribution of each system. For example, figure 6-2a shows the hysteric curves obtained from tests of a single story SPSW by Berman and Bruneau (2005). Note that the web-angle HBE-to-VBE connections in that specimen had a non-negligible moment resisting capacity. Berman and Bruneau subtracted the boundary frame contribution from the total hysteretic response of the SPSW and obtained the results of infill panel only as shown in figure 6-2b. Comparing the curves shown in figure 6-2a and 6-2b, it is observed that the overall strength of the wall reduces from 645 kN to about 400 kN due to the absence of the contribution of boundary frame and the hysteretic curves of infill panel only exhibit significantly pinching behavior.
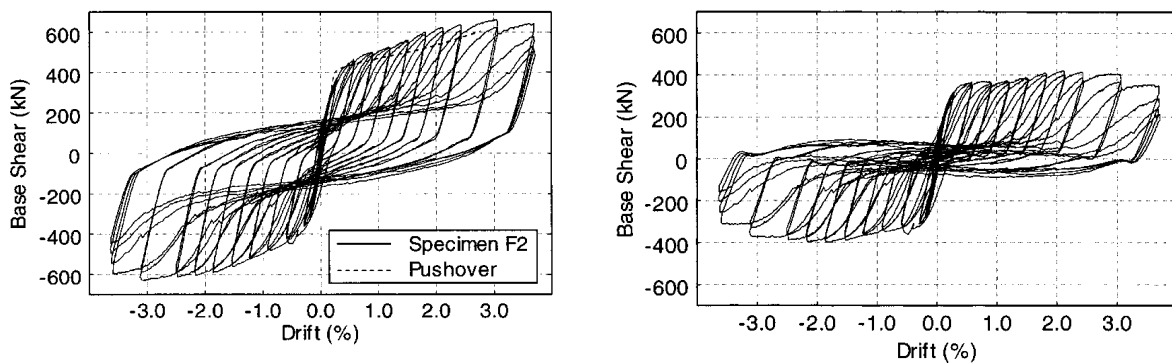
(a) Specimen Hystereses (b) Infill-Only Hystereses

FIGURE 6-2 Hystereses of a Single-Story SPSW
(Adapted from Berman and Bruneau 2005)

155

In another example of multistory SPSW with moment resisting HBE-to-VBE connections tested by Driver *et al.* (1997), the above observation was consistently obtained. Figure 6-3 presents the hysteretic curves and pushover curves of Driver *et al.* specimen. As shown, the strength due to the boundary frame moment resisting action contributes to about 25% of the global plastic strength of the wall.
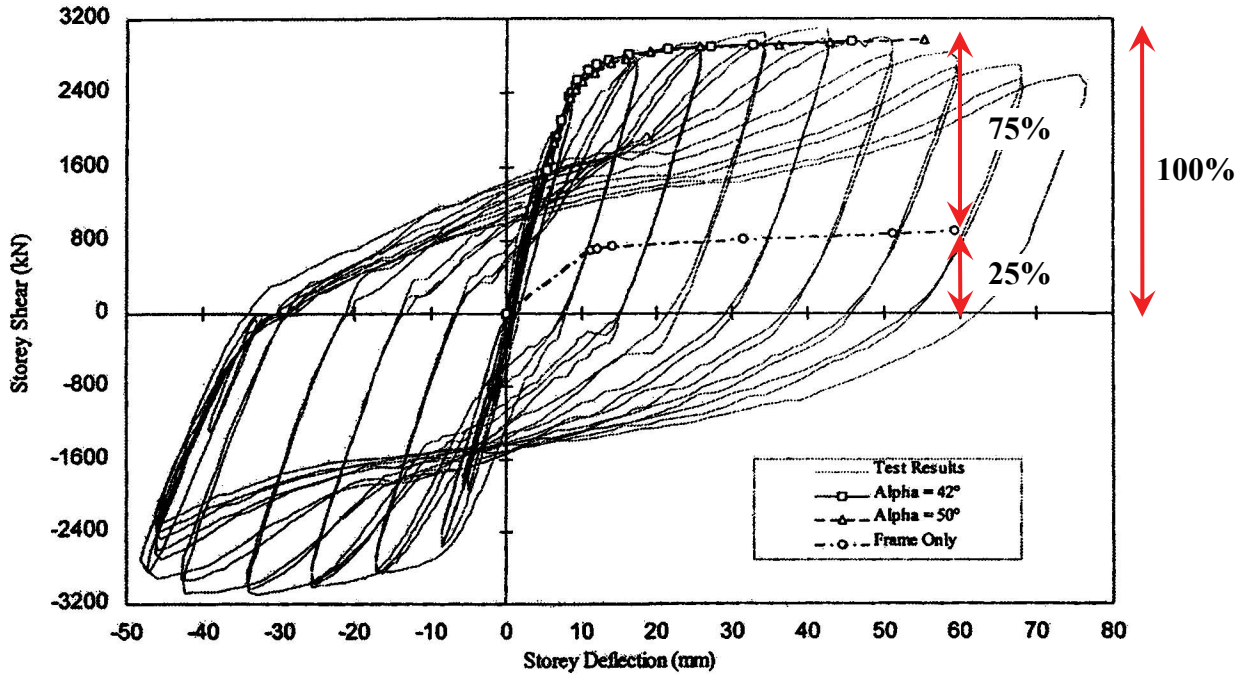
FIGURE 6-3 Test Results of a Multistory SPSW (Adapted from Driver *et al.* 1997)

6.3   Current Design Requirements

As shown in figure 6-2b, without the contribution of its boundary frame, the hysteresis loops of a SPSW exhibit severely pinching behavior, and, correspondingly, less energy dissipation would exist in a SPSW with simple HBE-to-VBE connections. Such a system would need to progressively drift to larger drifts to continue to dissipate substantial hysteretic energy. In addition, a SPSW with simple HBE-to-VBE connections will not have any additional lateral force resistance beyond that provided by the infill panel tension field actions, resulting in a system with less redundancy. Hence, the AISC Seismic Provisions requires the HBE-to-VBE connections to be rigid for the system. The CSA S16 Standard requires similarly for SPSW designs with the largest R factor and

allows SPSWs with simple HBE-to-VBE connections to be also implemented in seismic regions albeit with a significantly lower R factor ($R = 2.0$ versus 5.0, where 5.0 is the largest permitted for any systems by the CSA S16 Standard). However, neither design code takes into account the SPSW strength provided by the boundary frame moment resisting action as described below to resist the prescribed seismic loads.

Based on (6-1) presented in the previous section for the SPSW plastic strength one can obtain the following equation for calculating the shear strength of a single infill panel:

$$V_i = \frac{1}{2} R_{yp} f_{yp} L t_{wi} \sin(2\alpha_i)$$ (6-2)

where V_i is the expected strength of the considered infill panel and the other terms have been defined previously.

Dividing the infill panel strength determined from (6-2) by an overstrength factor, as defined by FEMA 369 (FEMA, 2001), and taken as 1.2 in this case (Berman and Bruneau, 2003), and also excluding the R_y factor used for calculating the expected plate strength, one can obtain the following infill panel nominal shear strength:

$$V_{ni} = 0.42 f_{yp} L t_{wi} \sin(2\alpha_i)$$ (6-3)

where V_{ni} is the nominal strength of the considered infill panel. This equation is implemented in the AISC Seismic Provisions and the CSA S16 Standard, and is used for sizing the thickness of infill panels of SPSWs.

Thus, by neglecting the contribution from the boundary frame moment resisting action on the SPSW strength, and solving for t_{wi} from (6-3), one can obtain the following design equation to select thickness of the infill panel.

$$t_{wi} = \frac{V_{ni}}{0.42 f_{yp} L \sin(2\alpha_i)}$$ (6-4)

Then, the AISC Seismic Provisions and the CSA S16 Standard require that the boundary frame members be designed using capacity design procedure to ensure that the boundary frame members can anchor the infill panel yield forces developed by the infill panel thickness determined from (6-4). As such, following this approach, strength provided by the boundary frame moment resisting action provides the SPSW with an overstrength (which has a positive impact on seismic performance). At the time of this writing, no analytical work had been done to quantify the magnitude of this overstrength in general terms and to investigate how to make use of it to achieve an optimum design of SPSWs. Such work is conducted in the following section.

6.4 SPSW Overstrength and Balanced Design

In order to best understand the SPSW overstrength resulting from the aforementioned design approach inferred by current design codes, which assumes that all the code-specified lateral forces applied on the wall are resisted by the infill panel tension field action alone, this section investigates the overstrength of SPSWs designed considering that various percentages of the lateral design forces are resisted by the infill panels. Both single-story and multistory SPSWs are considered.

6.4.1 Single-Story SPSW

A single-story SPSW is first studied here because this simple case provides some of the building blocks necessary to understand the more complex scenario (i.e. multistory SPSWs) presented later. Consider the single-story SPSW shown in figure 6-4 and expediently and conservatively assume that its VBEs are pinned to the ground. This assumption is done for two reasons, namely (i) the strengths of the plastic hinges at the column bases add very little to the lateral load resistance of a multistory SPSW, which is to be discussed later as an extension of the study of single-story SPSW, and (ii) taking into consideration of plastic hinges at the column bases will greatly increase the complexities of the equations derived below.
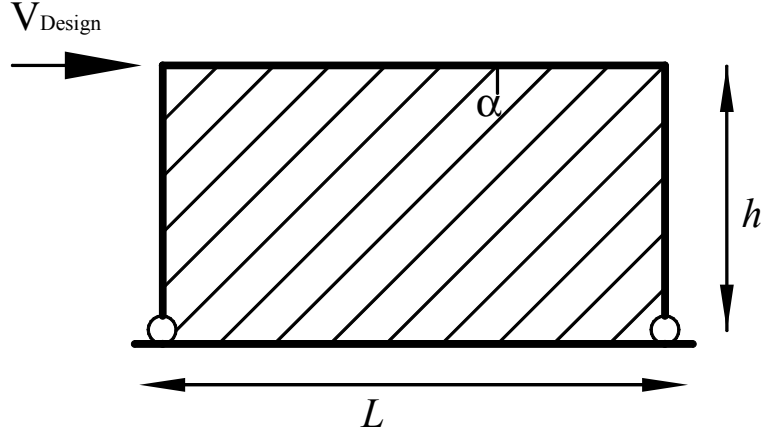
FIGURE 6-4 Single-Story SPSW Example

Assuming that the percentage of the total lateral design force assigned to the infill panel is κ, the required infill panel thickness is determined by solving for t_w from the following equation:

$$\kappa V_{design} = \frac{1}{2} R_{yp} f_{yp} L t_w \sin(2\alpha) \qquad (6\text{-}5)$$

where V_{design} is the lateral design force applied on the wall. Note that (6-5) is consistent with (6-2) when $\kappa = 1$ (i.e. when 100% of the lateral force is assumed to be resisted by the infill panel).

As described in Section 4, when the wall is fully yielded, the distributed loads to be applied along the VBEs (ω_{xc} and ω_{yc}) and HBEs (ω_{xb} and ω_{yb}) from infill panel yielding can be determined as:

$$\omega_{yc} = R_{yp} f_{yp} t_w \sin 2\alpha / 2 \qquad (6\text{-}6)$$

$$\omega_{xc} = R_{yp} f_{yp} t_w \left(\sin \alpha \right)^2 \qquad (6\text{-}7)$$

$$\omega_{yb} = R_{yp} f_{yp} t_w \left(\cos \alpha \right)^2 \qquad (6\text{-}8)$$

$$\omega_{xb} = R_{yp} f_{yp} t_w \sin 2\alpha / 2 \qquad (6\text{-}9)$$

159

Substituting (6-9) into(6-5), one can obtain the following relationship between lateral design force and horizontal tension field component along the HBEs:

$$\kappa V_{design} = \omega_{xb} L \tag{6-10}$$

Assuming that HBE plastic hinges (as normally the case rather than VBE plastic hinges) will form at the roof level, and following the plastic analysis procedure presented in Berman and Bruneau (2003), one can obtain the following equation for ultimate strength of the wall (equating the internal and external work)

$$V_p h = \omega_{xb} L h + 2 M_{pb} \tag{6-11}$$

where V_p is plastic strength of the wall; L and h are the wall width and height, respectively; and M_{pb} is the plastic strength of the HBE-to-VBE connections..

Assuming that the top HBE is proportioned using the design procedure proposed by Vian and Bruneau (2005), its resulting plastic section modulus is given as

$$Z_b = \frac{\omega_{yb} L^2}{4 f_y} \cdot \frac{1}{1+\sqrt{1-\eta^2}} \tag{6-12}$$

where η is the RBS plastic section modulus reduction ratio as described in Section 4; and f_y is the nominal yield strength of boundary frame.

Note that η in (6-12) may vary from unity (when there are no RBS connections in the top HBE) to the minimum value of RBS flange reduction permitted by the design specifications and guidelines (such as FEMA 350). Also note that (6-12) can be equivalently obtained from the HBE design equations presented in Section 4 when neglecting the reduction effects of HBE plastic moment due to the presence of internal forces. It is recognized that those reduction effects are expected to have negligible impacts on the global performance of the SPSW (although they should be taken into account if the focus is on understanding the local behavior and design of HBEs, as demonstrated in Section 4.).

Accordingly, the plastic strength of the top HBE-to-VBE connections is

$$M_{pb} = f_y \eta Z_b \qquad (6\text{-}13)$$

Substituting (6-12) into (6-13), the plastic strength of the top HBE-to-VBE connections can be further expressed as

$$M_{pb} = \frac{\omega_{yb} L^2}{4} \cdot \frac{\eta}{1 + \sqrt{1 - \eta^2}} \qquad (6\text{-}14)$$

Substituting (6-14) into (6-11) and solving for V_p

$$V_p = \omega_{xb} L + \frac{\omega_{yb} L^2}{2h} \cdot \frac{\eta}{1 + \sqrt{1 - \eta^2}} \qquad (6\text{-}15)$$

Based on (6-8) and (6-9), one can obtain the following relationship between ω_{xb} and ω_{yb}

$$\omega_{yb} = \tan^{-1}(\alpha) \omega_{xb} \qquad (6\text{-}16)$$

Substituting (6-16) into (6-15), the plastic strength of the wall becomes

$$V_p = \omega_{xb} L \left[1 + \frac{1}{2} \tan^{-1}(\alpha) \left(\frac{L}{h} \right) \cdot \frac{\eta}{1 + \sqrt{1 - \eta^2}} \right] \qquad (6\text{-}17)$$

Substituting (6-10) into (6-17), one can obtain a relationship between the SPSW plastic strength, V_p, and the lateral design force, V_{design}, namely

$$V_p = \kappa V_{design} \left[1 + \frac{1}{2} \tan^{-1}(\alpha) \left(\frac{L}{h} \right) \cdot \frac{\eta}{1 + \sqrt{1 - \eta^2}} \right] \qquad (6\text{-}18)$$

Here, the ratio of V_p to V_{design}, which is denoted as Ω_κ, is used to describe the overstrength of the SPSWs designed using different values of κ. Dividing by V_{design} on both sides of (6-18), one can determine Ω_κ as

$$\Omega_\kappa = \kappa \left[1 + \frac{1}{2} \tan^{-1}(\alpha) \left(\frac{L}{h} \right) \cdot \frac{\eta}{1 + \sqrt{1 - \eta^2}} \right] \qquad (6\text{-}19)$$

Explicitly shown in (6-19), the overstrength factor, Ω_κ, depends on a series of variables including, κ, α, L/h and η. The effects of those factors can be investigated based on (6-19). Here, a parametric study is conducted to discuss the impact of κ on Ω_κ for the given values of other terms.

Note that, for simplicity, the inclination angle of the tension field action is assumed to be 45° and η is assumed to be unity (i.e. no RBS connections are used in the HBEs). Note that results are not expected to vary substantially for other values of α. In addition, in the parametric study, the infill panel aspect ratio (i.e. L/h) was chosen to vary between 0.8 and 2.5, which are the limits allowed by the 2005 AISC Seismic Provisions.

The corresponding results are illustrated in figure 6-5. As shown, a higher percentage of the lateral design forces assigned to the infill panel (i.e. greater value of κ) results in a greater overstrength of the wall (i.e. greater value of Ω_κ). Under the design assumption presented in the AISC Seismic Provisions and the CSA S16 Standard (i.e. when $\kappa = 1.0$), the wall has a significant overstrength varying from 1.4 to 2.25 over the code-compliant range of infill panel aspect ratios of $0.8 \leq L/h \leq 2.5$. Note that the example wall assumes that the VBEs are pinned to the ground. It is recognized that, for the case that with VBEs fixed to the ground, the overstrength would be even greater.
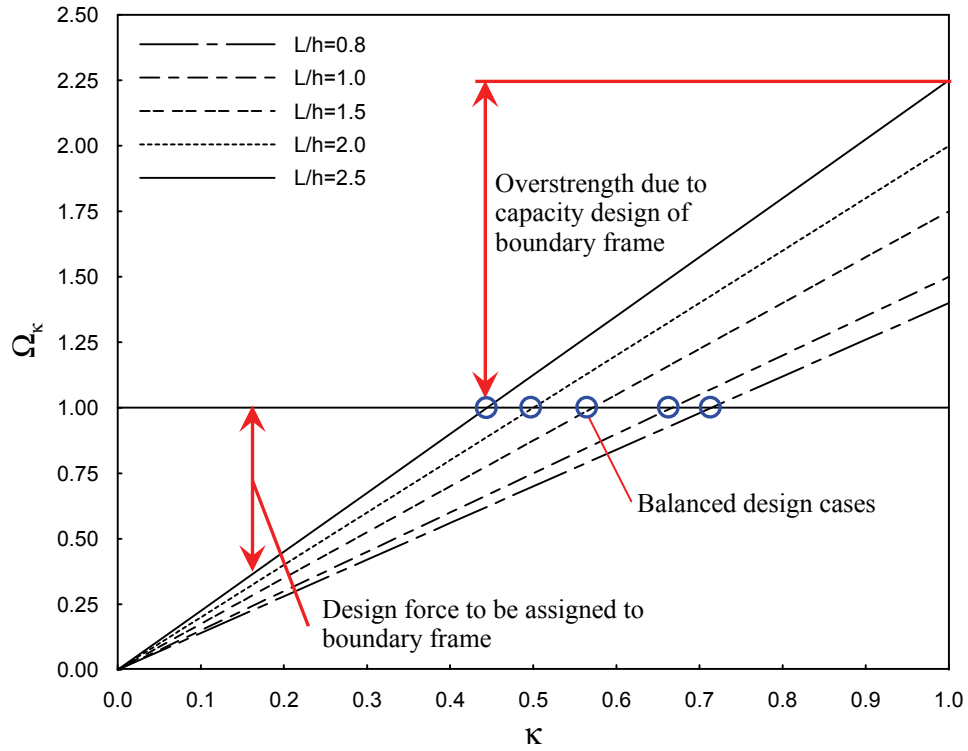
FIGURE 6-5 The Relationship between Ω_κ and κ (Assuming $\alpha = 45°$ and $\eta = 1.0$)

Also observed from figure 6-5, when κ is reduced to certain level, showed by the circles on that figure, the lateral force resisted by the boundary frame of the SPSW is exactly equal to that which will be required if that frame is designed to resist the yielding forces from the infill panel per capacity design principles. Therefore, at that particular point, the boundary frame does not provide any overstrength for the system as the division of the lateral load resistance and does not need to be made any stronger to satisfy all capacity design requirement, and the overstrength (Ω_κ) is therefore equal to unity. Such a design case is termed "balanced" design case in this report. For this case, the value of κ can be determined by setting the constraint $\Omega_\kappa = 1.0$ into (6-19) and solving for κ. The resulting value of κ for the balanced case, designated as $\kappa_{balanced}$, is therefore:

$$\kappa_{balanced} = \left[1 + \frac{1}{2} \tan^{-1}(\alpha) \left(\frac{L}{h} \right) \cdot \frac{\eta}{1 + \sqrt{1 - \eta^2}} \right]^{-1} \tag{6-20}$$

Figures 6-6 and 6-7 respectively plot, based on (6-20), the relationships between $\kappa_{balanced}$ and η for various L/h values, and $\kappa_{balanced}$ and L/h for various α values. As shown in figure 6-6, the value of $\kappa_{balanced}$ increases when η reduces. This observation is reasonable because the reserved strength of the wall due to the moment resisting action of the boundary frame decreases when RBS connections are introduced in the HBE (i.e. when $\eta \leq 1.0$), which means that, in this case, a higher percentage of lateral design force should be resisted by the infill panel tension field action. Note that, when η reduces to zero, which physically corresponds to simple HBE-to-VBE connections, $\kappa_{balanced}$ becomes unity, indicating that 100% of the lateral force is resisted by the infill panel.

Figure 6-7 illustrates the trends in $\kappa_{balanced}$ for the code-compliant range of infill panel aspect ratios and the typical range of tension field inclination angles. As shown, the value of $\kappa_{balanced}$ decreases when the aspect ratio increases. This is also reasonable since a bigger HBE member has to be used to anchor the tension field action in a "squat" wall (which has a greater aspect ratio) in comparison with a slender wall (which has a smaller aspect ratio), resulting in a higher strength of the wall due to the moment resisting action of the boundary frame.

As shown in figure 6-5, when reducing κ to a value below $\kappa_{balanced}$, the plastic strength of the wall is not sufficient to resist the lateral design force. In other words, the boundary frame designed only to resist the infill panel yield forces, per capacity design principles, has to be strengthened to fill the gap between the available strength of the wall and the expected lateral design demand. Incidentally, detailed information about the design of such SPSWs will be presented in Section 6.5.
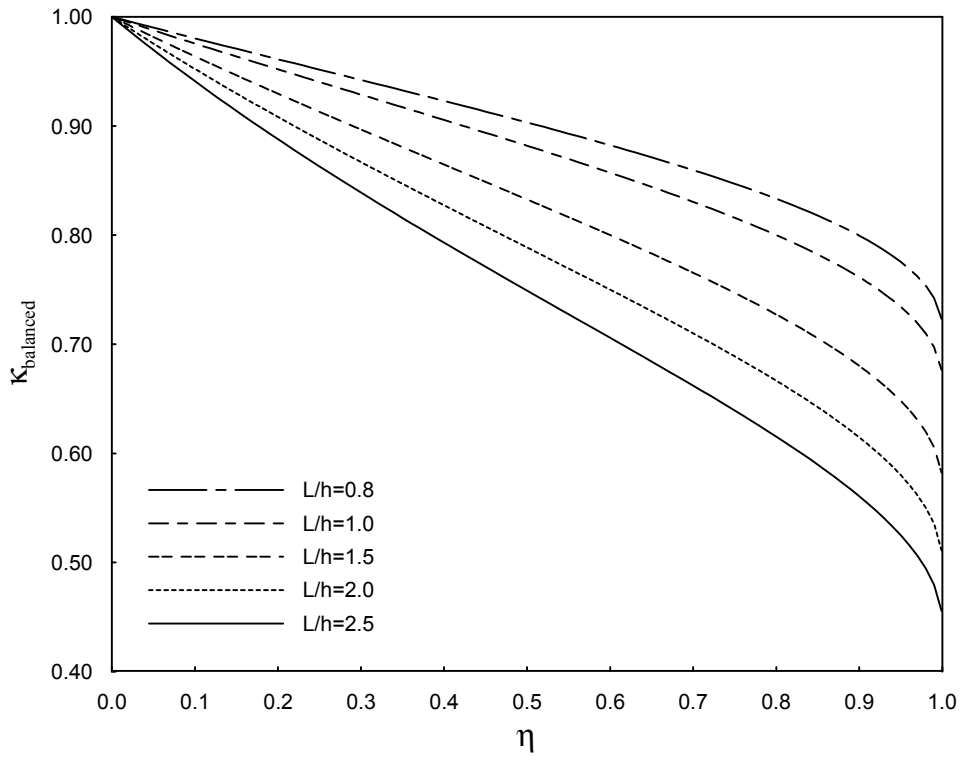
FIGURE 6-6 The Relationship between $\kappa_{balanced}$ and η (Assuming $\alpha = 45°$)
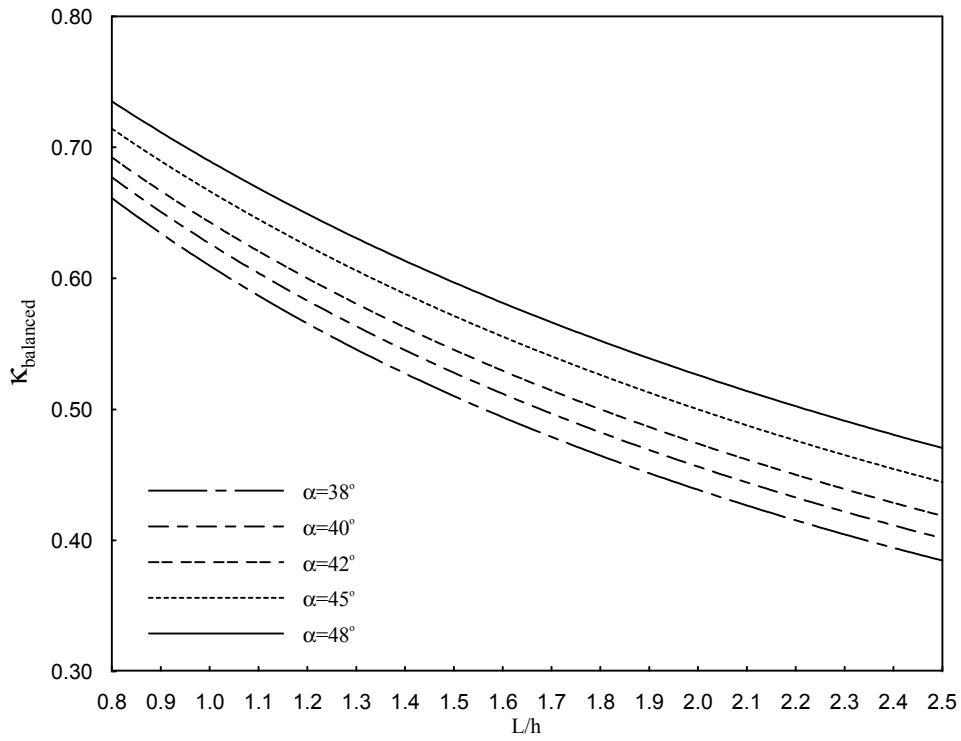
FIGURE 6-7 The Relationship between Aspect Ratio (L/h) and $\kappa_{balanced}$

(Assuming $\eta = 1.0$)

6.4.2 Multistory SPSW

The derivations presented in Section 6.4.1 for single-story SPSWs can be extended to the case of multistory SPSWs. The related procedures are briefly described below. Note that an index, i, is assigned to the variables associated with the ith floor level.

Consider a multistory SPSW with rigid HBE-to-VBE connections and VBEs pinned to the ground (for the same reasons as before) as shown in figure 6-8. Here, figure 6-8a shows the lateral design forces applied on the SPSW; figure 6-8b shows the modified lateral design force to size the infill panels and figure 6-8c shows the lateral force needed to develop the desired SPSW plastic mechanism. Based on those figures, the corresponding derivations are presented below.

(a) Lateral design force on SPSW (b) Modified lateral force to size infill panels (c) Lateral force to develop uniform yielding mechanism
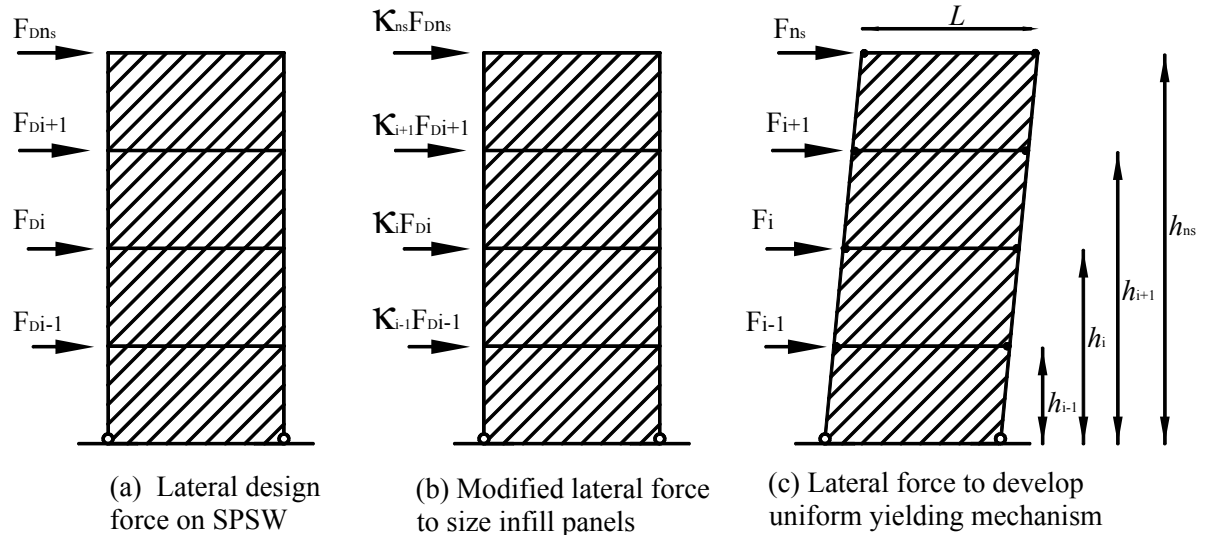
FIGURE 6-8 Schematic of a Typical Multistory SPSW

Similar to the procedure for single-story SPSWs, assigning part of the lateral design forces to the infill panel system, as shown in figure 6-8b and equating the infill panel shear strength and the corresponding design story shear at the ith and $i+1^{th}$ story, respectively, one can have

$$\omega_{xbi}L = \sum_{k=i}^{n_s} \kappa_k F_{Dk} \tag{6-21}$$

166

$$\omega_{xbi+1}L = \sum_{k=i+1}^{n_s} \kappa_k F_{Dk} \tag{6-22}$$

Subtracting (6-22) from (6-21)

$$\left(\omega_{xbi} - \omega_{xbi+1}\right)L = \kappa_i F_{Di} \tag{6-23}$$

It is assumed that the SPSW is able to develop the anticipated uniform plastic mechanism shown in figure 6-8c, and that HBE plastic hinges will form (instead of VBE plastic hinges) at the roof level. Consider an intermediate floor along the height of the wall as shown in figure 6-9a. Note that the derivations presented below are also valid for the top floor shown in figure 6-9b, simply by setting the magnitude of the tension field components of the upper story equal to zero.

(a) Intermediate Floor   **(b) Top Floor**
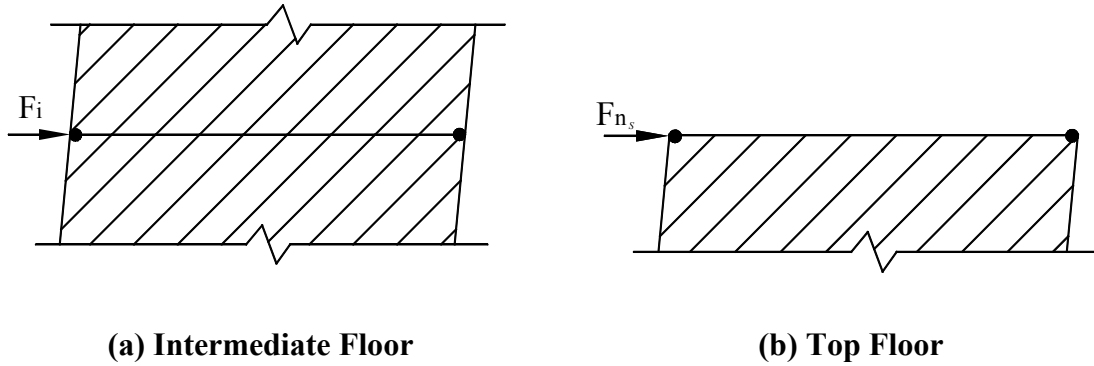
FIGURE 6-9 Segments of a Uniformly Yielded Multistory SPSW

Equating the internal and external work tributary to the considered intermediate floor, one can obtain the following equation:

$$F_i h_i = \left(\omega_{xbi} - \omega_{xbi+1}\right)L h_i + 2M_{pbi} \tag{6-24}$$

Assuming again that each intermediate HBE is proportioned using the design procedure proposed by Vian and Bruneau (2005), the resulting plastic section modulus is given as

$$Z_{bi} = \frac{\left(\omega_{ybi} - \omega_{ybi+1}\right)L^2}{4f_y} \cdot \frac{1}{1+\sqrt{1-\eta_i^2}} \tag{6-25}$$

167

Note that the procedure by Vian and Bruneau (2005) was originally developed for anchor HBE. However, that procedure can be alternatively used for intermediate HBE by considering the resulting vertical component of the tension field actions along the beam. Accordingly, the plastic moment of any HBE is determined as

$$M_{pbi} = \frac{\left(\omega_{ybi} - \omega_{ybi+1}\right)L^2}{4} \cdot \frac{\eta_i}{1+\sqrt{1-\eta_i^2}} \tag{6-26}$$

Substituting (6-26) and (6-23) into (6-24) , also considering (6-16) and solving for F_i, one can determine the force applied at each floor level to develop the expected mechanism, which is:

$$F_i = \kappa_i F_{Di} \left[1 + \frac{1}{2}\tan^{-1}(\alpha_i)\left(\frac{L}{h_i}\right) \cdot \frac{\eta_i}{1+\sqrt{1-\eta_i^2}}\right] \tag{6-27}$$

For the balanced design case,

$$F_i = F_{Di} \tag{6-28}$$

which physically means the lateral design force applied at each level of the SPSW is equal to that needed to develop the desirable mechanism.

Substituting (6-28) into (6-27), one can solve for κ_i for the balanced case:

$$\kappa_{balanced\,i} = \left[1 + \frac{1}{2}\tan^{-1}(\alpha_i)\left(\frac{L}{h_i}\right) \cdot \frac{\eta_i}{1+\sqrt{1-\eta_i^2}}\right]^{-1} \tag{6-29}$$

It is recognized that that (6-28) is a relatively "strong" constraint and may not be necessary for the global force equilibrium, which can be given as

$$\sum_{i=1}^{n_s} F_i = \sum_{i=1}^{n_s} F_{Di} \tag{6-30}$$

However, only based on (6-30), $\kappa_{balancedi}$ can not be determined. Hence, (6-28) is used herein.

To have a better understanding of the lateral forces respectively resisted by the infill panels and the boundary frame in the balanced design case for a multistory SPSW, consider a four-story SPSW without RBS connections as an example. Assume that the lateral design forces linearly distribute along the height of the wall as shown in figure 6-10 and the story heights and infill tension field inclination angles (45º) are constant in all stories. Figure 6-11 illustrates $\kappa_{balancedi}$ and the percentage of the story shear resisted by the infill panel at each level (i.e. to be considered to size the infill panels at each story). These results have been derived for the infill panel aspect ratios permitted by the 2005 AISC Seismic Provisions. For comparison purpose, the results for the case when 100% of the story shear is resisted by each infill panel (i.e. the design case implied by the AISC Seismic Provisions) are also provided in the figures.

As shown in figure 6-11, the lateral design forces and the corresponding story shears assigned to the infill panels are reduced in the balanced design case. For example, as shown in figure 6-11b, in the balanced design case, when the infill panel has an aspect ratio of 1.5, 78% of the base shear is resisted by the first-story infill panel when the wall develops the expected plastic mechanism.

(a) Lateral Design Forces   (b) Story Shear
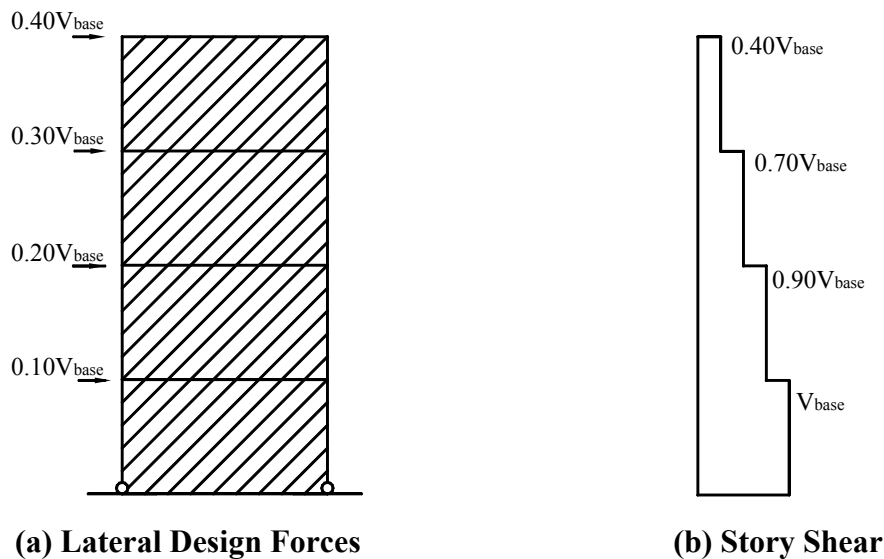
FIGURE 6-10 Description of Example Four-Story SPSW
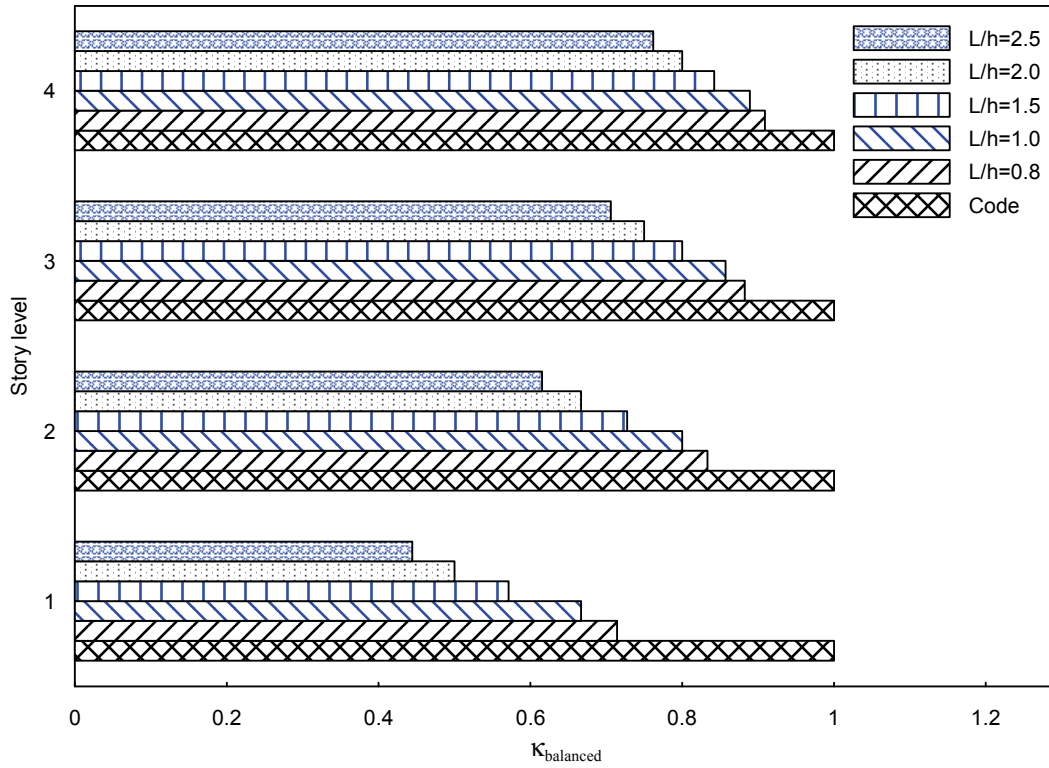
(a) Modified Lateral Design Forces along the Height of the Wall
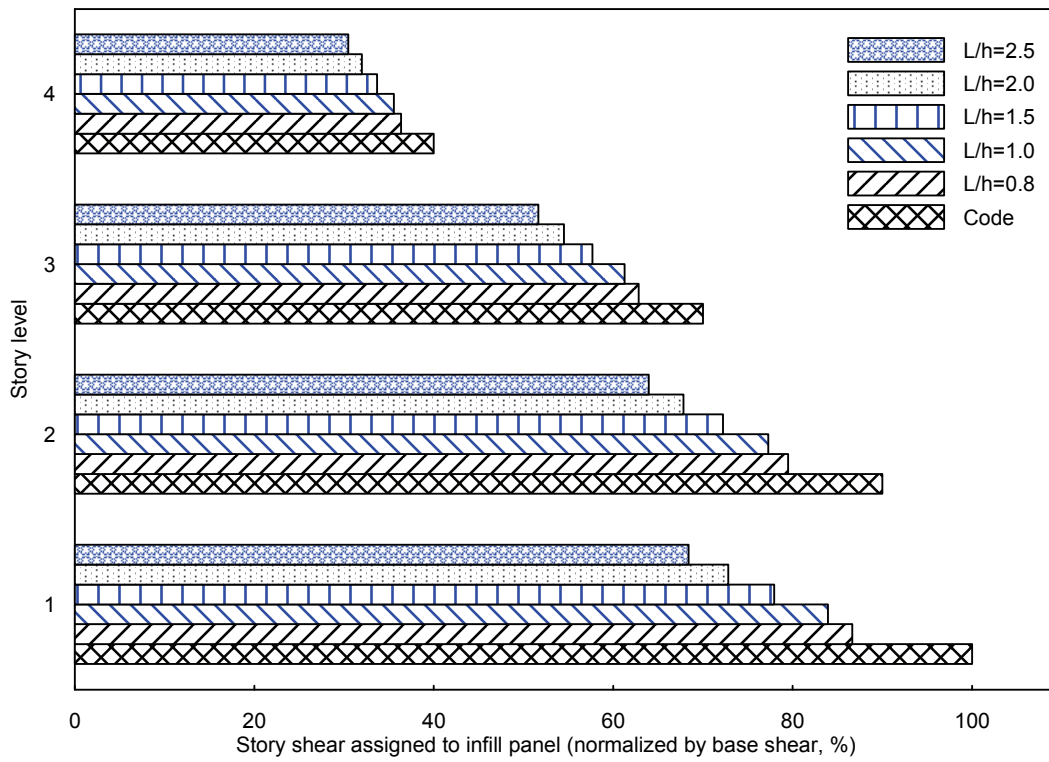
(b) Modified Story Shears to Size Infill Panels

FIGURE 6-11 Modified Design Forces of an Example Four-Story SPSW

170

6.5 Boundary Frame Design of SPSWs Having Weak Infill Panels

When the infill panel thickness is smaller than that corresponding to the balanced design case, the SPSW will not have sufficient strength to resist the lateral design force if the boundary frame is only proportioned using capacity design procedures (i.e. designed only to resist the infill panel yield forces). Here, such walls will be termed SPSWs having weak infill panels.

As a first step, the principle of SPSWs having weak infill panels is studied from a theoretical perspective to understand the implications of that concept. Intuitively, there would seem to be no benefits in using an infill panel thickness less than the balanced case that was discussed previously. However, without the knowledge of the equations presented in Section 6.4, an engineer may decide to apportion the percentage of the strength provided by the boundary frame and the infill panel arbitrarily to any number (e.g 50%-50%). When a weak infill panel is used, the boundary frame resulting from capacity design procedures needs to be strengthened to ensure that the overall SPSW (including both the infill panels and boundary frame) is able to resist the lateral design forces, i.e. in that case, capacity design considerations do not drive the design of the boundary frame.

To address the design procedures of the boundary frame of SPSWs having weak infill panels, consider the multistory SPSW shown in figure 6-12a. Assume the VBEs are pinned to the ground. Consistent with the definition of weak infill panels, the story shear assigned to each infill panel is smaller than that of the balanced case, which gives

$$\sum_{k=i}^{n_s} \kappa_k F_{Dk} \leq \sum_{k=i}^{n_s} \kappa_{balancedk} F_{Dk} \tag{6-31}$$

To better understand the lateral design demand resisted by the boundary frame, the SPSW is decomposed into two lateral force resisting systems as shown in figure 6-12, namely: (i) Frame B consisting of infill panels, which resists the lateral loads entirely through infill tension field actions together with a boundary frame without moment resisting connections; and (ii) Frame C as a frame without infill panels, which resists lateral loads

171

only through moment frame actions up to the development of plastic moments at the HBE-to-VBE connections. Note that the HBE end fixities and are removed in Frame B, since their contribution to lateral force resistance is taken into account in Frame C. The summation of lateral force resistances of the above two systems (i.e. Frames B and C) is equal to the SPSW lateral strength. Accordingly, the lateral force applied at each floor level of Frame C is $(1 - \kappa_i) F_{Di}$.

Design of Frame C can be achieved by following plastic analysis procedure and ensuring sufficient frame plastic strength. Three methods, which lead to different designs but same global plastic strength of the boundary frame, are presented below. What conceptually differs in the three methods considered below is that each case assumes a different distribution of HBE strength along the height of the SPSW for which the global plastic strength is satisfied but the local story-by-story strength is not necessarily satisfied. Note that the following derivations are based on plastic analysis and the yielding sequence of the members and the infill panels of the SPSW under the lateral forces is out of the scope of the work presented here.

For all methods used here to design the boundary frame, the resulting HBEs are checked to comply with the result determined from (6-25), i.e. capacity design is checked to ensure that all members are able to anchor their infill panel yield forces. In addition, the resulting designs are checked to satisfy the strong column and weak beam requirement to avoid undesirable behavior of the wall (e.g. soft story mechanism).
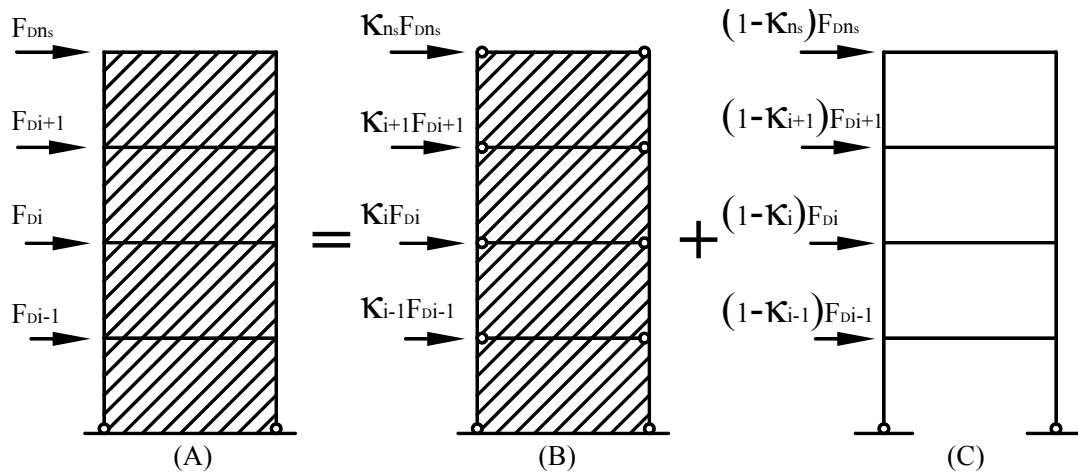
FIGURE 6-12 Decompositions of Lateral Forces and SPSW System

6.5.1 Design Method I

The first method to design the boundary frame assumes constant HBE cross-sections along the height of the wall. When the boundary frame as part of the wall develops the plastic mechanism shown in figure 6-13, equating the internal and external work of the boundary frame, one can derive the following equation:

$$\underbrace{\sum_{i=1}^{n_s}\left(1-\kappa_i\right)F_{Di}h_i}_{\text{External work}} = \underbrace{\sum_{i=1}^{n_s}2\cdot\eta_i\cdot f_y\cdot Z_b}_{\text{Internal work}} \tag{6-32}$$

Solving for Z_b gives,

$$Z_b = \frac{\displaystyle\sum_{i=1}^{n_s}\left(1-\kappa_i\right)F_{Di}h_i}{2f_y\displaystyle\sum_{i=1}^{n_s}\eta_i} \tag{6-33}$$

6.5.2 Design Method II

The second method to design the boundary frame determines HBEs from the virtual work equation of each story. For the plastic mechanism shown in figure 6-13, equating the internal and the external work tributary to the ith story, one can derive the following equation

$$\underbrace{\left(1-\kappa_i\right)F_{Di}h_i}_{\text{External work}} = \underbrace{2\cdot\eta_i\cdot f_y\cdot Z_{bi}}_{\text{Internal work}} \tag{6-34}$$

Solving for Z_{bi} gives,

$$Z_{bi} = \frac{\left(1-\kappa_i\right)F_{Di}h_i}{2f_y\eta_i} \tag{6-35}$$
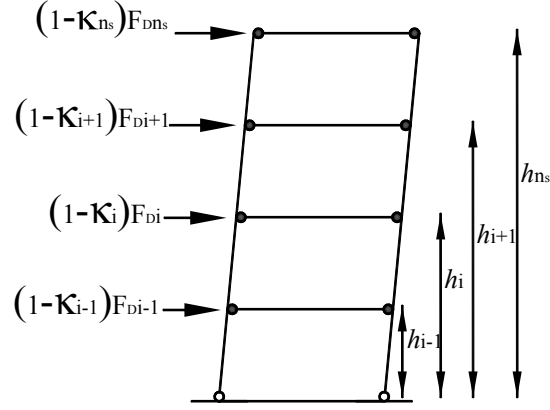
FIGURE 6-13 Plastic Mechanism of Boundary Frame

6.5.3 Design Method III

The third method to design the boundary frame determines HBEs from the virtual work equation of the sub-frame from the ith story to the top story. For the plastic mechanism shown in figure 6-13, equating the internal and external work of the $i+1^{th}$ sub-frame as shown in figure 6-14, one can derive the following equation

$$\underbrace{\sum_{j=i+1}^{n_s} \sum_{k=i+1}^{j} \left(1-\kappa_j\right) F_{Dj} h_{sk}}_{\text{External work}} = \underbrace{2f_y \cdot \left[\sum_{j=i+1}^{n_s} \eta_j Z_{b_j}\right]}_{\text{Internal work}} \tag{6-36}$$

where h_{si} is the ith story height, different from h_i used in the previous derivations (i.e. the ith story elevation).

Similarly, the equation for the ith sub-frame shown in figure 6-14 is

$$\underbrace{\sum_{j=i}^{n_s} \sum_{k=i}^{j} \left(1-\kappa_j\right) F_{Dj} h_{sk}}_{\text{External work}} = \underbrace{2f_y \cdot \left[\sum_{j=i}^{n_s} \eta_j Z_{b_j}\right]}_{\text{Internal work}} \tag{6-37}$$

Subtracting (6-36) from (6-37) and solving for Z_{bi}

$$Z_{bi} = \frac{\displaystyle\sum_{j=i}^{n_s} \left(1-\kappa_j\right) F_{Dj} h_{si}}{2f_y \eta_i} \tag{6-38}$$

174
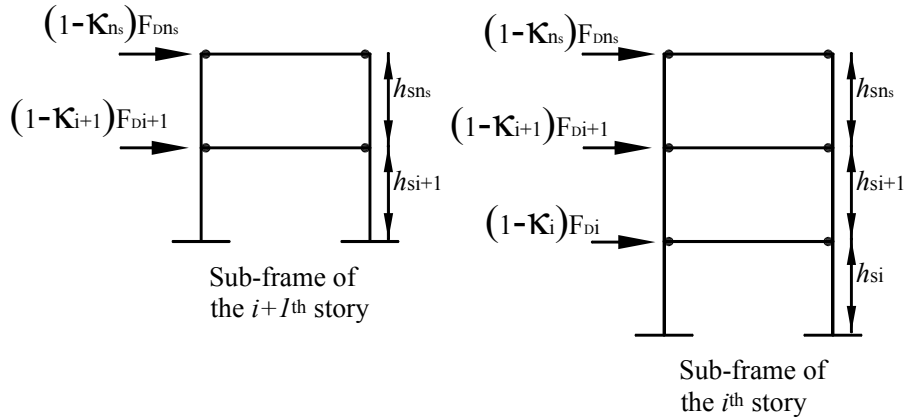
FIGURE 6-14 SPSW Sub-Frames

6.6 Case Study

Sections 6.4 and 6.5 presented different approaches for SPSW design. To be able to determine the relative merits of any of those designs which will provide the same lateral load resistance, it is important to conduct nonlinear time history analyses to compare the seismic performance of the walls respectively designed using various distributions of the lateral loads between the boundary frame and infill panels as well as various distributions of HBE strength that satisfy the total plastic strength of the structure. Such a study is conducted in this section. The following briefly describes assumptions, design results, and the performances of those differently designed SPSWs in the nonlinear time history analyses.

6.6.1 Assumption and Design Summary

An eight-story single-bay SPSW was used as the prototype structure in this study. The VBEs were assumed to be pinned to the ground and the first-story infill panel was assumed to be anchored to the ground rather than to an anchor beam at that level. The bay width and constant story height were assumed to be 10 and 18 ft, respectively, resulting in an infill panel aspect ratio of 1.8, which is within the range allowed in the 2005 AISC Seismic Provisions.

The structure was assumed to be located on class B soil in Northridge, CA. Its weight was assumed to be 5092.5 kips distributed as 652.5 kips at all stories except at the roof where it was 525 kips. Seismic design loads were calculated using FEMA 450 (FEMA,

2004) and the associated spectral acceleration maps. Design short and 1-second spectral ordinates, S_{DS} and S_{D1}, were calculated to be 1.43g and 0.50g, respectively. The period of the structure was estimated (using the FEMA procedures) to be 0.54 second, and using a response modification factor, R, of 7, and importance factor I, of 1, the base shear for the structure was found to be 674.5 kips.

Corresponding lateral loads up the height of the structure are presented in table 6-1. As shown in the table, the AISC design procedure, the developed procedure to achieve a balanced design, and the design procedure assuming 40% of the story shear is resisted by the infill panel at each story of the SPSW (i.e. the procedure for the SPSWs having weak infill panels) are considered to select the infill panel thicknesses of the SPSW. Note that it is assumed that the calculated infill panel thicknesses are available in all cases.

For the SPSW having weak infill panels, all three HBE design methods developed in Section 6.5 were considered for design of the boundary frame. As a result, a total of five SPSW designs were obtained, i.e. one from the AISC design procedure, one from the balanced design procedure, and three from the procedure for SPSWs having weak infill panels (respectively using methods I, II and III). The boundary frame members from those five designs are listed in table 6-2. Note that the three designs of the SPSW with weak infill panels had the same infill panels but different boundary frame members.

As shown in table 6-2, the boundary frame members from the balanced design are smaller than those from the AISC code design because the former considers the lateral force resistance of the SPSW due to the boundary frame moment resisting action. However, the boundary frame members are getting stronger at some stories of the SPSW having weak infill panels. This is because, in this study, each weak infill panel was sized to resist only 40% of the story shear and the boundary frame members proportioned using capacity design principles (i.e. designed only to resist the infill panel yield forces) are not sufficient to resist the remaining 60% of the story shear and therefore those boundary frame members had to be strengthened. Also shown in table 6-2, the HBE size distribution along the height of the SPSW, as expected, varies in the three designs using weak infill panels.

176

For comparison purpose, figure 6-15 illustrates the resulting steel weight for each design (also broken down in terms of each component). As shown, the balanced design is the most optimum in terms of the total weight of steel. Also shown in figure 6-15, for designs using weak infill panels, although the steel weight of infill panels decreases, the steel weight of boundary frame members increases for the reason presented earlier, resulting in an even higher value of the total steel weight in those designs.

TABLE 6-1 Summary of Design Story Shears and Infill Panel Thicknesses

Story Level	Elevation (ft)	Lateral Force (kip)	Modified Story Shear (kip)			Infill panel thickness (in)		
			AISC	Balanced design	Weak infills	AISC	Balanced design	Weak infills
8	80	127.1	127.1	113.0	50.8	0.033	0.029	0.013
7	70	137.9	264.9	233.6	106.0	0.069	0.060	0.027
6	60	117.9	382.8	335.5	153.1	0.099	0.087	0.040
5	50	97.9	480.7	422.9	192.3	0.124	0.109	0.050
4	40	78.0	558.7	492.0	223.5	0.144	0.127	0.058
3	30	58.2	616.9	542.8	246.8	0.160	0.140	0.064
2	20	38.5	655.5	575.8	262.2	0.170	0.149	0.068
1	10	19.0	674.5	590.1	269.8	0.174	0.153	0.070

TABLE 6-2 Design Summary of Boundary Frame Members

Boundary Frame Member ID[*]	AISC	Balanced design	Weak infills Method I	Weak infills Method II	Weak infills Method III
HBE-8	W18x76	W18x71	W18x158	W18x311	W18x50
HBE-7	W18x86	W18x71	W18x158	W18x311	W18x97
HBE-6	W18x65	W18x60	W18x158	W18x234	W18x130
HBE-5	W18x65	W18x60	W18x158	W18x158	W18x158
HBE-4	W18x60	W18x55	W18x158	W18x106	W18x192
HBE-3	W18x55	W18x50	W18x158	W18x65	W18x211
HBE-2	W18x50	W18x40	W18x158	W18x40	W18x211
HBE-1	W18x50	W18x40	W18x158	W18x40	W18x211
VBE-8	W30x116	W30x108	W40x167	W40x235	W40x149
VBE-7	W30x116	W30x108	W40x167	W40x235	W40x149
VBE-6	W40x183	W40x167	W40x235	W40x235	W40x235
VBE-5	W40x183	W40x167	W40x235	W40x235	W40x235
VBE-4	W40x277	W40x264	W40x264	W40x264	W40x264
VBE-3	W40x277	W40x264	W40x264	W40x264	W40x264
VBE-2	W40x431	W40x362	W40x362	W40x362	W40x362
VBE-1	W40x431	W40x362	W40x362	W40x362	W40x362

[*]HBE and VBE at the ith story are represented by HBE-i and VBE-i, respectively.
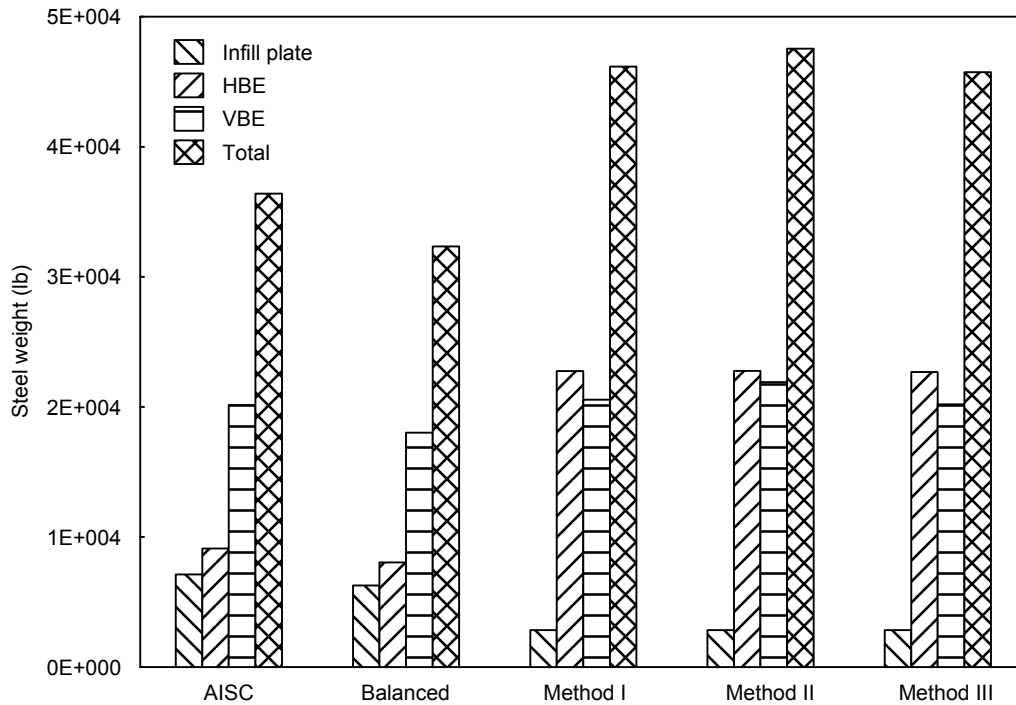
FIGURE 6-15 Comparison of Steel Weight

6.6.2 Analytical Model and Artificial Ground Motions

To quantify the seismic performance of those SPSWs designed using different procedures, nonlinear time history analyses were conducted on models constructed using the dual strip procedure described and validated in Qu *et al*. (2008). Three realizations of the target acceleration spectra compatible ground motion were obtained using the computer program, TARSCTHS, by Papageorgiou *et al.* (1999) and were used as ground excitations for the nonlinear time history analyses. The dual strip model, ground motion realizations and acceleration spectra are shown in figure 6-16.
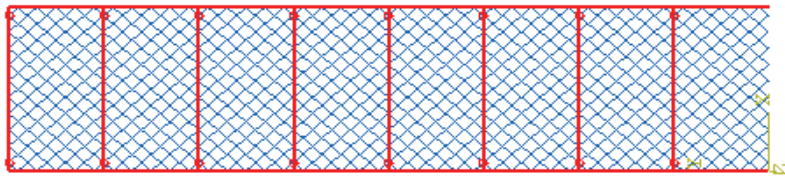
(a) Dual Strip Model
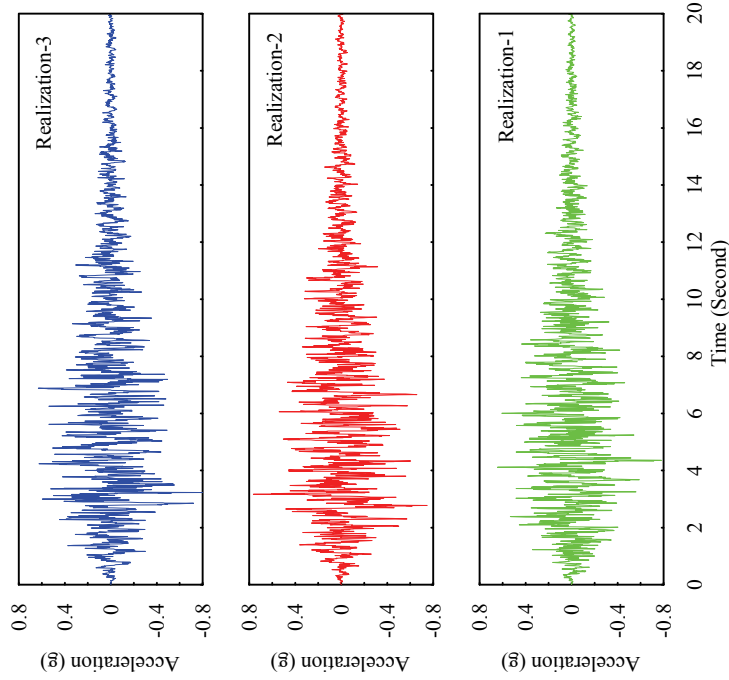
(b) Ground Motion Histories
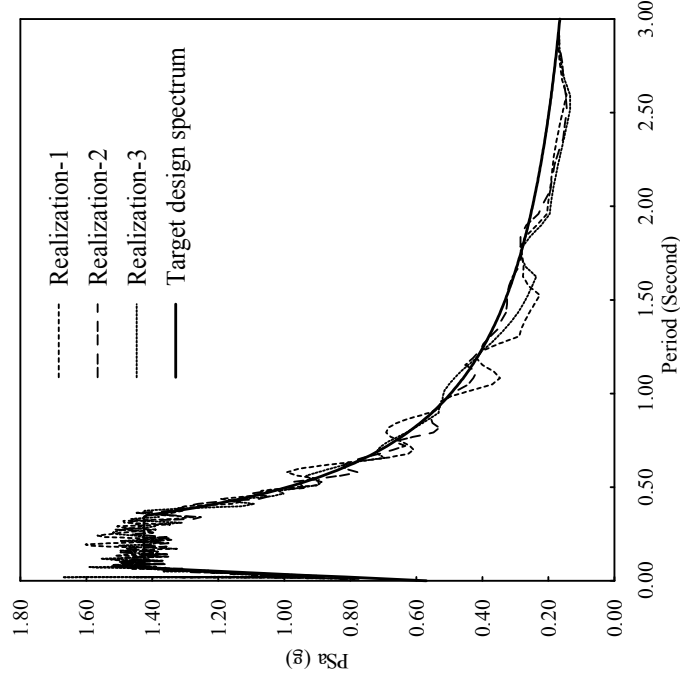
(c) Pseudoacceleration Spectra

FIGURE 6-16 Dual Strip Model and Ground Motion Information

179

6.6.3 Result Comparison

The maximum rotation of each HBE (including both elastic and plastic responses) and the maximum drift of each story were obtained from the nonlinear time history analyses to compare the seismic performances of the 5 different SPSWs designed in Section 6.6.1. Figure 6-17 presents the corresponding results along the height of the walls for each considered earthquake.

As shown, the wall from the balanced design exhibits similar performance to that of the wall designed using the AISC Seismic Provisions. For example, the average of the maximum first-story drifts of the wall designed using the balanced design procedure for the three earthquake realizations is 1.48%, which is close to the corresponding result of 1.30% from the wall designed using the AISC Seismic Provisions. For comparison purpose, the corresponding averages of the maximum first-story drifts the SPSWs having weak infill panels and designed using methods I, II and III are calculated to be 1.98%, 3.12% and 1.65%, respectively.

Another observation from figure 6-17 is that the maximum HBE rotations and story drifts are distributed in a uniform pattern along the heights of all SPSWs except for the wall having weak infill panels and designed using method II. As shown, significant deformations concentrated in the lower stories of that SPSW although less responses are observed in its upper stories.
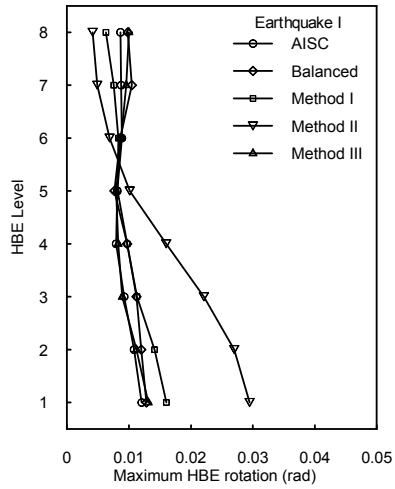
(a) Maximum HBE Rotation (EQ-1)   **(b) Maximum Story Drift (EQ-1)**
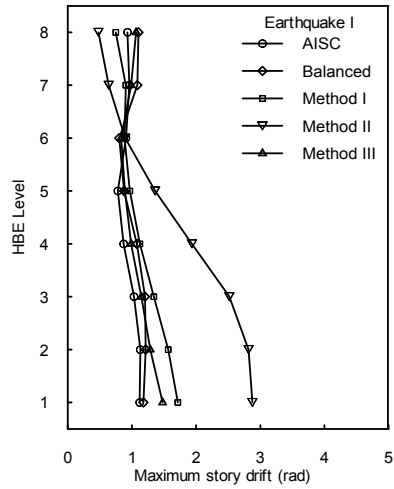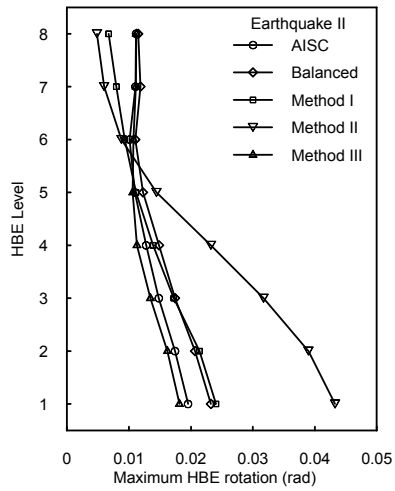
(c) Maximum HBE Rotation (EQ-2)   **(d) Maximum Story Drift (EQ-2)**
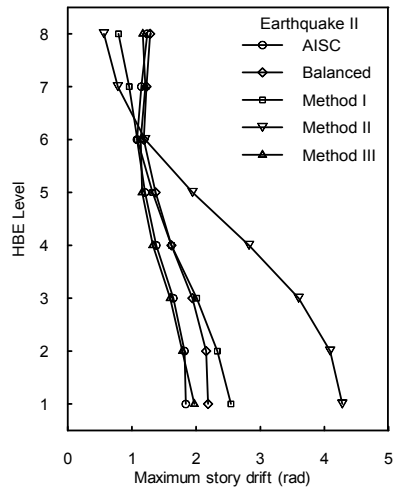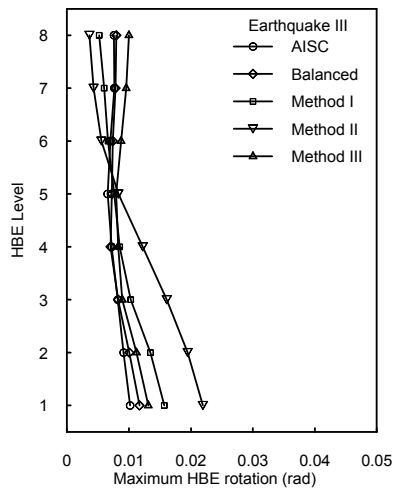
(e) Maximum HBE Rotation (EQ-3)   **(f) Maximum Story Drift (EQ-3)**
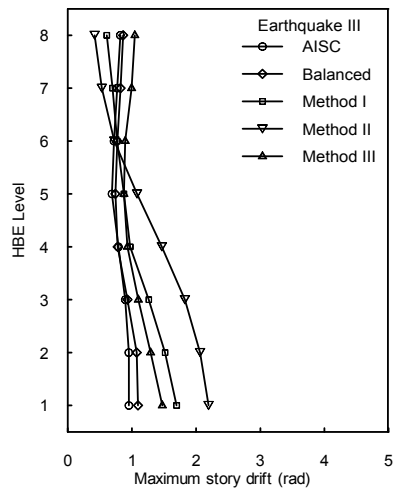
FIGURE 6-17 Results from Time History Analyses

181

6.7   Further Consideration

As observed in previous experimental research, SPSWs combine the behaviors of the moment resisting boundary frame and the infill panel system, which, taken alone, exhibit ductile and pinched hysteretic behaviors as schematically shown in figure 6-18a and 6-18b, respectively.

In the previous section, all the SPSWs were designed to resist the same level of lateral loads. Typically, the lateral loads are determined by code procedures which reduce the maximum elastic demands by the response modification factor (typically expressed by the parameter R). Traditionally, the R factor has been implicitly tied to the hysteretic energy dissipation capabilities of the structural systems. Those being more ductile are typically afforded larger R values. Traditionally; systems with highly pinched hysteretic behaviors have been penalized by having lower R values. While the previous parametric study in Section 6.6 is informative, it remains incomplete as it assumes that all SPSWs are designed for the same R value.
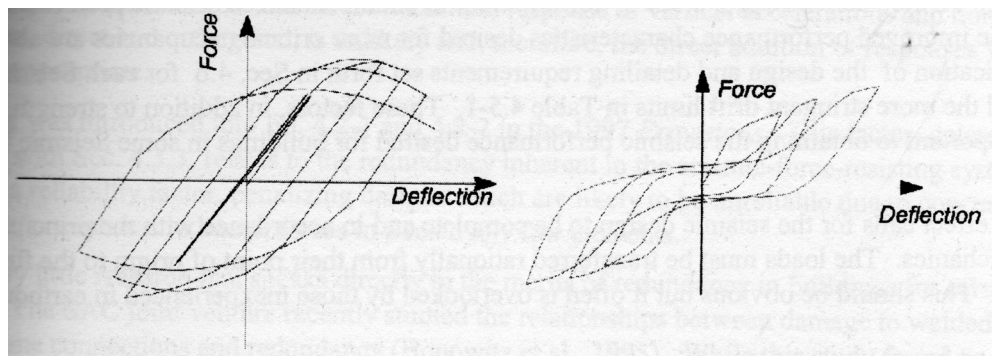
| (a) Ductile hysteretic loops | (b) Ductile hysteretic loops |

FIGURE 6-18 Typical Hysteretic Curves (from FEMA 450)

As stated in FEMA 450, "…Structural systems with larger energy dissipation capacity have larger R_d values, and hence are assigned higher R values, resulting in design for lower forces, than systems with relatively limited energy dissipation capacity. …" However, as typically done in conventional design, the same R value was used for all the SPSWs in the case study presented in Section 6.6. Opportunity exists for future research

to investigate what value of *R* should be used for those walls using different design assumptions and to provide greater insight as well as more definitive conclusions on the previously presented observations.

Given that some of the systems designed for the same level of lateral loads experienced greater story drifts and HBE rotations, it is conceivable that it might be desirable to reduce the R factor of the system that exhibits much greater inelastic response at specific stories. Therefore, if the parametric study was repeated with those systems designed for lower R values as a consequence of their decreased capability to dissipate hysteretic energy and to limit the drift and HBE rotation demands, it is quite possible that the savings in structural steel weights shown previously in figure 6-15 may not exhibit the same trends and that the apparent savings might be even eliminated.

In the past, R values have been assigned based on the judgment of code committee members on the respective and relative ability to dissipate energy of various structural systems as compared to each other. An effort is underway to develop a systematic and rigorous technical procedure to develop R factors, as documented in the ATC-63 90% Draft (FEMA, 2008). The recommended methodology for reliably quantifying R values as described in ATC-63 is based on a review of relevant research on nonlinear response and collapse simulation, benchmarking studies of selected structural system, feedback from an expanded group of experts and potential users, and evaluations of additional structural systems to verify the technical soundness and applicability of the approach.

At this point, it would be a major undertaking beyond the scope of this work to conduct such a derivation of appropriate R factors. However, the work undertaken in this section illustrates the technical issues that need to be resolved to establish to which degree the seismic loads applied to a SPSW could partly be resisted by the boundary frame surrounding the infill panels. While awaiting further results on such studies on R values, it is recommended for conservatism to continue designing SPSWs according to the AISC Seismic Provisions, or in the most permissive cases using the procedure corresponding to the balanced design. In other words, to design the infill panels of a SPSW for 100% of the story shears, based on the limited data provided here, or relax the design rule to design

the infill panels for the story shears determined from the procedure of the balanced design, for which a reasonable similarity in responses have been observed from the preliminary analysis results shown in figure 6-17.

6.8 Summary

This section investigated the lateral load resistance of SPSWs respectively provided by the boundary frame moment resisting action and the infill panel tension field action. Then, a procedure which considers the contributions of these two actions to the overall SPSW strength (i.e. a procedure to achieve a balanced design) was developed. Design of SPSWs having weak infill panels was also studied and three different methods that assume different HBE strength distributions along the SPSW height were developed.

A series of nonlinear time history analyses were conducted to evaluate the seismic performance of SPSWs designed using these different procedures (i.e. respectively designed using the AISC Seismic Provisions, using the developed balanced design procedure, and using the three methods for the SPSWs having weak infill panels). It was shown that the SPSW designed using the balanced design procedure exhibits similar performance to that designed using the AISC Seismic Provisions.

Finally, the future work to provide greater insight and more definitive conclusions on SPSW design is outlined.

SECTION 7

SUMMARY, CONCLUSIONS, AND RECOMMENDATIONS FOR FUTURE RESEARCH

7.1 Summary

In this report, the seismic behavior of boundary frame members (i.e. HBEs and VBEs) was investigated, and new design approaches were correspondingly proposed for those members.

- Analytical models were first developed for estimating the plastic moments of HBEs in SPSWs. Those procedures are based on classic plastic analysis and rely on calculation of the reduced axial yield strength of the HBE web accounting for the presence of shear and vertical stresses due to infill panel forces. Results from these procedures were shown to agree well with those from FE analysis. Simplified models were also developed for practical purposes and were shown to be accurate.

- The effects of axial and shear forces in intermediate HBEs were studied using plastic mechanisms and simple free body diagrams. A capacity design procedure was then proposed for intermediate HBEs. This procedure prevents HBE in-span plastic hinging and ensures adequate moment capacity at VBE faces when RBS connections are used. The proposed model differs from the current design approach in that it: (i) considers reduced HBE plastic moment strength to account for the presence of axial load, shear force, and vertical stresses in HBEs; (ii) is able to capture the fact that resultant action of the vertical tension field components is not equally resisted by each end of an HBE; and (iii) accounts for the variation of plastic hinge location in an HBE having RBS connections. FE analyses were used to validate the proposed approach. Finally, the intermediate HBE of a tested SPSW was examined and the observed HBE failure was explained using the knowledge and methodologies developed.

185

- For design of VBEs, analytical work was conducted to assess the adequacy of the VBE flexibility limit specified by the AISC Seismic Provisions and CSA S16-01. Derivation of the flexibility factor in plate girder theory and how that factor was incorporated into current design codes was reviewed. In addition, analytical models to estimate out-of-plane buckling strength and prevent shear yielding of VBEs were developed. It was shown that the flexibility factor, ω_t, is uncorrelated to satisfactory in-plane/out-of-plane VBE performance. Alternative analytical models were proposed and correlated well with the past experimental results.

- Finally, the contribution of boundary frame moment resisting action to the overall SPSW plastic strength was investigated. A procedure was developed to account for this moment resisting action to achieve a balanced design followed by the derivations of three different procedures for the SPSWs having weak infill panels. A case study was further developed to compare the performances of the SPSWs designed using different procedures. It was found that the wall designed according to the balanced design procedure may be optimum in terms of the total amount of steel and be able to exhibit acceptable seismic performance. However, SPSWs having weak infill panels may not necessarily be optimum in terms of seismic performance and amount of steel.

7.2 Conclusions

- In this research, an improved capacity design procedure was developed for HBEs accounting for the reduced HBE plastic moments due to the biaxial stress conditions in HBE webs and the complete free body diagrams of HBEs. Such a capacity design procedure can be used to explain the observed intermediate HBE failure reported in Qu et al (2008) and ensure a desirable ductile HBE behavior in future designs.

- Analytical investigations on VBEs showed that the existing VBE flexibility limit is uncorrelated to satisfactory in-plane and out-of-plane VBE performance. Alternatively, a proposed analytical model for preventing in-plane shear yielding

and out-of-plane buckling of VBEs predicted performance that correlates well with past experimental results, and can be used to ensure the desirable VBE behavior.

- An optimum SPSW design in terms of the total amount of steel and SPSW seismic performances can be achieved following the balanced design procedure developed accounting for the contribution of boundary frame moment resisting action to the overall SPSW plastic strength, although future research is needed to provide further insight for this procedure.

7.3 Recommendations for Future Research

The above results lead to the following recommendation for further research.

- Given that this research has explained that the observed patterns of yielding in the RBS details of SPSWs (which are different from those observed in conventional steel moment frame) depend on the significant axial force, shear force and vertical stresses acting in the HBE web and caused by infill panel yield forces, it would be interesting to explore if different geometries for the reduction of the flanges and webs of HBEs could be developed to enhance the ductile performance of HBE-to-VBE connections.

- The rational models developed to prevent the in-plane shear yielding and predict the out-of-plane buckling strength of VBEs, and validated by comparison with results from previous experimental studies on SPSWs, could be expanded by future analytical and experimental research to: (1) investigate whether in-plane buckling equations similar to those developed for the out-of-plane bucking cases could be equivalently derived and useful to enhance the interaction equations to calculate the beam-column strength of VBEs, and; (2) assess whether other concerns may exist to justify retaining the use of flexibility factor (i.e. ω_t) to achieve satisfactory seismic performance of VBEs in SPSWs.

- SPSWs explicitly designed to rely on the sum of the moment resisting boundary frame and infill panel system to resist lateral load might need, in some instances, to be assigned different R values than SPSWs for which the infill panel is designed to resist the totality of the code-specified lateral loads and for which the boundary frame provides a beneficial overstrength. Currently, in absence of guidance to the contrary, engineers could use the same R value for all SPSWs. Future research is needed to address how to determine the R value for each SPSW or whether it is appropriate to use the same R value for all cases.

SECTION 8

REFERENCES

AISC. (2005), "Seismic Provisions for Structural Steel Buildings." American Institute of Steel Construction, Chicago, Illinois.

Behbahanifard, M. R., Grondin, G. Y., and Elwi, A. E. (2003), "Experimental and Numerical Investigation of Steel Plate Shear Wall." Structural Engineering Report 254, University of Alberta, Department of Civil and Environmental Engineering, September 2003.

Berman, J. W. and Bruneau, M. (2003), "Experimental Investigation of Light-Gauge Steel Plate Shear Walls for the Seismic Retrofit Of Buildings. " Technical Report MCEER-03-0001, Multidisciplinary Center for Earthquake Engineering Research, Buffalo, N.Y., May 2, 2003.

Berman, J.W., and Bruneau, M. (2004), "Steel Plate Shear Walls are Not Plate Girders." AISC Engineering Journal Vol.41, No.3, pp.95-106.

Berman, J. W. and Bruneau, M. (2005), "Experimental Investigation of Light-Gauge Steel Plate Shear Walls." Journal of Structural Engineering, ASCE, Vol. 131, No. 2, pp. 259-267.

Berman, J.W., and Bruneau, M. (2008), "Capacity Design of Vertical Boundary Elements in Steel Plate Shear Walls." AISC Engineering Journal Vol.45, No.1., pp.57-71.

Bruneau, M., Uang, C-M, Whittaker, A.S. (1998), "Ductile Design of Steel Structures." McGraw-Hill, New York.

Canadian Standards Association (CSA). (1994), "Limit States Design of Steel Structures." CAN/CSA S16-95. Willowdale, Ontario, Canada.

Canadian Standards Association (CSA). (2000), "Limit States Design of Steel Structures." CAN/CSA S16-01. Willowdale, Ontario, Canada.

Driver, R. G., Kulak, G. L., Kennedy, D. J. L., and Elwi, A. E. (1997), "Seismic Behavior of Steel Plate Shear Walls. " Structural Engineering Report 215, University of Alberta, Department of Civil and Environmental Engineering, February 1997.

FEMA (2000), "FEMA 350: Recommended Seismic Design Criteria for New Steel Moment-Frame Buildings." SAC Joint Venture for the Federal Emergency Management Agency, Washington, D.C.

FEMA. (2001), "NEHRP recommended provisions for seismic regulations for new buildings and other structures, Part 2—commentary", FEMA 369, Building Seismic Safety Council for the Federal Emergency Management Agency, Washington, D.C.

FEMA (2004), "FEMA 450: NEHRP Recommended Provisions For Seismic Regulations For New Buildings And Other Structures." Building Seismic Safety Council for the Federal Emergency Management Agency, Washington, D.C.

FEMA (2008), "Quantification of Building Seismic Performance Factors" FEMA P695. Prepared by the Applied Technology Council for FEMA, Washington, D.C.

Jones, S. L., Fry, G. T., and Engelhardt, M. D. (2002) "Experimental Evaluation of Cyclically Loaded Reduced Beam Section Moment Connections." Journal of Structural Engineering, Vol. 128, No. 4, pp. 441-451.

Kharrazi, M. H. K., Ventura, C. E., Prion, H. G. L., and Sabouri-Ghomi, S. (2004), "Bending and Shear Analysis and Design of Ductile Steel Plate Walls." Proceedings of the 13th World Conference on Earthquake Engineering, Vancouver, B.C., Canada, August 1-6, 2004, Paper No. 77.

Kuhn, P., Peterson, J.P., and Levin, L.R. (1952), "A Summary of Diagonal Tension. Part I: Methods and Analysis." Technical Note 2661, National Advisory Committee for Aeronautics, Washington, D.C.

Lee, C.S. and Tsai, K.C. (2008), "Experimental Response of Four 2-Story Narrow Steel Plate Shear Walls" Proceeding of the 2008 Structures Congress. Vancouver, Canada.

Lopez-Garcia, D. and Bruneau, M. (2006), "Seismic Behavior of Intermediate beams in Steel Plate Shear Walls", Proceeding of the 8th U.S. National Conference on Earthquake Engineering, Paper No.1089, San Francisco, CA.

Lubell, A.S., Prion, H.G.L., Ventura, C.E., and Rezai, M. (2000), "Unstiffened Steel Plate Shear Wall Performance under Cyclic Loading." Journal of Structural Engineering, Vol.126, No.4, pp.453-460.

Montgomery, C.J., and Medhekar, M. (2001), "Discussion on Unstiffened Steel Plate Shear Wall Performance under Cyclic Loading", Journal of Structural Engineering, Vol. 127, No. 8, pp. 973.

Papageorgiou, A., Halldorsson B., and Dong G. (1999), "Target Acceleration Spectra Compatible Time Histories." TARSCTHS - User's Manual, Engineering Seismology Laboratory, State University of New York, Buffalo.

Park, H.G., Kwack, J.H., Jeon, S.W., Kim, W.K., and Choi, I.R. (2007), "Framed Steel Plate Wall Behavior under Cyclic Later Loading", Journal of Structural Engineering, Vol.133, No.3, pp.378-388.

Purba, R.and Bruneau, M. (2007), "Design Recommendations for Perforated Steel Plate Shear Walls" Technical Report MCEER-07-0011, Multidisciplinary Center for Earthquake Engineering Research, Buffalo, N.Y., June 18, 2007.

Qu, B., and Bruneau. M. (2008). "Experimental Investigation of Full-Scale Two-Story Steel Plate Shear Walls with Reduced Beam Section Connections" Technical Report MCEER-08-0010, Multidisciplinary Center for Earthquake Engineering Research, Buffalo, New York.

Qu, B., Bruneau. M., Lin, C.H., and Tsai, K.C. (2008), "Testing of Full Scale Two-story Steel Plate Shear Walls with RBS Connections and Composite Floor.", Journal of Structural Engineering, Vol. 134, No. 3, pp.364-373.

Sabelli, R., and Bruneau, M. (2007), "Steel Plate Shear Walls (AISC Design Guide).", American Institute of Steel Construction, Chicago, Illinois.

Sabouri-Ghomi, S. (2005), "Discussion of Plastic Analysis and Design of Steel Plate Shear Walls", Journal of Structural Engineering, Vol.131, No. 4, pp.695-697.

Shishkin, J. J., Driver, R. G., and Grondin, G. Y. (2005), "Analysis of Steel Plate Shear Walls using the Modified Strip Model", Structural Engineering Report No. 261, Department of Civil Engineering, University of Alberta, Edmonton, Alberta, Canada.

Timler, P. A. and Kulak, G. L. (1983), "Experimental Study of Steel Plate Shear Walls." Structural Engineering Report No. 114, Department of Civil Engineering, The University of Alberta, Edmonton, Alberta, November 1983.

Timoshenko, S.P., and Gere, J.M. (1961), "Theory of Elastic Stability." Second Edition, McGraw-Hill Book Company, Inc., New York, NY.

Thorburn, L. Jane, Kulak, G. L., and Montgomery, C. J. (1983), "Analysis of Steel Plate Shear Walls." Structural Engineering Report No. 107, Department of Civil Engineering, The University of Alberta, Edmonton, Alberta, May 1983.

Vian D. and Bruneau M.(2005), "Steel Plate Shear Walls for Seismic Design and Retrofit of Building Structure", Technical Report MCEER-05-0010, Multidisciplinary Center for Earthquake Engineering Research, Buffalo, N.Y.

Wagner, H. (1931), "Flat Sheet Metal Girders with Very Thin Webs, Part III: Sheet Metal Girders with Spars Resistant to Bending – The Stress in Uprights – Diagonal Tension Fields." Technical Memorandum No.606, National Advisory Committee for Aeronautics, Washington, D.C.

Zhang, X., and Ricles, J.(2006), "Experimental Evaluation of Reduced Beam Section Connections to Deep-Columns." Journal of Structural Engineering, Vol. 132 No.3, pp. 346-357

APPENDIX A

SHEAR EFFECTS AT THE END OF INTERMEDIATE HBE DUE TO TENSION FIELDS

A.1 General

In Section 4.4.1, two analytical procedures were presented to estimate the shear effects at the end of a statically determinate beam under uniform loads from fully yielded infill panels. These two procedures, both employing the principle of superposition, either combine the shear effects from different sub-tension fields, or sum up the shear effects from different components of the tension fields. Although different resulting expressions for the HBE end shear were obtained based on different free body diagrams, the derivations in this appendix demonstrates that the results from these two procedures are identical.

A.2 Method 1 (superposing shear effects from sub-tension fields)

In this method, the tension fields were divided into one middle part and two end parts. According to the geometry shown in figure A-1, the location factors, x_E and x_M, used to locate the end and middle part of the tension fields can be determined as:

$$x_E = d_f + \left(d + 2h_f\right)\tan\alpha \qquad\qquad \text{(A-1)}$$

$$x_M = d_f + \left(\frac{d}{2} + h_f\right)\tan\alpha \qquad\qquad \text{(A-2)}$$

Based on the general static analysis procedure and superposing the shear effects from each part of the tension fields, the shear force at the right and left end of the intermediate HBE can be obtained:

$$V_{SR} = \frac{\left(\omega_{ybi} - \omega_{ybi+1}\right)\left(L - 2x_M\right)}{2} + \theta\omega_{ybi}\left(x_E - d_f\right)$$

$$-(1-\theta)\omega_{ybi+1}\left(x_E - d_f\right) + \frac{\left(\omega_{xbi} + \omega_{xbi+1}\right)\left(x_E - d_f\right)\left(\dfrac{d}{2} + h_f\right)}{L}$$

(A-3)

$$V_{SL} = \frac{\left(\omega_{ybi} - \omega_{ybi+1}\right)\left(L - 2x_M\right)}{2} + (1-\theta)\omega_{ybi}\left(x_E - d_f\right)$$

$$-\theta\omega_{ybi+1}\left(x_E - d_f\right) - \frac{\left(\omega_{xbi} + \omega_{xbi+1}\right)\left(x_E - d_f\right)\left(\dfrac{d}{2} + h_f\right)}{L}$$

(A-4)

where θ is the load distribution factor

$$\theta = 1 - x_M / L$$

(A-5)

Substituting (A-1) and (A-2) into (A-3)

$$V_{SR} = \frac{\left(\omega_{ybi} - \omega_{ybi+1}\right)\left(L - 2d_f\right)}{2} - \frac{\left(\omega_{ybi} - \omega_{ybi+1}\right)\left(d + 2h_f\right)\tan\alpha}{2} + \theta\omega_{ybi}\left(d + 2h_f\right)\tan\alpha$$

$$-(1-\theta)\omega_{ybi+1}\left(d + 2h_f\right)\tan\alpha + \frac{\left(\omega_{xbi} + \omega_{xbi+1}\right)\left(x_E - d_f\right)\left(\dfrac{d}{2} + h_f\right)}{L}$$

(A-6)

The second, third and fourth term in the above expression include the common factor $\left(d + 2h_f\right)\tan\alpha$, therefore, (A-6) can be reorganized as

$$V_{SR} = \frac{\left(\omega_{ybi} - \omega_{ybi+1}\right)\left(L - 2d_f\right)}{2}$$

$$+ \left(d + 2h_f\right)\tan\alpha \cdot \left(\omega_{ybi} + \omega_{ybi+1}\right) \cdot (\theta - 0.5)$$

$$+ \frac{\left(\omega_{xbi} + \omega_{xbi+1}\right)\left(x_E - d_f\right)\left(\dfrac{d}{2} + h_f\right)}{L}$$

(A-7)

Substituting (A-5) into (A-7)

$$V_{SR} = \frac{\left(\omega_{ybi} - \omega_{ybi+1}\right)\left(L - 2d_f\right)}{2}$$
$$+\left(\frac{d}{2} + h_f\right)\tan\alpha \cdot \left(\omega_{ybi} + \omega_{ybi+1}\right) \cdot \frac{\left(L - 2x_M\right)}{L} \qquad \text{(A-8)}$$
$$+ \frac{\left(\omega_{xbi} + \omega_{xbi+1}\right)\left(x_E - d_f\right)\left(\frac{d}{2} + h_f\right)}{L}$$

From the tension field geometry

$$\omega_{xbi} = \omega_{ybi}\tan\alpha \qquad \text{(A-9)}$$

$$\omega_{xbi+1} = \omega_{ybi+1}\tan\alpha \qquad \text{(A-10)}$$

Adding up (A-9)and(A-10):

$$\omega_{xbi} + \omega_{xbi} = \left(\omega_{ybi} + \omega_{ybi+1}\right)\tan\alpha \qquad \text{(A-11)}$$

Substituting (A-11) into (A-8)

$$V_{SR} = \frac{\left(\omega_{ybi} - \omega_{ybi+1}\right)\left(L - 2d_f\right)}{2}$$
$$+\left(\frac{d}{2} + h_f\right)\left(\omega_{xbi} + \omega_{xbi+1}\right) \cdot \frac{\left(L - 2x_M\right)}{L} \qquad \text{(A-12)}$$
$$+ \frac{\left(\omega_{xbi} + \omega_{xbi+1}\right)\left(x_E - d_f\right)\left(\frac{d}{2} + h_f\right)}{L}$$

The second and third term in the above expression include the common

factor $\left(\frac{d}{2} + h_f\right)\left(\omega_{xbi} + \omega_{xbi+1}\right)$, therefore, (A-12)can be reorganized as

$$V_{SR} = \frac{\left(\omega_{ybi} - \omega_{ybi+1}\right)\left(L - 2d_f\right)}{2}$$
$$+\left(\frac{d}{2} + h_f\right)\left(\omega_{xbi} + \omega_{xbi+1}\right) \cdot \frac{\left(L - 2x_M + x_E - d_f\right)}{L} \qquad \text{(A-13)}$$

Substituting (A-1) and (A-2) into (A-13)

$$V_{SR} = \frac{\left(\omega_{ybi} - \omega_{ybi+1}\right)\left(L - 2d_f\right)}{2} + \frac{\left(d + 2h_f\right)\left(\omega_{xbi} + \omega_{xbi+1}\right)\left(L - 2d_f\right)}{2L} \qquad \text{(A-14)}$$

Similarly,

$$V_{SL} = \frac{\left(\omega_{ybi} - \omega_{ybi+1}\right)\left(L - 2d_f\right)}{2} - \frac{\left(d + 2h_f\right)\left(\omega_{xbi} + \omega_{xbi+1}\right)\left(L - 2d_f\right)}{2L} \qquad \text{(A-15)}$$

A.2 Method 2 (combining shear effects from tension field components)

In this method, the tension fields were decomposed into horizontal and vertical components. Following the static analysis procedure, the shear effects in an HBE can be obtained by combining the shear forces due to each component. The resulting shear at the right and left end can be respectively expressed as below

$$V_{SR} = \frac{\left(\omega_{ybi} - \omega_{ybi+1}\right)\left(L - 2d_f\right)}{2} + \frac{\left(d + 2h_f\right)\left(\omega_{xbi} + \omega_{xbi+1}\right)\left(L - 2d_f\right)}{2L} \qquad \text{(A-16)}$$

$$V_{SL} = \frac{\left(\omega_{ybi} - \omega_{ybi+1}\right)\left(L - 2d_f\right)}{2} - \frac{\left(d + 2h_f\right)\left(\omega_{xbi} + \omega_{xbi+1}\right)\left(L - 2d_f\right)}{2L} \qquad \text{(A-17)}$$

Comparing (A-14) and (A-15) with (A-16) and (A-17) respectively, the identical equations demonstrate that the two methods provide identical results, although they are originally differently expressed.
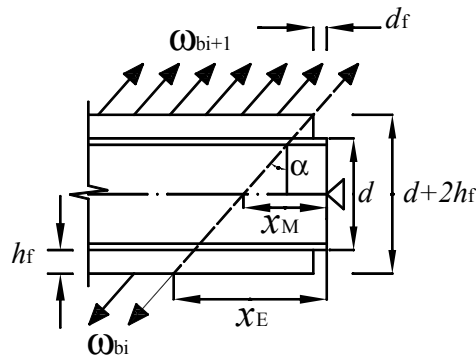
FIGURE A-1 Intermediate HBE End

Units Definition

$$\text{kip} := 1000\text{lb} \qquad \text{ksi} := 1000\,\frac{\text{lb}}{\text{in}^2} \qquad E := 29000\text{ksi} \qquad N := \frac{1}{9.8}\text{kg} \qquad \text{MPa} := 1\,\frac{N}{\text{mm}^2}$$

Geometries and Material Properties

$L_c := 4000\text{mm}$ *Distance between VBE centerline*

$L := 3508\text{mm}$ *Net span of intermediate HBE*

$h_1 := 4000\text{mm}$ *1st story height*

$h_2 := 4000\text{mm}$ *2nd story height*

$t_{w1} := 1 \cdot 3.2 \cdot \text{mm}$ *1F panel thickness*

$t_{w2} := 1 \cdot 2.3 \cdot \text{mm}$ *2F panel thickness*

$h_f := 0\text{mm}$ *Fishplate details: hf =0*

$d_f := 0\text{mm}$ *Fishplate details: df =0*

$A_{top} := 1.851 \cdot 10^4 \text{mm}^2$ *Cross section area of top HBE*

$A_{bottom} := 2.477 \cdot 10^4 \text{mm}^2$ *Cross section area of bottom HBE*

$A_c := 3.642 \cdot 10^4 \text{mm}^2$ *Cross section area of VBE*

$I_c := 1.716 \times 10^9 \cdot \text{mm}^4$ *Moment of inertia of VBE*

$f_y := 346\text{MPa}$ *Yield strength of A572Gr50, to be used for HBE*

$\nu := 0.3$ *Possion's ratio*

$f_{yp1} := 310\text{MPa}$ *Yield strength of 1F infill panel (From coupon test)*

$f_{yp2} := 285\text{MPa}$ *Yield strength of 2F infill panel (From coupon test)*

$R_{yp1} := 1.0$

$R_{yp2} := 1.0$ *Ratio of expected to nominal yield stress, assumed to be unity since yield strength is from coupon test.*

Preliminary Intermediate HBE Section and RBS Geometry

*Try **W24x76** for the intermediate HBE*

$d := 23.9 \text{in}$ *Depth of W24x76*

$b_f := 8.99 \text{in}$ *Flange width of W24x76*

$t_w := 0.44 \text{in}$ *Web thickness of W24x76*

$t_f := 0.68 \text{in}$ *Flange thickness of W24x76*

$h_w := d - t_f$ *Web depth of W24x76*

Use $h_w = d - t_f$ instead of $h_w = d - 2t_f$ to calculate web depth, since the corresponding FE model employed shell element, which assume flange and web area concentrated at mid-surface.

$a := 0.7 \cdot b_f$ *Parameter of RBS, Pls Refer to Fig 3-12 of FEMA 350*

$b := 0.8 d$ *Parameter of RBS, Pls Refer to Fig 3-12 of FEMA 350*

$c := 0.25 \cdot b_f$ *Parameter of RBS, Pls Refer to Fig 3-12 of FEMA 350*

$R := \dfrac{4 \cdot c^2 + b^2}{8c}$ *Parameter of RBS, Pls Refer to Fig 3-12 of FEMA 350*

$e := a + \dfrac{b}{2}$ *Distance between RBS center to HBE end*

$Z := b_f t_f (d - t_f) + \dfrac{1}{4} \cdot t_w \cdot (d - t_f)^2$ *Section modulus of W24x76*

$A := 2 b_f t_f + t_w \cdot (d - t_f)$ *Cross section area of W24x76*

$Z_{RBS} := (b_f - 2 \cdot c) \cdot t_f (d - t_f) + \dfrac{1}{4} \cdot t_w \cdot (d - t_f)^2$ *Section modulus of RBS*

$A_{RBS} := 2 \cdot (b_f - 2 \cdot c) \cdot t_f + t_w \cdot (d - t_f)$ *Cross section area of RBS*

$\eta := \dfrac{Z_{RBS}}{Z}$ $\eta = 0.6473$ *Ratio of RBS section modulus to original section modulus*

Forces Resulting from Infill Panel Yielding

Estimation of tension field angles at 1F and 2F respectively

$$\alpha_1 := \text{atan}\left[\sqrt[4]{\dfrac{1 + \dfrac{t_{w1} \cdot L_c}{2A_c}}{1 + t_{w1} \cdot h_1 \cdot \left[\dfrac{1}{0.5\left(A + A_{bottom}\right)} + \dfrac{h_1^3}{360 \cdot I_c \cdot L_c}\right]}}\right]$$

1F tension field angle

$$\alpha_2 := \text{atan}\left[\sqrt[4]{\dfrac{1 + \dfrac{t_{w2} \cdot L_c}{2A_c}}{1 + t_{w2} \cdot h_2 \cdot \left[\dfrac{1}{0.5\left(A + A_{top}\right)} + \dfrac{h_2^3}{360 \cdot I_c \cdot L_c}\right]}}\right]$$

2F tension field angle

$$\alpha := \frac{\left(\alpha_1 + \alpha_2\right)}{2}$$

Average inclination angle of tension fields

$$\omega_{xc1} := R_{yp1} \cdot f_{yp1} \cdot t_{w1} \cdot \sin(\alpha)^2$$

Horizontal component of the tension field along VBE at 1F

$$\omega_{xc2} := R_{yp1} \cdot f_{yp1} \cdot t_{w2} \cdot \sin(\alpha)^2$$

Horizontal component of the tension field along VBE at 2F

$$\omega_{yb1} := R_{yp1} \cdot f_{yp1} \cdot t_{w1} \cdot \cos(\alpha)^2$$

Vertical component of the tension field along HBE at 1F

$$\omega_{yb2} := R_{yp1} \cdot f_{yp1} \cdot t_{w2} \cdot \cos(\alpha)^2$$

Vertical component of the tension field along HBE at 2F

$$\omega_{xb1} := \frac{1}{2} R_{yp1} \cdot f_{yp1} \cdot t_{w1} \cdot \sin(2 \cdot \alpha)$$

Horizontal component of the tension field along HBE at 1F

$$\omega_{xb2} := \frac{1}{2} R_{yp1} \cdot f_{yp1} \cdot t_{w2} \cdot \sin(2 \cdot \alpha)$$

Horizontal component of the tension field along HBE at 2F

Axial Force in the Intermediate HBE

Assume the earthquake loads concentrate at both ends of the intermediate HBE

Axial force at the left and right end of HBE

$$P_L := -\omega_{xc1} \cdot \left(\frac{h_1}{2} - \frac{d}{2}\right) - \omega_{xc2} \cdot \left(\frac{h_2}{2} - \frac{d}{2}\right) - \left(\omega_{xb1} - \omega_{xb2}\right) \cdot \frac{L}{2} + \frac{v}{2} \cdot \left(\omega_{yb1} + \omega_{yb2}\right) \cdot h_w$$

$$P_R := -\omega_{xc1} \cdot \left(\frac{h_1}{2} - \frac{d}{2}\right) - \omega_{xc2} \cdot \left(\frac{h_2}{2} - \frac{d}{2}\right) + \left(\omega_{xb1} - \omega_{xb2}\right) \cdot \frac{L}{2} + \frac{v}{2} \cdot \left(\omega_{yb1} + \omega_{yb2}\right) \cdot h_w$$

$$P_L = -1.4263 \times 10^6 \, N \qquad\qquad P_R = -940.7014 \times 10^3 \, N$$

Axial force at the left and right RBS center

$$P_{RBSL} := -\omega_{xc1} \cdot \left(\frac{h_1}{2} - \frac{d}{2}\right) - \omega_{xc2} \cdot \left(\frac{h_2}{2} - \frac{d}{2}\right) - \left(\omega_{xb1} - \omega_{xb2}\right) \cdot \left(\frac{L}{2} - e\right) + \frac{v}{2} \cdot \left(\omega_{yb1} + \omega_{yb2}\right) \cdot h_w$$

$$P_{RBSR} := -\omega_{xc1} \cdot \left(\frac{h_1}{2} - \frac{d}{2}\right) - \omega_{xc2} \cdot \left(\frac{h_2}{2} - \frac{d}{2}\right) + \left(\omega_{xb1} - \omega_{xb2}\right) \cdot \left(\frac{L}{2} - e\right) + \frac{v}{2} \cdot \left(\omega_{yb1} + \omega_{yb2}\right) \cdot h_w$$

$$P_{RBSL} = -1.3706 \times 10^6 \, N \qquad\qquad P_{RBSR} = -996.4462 \times 10^3 \, N$$

Shear Force in the Intermediate HBE

Assume the following cross section plastic moment reduction factors at the left and right plastic hinging respectively

$$\beta_{RBSL} := 0.74 \qquad\qquad \beta_{RBSR} := 0.77$$

Shears developed in the left and right plastic hinging

$$V_{RBSL} := -\frac{\left(\beta_{RBSL} + \beta_{RBSR}\right) \cdot f_y \cdot Z_{RBS}}{L - 2e} + \frac{\left(\omega_{yb1} - \omega_{yb2}\right) \cdot (L - 2e)}{2} - \frac{\left(\omega_{xb1} + \omega_{xb2}\right) \cdot \left(h_w + 2h_f\right)}{2}$$

$$V_{RBSR} := \frac{f_y \cdot Z_{RBS}}{L - 2e} + \frac{\left(\omega_{yb1} - \omega_{yb2}\right) \cdot (L - 2e)}{2} + \frac{\left(\omega_{xb1} + \omega_{xb2}\right) \cdot \left(h_w + 2h_f\right)}{2}$$

Shear Force in the Intermediate HBE (cont'd)

Estimation of the cross section plastic moment reduction factor at the left plastic hinging

$$V_{RBSL} = -450.4844 \times 10^3 \, N \qquad\qquad P_{RBSL} = -1.3706 \times 10^6 \, N$$

Positive flexure

$$\sigma_y := \frac{\left(\omega_{yb1} + \omega_{yb2}\right)}{2t_w} - \frac{\left(\omega_{yb1} - \omega_{yb2}\right)}{4t_w}$$

$$\frac{\sigma_y}{f_y} = 0.11 \qquad\qquad \beta_w := \frac{-P_{RBSL}}{h_w \cdot t_w \cdot f_y} \qquad\qquad \tau_{xy} := \frac{V_{RBSL}}{t_w \cdot h_w}$$

$$\frac{1}{3} - \frac{1}{3} \cdot \left(\frac{\sigma_y}{f_y}\right)^2 - \frac{\beta_w}{3} \cdot \left[\beta_w + \left(\frac{\sigma_y}{f_y}\right)\right] - \left(\frac{\tau_{xy}}{f_y}\right)^2 = 0.15$$

$$\sigma_T := \left[\frac{1}{2} \cdot \left(\frac{\sigma_y}{f_y}\right) + \frac{1}{2} \cdot \sqrt{4 - 3 \cdot \left(\frac{\sigma_y}{f_y}\right)^2 - 12 \cdot \left(\frac{\tau_{xy}}{f_y}\right)^2}\right] \cdot f_y \qquad \sigma_T = 342.997 \, MPa$$

$$\sigma_C := \left[\frac{1}{2} \cdot \left(\frac{\sigma_y}{f_y}\right) - \frac{1}{2} \cdot \sqrt{4 - 3 \cdot \left(\frac{\sigma_y}{f_y}\right)^2 - 12 \cdot \left(\frac{\tau_{xy}}{f_y}\right)^2}\right] \cdot f_y \qquad \sigma_C = -303.667 \, MPa$$

$$y_C := \frac{\left(\frac{\sigma_T}{f_y}\right) + \beta_w}{\left(\frac{\sigma_T}{f_y}\right) - \left(\frac{\sigma_C}{f_y}\right)} \cdot h_w \qquad\qquad \frac{y_C}{h_w} = 0.852 \qquad\qquad y_T := h_w - y_C$$

$$M_{P.Flange} := \left(b_f - 2c\right) \cdot t_f h_w \cdot f_y$$

$$M_{P.Web} := \sigma_T \cdot t_w \cdot y_T \cdot \left(\frac{h_w}{2} - \frac{y_T}{2}\right) - \sigma_C \cdot t_w \cdot y_C \cdot \left(\frac{h_w}{2} - \frac{y_C}{2}\right)$$

$$M_{P.Capacity} := M_{P.Flange} + M_{P.Web} \qquad\qquad \beta_{RBSL} := \frac{M_{P.Capacity}}{f_y \cdot Z_{RBS}}$$

Shear Force in the Intermediate HBE (cont'd)

Estimation of the cross section plastic moment reduction factor at the right plastic hinging

$$V_{RBSR} = 734.5201 \times 10^3 \, N \qquad\qquad P_{RBSR} = -996.4462 \times 10^3 \, N$$

Negative flexure

$$\sigma_y := \frac{\left(\omega_{yb1} + \omega_{yb2}\right)}{2t_w} + \frac{\left(\omega_{yb1} - \omega_{yb2}\right)}{4t_w}$$

$$\frac{\sigma_y}{f_y} = 0.13 \qquad\qquad \beta_w := \frac{-P_{RBSR}}{h_w \cdot t_w \cdot f_y} \qquad\qquad \tau_{xy} := \frac{V_{RBSR}}{t_w \cdot h_w}$$

$$\frac{1}{3} - \frac{1}{3} \cdot \left(\frac{\sigma_y}{f_y}\right)^2 - \frac{\beta_w}{3} \cdot \left[\beta_w + \left(\frac{\sigma_y}{f_y}\right)\right] - \left(\frac{\tau_{xy}}{f_y}\right)^2 = 0.14$$

$$\sigma_T := \left[\frac{1}{2} \cdot \left(\frac{\sigma_y}{f_y}\right) + \frac{1}{2} \cdot \sqrt{4 - 3 \cdot \left(\frac{\sigma_y}{f_y}\right)^2 - 12 \cdot \left(\frac{\tau_{xy}}{f_y}\right)^2}\right] \cdot f_y \qquad \sigma_T = 307.515 \, MPa$$

$$\sigma_C := \left[\frac{1}{2} \cdot \left(\frac{\sigma_y}{f_y}\right) - \frac{1}{2} \cdot \sqrt{4 - 3 \cdot \left(\frac{\sigma_y}{f_y}\right)^2 - 12 \cdot \left(\frac{\tau_{xy}}{f_y}\right)^2}\right] \cdot f_y \qquad \sigma_C = -261.176 \, MPa$$

$$y_C := \frac{\left(\frac{\sigma_T}{f_y}\right) + \beta_w}{\left(\frac{\sigma_T}{f_y}\right) - \left(\frac{\sigma_C}{f_y}\right)} \cdot h_w \qquad\qquad \frac{y_C}{h_w} = 0.807 \qquad y_T := h_w - y_C$$

$$M_{P.Flange} := \left(b_f - 2c\right) \cdot t_f \cdot h_w \cdot f_y$$

$$M_{P.Web} := \sigma_T \cdot t_w \cdot y_T \cdot \left(\frac{h_w}{2} - \frac{y_T}{2}\right) - \sigma_C \cdot t_w \cdot y_C \cdot \left(\frac{h_w}{2} - \frac{y_C}{2}\right)$$

$$M_{P.Capacity} := M_{P.Flange} + M_{P.Web} \qquad\qquad \beta_{RBSR} := \frac{M_{P.Capacity}}{f_y \cdot Z_{RBS}}$$

Shear Force in the Intermediate HBE (cont'd)

$$\beta_{RBSL} = 0.7594 \qquad\qquad \beta_{RBSR} = 0.7782$$

The cross section plastic moment reduction factors from calculation are close enough to those assumed. Thus, the shear developed at the left and right plastic hinging can be calculated as:

$$V_{RBSL} := -\frac{\left(\beta_{RBSL} + \beta_{RBSR}\right) \cdot f_y \cdot Z_{RBS}}{L - 2e} + \frac{\left(\omega_{yb1} - \omega_{yb2}\right) \cdot (L - 2e)}{2} - \frac{\left(\omega_{xb1} + \omega_{xb2}\right) \cdot \left(h_w + 2h_f\right)}{2}$$

$$V_{RBSR} := \frac{\left(\beta_{RBSL} + \beta_{RBSR}\right) \cdot f_y \cdot Z_{RBS}}{L - 2e} + \frac{\left(\omega_{yb1} - \omega_{yb2}\right) \cdot (L - 2e)}{2} + \frac{\left(\omega_{xb1} + \omega_{xb2}\right) \cdot \left(h_w + 2h_f\right)}{2}$$

$$V_{RBSL} = -458.0351 \times 10^3 \, N \qquad\qquad V_{RBSR} = 881.4640 \times 10^3 \, N$$

The shear demand at the left and right plastic hinging can be calculated as:

$$V_R := V_{RBSR} + \left(\omega_{yb1} - \omega_{yb2}\right) \cdot e$$

$$V_L := V_{RBSL} + \left(\omega_{yb1} - \omega_{yb2}\right) \cdot e$$

$$V_L = -394.9491 \times 10^3 \, N \qquad\qquad V_R = 944.5501 \times 10^3 \, N$$

Prevention of In-Span Plastic Hinging

Possible plastic hinging location

$$x_{span} := \max\left[\frac{L - 2e}{2} - \frac{\beta_{RBSL} + \beta_{RBSR}}{\left(\omega_{yb1} - \omega_{yb2}\right) \cdot (L - 2e)} \cdot f_y \cdot Z_{RBS}, 0\right]$$

$$x_{span} = 0.0000 \, mm$$

So, in span plastic hing will not form.

Moment at the Right Column Face

Demand at the right end

$$M_{R.demand} := \beta_{RBSR} \cdot f_y \cdot Z_{RBS} + V_{RBSR} \cdot e \ldots$$
$$+ \frac{(\omega_{yb1} - \omega_{yb2})}{2} \cdot (e - d_f) \cdot (e + d_f) - \frac{(\omega_{xb1} + \omega_{xb2})}{2} \cdot (e - d_f) \cdot (h_w + 2h_f)$$

$$M_{R.demand} = 842.0595 \times 10^6 \, N \cdot mm$$

Estimation of cross-section moment capacity at right end

$$P_R = -940.7014 \times 10^3 \, N \qquad V_R = 944.5501 \times 10^3 \, N$$

Negative flexure

$$\sigma_y := \frac{(\omega_{yb1} + \omega_{yb2})}{2t_w} + \frac{(\omega_{yb1} - \omega_{yb2})}{4t_w} \qquad \beta_w := \frac{-P_R}{h_w \cdot t_w \cdot f_y} \qquad \tau_{xy} := \frac{V_R}{t_w \cdot h_w}$$

$$\frac{\sigma_y}{f_y} = 0.13 \qquad \beta_w = 0.412 \qquad \frac{\tau_{xy}}{f_y} = 0.414$$

$$\frac{1}{3} - \frac{1}{3} \cdot \left(\frac{\sigma_y}{f_y}\right)^2 - \frac{\beta_w}{3} \cdot \left[\beta_w + \left(\frac{\sigma_y}{f_y}\right)\right] - \left(\frac{\tau_{xy}}{f_y}\right)^2 = 0.08$$

$$\sigma_T := \left[\frac{1}{2} \cdot \left(\frac{\sigma_y}{f_y}\right) + \frac{1}{2} \cdot \sqrt{4 - 3 \cdot \left(\frac{\sigma_y}{f_y}\right)^2 - 12 \cdot \left(\frac{\tau_{xy}}{f_y}\right)^2}\right] \cdot f_y \qquad \sigma_T = 260.871 \, MPa$$

$$\sigma_C := \left[\frac{1}{2} \cdot \left(\frac{\sigma_y}{f_y}\right) - \frac{1}{2} \cdot \sqrt{4 - 3 \cdot \left(\frac{\sigma_y}{f_y}\right)^2 - 12 \cdot \left(\frac{\tau_{xy}}{f_y}\right)^2}\right] \cdot f_y \qquad \sigma_C = -214.532 \, MPa$$

$$y_C := \frac{\left(\frac{\sigma_T}{f_y}\right) + \beta_w}{\left(\frac{\sigma_T}{f_y}\right) - \left(\frac{\sigma_C}{f_y}\right)} \cdot h_w \qquad \frac{y_C}{h_w} = 0.849 \qquad y_T := h_w - y_C$$

$$M_{P.Flange} := b_f \cdot t_f \cdot h_w \cdot f_y$$

Moment at the Right Column Face(cont'd)

$$M_{P.Web} := \sigma_T \cdot t_w \cdot y_T \cdot \left(\frac{h_w}{2} - \frac{y_T}{2} \right) - \sigma_C \cdot t_w \cdot y_C \cdot \left(\frac{h_w}{2} - \frac{y_C}{2} \right)$$

$$M_{R.Capacity} := M_{P.Flange} + M_{P.Web}$$

$$M_{R.demand} = 842.0595 \times 10^6 \, N \cdot mm \qquad M_{R.Capacity} = 923.3455 \times 10^6 \, N \cdot mm$$

Capacity is greater than demand, **OK**

Moment at the Left Column Face

Demand at the left end

$$M_{L.demand} := \beta_{RBSL} \cdot f_y \cdot Z_{RBS} - V_{RBSL} \cdot e - \frac{\left(\omega_{xb1} + \omega_{xb2} \right)}{2} \cdot \left(e - d_f \right) \cdot \left(h_w + 2h_f \right) \dots$$
$$+ \frac{-\left(\omega_{yb1} - \omega_{yb2} \right)}{2} \cdot \left(e - d_f \right) \cdot \left(e + d_f \right)$$

$$M_{L.demand} = 632.2270 \times 10^6 \, N \cdot mm$$

Estimation of moment capacity at left end

$$P_L = -1.4263 \times 10^6 \, N \qquad V_L = -394.9491 \times 10^3 \, N$$

Positive flexure

$$\sigma_y := \frac{\left(\omega_{yb1} + \omega_{yb2} \right)}{2t_w} - \frac{\left(\omega_{yb1} - \omega_{yb2} \right)}{4t_w} \qquad \beta_w := \frac{-P_L}{h_w \cdot t_w \cdot f_y} \qquad \tau_{xy} := \frac{V_L}{t_w \cdot h_w}$$

$$\frac{\sigma_y}{f_y} = 0.11 \qquad \beta_w = 0.625 \qquad \frac{\tau_{xy}}{f_y} = -0.173$$

$$\frac{1}{3} - \frac{1}{3} \cdot \left(\frac{\sigma_y}{f_y} \right)^2 - \frac{\beta_w}{3} \cdot \left[\beta_w + \left(\frac{\sigma_y}{f_y} \right) \right] - \left(\frac{\tau_{xy}}{f_y} \right)^2 = 0.14$$

Moment at the Left Column Face(cont'd)

$$\sigma_T := \left[\frac{1}{2} \cdot \left(\frac{\sigma_y}{f_y} \right) + \frac{1}{2} \cdot \sqrt{4 - 3 \cdot \left(\frac{\sigma_y}{f_y} \right)^2 - 12 \cdot \left(\frac{\tau_{xy}}{f_y} \right)^2} \right] \cdot f_y \qquad \sigma_T = 347.972 \text{ MPa}$$

$$\sigma_C := \left[\frac{1}{2} \cdot \left(\frac{\sigma_y}{f_y} \right) - \frac{1}{2} \cdot \sqrt{4 - 3 \cdot \left(\frac{\sigma_y}{f_y} \right)^2 - 12 \cdot \left(\frac{\tau_{xy}}{f_y} \right)^2} \right] \cdot f_y \qquad \sigma_C = -308.642 \text{ MPa}$$

$$y_C := \frac{\left(\frac{\sigma_T}{f_y} \right) + \beta_w}{\left(\frac{\sigma_T}{f_y} \right) - \left(\frac{\sigma_C}{f_y} \right)} \cdot h_w \qquad\qquad \frac{y_C}{h_w} = 0.860$$

$$y_T := h_w - y_C$$

$$M_{P.Flange} := b_f \, t_f \, h_w \cdot f_y$$

$$M_{P.Web} := \sigma_T \cdot t_w \cdot y_T \cdot \left(\frac{h_w}{2} - \frac{y_T}{2} \right) - \sigma_C \cdot t_w \cdot y_C \cdot \left(\frac{h_w}{2} - \frac{y_C}{2} \right)$$

$$M_{L.Capacity} := M_{P.Flange} + M_{P.Web}$$

$$M_{L.demand} = 632.2270 \times 10^6 \, \text{N·mm} \qquad\qquad M_{L.Capacity} = 958.9578 \times 10^6 \, \text{N·mm}$$

Capacity is greater than demand, **OK**

Summary of Intermediate HBE Design Loads

Shear force

$$V_R = 944.5501 \times 10^3 \, N \qquad V_L = -394.9491 \times 10^3 \, N$$

Axial Force

$$P_R = -940.7014 \times 10^3 \, N \qquad P_L = -1.4263 \times 10^6 \, N$$

Moment Demand

$$M_{R.demand} = 842.0595 \times 10^6 \, N{\cdot}mm \qquad M_{L.demand} = 632.2270 \times 10^6 \, N{\cdot}mm$$

Units Definition

$$\text{kip} := 1000\text{lb} \qquad \text{ksi} := 1000\frac{\text{lb}}{\text{in}^2} \qquad E := 29000\text{ksi} \qquad N := \frac{1}{9.8}\text{kg} \qquad \text{MPa} := 1\frac{N}{\text{mm}^2}$$

Geometries and Material Properties

$L_c := 4000\text{mm}$ *Distance between VBE centerline*

$L := 3508\text{mm}$ *Net span of intermediate HBE*

$h_1 := 4000\text{mm}$ *1st story height*

$h_2 := 4000\text{mm}$ *2nd story height*

$t_{w1} := 1 \cdot 3.2 \cdot \text{mm}$ *1F panel thickness*

$t_{w2} := 1 \cdot 2.3\text{mm}$ *2F panel thickness*

$h_f := 0\text{mm}$ *Fishplate details: hf =0mm*

$d_f := 0\text{mm}$ *Fishplate details: df =0mm*

$A_{top} := 1.851 \cdot 10^4 \text{mm}^2$ *Cross section area of top HBE*

$A_{bottom} := 2.477 \cdot 10^4 \text{mm}^2$ *Cross section area of bottom HBE*

$A_c := 3.642 \cdot 10^4 \text{mm}^2$ *Cross section area of VBE*

$I_c := 1.716 \times 10^9 \cdot \text{mm}^4$ *Moment of inertia of VBE*

$f_y := 346\text{MPa}$ *Yield strength of A572Gr50, to be used for HBE*

$\nu := 0.3$ *Possion's ratio*

$f_{yp1} := 310\text{MPa}$ *Yield strength of 1F infill panel (From coupon test)*

$f_{yp2} := 285\text{MPa}$ *Yield strength of 2F infill panel (From coupon test)*

$R_{yp1} := 1.0$

$R_{yp2} := 1.0$ *Ratio of expected to nominal yield stress, assumed to be unity since yield strength is from coupon test.*

Preliminary Intermediate HBE Section and RBS Geometry

*Try **W24x76** for the intermediate HBE*

$d := 23.9in$ *Depth of W24x76*

$b_f := 8.99in$ *Flange width of W24x76*

$t_w := 0.44in$ *Web thickness of W24x76*

$t_f := 0.68in$ *Flange thickness of W24x76*

$h_w := d - t_f$ *Web depth of W24x76*

Note use $h_w=d-t_f$ instead of $h_w=d-2t_f$ to estimate web depth, since the corresponding FE model employed shell element, which assume flange and web area concentrated at mid-surface.

$a := 0.7 \cdot b_f$ *Parameter of RBS, Pls Refer to Fig 3-12 of FEMA 350*

$b := 0.8d$ *Parameter of RBS, Pls Refer to Fig 3-12 of FEMA 350*

$c := 0.25 \cdot b_f$ *Parameter of RBS, Pls Refer to Fig 3-12 of FEMA 350*

$R := \dfrac{4 \cdot c^2 + b^2}{8c}$ *Parameter of RBS, Pls Refer to Fig 3-12 of FEMA 350*

$dx := 0.36 \cdot b$ *Distance between RBS center and plastic hinging, determined from 7-66*

$e := a + \dfrac{b}{2} - dx$ *Distance between plastic hinging and HBE end*

$dy := R - \sqrt{R^2 - dx^2}$ *Flange width increament considering location variation of plastic hinging*

$Z := b_f t_f (d - t_f) + \dfrac{1}{4} \cdot t_w \cdot (d - t_f)^2$ *Section modulus of W24x76*

$A := 2 b_f t_f + t_w \cdot (d - t_f)$ *Cross section area of W24x76*

$Z_{RBS} := (b_f - 2 \cdot c + 2dy) \cdot t_f (d - t_f) + \dfrac{1}{4} \cdot t_w \cdot (d - t_f)^2$ *Section modulus of plastic hinging*

Forces Resulting from Infill Panel Yielding

Estimation of tension field angles at 1F and 2F respectively

$$\alpha_1 := atan\left[\sqrt[4]{\dfrac{1 + \dfrac{t_{w1} \cdot L_c}{2A_c}}{1 + t_{w1} \cdot h_1 \cdot \left[\dfrac{1}{0.5(A + A_{bottom})} + \dfrac{h_1^3}{360 \cdot I_c \cdot L_c}\right]}}\right]$$ *1F tension field angle*

$$\alpha_2 := atan\left[\sqrt[4]{\dfrac{1 + \dfrac{t_{w2} \cdot L_c}{2A_c}}{1 + t_{w2} \cdot h_2 \cdot \left[\dfrac{1}{0.5(A + A_{top})} + \dfrac{h_2^3}{360 \cdot I_c \cdot L_c}\right]}}\right]$$ *2F tension field angle*

$$\alpha := \frac{(\alpha_1 + \alpha_2)}{2}$$ Average inclination angle of tension fields

$\omega_{xc1} := R_{yp1} \cdot f_{yp1} \cdot t_{w1} \cdot \sin(\alpha)^2$ Horizontal component of the tension field along VBE at 1F

$\omega_{xc2} := R_{yp1} \cdot f_{yp1} \cdot t_{w2} \cdot \sin(\alpha)^2$ Horizontal component of the tension field along VBE at 2F

$\omega_{yb1} := R_{yp1} \cdot f_{yp1} \cdot t_{w1} \cdot \cos(\alpha)^2$ Vertical component of the tension field along HBE at 1F

$\omega_{yb2} := R_{yp1} \cdot f_{yp1} \cdot t_{w2} \cdot \cos(\alpha)^2$ Vertical component of the tension field along HBE at 2F

$\omega_{xb1} := \frac{1}{2} R_{yp1} \cdot f_{yp1} \cdot t_{w1} \cdot \sin(2 \cdot \alpha)$ Horizontal component of the tension field along HBE at 1F

$\omega_{xb2} := \frac{1}{2} R_{yp1} \cdot f_{yp1} \cdot t_{w2} \cdot \sin(2 \cdot \alpha)$ Horizontal component of the tension field along HBE at 2F

Axial Force in the Intermediate HBE

Assume the earthquake loads concentrate at both ends of the intermediate HBE

Axial force at the left and right end of HBE

$$P_L := -\omega_{xc1} \cdot \left(\frac{h_1}{2} - \frac{d}{2} \right) - \omega_{xc2} \cdot \left(\frac{h_2}{2} - \frac{d}{2} \right) - \left(\omega_{xb1} - \omega_{xb2} \right) \cdot \frac{L}{2} + \frac{v}{2} \cdot \left(\omega_{yb1} + \omega_{yb2} \right) \cdot h_w$$

$$P_R := -\omega_{xc1} \cdot \left(\frac{h_1}{2} - \frac{d}{2} \right) - \omega_{xc2} \cdot \left(\frac{h_2}{2} - \frac{d}{2} \right) + \left(\omega_{xb1} - \omega_{xb2} \right) \cdot \frac{L}{2} + \frac{v}{2} \cdot \left(\omega_{yb1} + \omega_{yb2} \right) \cdot h_w$$

$$P_L = -1.4263 \times 10^6 \, N \qquad\qquad P_R = -940.7014 \times 10^3 \, N$$

Axial force at the left and right plastic hinging

$$P_{RBSL} := -\omega_{xc1} \cdot \left(\frac{h_1}{2} - \frac{d}{2} \right) - \omega_{xc2} \cdot \left(\frac{h_2}{2} - \frac{d}{2} \right) - \left(\omega_{xb1} - \omega_{xb2} \right) \cdot \left(\frac{L}{2} - e \right) + \frac{v}{2} \cdot \left(\omega_{yb1} + \omega_{yb2} \right) \cdot h_w$$

$$P_{RBSR} := -\omega_{xc1} \cdot \left(\frac{h_1}{2} - \frac{d}{2} \right) - \omega_{xc2} \cdot \left(\frac{h_2}{2} - \frac{d}{2} \right) + \left(\omega_{xb1} - \omega_{xb2} \right) \cdot \left(\frac{L}{2} - e \right) + \frac{v}{2} \cdot \left(\omega_{yb1} + \omega_{yb2} \right) \cdot h_w$$

$$P_{RBSL} = -1.3948 \times 10^6 \, N \qquad\qquad P_{RBSR} = -972.2424 \times 10^3 \, N$$

Shear Force in the Intermediate HBE

Assume the following cross section plastic moment reduction factors at the left and right plastic hinging respectively

$$\beta_{RBSL} := 0.80 \qquad\qquad \beta_{RBSR} := 0.75$$

Shears developed in the left and right plastic hinging

$$V_{RBSL} := -\frac{\left(\beta_{RBSL} + \beta_{RBSR} \right) \cdot f_y \cdot Z_{RBS}}{L - e} + \frac{\left(\omega_{yb1} - \omega_{yb2} \right) \cdot (L - 2e)}{2} - \frac{\left(\omega_{xb1} + \omega_{xb2} \right) \cdot \left(h_w + 2h_f \right)}{2}$$

$$V_{RBSR} := \frac{\left(\beta_{RBSL} + \beta_{RBSR} \right) \cdot f_y \cdot Z_{RBS}}{L - 2e} + \frac{\left(\omega_{yb1} - \omega_{yb2} \right) \cdot (L - 2e)}{2} + \frac{\left(\omega_{xb1} + \omega_{xb2} \right) \cdot \left(h_w + 2h_f \right)}{2}$$

Shear Force in the Intermediate HBE (cont'd)

Estimation of the cross section plastic moment reduction factor at the left plastic hinging

$$V_{RBSL} = -455.3901 \times 10^3 \, N \qquad\qquad P_{RBSL} = -1.3948 \times 10^6 \, N$$

Positive flexure

$$\sigma_y := \frac{\left(\omega_{yb1} + \omega_{yb2}\right)}{2t_w} - \frac{\left(\omega_{yb1} - \omega_{yb2}\right)}{4t_w}$$

$$\frac{\sigma_y}{f_y} = 0.11 \qquad\qquad \beta_w := \frac{-P_{RBSL}}{h_w \cdot t_w \cdot f_y} \qquad\qquad \tau_{xy} := \frac{V_{RBSL}}{t_w \cdot h_w}$$

$$\frac{1}{3} - \frac{1}{3} \cdot \left(\frac{\sigma_y}{f_y}\right)^2 - \frac{\beta_w}{3} \cdot \left[\beta_w + \left(\frac{\sigma_y}{f_y}\right)\right] - \left(\frac{\tau_{xy}}{f_y}\right)^2 = 0.14$$

$$\sigma_T := \left[\frac{1}{2} \cdot \left(\frac{\sigma_y}{f_y}\right) + \frac{1}{2} \cdot \sqrt{4 - 3 \cdot \left(\frac{\sigma_y}{f_y}\right)^2 - 12 \cdot \left(\frac{\tau_{xy}}{f_y}\right)^2}\right] \cdot f_y \qquad \sigma_T = 342.522 \, MPa$$

$$\sigma_C := \left[\frac{1}{2} \cdot \left(\frac{\sigma_y}{f_y}\right) - \frac{1}{2} \cdot \sqrt{4 - 3 \cdot \left(\frac{\sigma_y}{f_y}\right)^2 - 12 \cdot \left(\frac{\tau_{xy}}{f_y}\right)^2}\right] \cdot f_y \qquad \sigma_C = -303.192 \, MPa$$

$$y_C := \frac{\left(\frac{\sigma_T}{f_y}\right) + \beta_w}{\left(\frac{\sigma_T}{f_y}\right) - \left(\frac{\sigma_C}{f_y}\right)} \cdot h_w \qquad\qquad \frac{y_C}{h_w} = 0.858 \qquad\qquad y_T := h_w - y_C$$

$$M_{P.Flange} := \left(b_f - 2c + 2dy\right) \cdot t_f h_w f_y$$

$$M_{P.Web} := \sigma_T \cdot t_w \cdot y_T \cdot \left(\frac{h_w}{2} - \frac{y_T}{2}\right) - \sigma_C \cdot t_w \cdot y_C \cdot \left(\frac{h_w}{2} - \frac{y_C}{2}\right)$$

$$M_{P.Capacity} := M_{P.Flange} + M_{P.Web} \qquad\qquad \beta_{RBSL} := \frac{M_{P.Capacity}}{f_y \cdot Z_{RBS}}$$

Shear Force in the Intermediate HBE (cont'd)

Estimation of the cross section plastic moment reduction factor at the right plastic hinging

$$V_{RBSR} = 966.8181 \times 10^3 \, N \qquad\qquad P_{RBSR} = -972.2424 \times 10^3 \, N$$

Negative flexure

$$\sigma_y := \frac{(\omega_{yb1} + \omega_{yb2})}{2t_w} + \frac{(\omega_{yb1} - \omega_{yb2})}{4t_w}$$

$$\frac{\sigma_y}{f_y} = 0.13 \qquad\qquad \beta_w := \frac{-P_{RBSR}}{h_w \cdot t_w \cdot f_y} \qquad\qquad \tau_{xy} := \frac{V_{RBSR}}{t_w \cdot h_w}$$

$$\frac{1}{3} - \frac{1}{3} \cdot \left(\frac{\sigma_y}{f_y}\right)^2 - \frac{\beta_w}{3} \cdot \left[\beta_w + \left(\frac{\sigma_y}{f_y}\right)\right] - \left(\frac{\tau_{xy}}{f_y}\right)^2 = 0.07$$

$$\sigma_T := \left[\frac{1}{2} \cdot \left(\frac{\sigma_y}{f_y}\right) + \frac{1}{2} \cdot \sqrt{4 - 3 \cdot \left(\frac{\sigma_y}{f_y}\right)^2 - 12 \cdot \left(\frac{\tau_{xy}}{f_y}\right)^2}\right] \cdot f_y \qquad \sigma_T = 254.606 \, MPa$$

$$\sigma_C := \left[\frac{1}{2} \cdot \left(\frac{\sigma_y}{f_y}\right) - \frac{1}{2} \cdot \sqrt{4 - 3 \cdot \left(\frac{\sigma_y}{f_y}\right)^2 - 12 \cdot \left(\frac{\tau_{xy}}{f_y}\right)^2}\right] \cdot f_y \qquad \sigma_C = -208.267 \, MPa$$

$$y_C := \frac{\left(\frac{\sigma_T}{f_y}\right) + \beta_w}{\left(\frac{\sigma_T}{f_y}\right) - \left(\frac{\sigma_C}{f_y}\right)} \cdot h_w \qquad\qquad \frac{y_C}{h_w} = 0.869 \qquad y_T := h_w - y_C$$

$$M_{P.Flange} := (b_f - 2c + 2dy) \cdot t_f \cdot h_w \cdot f_y$$

$$M_{P.Web} := \sigma_T \cdot t_w \cdot y_T \cdot \left(\frac{h_w}{2} - \frac{y_T}{2}\right) - \sigma_C \cdot t_w \cdot y_C \cdot \left(\frac{h_w}{2} - \frac{y_C}{2}\right)$$

$$M_{P.Capacity} := M_{P.Flange} + M_{P.Web} \qquad\qquad \beta_{RBSR} := \frac{M_{P.Capacity}}{f_y \cdot Z_{RBS}}$$

Shear Force in the Intermediate HBE (cont'd)

$$\beta_{RBSL} = 0.8051 \qquad\qquad \beta_{RBSR} = 0.7519$$

The cross section plastic moment reduction factors from calculation are close enough to those assumed.Thus, the shear developed at the left and right plastic hinging can be calculated as:

$$V_{RBSL} := -\frac{\left(\beta_{RBSL} + \beta_{RBSR}\right)\cdot f_y \cdot Z_{RBS}}{L - 2e} + \frac{\left(\omega_{yb1} - \omega_{yb2}\right)\cdot(L - 2e)}{2} - \frac{\left(\omega_{xb1} + \omega_{xb2}\right)\cdot\left(h_w + 2h_f\right)}{2}$$

$$V_{RBSR} := \frac{\left(\beta_{RBSL} + \beta_{RBSR}\right)\cdot f_y \cdot Z_{RBS}}{L - 2e} + \frac{\left(\omega_{yb1} - \omega_{yb2}\right)\cdot(L - 2e)}{2} + \frac{\left(\omega_{xb1} + \omega_{xb2}\right)\cdot\left(h_w + 2h_f\right)}{2}$$

$$V_{RBSL} = -490.7752 \times 10^3\,N \qquad\qquad V_{RBSR} = 968.9867 \times 10^3\,N$$

The shear demand at the left and right plastic hinging can be calculated as:

$$V_R := V_{RBSR} + \left(\omega_{yb1} - \omega_{yb2}\right)\cdot e$$

$$V_L := V_{RBSL} + \left(\omega_{yb1} - \omega_{yb2}\right)\cdot e$$

$$V_L = -455.0805 \times 10^3\,N \qquad\qquad V_R = 1.0047 \times 10^6\,N$$

Prevention of In-Span Plastic Hinging

Possible plastic hinging location

$$x_{span} := \max\left[\frac{L - 2e}{2} - \frac{\beta_{RBSL} + \beta_{RBSR}}{\left(\omega_{yb1} - \omega_{yb2}\right)\cdot(L - 2e)}\cdot f_y \cdot Z_{RBS}, 0\right]$$

$$x_{span} = 0.0000\,mm$$

So, in span plastic hing will not form.

Moment at the Right Column Face

Demand at the right end

$$M_{R.demand} := \beta_{RBSR} \cdot f_y \cdot Z_{RBS} + V_{RBSR} \cdot e \ldots$$
$$+ \frac{(\omega_{yb1} - \omega_{yb2})}{2} \cdot (e - d_f) \cdot (e + d_f) - \frac{(\omega_{xb1} + \omega_{xb2})}{2} \cdot (e - d_f) \cdot (h_w + 2h_f)$$

$$M_{R.demand} = 876.0764 \times 10^6 \, N \cdot mm$$

Estimation of cross-section moment capacity at right end

$$P_R = -940.7014 \times 10^3 \, N \qquad V_R = 1.0047 \times 10^6 \, N$$

Negative flexure

$$\sigma_y := \frac{(\omega_{yb1} + \omega_{yb2})}{2t_w} + \frac{(\omega_{yb1} - \omega_{yb2})}{4t_w} \qquad \beta_w := \frac{-P_R}{h_w \cdot t_w \cdot f_y} \qquad \tau_{xy} := \frac{V_R}{t_w \cdot h_w}$$

$$\frac{\sigma_y}{f_y} = 0.13 \qquad \beta_w = 0.412 \qquad \frac{\tau_{xy}}{f_y} = 0.441$$

$$\frac{1}{3} - \frac{1}{3} \cdot \left(\frac{\sigma_y}{f_y}\right)^2 - \frac{\beta_w}{3} \cdot \left[\beta_w + \left(\frac{\sigma_y}{f_y}\right)\right] - \left(\frac{\tau_{xy}}{f_y}\right)^2 = 0.06$$

$$\sigma_T := \left[\frac{1}{2} \cdot \left(\frac{\sigma_y}{f_y}\right) + \frac{1}{2} \cdot \sqrt{4 - 3 \cdot \left(\frac{\sigma_y}{f_y}\right)^2 - 12 \cdot \left(\frac{\tau_{xy}}{f_y}\right)^2}\right] \cdot f_y \qquad \sigma_T = 243.189 \, MPa$$

$$\sigma_C := \left[\frac{1}{2} \cdot \left(\frac{\sigma_y}{f_y}\right) - \frac{1}{2} \cdot \sqrt{4 - 3 \cdot \left(\frac{\sigma_y}{f_y}\right)^2 - 12 \cdot \left(\frac{\tau_{xy}}{f_y}\right)^2}\right] \cdot f_y \qquad \sigma_C = -196.850 \, MPa$$

$$y_C := \frac{\left(\frac{\sigma_T}{f_y}\right) + \beta_w}{\left(\frac{\sigma_T}{f_y}\right) - \left(\frac{\sigma_C}{f_y}\right)} \cdot h_w \qquad \frac{y_C}{h_w} = 0.877 \qquad y_T := h_w - y_C$$

$$M_{P.Flange} := b_f \cdot t_f \cdot h_w \cdot f_y$$

Moment at the Right Column Face(cont'd)

$$M_{P.Web} := \sigma_T \cdot t_w \cdot y_T \cdot \left(\frac{h_w}{2} - \frac{y_T}{2} \right) - \sigma_C \cdot t_w \cdot y_C \cdot \left(\frac{h_w}{2} - \frac{y_C}{2} \right)$$

$$M_{R.Capacity} := M_{P.Flange} + M_{P.Web}$$

$$M_{R.demand} = 876.0764 \times 10^6 \, N \cdot mm \qquad M_{R.Capacity} = 897.1191 \times 10^6 \, N \cdot mm$$

Capacity is greater than demand, **OK**

Moment at the Left Column Face

Demand at the left end

$$M_{L.demand} := \beta_{RBSL} \cdot f_y \cdot Z_{RBS} - V_{RBSL} \cdot e - \frac{(\omega_{xb1} + \omega_{xb2})}{2} \cdot (e - d_f) \cdot (h_w + 2h_f) \, ... \\ + \frac{-(\omega_{yb1} - \omega_{yb2})}{2} \cdot (e - d_f) \cdot (e + d_f)$$

$$M_{L.demand} = 809.1511 \times 10^6 \, N \cdot mm$$

Estimation of moment capacity at left end

$$P_L = -1.4263 \times 10^6 \, N \qquad V_L = -455.0805 \times 10^3 \, N$$

Positive flexure

$$\sigma_y := \frac{(\omega_{yb1} + \omega_{yb2})}{2t_w} - \frac{(\omega_{yb1} - \omega_{yb2})}{4t_w} \qquad \beta_w := \frac{-P_L}{h_w \cdot t_w \cdot f_y} \qquad \tau_{xy} := \frac{V_L}{t_w \cdot h_w}$$

$$\frac{\sigma_y}{f_y} = 0.11 \qquad \beta_w = 0.625 \qquad \frac{\tau_{xy}}{f_y} = -0.200$$

$$\frac{1}{3} - \frac{1}{3} \cdot \left(\frac{\sigma_y}{f_y} \right)^2 - \frac{\beta_w}{3} \cdot \left[\beta_w + \left(\frac{\sigma_y}{f_y} \right) \right] - \left(\frac{\tau_{xy}}{f_y} \right)^2 = 0.14$$

Moment at the Left Column Face(cont'd)

$$\sigma_T := \left[\frac{1}{2} \cdot \left(\frac{\sigma_y}{f_y} \right) + \frac{1}{2} \cdot \sqrt{4 - 3 \cdot \left(\frac{\sigma_y}{f_y} \right)^2 - 12 \cdot \left(\frac{\tau_{xy}}{f_y} \right)^2} \right] \cdot f_y \qquad \sigma_T = 342.552\,\text{MPa}$$

$$\sigma_C := \left[\frac{1}{2} \cdot \left(\frac{\sigma_y}{f_y} \right) - \frac{1}{2} \cdot \sqrt{4 - 3 \cdot \left(\frac{\sigma_y}{f_y} \right)^2 - 12 \cdot \left(\frac{\tau_{xy}}{f_y} \right)^2} \right] \cdot f_y \qquad \sigma_C = -303.222\,\text{MPa}$$

$$y_C := \frac{\left(\dfrac{\sigma_T}{f_y} \right) + \beta_w}{\left(\dfrac{\sigma_T}{f_y} \right) - \left(\dfrac{\sigma_C}{f_y} \right)} \cdot h_w \qquad \frac{y_C}{h_w} = 0.866$$

$$y_T := h_w - y_C$$

$$M_{P.Flange} := b_f\, t_f\, h_w \cdot f_y$$

$$M_{P.Web} := \sigma_T \cdot t_w \cdot y_T \cdot \left(\frac{h_w}{2} - \frac{y_T}{2} \right) - \sigma_C \cdot t_w \cdot y_C \cdot \left(\frac{h_w}{2} - \frac{y_C}{2} \right)$$

$$M_{L.Capacity} := M_{P.Flange} + M_{P.Web}$$

$$M_{L.demand} = 809.1511 \times 10^6\,\text{N·mm} \qquad M_{L.Capacity} = 950.9215 \times 10^6\,\text{N·mm}$$

Capacity is greater than demand, **OK**

Summary of Design Loads at HBE Ends

Shear force

$$V_R = 1.0047 \times 10^6\,\text{N} \qquad\qquad V_L = -455.0805 \times 10^3\,\text{N}$$

Moment

$$M_{R.demand} = 876.0764 \times 10^6\,\text{N·mm} \qquad M_{L.demand} = 809.1511 \times 10^6\,\text{N·mm}$$

Axial force

$$P_R = -940.7014 \times 10^3\,\text{N} \qquad\qquad P_L = -1.4263 \times 10^6\,\text{N}$$

MCEER Technical Reports

MCEER publishes technical reports on a variety of subjects written by authors funded through MCEER. These reports are available from both MCEER Publications and the National Technical Information Service (NTIS). Requests for reports should be directed to MCEER Publications, MCEER, University at Buffalo, State University of New York, Red Jacket Quadrangle, Buffalo, New York 14261. Reports can also be requested through NTIS, 5285 Port Royal Road, Springfield, Virginia 22161. NTIS accession numbers are shown in parenthesis, if available.

NCEER-87-0001   "First-Year Program in Research, Education and Technology Transfer," 3/5/87, (PB88-134275, A04, MF-A01).

NCEER-87-0002   "Experimental Evaluation of Instantaneous Optimal Algorithms for Structural Control," by R.C. Lin, T.T. Soong and A.M. Reinhorn, 4/20/87, (PB88-134341, A04, MF-A01).

NCEER-87-0003   "Experimentation Using the Earthquake Simulation Facilities at University at Buffalo," by A.M. Reinhorn and R.L. Ketter, to be published.

NCEER-87-0004   "The System Characteristics and Performance of a Shaking Table," by J.S. Hwang, K.C. Chang and G.C. Lee, 6/1/87, (PB88-134259, A03, MF-A01). This report is available only through NTIS (see address given above).

NCEER-87-0005   "A Finite Element Formulation for Nonlinear Viscoplastic Material Using a Q Model," by O. Gyebi and G. Dasgupta, 11/2/87, (PB88-213764, A08, MF-A01).

NCEER-87-0006   "Symbolic Manipulation Program (SMP) - Algebraic Codes for Two and Three Dimensional Finite Element Formulations," by X. Lee and G. Dasgupta, 11/9/87, (PB88-218522, A05, MF-A01).

NCEER-87-0007   "Instantaneous Optimal Control Laws for Tall Buildings Under Seismic Excitations," by J.N. Yang, A. Akbarpour and P. Ghaemmaghami, 6/10/87, (PB88-134333, A06, MF-A01). This report is only available through NTIS (see address given above).

NCEER-87-0008   "IDARC: Inelastic Damage Analysis of Reinforced Concrete Frame - Shear-Wall Structures," by Y.J. Park, A.M. Reinhorn and S.K. Kunnath, 7/20/87, (PB88-134325, A09, MF-A01). This report is only available through NTIS (see address given above).

NCEER-87-0009   "Liquefaction Potential for New York State: A Preliminary Report on Sites in Manhattan and Buffalo," by M. Budhu, V. Vijayakumar, R.F. Giese and L. Baumgras, 8/31/87, (PB88-163704, A03, MF-A01). This report is available only through NTIS (see address given above).

NCEER-87-0010   "Vertical and Torsional Vibration of Foundations in Inhomogeneous Media," by A.S. Veletsos and K.W. Dotson, 6/1/87, (PB88-134291, A03, MF-A01). This report is only available through NTIS (see address given above).

NCEER-87-0011   "Seismic Probabilistic Risk Assessment and Seismic Margins Studies for Nuclear Power Plants," by Howard H.M. Hwang, 6/15/87, (PB88-134267, A03, MF-A01). This report is only available through NTIS (see address given above).

NCEER-87-0012   "Parametric Studies of Frequency Response of Secondary Systems Under Ground-Acceleration Excitations," by Y. Yong and Y.K. Lin, 6/10/87, (PB88-134309, A03, MF-A01). This report is only available through NTIS (see address given above).

NCEER-87-0013   "Frequency Response of Secondary Systems Under Seismic Excitation," by J.A. HoLung, J. Cai and Y.K. Lin, 7/31/87, (PB88-134317, A05, MF-A01). This report is only available through NTIS (see address given above).

NCEER-87-0014   "Modelling Earthquake Ground Motions in Seismically Active Regions Using Parametric Time Series Methods," by G.W. Ellis and A.S. Cakmak, 8/25/87, (PB88-134283, A08, MF-A01). This report is only available through NTIS (see address given above).

NCEER-87-0015   "Detection and Assessment of Seismic Structural Damage," by E. DiPasquale and A.S. Cakmak, 8/25/87, (PB88-163712, A05, MF-A01). This report is only available through NTIS (see address given above).

NCEER-87-0016   "Pipeline Experiment at Parkfield, California," by J. Isenberg and E. Richardson, 9/15/87, (PB88-163720, A03, MF-A01). This report is available only through NTIS (see address given above).

NCEER-87-0017   "Digital Simulation of Seismic Ground Motion," by M. Shinozuka, G. Deodatis and T. Harada, 8/31/87, (PB88-155197, A04, MF-A01). This report is available only through NTIS (see address given above).

NCEER-87-0018   "Practical Considerations for Structural Control: System Uncertainty, System Time Delay and Truncation of Small Control Forces," J.N. Yang and A. Akbarpour, 8/10/87, (PB88-163738, A08, MF-A01). This report is only available through NTIS (see address given above).

NCEER-87-0019   "Modal Analysis of Nonclassically Damped Structural Systems Using Canonical Transformation," by J.N. Yang, S. Sarkani and F.X. Long, 9/27/87, (PB88-187851, A04, MF-A01).

NCEER-87-0020   "A Nonstationary Solution in Random Vibration Theory," by J.R. Red-Horse and P.D. Spanos, 11/3/87, (PB88-163746, A03, MF-A01).

NCEER-87-0021   "Horizontal Impedances for Radially Inhomogeneous Viscoelastic Soil Layers," by A.S. Veletsos and K.W. Dotson, 10/15/87, (PB88-150859, A04, MF-A01).

NCEER-87-0022   "Seismic Damage Assessment of Reinforced Concrete Members," by Y.S. Chung, C. Meyer and M. Shinozuka, 10/9/87, (PB88-150867, A05, MF-A01). This report is available only through NTIS (see address given above).

NCEER-87-0023   "Active Structural Control in Civil Engineering," by T.T. Soong, 11/11/87, (PB88-187778, A03, MF-A01).

NCEER-87-0024   "Vertical and Torsional Impedances for Radially Inhomogeneous Viscoelastic Soil Layers," by K.W. Dotson and A.S. Veletsos, 12/87, (PB88-187786, A03, MF-A01).

NCEER-87-0025   "Proceedings from the Symposium on Seismic Hazards, Ground Motions, Soil-Liquefaction and Engineering Practice in Eastern North America," October 20-22, 1987, edited by K.H. Jacob, 12/87, (PB88-188115, A23, MF-A01). This report is available only through NTIS (see address given above).

NCEER-87-0026   "Report on the Whittier-Narrows, California, Earthquake of October 1, 1987," by J. Pantelic and A. Reinhorn, 11/87, (PB88-187752, A03, MF-A01). This report is available only through NTIS (see address given above).

NCEER-87-0027   "Design of a Modular Program for Transient Nonlinear Analysis of Large 3-D Building Structures," by S. Srivastav and J.F. Abel, 12/30/87, (PB88-187950, A05, MF-A01). This report is only available through NTIS (see address given above).

NCEER-87-0028   "Second-Year Program in Research, Education and Technology Transfer," 3/8/88, (PB88-219480, A04, MF-A01).

NCEER-88-0001   "Workshop on Seismic Computer Analysis and Design of Buildings With Interactive Graphics," by W. McGuire, J.F. Abel and C.H. Conley, 1/18/88, (PB88-187760, A03, MF-A01). This report is only available through NTIS (see address given above).

NCEER-88-0002   "Optimal Control of Nonlinear Flexible Structures," by J.N. Yang, F.X. Long and D. Wong, 1/22/88, (PB88-213772, A06, MF-A01).

NCEER-88-0003   "Substructuring Techniques in the Time Domain for Primary-Secondary Structural Systems," by G.D. Manolis and G. Juhn, 2/10/88, (PB88-213780, A04, MF-A01).

NCEER-88-0004   "Iterative Seismic Analysis of Primary-Secondary Systems," by A. Singhal, L.D. Lutes and P.D. Spanos, 2/23/88, (PB88-213798, A04, MF-A01).

NCEER-88-0005   "Stochastic Finite Element Expansion for Random Media," by P.D. Spanos and R. Ghanem, 3/14/88, (PB88-213806, A03, MF-A01).

NCEER-88-0006   "Combining Structural Optimization and Structural Control," by F.Y. Cheng and C.P. Pantelides, 1/10/88, (PB88-213814, A05, MF-A01).

NCEER-88-0007   "Seismic Performance Assessment of Code-Designed Structures," by H.H-M. Hwang, J-W. Jaw and H-J. Shau, 3/20/88, (PB88-219423, A04, MF-A01). This report is only available through NTIS (see address given above).

NCEER-88-0008   "Reliability Analysis of Code-Designed Structures Under Natural Hazards," by H.H-M. Hwang, H. Ushiba and M. Shinozuka, 2/29/88, (PB88-229471, A07, MF-A01). This report is only available through NTIS (see address given above).

NCEER-88-0009   "Seismic Fragility Analysis of Shear Wall Structures," by J-W Jaw and H.H-M. Hwang, 4/30/88, (PB89-102867, A04, MF-A01).

NCEER-88-0010   "Base Isolation of a Multi-Story Building Under a Harmonic Ground Motion - A Comparison of Performances of Various Systems," by F-G Fan, G. Ahmadi and I.G. Tadjbakhsh, 5/18/88, (PB89-122238, A06, MF-A01). This report is only available through NTIS (see address given above).

NCEER-88-0011   "Seismic Floor Response Spectra for a Combined System by Green's Functions," by F.M. Lavelle, L.A. Bergman and P.D. Spanos, 5/1/88, (PB89-102875, A03, MF-A01).

NCEER-88-0012   "A New Solution Technique for Randomly Excited Hysteretic Structures," by G.Q. Cai and Y.K. Lin, 5/16/88, (PB89-102883, A03, MF-A01).

NCEER-88-0013   "A Study of Radiation Damping and Soil-Structure Interaction Effects in the Centrifuge," by K. Weissman, supervised by J.H. Prevost, 5/24/88, (PB89-144703, A06, MF-A01).

NCEER-88-0014   "Parameter Identification and Implementation of a Kinematic Plasticity Model for Frictional Soils," by J.H. Prevost and D.V. Griffiths, to be published.

NCEER-88-0015   "Two- and Three- Dimensional Dynamic Finite Element Analyses of the Long Valley Dam," by D.V. Griffiths and J.H. Prevost, 6/17/88, (PB89-144711, A04, MF-A01).

NCEER-88-0016   "Damage Assessment of Reinforced Concrete Structures in Eastern United States," by A.M. Reinhorn, M.J. Seidel, S.K. Kunnath and Y.J. Park, 6/15/88, (PB89-122220, A04, MF-A01). This report is only available through NTIS (see address given above).

NCEER-88-0017   "Dynamic Compliance of Vertically Loaded Strip Foundations in Multilayered Viscoelastic Soils," by S. Ahmad and A.S.M. Israil, 6/17/88, (PB89-102891, A04, MF-A01).

NCEER-88-0018   "An Experimental Study of Seismic Structural Response With Added Viscoelastic Dampers," by R.C. Lin, Z. Liang, T.T. Soong and R.H. Zhang, 6/30/88, (PB89-122212, A05, MF-A01). This report is available only through NTIS (see address given above).

NCEER-88-0019   "Experimental Investigation of Primary - Secondary System Interaction," by G.D. Manolis, G. Juhn and A.M. Reinhorn, 5/27/88, (PB89-122204, A04, MF-A01).

NCEER-88-0020   "A Response Spectrum Approach For Analysis of Nonclassically Damped Structures," by J.N. Yang, S. Sarkani and F.X. Long, 4/22/88, (PB89-102909, A04, MF-A01).

NCEER-88-0021   "Seismic Interaction of Structures and Soils: Stochastic Approach," by A.S. Veletsos and A.M. Prasad, 7/21/88, (PB89-122196, A04, MF-A01). This report is only available through NTIS (see address given above).

NCEER-88-0022   "Identification of the Serviceability Limit State and Detection of Seismic Structural Damage," by E. DiPasquale and A.S. Cakmak, 6/15/88, (PB89-122188, A05, MF-A01). This report is available only through NTIS (see address given above).

NCEER-88-0023   "Multi-Hazard Risk Analysis: Case of a Simple Offshore Structure," by B.K. Bhartia and E.H. Vanmarcke, 7/21/88, (PB89-145213, A05, MF-A01).

NCEER-88-0024   "Automated Seismic Design of Reinforced Concrete Buildings," by Y.S. Chung, C. Meyer and M. Shinozuka, 7/5/88, (PB89-122170, A06, MF-A01). This report is available only through NTIS (see address given above).

NCEER-88-0025   "Experimental Study of Active Control of MDOF Structures Under Seismic Excitations," by L.L. Chung, R.C. Lin, T.T. Soong and A.M. Reinhorn, 7/10/88, (PB89-122600, A04, MF-A01).

NCEER-88-0026   "Earthquake Simulation Tests of a Low-Rise Metal Structure," by J.S. Hwang, K.C. Chang, G.C. Lee and R.L. Ketter, 8/1/88, (PB89-102917, A04, MF-A01).

NCEER-88-0027   "Systems Study of Urban Response and Reconstruction Due to Catastrophic Earthquakes," by F. Kozin and H.K. Zhou, 9/22/88, (PB90-162348, A04, MF-A01).

NCEER-88-0028   "Seismic Fragility Analysis of Plane Frame Structures," by H.H-M. Hwang and Y.K. Low, 7/31/88, (PB89-131445, A06, MF-A01).

NCEER-88-0029   "Response Analysis of Stochastic Structures," by A. Kardara, C. Bucher and M. Shinozuka, 9/22/88, (PB89-174429, A04, MF-A01).

NCEER-88-0030   "Nonnormal Accelerations Due to Yielding in a Primary Structure," by D.C.K. Chen and L.D. Lutes, 9/19/88, (PB89-131437, A04, MF-A01).

NCEER-88-0031   "Design Approaches for Soil-Structure Interaction," by A.S. Veletsos, A.M. Prasad and Y. Tang, 12/30/88, (PB89-174437, A03, MF-A01). This report is available only through NTIS (see address given above).

NCEER-88-0032   "A Re-evaluation of Design Spectra for Seismic Damage Control," by C.J. Turkstra and A.G. Tallin, 11/7/88, (PB89-145221, A05, MF-A01).

NCEER-88-0033   "The Behavior and Design of Noncontact Lap Splices Subjected to Repeated Inelastic Tensile Loading," by V.E. Sagan, P. Gergely and R.N. White, 12/8/88, (PB89-163737, A08, MF-A01).

NCEER-88-0034   "Seismic Response of Pile Foundations," by S.M. Mamoon, P.K. Banerjee and S. Ahmad, 11/1/88, (PB89-145239, A04, MF-A01).

NCEER-88-0035   "Modeling of R/C Building Structures With Flexible Floor Diaphragms (IDARC2)," by A.M. Reinhorn, S.K. Kunnath and N. Panahshahi, 9/7/88, (PB89-207153, A07, MF-A01).

NCEER-88-0036   "Solution of the Dam-Reservoir Interaction Problem Using a Combination of FEM, BEM with Particular Integrals, Modal Analysis, and Substructuring," by C-S. Tsai, G.C. Lee and R.L. Ketter, 12/31/88, (PB89-207146, A04, MF-A01).

NCEER-88-0037   "Optimal Placement of Actuators for Structural Control," by F.Y. Cheng and C.P. Pantelides, 8/15/88, (PB89-162846, A05, MF-A01).

NCEER-88-0038   "Teflon Bearings in Aseismic Base Isolation: Experimental Studies and Mathematical Modeling," by A. Mokha, M.C. Constantinou and A.M. Reinhorn, 12/5/88, (PB89-218457, A10, MF-A01). This report is available only through NTIS (see address given above).

NCEER-88-0039   "Seismic Behavior of Flat Slab High-Rise Buildings in the New York City Area," by P. Weidlinger and M. Ettouney, 10/15/88, (PB90-145681, A04, MF-A01).

NCEER-88-0040   "Evaluation of the Earthquake Resistance of Existing Buildings in New York City," by P. Weidlinger and M. Ettouney, 10/15/88, to be published.

NCEER-88-0041   "Small-Scale Modeling Techniques for Reinforced Concrete Structures Subjected to Seismic Loads," by W. Kim, A. El-Attar and R.N. White, 11/22/88, (PB89-189625, A05, MF-A01).

NCEER-88-0042   "Modeling Strong Ground Motion from Multiple Event Earthquakes," by G.W. Ellis and A.S. Cakmak, 10/15/88, (PB89-174445, A03, MF-A01).

NCEER-88-0043 "Nonstationary Models of Seismic Ground Acceleration," by M. Grigoriu, S.E. Ruiz and E. Rosenblueth, 7/15/88, (PB89-189617, A04, MF-A01).

NCEER-88-0044 "SARCF User's Guide: Seismic Analysis of Reinforced Concrete Frames," by Y.S. Chung, C. Meyer and M. Shinozuka, 11/9/88, (PB89-174452, A08, MF-A01).

NCEER-88-0045 "First Expert Panel Meeting on Disaster Research and Planning," edited by J. Pantelic and J. Stoyle, 9/15/88, (PB89-174460, A05, MF-A01).

NCEER-88-0046 "Preliminary Studies of the Effect of Degrading Infill Walls on the Nonlinear Seismic Response of Steel Frames," by C.Z. Chrysostomou, P. Gergely and J.F. Abel, 12/19/88, (PB89-208383, A05, MF-A01).

NCEER-88-0047 "Reinforced Concrete Frame Component Testing Facility - Design, Construction, Instrumentation and Operation," by S.P. Pessiki, C. Conley, T. Bond, P. Gergely and R.N. White, 12/16/88, (PB89-174478, A04, MF-A01).

NCEER-89-0001 "Effects of Protective Cushion and Soil Compliancy on the Response of Equipment Within a Seismically Excited Building," by J.A. HoLung, 2/16/89, (PB89-207179, A04, MF-A01).

NCEER-89-0002 "Statistical Evaluation of Response Modification Factors for Reinforced Concrete Structures," by H.H-M. Hwang and J-W. Jaw, 2/17/89, (PB89-207187, A05, MF-A01).

NCEER-89-0003 "Hysteretic Columns Under Random Excitation," by G-Q. Cai and Y.K. Lin, 1/9/89, (PB89-196513, A03, MF-A01).

NCEER-89-0004 "Experimental Study of `Elephant Foot Bulge' Instability of Thin-Walled Metal Tanks," by Z-H. Jia and R.L. Ketter, 2/22/89, (PB89-207195, A03, MF-A01).

NCEER-89-0005 "Experiment on Performance of Buried Pipelines Across San Andreas Fault," by J. Isenberg, E. Richardson and T.D. O'Rourke, 3/10/89, (PB89-218440, A04, MF-A01). This report is available only through NTIS (see address given above).

NCEER-89-0006 "A Knowledge-Based Approach to Structural Design of Earthquake-Resistant Buildings," by M. Subramani, P. Gergely, C.H. Conley, J.F. Abel and A.H. Zaghw, 1/15/89, (PB89-218465, A06, MF-A01).

NCEER-89-0007 "Liquefaction Hazards and Their Effects on Buried Pipelines," by T.D. O'Rourke and P.A. Lane, 2/1/89, (PB89-218481, A09, MF-A01).

NCEER-89-0008 "Fundamentals of System Identification in Structural Dynamics," by H. Imai, C-B. Yun, O. Maruyama and M. Shinozuka, 1/26/89, (PB89-207211, A04, MF-A01).

NCEER-89-0009 "Effects of the 1985 Michoacan Earthquake on Water Systems and Other Buried Lifelines in Mexico," by A.G. Ayala and M.J. O'Rourke, 3/8/89, (PB89-207229, A06, MF-A01).

NCEER-89-R010 "NCEER Bibliography of Earthquake Education Materials," by K.E.K. Ross, Second Revision, 9/1/89, (PB90-125352, A05, MF-A01). This report is replaced by NCEER-92-0018.

NCEER-89-0011 "Inelastic Three-Dimensional Response Analysis of Reinforced Concrete Building Structures (IDARC-3D), Part I - Modeling," by S.K. Kunnath and A.M. Reinhorn, 4/17/89, (PB90-114612, A07, MF-A01). This report is available only through NTIS (see address given above).

NCEER-89-0012 "Recommended Modifications to ATC-14," by C.D. Poland and J.O. Malley, 4/12/89, (PB90-108648, A15, MF-A01).

NCEER-89-0013 "Repair and Strengthening of Beam-to-Column Connections Subjected to Earthquake Loading," by M. Corazao and A.J. Durrani, 2/28/89, (PB90-109885, A06, MF-A01).

NCEER-89-0014 "Program EXKAL2 for Identification of Structural Dynamic Systems," by O. Maruyama, C-B. Yun, M. Hoshiya and M. Shinozuka, 5/19/89, (PB90-109877, A09, MF-A01).

NCEER-89-0015   "Response of Frames With Bolted Semi-Rigid Connections, Part I - Experimental Study and Analytical Predictions," by P.J. DiCorso, A.M. Reinhorn, J.R. Dickerson, J.B. Radziminski and W.L. Harper, 6/1/89, to be published.

NCEER-89-0016   "ARMA Monte Carlo Simulation in Probabilistic Structural Analysis," by P.D. Spanos and M.P. Mignolet, 7/10/89, (PB90-109893, A03, MF-A01).

NCEER-89-P017   "Preliminary Proceedings from the Conference on Disaster Preparedness - The Place of Earthquake Education in Our Schools," Edited by K.E.K. Ross, 6/23/89, (PB90-108606, A03, MF-A01).

NCEER-89-0017   "Proceedings from the Conference on Disaster Preparedness - The Place of Earthquake Education in Our Schools," Edited by K.E.K. Ross, 12/31/89, (PB90-207895, A012, MF-A02). This report is available only through NTIS (see address given above).

NCEER-89-0018   "Multidimensional Models of Hysteretic Material Behavior for Vibration Analysis of Shape Memory Energy Absorbing Devices, by E.J. Graesser and F.A. Cozzarelli, 6/7/89, (PB90-164146, A04, MF-A01).

NCEER-89-0019   "Nonlinear Dynamic Analysis of Three-Dimensional Base Isolated Structures (3D-BASIS)," by S. Nagarajaiah, A.M. Reinhorn and M.C. Constantinou, 8/3/89, (PB90-161936, A06, MF-A01). This report has been replaced by NCEER-93-0011.

NCEER-89-0020   "Structural Control Considering Time-Rate of Control Forces and Control Rate Constraints," by F.Y. Cheng and C.P. Pantelides, 8/3/89, (PB90-120445, A04, MF-A01).

NCEER-89-0021   "Subsurface Conditions of Memphis and Shelby County," by K.W. Ng, T-S. Chang and H-H.M. Hwang, 7/26/89, (PB90-120437, A03, MF-A01).

NCEER-89-0022   "Seismic Wave Propagation Effects on Straight Jointed Buried Pipelines," by K. Elhmadi and M.J. O'Rourke, 8/24/89, (PB90-162322, A10, MF-A02).

NCEER-89-0023   "Workshop on Serviceability Analysis of Water Delivery Systems," edited by M. Grigoriu, 3/6/89, (PB90-127424, A03, MF-A01).

NCEER-89-0024   "Shaking Table Study of a 1/5 Scale Steel Frame Composed of Tapered Members," by K.C. Chang, J.S. Hwang and G.C. Lee, 9/18/89, (PB90-160169, A04, MF-A01).

NCEER-89-0025   "DYNA1D: A Computer Program for Nonlinear Seismic Site Response Analysis - Technical Documentation," by Jean H. Prevost, 9/14/89, (PB90-161944, A07, MF-A01). This report is available only through NTIS (see address given above).

NCEER-89-0026   "1:4 Scale Model Studies of Active Tendon Systems and Active Mass Dampers for Aseismic Protection," by A.M. Reinhorn, T.T. Soong, R.C. Lin, Y.P. Yang, Y. Fukao, H. Abe and M. Nakai, 9/15/89, (PB90-173246, A10, MF-A02). This report is available only through NTIS (see address given above).

NCEER-89-0027   "Scattering of Waves by Inclusions in a Nonhomogeneous Elastic Half Space Solved by Boundary Element Methods," by P.K. Hadley, A. Askar and A.S. Cakmak, 6/15/89, (PB90-145699, A07, MF-A01).

NCEER-89-0028   "Statistical Evaluation of Deflection Amplification Factors for Reinforced Concrete Structures," by H.H.M. Hwang, J-W. Jaw and A.L. Ch'ng, 8/31/89, (PB90-164633, A05, MF-A01).

NCEER-89-0029   "Bedrock Accelerations in Memphis Area Due to Large New Madrid Earthquakes," by H.H.M. Hwang, C.H.S. Chen and G. Yu, 11/7/89, (PB90-162330, A04, MF-A01).

NCEER-89-0030   "Seismic Behavior and Response Sensitivity of Secondary Structural Systems," by Y.Q. Chen and T.T. Soong, 10/23/89, (PB90-164658, A08, MF-A01).

NCEER-89-0031   "Random Vibration and Reliability Analysis of Primary-Secondary Structural Systems," by Y. Ibrahim, M. Grigoriu and T.T. Soong, 11/10/89, (PB90-161951, A04, MF-A01).

NCEER-89-0032   "Proceedings from the Second U.S. - Japan Workshop on Liquefaction, Large Ground Deformation and Their Effects on Lifelines, September 26-29, 1989," Edited by T.D. O'Rourke and M. Hamada, 12/1/89, (PB90-209388, A22, MF-A03).

NCEER-89-0033   "Deterministic Model for Seismic Damage Evaluation of Reinforced Concrete Structures," by J.M. Bracci, A.M. Reinhorn, J.B. Mander and S.K. Kunnath, 9/27/89, (PB91-108803, A06, MF-A01).

NCEER-89-0034   "On the Relation Between Local and Global Damage Indices," by E. DiPasquale and A.S. Cakmak, 8/15/89, (PB90-173865, A05, MF-A01).

NCEER-89-0035   "Cyclic Undrained Behavior of Nonplastic and Low Plasticity Silts," by A.J. Walker and H.E. Stewart, 7/26/89, (PB90-183518, A10, MF-A01).

NCEER-89-0036   "Liquefaction Potential of Surficial Deposits in the City of Buffalo, New York," by M. Budhu, R. Giese and L. Baumgrass, 1/17/89, (PB90-208455, A04, MF-A01).

NCEER-89-0037   "A Deterministic Assessment of Effects of Ground Motion Incoherence," by A.S. Veletsos and Y. Tang, 7/15/89, (PB90-164294, A03, MF-A01).

NCEER-89-0038   "Workshop on Ground Motion Parameters for Seismic Hazard Mapping," July 17-18, 1989, edited by R.V. Whitman, 12/1/89, (PB90-173923, A04, MF-A01).

NCEER-89-0039   "Seismic Effects on Elevated Transit Lines of the New York City Transit Authority," by C.J. Costantino, C.A. Miller and E. Heymsfield, 12/26/89, (PB90-207887, A06, MF-A01).

NCEER-89-0040   "Centrifugal Modeling of Dynamic Soil-Structure Interaction," by K. Weissman, Supervised by J.H. Prevost, 5/10/89, (PB90-207879, A07, MF-A01).

NCEER-89-0041   "Linearized Identification of Buildings With Cores for Seismic Vulnerability Assessment," by I-K. Ho and A.E. Aktan, 11/1/89, (PB90-251943, A07, MF-A01).

NCEER-90-0001   "Geotechnical and Lifeline Aspects of the October 17, 1989 Loma Prieta Earthquake in San Francisco," by T.D. O'Rourke, H.E. Stewart, F.T. Blackburn and T.S. Dickerman, 1/90, (PB90-208596, A05, MF-A01).

NCEER-90-0002   "Nonnormal Secondary Response Due to Yielding in a Primary Structure," by D.C.K. Chen and L.D. Lutes, 2/28/90, (PB90-251976, A07, MF-A01).

NCEER-90-0003   "Earthquake Education Materials for Grades K-12," by K.E.K. Ross, 4/16/90, (PB91-251984, A05, MF-A05). This report has been replaced by NCEER-92-0018.

NCEER-90-0004   "Catalog of Strong Motion Stations in Eastern North America," by R.W. Busby, 4/3/90, (PB90-251984, A05, MF-A01).

NCEER-90-0005   "NCEER Strong-Motion Data Base: A User Manual for the GeoBase Release (Version 1.0 for the Sun3)," by P. Friberg and K. Jacob, 3/31/90 (PB90-258062, A04, MF-A01).

NCEER-90-0006   "Seismic Hazard Along a Crude Oil Pipeline in the Event of an 1811-1812 Type New Madrid Earthquake," by H.H.M. Hwang and C-H.S. Chen, 4/16/90, (PB90-258054, A04, MF-A01).

NCEER-90-0007   "Site-Specific Response Spectra for Memphis Sheahan Pumping Station," by H.H.M. Hwang and C.S. Lee, 5/15/90, (PB91-108811, A05, MF-A01).

NCEER-90-0008   "Pilot Study on Seismic Vulnerability of Crude Oil Transmission Systems," by T. Ariman, R. Dobry, M. Grigoriu, F. Kozin, M. O'Rourke, T. O'Rourke and M. Shinozuka, 5/25/90, (PB91-108837, A06, MF-A01).

NCEER-90-0009   "A Program to Generate Site Dependent Time Histories: EQGEN," by G.W. Ellis, M. Srinivasan and A.S. Cakmak, 1/30/90, (PB91-108829, A04, MF-A01).

NCEER-90-0010   "Active Isolation for Seismic Protection of Operating Rooms," by M.E. Talbott, Supervised by M. Shinozuka, 6/8/9, (PB91-110205, A05, MF-A01).

NCEER-90-0011   "Program LINEARID for Identification of Linear Structural Dynamic Systems," by C-B. Yun and M. Shinozuka, 6/25/90, (PB91-110312, A08, MF-A01).

NCEER-90-0012   "Two-Dimensional Two-Phase Elasto-Plastic Seismic Response of Earth Dams," by A.N. Yiagos, Supervised by J.H. Prevost, 6/20/90, (PB91-110197, A13, MF-A02).

NCEER-90-0013   "Secondary Systems in Base-Isolated Structures: Experimental Investigation, Stochastic Response and Stochastic Sensitivity," by G.D. Manolis, G. Juhn, M.C. Constantinou and A.M. Reinhorn, 7/1/90, (PB91-110320, A08, MF-A01).

NCEER-90-0014   "Seismic Behavior of Lightly-Reinforced Concrete Column and Beam-Column Joint Details," by S.P. Pessiki, C.H. Conley, P. Gergely and R.N. White, 8/22/90, (PB91-108795, A11, MF-A02).

NCEER-90-0015   "Two Hybrid Control Systems for Building Structures Under Strong Earthquakes," by J.N. Yang and A. Danielians, 6/29/90, (PB91-125393, A04, MF-A01).

NCEER-90-0016   "Instantaneous Optimal Control with Acceleration and Velocity Feedback," by J.N. Yang and Z. Li, 6/29/90, (PB91-125401, A03, MF-A01).

NCEER-90-0017   "Reconnaissance Report on the Northern Iran Earthquake of June 21, 1990," by M. Mehrain, 10/4/90, (PB91-125377, A03, MF-A01).

NCEER-90-0018   "Evaluation of Liquefaction Potential in Memphis and Shelby County," by T.S. Chang, P.S. Tang, C.S. Lee and H. Hwang, 8/10/90, (PB91-125427, A09, MF-A01).

NCEER-90-0019   "Experimental and Analytical Study of a Combined Sliding Disc Bearing and Helical Steel Spring Isolation System," by M.C. Constantinou, A.S. Mokha and A.M. Reinhorn, 10/4/90, (PB91-125385, A06, MF-A01). This report is available only through NTIS (see address given above).

NCEER-90-0020   "Experimental Study and Analytical Prediction of Earthquake Response of a Sliding Isolation System with a Spherical Surface," by A.S. Mokha, M.C. Constantinou and A.M. Reinhorn, 10/11/90, (PB91-125419, A05, MF-A01).

NCEER-90-0021   "Dynamic Interaction Factors for Floating Pile Groups," by G. Gazetas, K. Fan, A. Kaynia and E. Kausel, 9/10/90, (PB91-170381, A05, MF-A01).

NCEER-90-0022   "Evaluation of Seismic Damage Indices for Reinforced Concrete Structures," by S. Rodriguez-Gomez and A.S. Cakmak, 9/30/90, PB91-171322, A06, MF-A01).

NCEER-90-0023   "Study of Site Response at a Selected Memphis Site," by H. Desai, S. Ahmad, E.S. Gazetas and M.R. Oh, 10/11/90, (PB91-196857, A03, MF-A01).

NCEER-90-0024   "A User's Guide to Strongmo: Version 1.0 of NCEER's Strong-Motion Data Access Tool for PCs and Terminals," by P.A. Friberg and C.A.T. Susch, 11/15/90, (PB91-171272, A03, MF-A01).

NCEER-90-0025   "A Three-Dimensional Analytical Study of Spatial Variability of Seismic Ground Motions," by L-L. Hong and A.H.-S. Ang, 10/30/90, (PB91-170399, A09, MF-A01).

NCEER-90-0026   "MUMOID User's Guide - A Program for the Identification of Modal Parameters," by S. Rodriguez-Gomez and E. DiPasquale, 9/30/90, (PB91-171298, A04, MF-A01).

NCEER-90-0027   "SARCF-II User's Guide - Seismic Analysis of Reinforced Concrete Frames," by S. Rodriguez-Gomez, Y.S. Chung and C. Meyer, 9/30/90, (PB91-171280, A05, MF-A01).

NCEER-90-0028   "Viscous Dampers: Testing, Modeling and Application in Vibration and Seismic Isolation," by N. Makris and M.C. Constantinou, 12/20/90 (PB91-190561, A06, MF-A01).

NCEER-90-0029   "Soil Effects on Earthquake Ground Motions in the Memphis Area," by H. Hwang, C.S. Lee, K.W. Ng and T.S. Chang, 8/2/90, (PB91-190751, A05, MF-A01).

NCEER-91-0001   "Proceedings from the Third Japan-U.S. Workshop on Earthquake Resistant Design of Lifeline Facilities and Countermeasures for Soil Liquefaction, December 17-19, 1990," edited by T.D. O'Rourke and M. Hamada, 2/1/91, (PB91-179259, A99, MF-A04).

NCEER-91-0002   "Physical Space Solutions of Non-Proportionally Damped Systems," by M. Tong, Z. Liang and G.C. Lee, 1/15/91, (PB91-179242, A04, MF-A01).

NCEER-91-0003   "Seismic Response of Single Piles and Pile Groups," by K. Fan and G. Gazetas, 1/10/91, (PB92-174994, A04, MF-A01).

NCEER-91-0004   "Damping of Structures: Part 1 - Theory of Complex Damping," by Z. Liang and G. Lee, 10/10/91, (PB92-197235, A12, MF-A03).

NCEER-91-0005   "3D-BASIS - Nonlinear Dynamic Analysis of Three Dimensional Base Isolated Structures: Part II," by S. Nagarajaiah, A.M. Reinhorn and M.C. Constantinou, 2/28/91, (PB91-190553, A07, MF-A01). This report has been replaced by NCEER-93-0011.

NCEER-91-0006   "A Multidimensional Hysteretic Model for Plasticity Deforming Metals in Energy Absorbing Devices," by E.J. Graesser and F.A. Cozzarelli, 4/9/91, (PB92-108364, A04, MF-A01).

NCEER-91-0007   "A Framework for Customizable Knowledge-Based Expert Systems with an Application to a KBES for Evaluating the Seismic Resistance of Existing Buildings," by E.G. Ibarra-Anaya and S.J. Fenves, 4/9/91, (PB91-210930, A08, MF-A01).

NCEER-91-0008   "Nonlinear Analysis of Steel Frames with Semi-Rigid Connections Using the Capacity Spectrum Method," by G.G. Deierlein, S-H. Hsieh, Y-J. Shen and J.F. Abel, 7/2/91, (PB92-113828, A05, MF-A01).

NCEER-91-0009   "Earthquake Education Materials for Grades K-12," by K.E.K. Ross, 4/30/91, (PB91-212142, A06, MF-A01). This report has been replaced by NCEER-92-0018.

NCEER-91-0010   "Phase Wave Velocities and Displacement Phase Differences in a Harmonically Oscillating Pile," by N. Makris and G. Gazetas, 7/8/91, (PB92-108356, A04, MF-A01).

NCEER-91-0011   "Dynamic Characteristics of a Full-Size Five-Story Steel Structure and a 2/5 Scale Model," by K.C. Chang, G.C. Yao, G.C. Lee, D.S. Hao and Y.C. Yeh," 7/2/91, (PB93-116648, A06, MF-A02).

NCEER-91-0012   "Seismic Response of a 2/5 Scale Steel Structure with Added Viscoelastic Dampers," by K.C. Chang, T.T. Soong, S-T. Oh and M.L. Lai, 5/17/91, (PB92-110816, A05, MF-A01).

NCEER-91-0013   "Earthquake Response of Retaining Walls; Full-Scale Testing and Computational Modeling," by S. Alampalli and A-W.M. Elgamal, 6/20/91, to be published.

NCEER-91-0014   "3D-BASIS-M: Nonlinear Dynamic Analysis of Multiple Building Base Isolated Structures," by P.C. Tsopelas, S. Nagarajaiah, M.C. Constantinou and A.M. Reinhorn, 5/28/91, (PB92-113885, A09, MF-A02).

NCEER-91-0015   "Evaluation of SEAOC Design Requirements for Sliding Isolated Structures," by D. Theodossiou and M.C. Constantinou, 6/10/91, (PB92-114602, A11, MF-A03).

NCEER-91-0016   "Closed-Loop Modal Testing of a 27-Story Reinforced Concrete Flat Plate-Core Building," by H.R. Somaprasad, T. Toksoy, H. Yoshiyuki and A.E. Aktan, 7/15/91, (PB92-129980, A07, MF-A02).

NCEER-91-0017   "Shake Table Test of a 1/6 Scale Two-Story Lightly Reinforced Concrete Building," by A.G. El-Attar, R.N. White and P. Gergely, 2/28/91, (PB92-222447, A06, MF-A02).

NCEER-91-0018   "Shake Table Test of a 1/8 Scale Three-Story Lightly Reinforced Concrete Building," by A.G. El-Attar, R.N. White and P. Gergely, 2/28/91, (PB93-116630, A08, MF-A02).

NCEER-91-0019   "Transfer Functions for Rigid Rectangular Foundations," by A.S. Veletsos, A.M. Prasad and W.H. Wu, 7/31/91, to be published.

NCEER-91-0020   "Hybrid Control of Seismic-Excited Nonlinear and Inelastic Structural Systems," by J.N. Yang, Z. Li and A. Danielians, 8/1/91, (PB92-143171, A06, MF-A02).

NCEER-91-0021   "The NCEER-91 Earthquake Catalog: Improved Intensity-Based Magnitudes and Recurrence Relations for U.S. Earthquakes East of New Madrid," by L. Seeber and J.G. Armbruster, 8/28/91, (PB92-176742, A06, MF-A02).

NCEER-91-0022   "Proceedings from the Implementation of Earthquake Planning and Education in Schools: The Need for Change - The Roles of the Changemakers," by K.E.K. Ross and F. Winslow, 7/23/91, (PB92-129998, A12, MF-A03).

NCEER-91-0023   "A Study of Reliability-Based Criteria for Seismic Design of Reinforced Concrete Frame Buildings," by H.H.M. Hwang and H-M. Hsu, 8/10/91, (PB92-140235, A09, MF-A02).

NCEER-91-0024   "Experimental Verification of a Number of Structural System Identification Algorithms," by R.G. Ghanem, H. Gavin and M. Shinozuka, 9/18/91, (PB92-176577, A18, MF-A04).

NCEER-91-0025   "Probabilistic Evaluation of Liquefaction Potential," by H.H.M. Hwang and C.S. Lee," 11/25/91, (PB92-143429, A05, MF-A01).

NCEER-91-0026   "Instantaneous Optimal Control for Linear, Nonlinear and Hysteretic Structures - Stable Controllers," by J.N. Yang and Z. Li, 11/15/91, (PB92-163807, A04, MF-A01).

NCEER-91-0027   "Experimental and Theoretical Study of a Sliding Isolation System for Bridges," by M.C. Constantinou, A. Kartoum, A.M. Reinhorn and P. Bradford, 11/15/91, (PB92-176973, A10, MF-A03).

NCEER-92-0001   "Case Studies of Liquefaction and Lifeline Performance During Past Earthquakes, Volume 1: Japanese Case Studies," Edited by M. Hamada and T. O'Rourke, 2/17/92, (PB92-197243, A18, MF-A04).

NCEER-92-0002   "Case Studies of Liquefaction and Lifeline Performance During Past Earthquakes, Volume 2: United States Case Studies," Edited by T. O'Rourke and M. Hamada, 2/17/92, (PB92-197250, A20, MF-A04).

NCEER-92-0003   "Issues in Earthquake Education," Edited by K. Ross, 2/3/92, (PB92-222389, A07, MF-A02).

NCEER-92-0004   "Proceedings from the First U.S. - Japan Workshop on Earthquake Protective Systems for Bridges," Edited by I.G. Buckle, 2/4/92, (PB94-142239, A99, MF-A06).

NCEER-92-0005   "Seismic Ground Motion from a Haskell-Type Source in a Multiple-Layered Half-Space," A.P. Theoharis, G. Deodatis and M. Shinozuka, 1/2/92, to be published.

NCEER-92-0006   "Proceedings from the Site Effects Workshop," Edited by R. Whitman, 2/29/92, (PB92-197201, A04, MF-A01).

NCEER-92-0007   "Engineering Evaluation of Permanent Ground Deformations Due to Seismically-Induced Liquefaction," by M.H. Baziar, R. Dobry and A-W.M. Elgamal, 3/24/92, (PB92-222421, A13, MF-A03).

NCEER-92-0008   "A Procedure for the Seismic Evaluation of Buildings in the Central and Eastern United States," by C.D. Poland and J.O. Malley, 4/2/92, (PB92-222439, A20, MF-A04).

NCEER-92-0009   "Experimental and Analytical Study of a Hybrid Isolation System Using Friction Controllable Sliding Bearings," by M.Q. Feng, S. Fujii and M. Shinozuka, 5/15/92, (PB93-150282, A06, MF-A02).

NCEER-92-0010   "Seismic Resistance of Slab-Column Connections in Existing Non-Ductile Flat-Plate Buildings," by A.J. Durrani and Y. Du, 5/18/92, (PB93-116812, A06, MF-A02).

NCEER-92-0011   "The Hysteretic and Dynamic Behavior of Brick Masonry Walls Upgraded by Ferrocement Coatings Under Cyclic Loading and Strong Simulated Ground Motion," by H. Lee and S.P. Prawel, 5/11/92, to be published.

NCEER-92-0012   "Study of Wire Rope Systems for Seismic Protection of Equipment in Buildings," by G.F. Demetriades, M.C. Constantinou and A.M. Reinhorn, 5/20/92, (PB93-116655, A08, MF-A02).

NCEER-92-0013   "Shape Memory Structural Dampers: Material Properties, Design and Seismic Testing," by P.R. Witting and F.A. Cozzarelli, 5/26/92, (PB93-116663, A05, MF-A01).

NCEER-92-0014   "Longitudinal Permanent Ground Deformation Effects on Buried Continuous Pipelines," by M.J. O'Rourke, and C. Nordberg, 6/15/92, (PB93-116671, A08, MF-A02).

NCEER-92-0015   "A Simulation Method for Stationary Gaussian Random Functions Based on the Sampling Theorem," by M. Grigoriu and S. Balopoulou, 6/11/92, (PB93-127496, A05, MF-A01).

NCEER-92-0016   "Gravity-Load-Designed Reinforced Concrete Buildings: Seismic Evaluation of Existing Construction and Detailing Strategies for Improved Seismic Resistance," by G.W. Hoffmann, S.K. Kunnath, A.M. Reinhorn and J.B. Mander, 7/15/92, (PB94-142007, A08, MF-A02).

NCEER-92-0017   "Observations on Water System and Pipeline Performance in the Limón Area of Costa Rica Due to the April 22, 1991 Earthquake," by M. O'Rourke and D. Ballantyne, 6/30/92, (PB93-126811, A06, MF-A02).

NCEER-92-0018   "Fourth Edition of Earthquake Education Materials for Grades K-12," Edited by K.E.K. Ross, 8/10/92, (PB93-114023, A07, MF-A02).

NCEER-92-0019   "Proceedings from the Fourth Japan-U.S. Workshop on Earthquake Resistant Design of Lifeline Facilities and Countermeasures for Soil Liquefaction," Edited by M. Hamada and T.D. O'Rourke, 8/12/92, (PB93-163939, A99, MF-E11).

NCEER-92-0020   "Active Bracing System: A Full Scale Implementation of Active Control," by A.M. Reinhorn, T.T. Soong, R.C. Lin, M.A. Riley, Y.P. Wang, S. Aizawa and M. Higashino, 8/14/92, (PB93-127512, A06, MF-A02).

NCEER-92-0021   "Empirical Analysis of Horizontal Ground Displacement Generated by Liquefaction-Induced Lateral Spreads," by S.F. Bartlett and T.L. Youd, 8/17/92, (PB93-188241, A06, MF-A02).

NCEER-92-0022   "IDARC Version 3.0: Inelastic Damage Analysis of Reinforced Concrete Structures," by S.K. Kunnath, A.M. Reinhorn and R.F. Lobo, 8/31/92, (PB93-227502, A07, MF-A02).

NCEER-92-0023   "A Semi-Empirical Analysis of Strong-Motion Peaks in Terms of Seismic Source, Propagation Path and Local Site Conditions, by M. Kamiyama, M.J. O'Rourke and R. Flores-Berrones, 9/9/92, (PB93-150266, A08, MF-A02).

NCEER-92-0024   "Seismic Behavior of Reinforced Concrete Frame Structures with Nonductile Details, Part I: Summary of Experimental Findings of Full Scale Beam-Column Joint Tests," by A. Beres, R.N. White and P. Gergely, 9/30/92, (PB93-227783, A05, MF-A01).

NCEER-92-0025   "Experimental Results of Repaired and Retrofitted Beam-Column Joint Tests in Lightly Reinforced Concrete Frame Buildings," by A. Beres, S. El-Borgi, R.N. White and P. Gergely, 10/29/92, (PB93-227791, A05, MF-A01).

NCEER-92-0026   "A Generalization of Optimal Control Theory: Linear and Nonlinear Structures," by J.N. Yang, Z. Li and S. Vongchavalitkul, 11/2/92, (PB93-188621, A05, MF-A01).

NCEER-92-0027   "Seismic Resistance of Reinforced Concrete Frame Structures Designed Only for Gravity Loads: Part I - Design and Properties of a One-Third Scale Model Structure," by J.M. Bracci, A.M. Reinhorn and J.B. Mander, 12/1/92, (PB94-104502, A08, MF-A02).

NCEER-92-0028   "Seismic Resistance of Reinforced Concrete Frame Structures Designed Only for Gravity Loads: Part II - Experimental Performance of Subassemblages," by L.E. Aycardi, J.B. Mander and A.M. Reinhorn, 12/1/92, (PB94-104510, A08, MF-A02).

NCEER-92-0029   "Seismic Resistance of Reinforced Concrete Frame Structures Designed Only for Gravity Loads: Part III - Experimental Performance and Analytical Study of a Structural Model," by J.M. Bracci, A.M. Reinhorn and J.B. Mander, 12/1/92, (PB93-227528, A09, MF-A01).

NCEER-92-0030 "Evaluation of Seismic Retrofit of Reinforced Concrete Frame Structures: Part I - Experimental Performance of Retrofitted Subassemblages," by D. Choudhuri, J.B. Mander and A.M. Reinhorn, 12/8/92, (PB93-198307, A07, MF-A02).

NCEER-92-0031 "Evaluation of Seismic Retrofit of Reinforced Concrete Frame Structures: Part II - Experimental Performance and Analytical Study of a Retrofitted Structural Model," by J.M. Bracci, A.M. Reinhorn and J.B. Mander, 12/8/92, (PB93-198315, A09, MF-A03).

NCEER-92-0032 "Experimental and Analytical Investigation of Seismic Response of Structures with Supplemental Fluid Viscous Dampers," by M.C. Constantinou and M.D. Symans, 12/21/92, (PB93-191435, A10, MF-A03). This report is available only through NTIS (see address given above).

NCEER-92-0033 "Reconnaissance Report on the Cairo, Egypt Earthquake of October 12, 1992," by M. Khater, 12/23/92, (PB93-188621, A03, MF-A01).

NCEER-92-0034 "Low-Level Dynamic Characteristics of Four Tall Flat-Plate Buildings in New York City," by H. Gavin, S. Yuan, J. Grossman, E. Pekelis and K. Jacob, 12/28/92, (PB93-188217, A07, MF-A02).

NCEER-93-0001 "An Experimental Study on the Seismic Performance of Brick-Infilled Steel Frames With and Without Retrofit," by J.B. Mander, B. Nair, K. Wojtkowski and J. Ma, 1/29/93, (PB93-227510, A07, MF-A02).

NCEER-93-0002 "Social Accounting for Disaster Preparedness and Recovery Planning," by S. Cole, E. Pantoja and V. Razak, 2/22/93, (PB94-142114, A12, MF-A03).

NCEER-93-0003 "Assessment of 1991 NEHRP Provisions for Nonstructural Components and Recommended Revisions," by T.T. Soong, G. Chen, Z. Wu, R-H. Zhang and M. Grigoriu, 3/1/93, (PB93-188639, A06, MF-A02).

NCEER-93-0004 "Evaluation of Static and Response Spectrum Analysis Procedures of SEAOC/UBC for Seismic Isolated Structures," by C.W. Winters and M.C. Constantinou, 3/23/93, (PB93-198299, A10, MF-A03).

NCEER-93-0005 "Earthquakes in the Northeast - Are We Ignoring the Hazard? A Workshop on Earthquake Science and Safety for Educators," edited by K.E.K. Ross, 4/2/93, (PB94-103066, A09, MF-A02).

NCEER-93-0006 "Inelastic Response of Reinforced Concrete Structures with Viscoelastic Braces," by R.F. Lobo, J.M. Bracci, K.L. Shen, A.M. Reinhorn and T.T. Soong, 4/5/93, (PB93-227486, A05, MF-A02).

NCEER-93-0007 "Seismic Testing of Installation Methods for Computers and Data Processing Equipment," by K. Kosar, T.T. Soong, K.L. Shen, J.A. HoLung and Y.K. Lin, 4/12/93, (PB93-198299, A07, MF-A02).

NCEER-93-0008 "Retrofit of Reinforced Concrete Frames Using Added Dampers," by A. Reinhorn, M. Constantinou and C. Li, to be published.

NCEER-93-0009 "Seismic Behavior and Design Guidelines for Steel Frame Structures with Added Viscoelastic Dampers," by K.C. Chang, M.L. Lai, T.T. Soong, D.S. Hao and Y.C. Yeh, 5/1/93, (PB94-141959, A07, MF-A02).

NCEER-93-0010 "Seismic Performance of Shear-Critical Reinforced Concrete Bridge Piers," by J.B. Mander, S.M. Waheed, M.T.A. Chaudhary and S.S. Chen, 5/12/93, (PB93-227494, A08, MF-A02).

NCEER-93-0011 "3D-BASIS-TABS: Computer Program for Nonlinear Dynamic Analysis of Three Dimensional Base Isolated Structures," by S. Nagarajaiah, C. Li, A.M. Reinhorn and M.C. Constantinou, 8/2/93, (PB94-141819, A09, MF-A02).

NCEER-93-0012 "Effects of Hydrocarbon Spills from an Oil Pipeline Break on Ground Water," by O.J. Helweg and H.H.M. Hwang, 8/3/93, (PB94-141942, A06, MF-A02).

NCEER-93-0013 "Simplified Procedures for Seismic Design of Nonstructural Components and Assessment of Current Code Provisions," by M.P. Singh, L.E. Suarez, E.E. Matheu and G.O. Maldonado, 8/4/93, (PB94-141827, A09, MF-A02).

NCEER-93-0014 "An Energy Approach to Seismic Analysis and Design of Secondary Systems," by G. Chen and T.T. Soong, 8/6/93, (PB94-142767, A11, MF-A03).

NCEER-93-0015   "Proceedings from School Sites: Becoming Prepared for Earthquakes - Commemorating the Third Anniversary of the Loma Prieta Earthquake," Edited by F.E. Winslow and K.E.K. Ross, 8/16/93, (PB94-154275, A16, MF-A02).

NCEER-93-0016   "Reconnaissance Report of Damage to Historic Monuments in Cairo, Egypt Following the October 12, 1992 Dahshur Earthquake," by D. Sykora, D. Look, G. Croci, E. Karaesmen and E. Karaesmen, 8/19/93, (PB94-142221, A08, MF-A02).

NCEER-93-0017   "The Island of Guam Earthquake of August 8, 1993," by S.W. Swan and S.K. Harris, 9/30/93, (PB94-141843, A04, MF-A01).

NCEER-93-0018   "Engineering Aspects of the October 12, 1992 Egyptian Earthquake," by A.W. Elgamal, M. Amer, K. Adalier and A. Abul-Fadl, 10/7/93, (PB94-141983, A05, MF-A01).

NCEER-93-0019   "Development of an Earthquake Motion Simulator and its Application in Dynamic Centrifuge Testing," by I. Krstelj, Supervised by J.H. Prevost, 10/23/93, (PB94-181773, A-10, MF-A03).

NCEER-93-0020   "NCEER-Taisei Corporation Research Program on Sliding Seismic Isolation Systems for Bridges: Experimental and Analytical Study of a Friction Pendulum System (FPS)," by M.C. Constantinou, P. Tsopelas, Y-S. Kim and S. Okamoto, 11/1/93, (PB94-142775, A08, MF-A02).

NCEER-93-0021   "Finite Element Modeling of Elastomeric Seismic Isolation Bearings," by L.J. Billings, Supervised by R. Shepherd, 11/8/93, to be published.

NCEER-93-0022   "Seismic Vulnerability of Equipment in Critical Facilities: Life-Safety and Operational Consequences," by K. Porter, G.S. Johnson, M.M. Zadeh, C. Scawthorn and S. Eder, 11/24/93, (PB94-181765, A16, MF-A03).

NCEER-93-0023   "Hokkaido Nansei-oki, Japan Earthquake of July 12, 1993, by P.I. Yanev and C.R. Scawthorn, 12/23/93, (PB94-181500, A07, MF-A01).

NCEER-94-0001   "An Evaluation of Seismic Serviceability of Water Supply Networks with Application to the San Francisco Auxiliary Water Supply System," by I. Markov, Supervised by M. Grigoriu and T. O'Rourke, 1/21/94, (PB94-204013, A07, MF-A02).

NCEER-94-0002   "NCEER-Taisei Corporation Research Program on Sliding Seismic Isolation Systems for Bridges: Experimental and Analytical Study of Systems Consisting of Sliding Bearings, Rubber Restoring Force Devices and Fluid Dampers," Volumes I and II, by P. Tsopelas, S. Okamoto, M.C. Constantinou, D. Ozaki and S. Fujii, 2/4/94, (PB94-181740, A09, MF-A02 and PB94-181757, A12, MF-A03).

NCEER-94-0003   "A Markov Model for Local and Global Damage Indices in Seismic Analysis," by S. Rahman and M. Grigoriu, 2/18/94, (PB94-206000, A12, MF-A03).

NCEER-94-0004   "Proceedings from the NCEER Workshop on Seismic Response of Masonry Infills," edited by D.P. Abrams, 3/1/94, (PB94-180783, A07, MF-A02).

NCEER-94-0005   "The Northridge, California Earthquake of January 17, 1994: General Reconnaissance Report," edited by J.D. Goltz, 3/11/94, (PB94-193943, A10, MF-A03).

NCEER-94-0006   "Seismic Energy Based Fatigue Damage Analysis of Bridge Columns: Part I - Evaluation of Seismic Capacity," by G.A. Chang and J.B. Mander, 3/14/94, (PB94-219185, A11, MF-A03).

NCEER-94-0007   "Seismic Isolation of Multi-Story Frame Structures Using Spherical Sliding Isolation Systems," by T.M. Al-Hussaini, V.A. Zayas and M.C. Constantinou, 3/17/94, (PB94-193745, A09, MF-A02).

NCEER-94-0008   "The Northridge, California Earthquake of January 17, 1994: Performance of Highway Bridges," edited by I.G. Buckle, 3/24/94, (PB94-193851, A06, MF-A02).

NCEER-94-0009   "Proceedings of the Third U.S.-Japan Workshop on Earthquake Protective Systems for Bridges," edited by I.G. Buckle and I. Friedland, 3/31/94, (PB94-195815, A99, MF-A06).

NCEER-94-0010   "3D-BASIS-ME: Computer Program for Nonlinear Dynamic Analysis of Seismically Isolated Single and Multiple Structures and Liquid Storage Tanks," by P.C. Tsopelas, M.C. Constantinou and A.M. Reinhorn, 4/12/94, (PB94-204922, A09, MF-A02).

NCEER-94-0011   "The Northridge, California Earthquake of January 17, 1994: Performance of Gas Transmission Pipelines," by T.D. O'Rourke and M.C. Palmer, 5/16/94, (PB94-204989, A05, MF-A01).

NCEER-94-0012   "Feasibility Study of Replacement Procedures and Earthquake Performance Related to Gas Transmission Pipelines," by T.D. O'Rourke and M.C. Palmer, 5/25/94, (PB94-206638, A09, MF-A02).

NCEER-94-0013   "Seismic Energy Based Fatigue Damage Analysis of Bridge Columns: Part II - Evaluation of Seismic Demand," by G.A. Chang and J.B. Mander, 6/1/94, (PB95-18106, A08, MF-A02).

NCEER-94-0014   "NCEER-Taisei Corporation Research Program on Sliding Seismic Isolation Systems for Bridges: Experimental and Analytical Study of a System Consisting of Sliding Bearings and Fluid Restoring Force/Damping Devices," by P. Tsopelas and M.C. Constantinou, 6/13/94, (PB94-219144, A10, MF-A03).

NCEER-94-0015   "Generation of Hazard-Consistent Fragility Curves for Seismic Loss Estimation Studies," by H. Hwang and J-R. Huo, 6/14/94, (PB95-181996, A09, MF-A02).

NCEER-94-0016   "Seismic Study of Building Frames with Added Energy-Absorbing Devices," by W.S. Pong, C.S. Tsai and G.C. Lee, 6/20/94, (PB94-219136, A10, A03).

NCEER-94-0017   "Sliding Mode Control for Seismic-Excited Linear and Nonlinear Civil Engineering Structures," by J. Yang, J. Wu, A. Agrawal and Z. Li, 6/21/94, (PB95-138483, A06, MF-A02).

NCEER-94-0018   "3D-BASIS-TABS Version 2.0: Computer Program for Nonlinear Dynamic Analysis of Three Dimensional Base Isolated Structures," by A.M. Reinhorn, S. Nagarajaiah, M.C. Constantinou, P. Tsopelas and R. Li, 6/22/94, (PB95-182176, A08, MF-A02).

NCEER-94-0019   "Proceedings of the International Workshop on Civil Infrastructure Systems: Application of Intelligent Systems and Advanced Materials on Bridge Systems," Edited by G.C. Lee and K.C. Chang, 7/18/94, (PB95-252474, A20, MF-A04).

NCEER-94-0020   "Study of Seismic Isolation Systems for Computer Floors," by V. Lambrou and M.C. Constantinou, 7/19/94, (PB95-138533, A10, MF-A03).

NCEER-94-0021   "Proceedings of the U.S.-Italian Workshop on Guidelines for Seismic Evaluation and Rehabilitation of Unreinforced Masonry Buildings," Edited by D.P. Abrams and G.M. Calvi, 7/20/94, (PB95-138749, A13, MF-A03).

NCEER-94-0022   "NCEER-Taisei Corporation Research Program on Sliding Seismic Isolation Systems for Bridges: Experimental and Analytical Study of a System Consisting of Lubricated PTFE Sliding Bearings and Mild Steel Dampers," by P. Tsopelas and M.C. Constantinou, 7/22/94, (PB95-182184, A08, MF-A02).

NCEER-94-0023   "Development of Reliability-Based Design Criteria for Buildings Under Seismic Load," by Y.K. Wen, H. Hwang and M. Shinozuka, 8/1/94, (PB95-211934, A08, MF-A02).

NCEER-94-0024   "Experimental Verification of Acceleration Feedback Control Strategies for an Active Tendon System," by S.J. Dyke, B.F. Spencer, Jr., P. Quast, M.K. Sain, D.C. Kaspari, Jr. and T.T. Soong, 8/29/94, (PB95-212320, A05, MF-A01).

NCEER-94-0025   "Seismic Retrofitting Manual for Highway Bridges," Edited by I.G. Buckle and I.F. Friedland, published by the Federal Highway Administration (PB95-212676, A15, MF-A03).

NCEER-94-0026   "Proceedings from the Fifth U.S.-Japan Workshop on Earthquake Resistant Design of Lifeline Facilities and Countermeasures Against Soil Liquefaction," Edited by T.D. O'Rourke and M. Hamada, 11/7/94, (PB95-220802, A99, MF-E08).

NCEER-95-0001 "Experimental and Analytical Investigation of Seismic Retrofit of Structures with Supplemental Damping: Part 1 - Fluid Viscous Damping Devices," by A.M. Reinhorn, C. Li and M.C. Constantinou, 1/3/95, (PB95-266599, A09, MF-A02).

NCEER-95-0002 "Experimental and Analytical Study of Low-Cycle Fatigue Behavior of Semi-Rigid Top-And-Seat Angle Connections," by G. Pekcan, J.B. Mander and S.S. Chen, 1/5/95, (PB95-220042, A07, MF-A02).

NCEER-95-0003 "NCEER-ATC Joint Study on Fragility of Buildings," by T. Anagnos, C. Rojahn and A.S. Kiremidjian, 1/20/95, (PB95-220026, A06, MF-A02).

NCEER-95-0004 "Nonlinear Control Algorithms for Peak Response Reduction," by Z. Wu, T.T. Soong, V. Gattulli and R.C. Lin, 2/16/95, (PB95-220349, A05, MF-A01).

NCEER-95-0005 "Pipeline Replacement Feasibility Study: A Methodology for Minimizing Seismic and Corrosion Risks to Underground Natural Gas Pipelines," by R.T. Eguchi, H.A. Seligson and D.G. Honegger, 3/2/95, (PB95-252326, A06, MF-A02).

NCEER-95-0006 "Evaluation of Seismic Performance of an 11-Story Frame Building During the 1994 Northridge Earthquake," by F. Naeim, R. DiSulio, K. Benuska, A. Reinhorn and C. Li, to be published.

NCEER-95-0007 "Prioritization of Bridges for Seismic Retrofitting," by N. Basöz and A.S. Kiremidjian, 4/24/95, (PB95-252300, A08, MF-A02).

NCEER-95-0008 "Method for Developing Motion Damage Relationships for Reinforced Concrete Frames," by A. Singhal and A.S. Kiremidjian, 5/11/95, (PB95-266607, A06, MF-A02).

NCEER-95-0009 "Experimental and Analytical Investigation of Seismic Retrofit of Structures with Supplemental Damping: Part II - Friction Devices," by C. Li and A.M. Reinhorn, 7/6/95, (PB96-128087, A11, MF-A03).

NCEER-95-0010 "Experimental Performance and Analytical Study of a Non-Ductile Reinforced Concrete Frame Structure Retrofitted with Elastomeric Spring Dampers," by G. Pekcan, J.B. Mander and S.S. Chen, 7/14/95, (PB96-137161, A08, MF-A02).

NCEER-95-0011 "Development and Experimental Study of Semi-Active Fluid Damping Devices for Seismic Protection of Structures," by M.D. Symans and M.C. Constantinou, 8/3/95, (PB96-136940, A23, MF-A04).

NCEER-95-0012 "Real-Time Structural Parameter Modification (RSPM): Development of Innervated Structures," by Z. Liang, M. Tong and G.C. Lee, 4/11/95, (PB96-137153, A06, MF-A01).

NCEER-95-0013 "Experimental and Analytical Investigation of Seismic Retrofit of Structures with Supplemental Damping: Part III - Viscous Damping Walls," by A.M. Reinhorn and C. Li, 10/1/95, (PB96-176409, A11, MF-A03).

NCEER-95-0014 "Seismic Fragility Analysis of Equipment and Structures in a Memphis Electric Substation," by J-R. Huo and H.H.M. Hwang, 8/10/95, (PB96-128087, A09, MF-A02).

NCEER-95-0015 "The Hanshin-Awaji Earthquake of January 17, 1995: Performance of Lifelines," Edited by M. Shinozuka, 11/3/95, (PB96-176383, A15, MF-A03).

NCEER-95-0016 "Highway Culvert Performance During Earthquakes," by T.L. Youd and C.J. Beckman, available as NCEER-96-0015.

NCEER-95-0017 "The Hanshin-Awaji Earthquake of January 17, 1995: Performance of Highway Bridges," Edited by I.G. Buckle, 12/1/95, to be published.

NCEER-95-0018 "Modeling of Masonry Infill Panels for Structural Analysis," by A.M. Reinhorn, A. Madan, R.E. Valles, Y. Reichmann and J.B. Mander, 12/8/95, (PB97-110886, MF-A01, A06).

NCEER-95-0019 "Optimal Polynomial Control for Linear and Nonlinear Structures," by A.K. Agrawal and J.N. Yang, 12/11/95, (PB96-168737, A07, MF-A02).

NCEER-95-0020   "Retrofit of Non-Ductile Reinforced Concrete Frames Using Friction Dampers," by R.S. Rao, P. Gergely and R.N. White, 12/22/95, (PB97-133508, A10, MF-A02).

NCEER-95-0021   "Parametric Results for Seismic Response of Pile-Supported Bridge Bents," by G. Mylonakis, A. Nikolaou and G. Gazetas, 12/22/95, (PB97-100242, A12, MF-A03).

NCEER-95-0022   "Kinematic Bending Moments in Seismically Stressed Piles," by A. Nikolaou, G. Mylonakis and G. Gazetas, 12/23/95, (PB97-113914, MF-A03, A13).

NCEER-96-0001   "Dynamic Response of Unreinforced Masonry Buildings with Flexible Diaphragms," by A.C. Costley and D.P. Abrams," 10/10/96, (PB97-133573, MF-A03, A15).

NCEER-96-0002   "State of the Art Review: Foundations and Retaining Structures," by I. Po Lam, to be published.

NCEER-96-0003   "Ductility of Rectangular Reinforced Concrete Bridge Columns with Moderate Confinement," by N. Wehbe, M. Saiidi, D. Sanders and B. Douglas, 11/7/96, (PB97-133557, A06, MF-A02).

NCEER-96-0004   "Proceedings of the Long-Span Bridge Seismic Research Workshop," edited by I.G. Buckle and I.M. Friedland, to be published.

NCEER-96-0005   "Establish Representative Pier Types for Comprehensive Study: Eastern United States," by J. Kulicki and Z. Prucz, 5/28/96, (PB98-119217, A07, MF-A02).

NCEER-96-0006   "Establish Representative Pier Types for Comprehensive Study: Western United States," by R. Imbsen, R.A. Schamber and T.A. Osterkamp, 5/28/96, (PB98-118607, A07, MF-A02).

NCEER-96-0007   "Nonlinear Control Techniques for Dynamical Systems with Uncertain Parameters," by R.G. Ghanem and M.I. Bujakov, 5/27/96, (PB97-100259, A17, MF-A03).

NCEER-96-0008   "Seismic Evaluation of a 30-Year Old Non-Ductile Highway Bridge Pier and Its Retrofit," by J.B. Mander, B. Mahmoodzadegan, S. Bhadra and S.S. Chen, 5/31/96, (PB97-110902, MF-A03, A10).

NCEER-96-0009   "Seismic Performance of a Model Reinforced Concrete Bridge Pier Before and After Retrofit," by J.B. Mander, J.H. Kim and C.A. Ligozio, 5/31/96, (PB97-110910, MF-A02, A10).

NCEER-96-0010   "IDARC2D Version 4.0: A Computer Program for the Inelastic Damage Analysis of Buildings," by R.E. Valles, A.M. Reinhorn, S.K. Kunnath, C. Li and A. Madan, 6/3/96, (PB97-100234, A17, MF-A03).

NCEER-96-0011   "Estimation of the Economic Impact of Multiple Lifeline Disruption: Memphis Light, Gas and Water Division Case Study," by S.E. Chang, H.A. Seligson and R.T. Eguchi, 8/16/96, (PB97-133490, A11, MF-A03).

NCEER-96-0012   "Proceedings from the Sixth Japan-U.S. Workshop on Earthquake Resistant Design of Lifeline Facilities and Countermeasures Against Soil Liquefaction, Edited by M. Hamada and T. O'Rourke, 9/11/96, (PB97-133581, A99, MF-A06).

NCEER-96-0013   "Chemical Hazards, Mitigation and Preparedness in Areas of High Seismic Risk: A Methodology for Estimating the Risk of Post-Earthquake Hazardous Materials Release," by H.A. Seligson, R.T. Eguchi, K.J. Tierney and K. Richmond, 11/7/96, (PB97-133565, MF-A02, A08).

NCEER-96-0014   "Response of Steel Bridge Bearings to Reversed Cyclic Loading," by J.B. Mander, D-K. Kim, S.S. Chen and G.J. Premus, 11/13/96, (PB97-140735, A12, MF-A03).

NCEER-96-0015   "Highway Culvert Performance During Past Earthquakes," by T.L. Youd and C.J. Beckman, 11/25/96, (PB97-133532, A06, MF-A01).

NCEER-97-0001   "Evaluation, Prevention and Mitigation of Pounding Effects in Building Structures," by R.E. Valles and A.M. Reinhorn, 2/20/97, (PB97-159552, A14, MF-A03).

NCEER-97-0002   "Seismic Design Criteria for Bridges and Other Highway Structures," by C. Rojahn, R. Mayes, D.G. Anderson, J. Clark, J.H. Hom, R.V. Nutt and M.J. O'Rourke, 4/30/97, (PB97-194658, A06, MF-A03).

NCEER-97-0003   "Proceedings of the U.S.-Italian Workshop on Seismic Evaluation and Retrofit," Edited by D.P. Abrams and G.M. Calvi, 3/19/97, (PB97-194666, A13, MF-A03).

NCEER-97-0004   "Investigation of Seismic Response of Buildings with Linear and Nonlinear Fluid Viscous Dampers," by A.A. Seleemah and M.C. Constantinou, 5/21/97, (PB98-109002, A15, MF-A03).

NCEER-97-0005   "Proceedings of the Workshop on Earthquake Engineering Frontiers in Transportation Facilities," edited by G.C. Lee and I.M. Friedland, 8/29/97, (PB98-128911, A25, MR-A04).

NCEER-97-0006   "Cumulative Seismic Damage of Reinforced Concrete Bridge Piers," by S.K. Kunnath, A. El-Bahy, A. Taylor and W. Stone, 9/2/97, (PB98-108814, A11, MF-A03).

NCEER-97-0007   "Structural Details to Accommodate Seismic Movements of Highway Bridges and Retaining Walls," by R.A. Imbsen, R.A. Schamber, E. Thorkildsen, A. Kartoum, B.T. Martin, T.N. Rosser and J.M. Kulicki, 9/3/97, (PB98-108996, A09, MF-A02).

NCEER-97-0008   "A Method for Earthquake Motion-Damage Relationships with Application to Reinforced Concrete Frames," by A. Singhal and A.S. Kiremidjian, 9/10/97, (PB98-108988, A13, MF-A03).

NCEER-97-0009   "Seismic Analysis and Design of Bridge Abutments Considering Sliding and Rotation," by K. Fishman and R. Richards, Jr., 9/15/97, (PB98-108897, A06, MF-A02).

NCEER-97-0010   "Proceedings of the FHWA/NCEER Workshop on the National Representation of Seismic Ground Motion for New and Existing Highway Facilities," edited by I.M. Friedland, M.S. Power and R.L. Mayes, 9/22/97, (PB98-128903, A21, MF-A04).

NCEER-97-0011   "Seismic Analysis for Design or Retrofit of Gravity Bridge Abutments," by K.L. Fishman, R. Richards, Jr. and R.C. Divito, 10/2/97, (PB98-128937, A08, MF-A02).

NCEER-97-0012   "Evaluation of Simplified Methods of Analysis for Yielding Structures," by P. Tsopelas, M.C. Constantinou, C.A. Kircher and A.S. Whittaker, 10/31/97, (PB98-128929, A10, MF-A03).

NCEER-97-0013   "Seismic Design of Bridge Columns Based on Control and Repairability of Damage," by C-T. Cheng and J.B. Mander, 12/8/97, (PB98-144249, A11, MF-A03).

NCEER-97-0014   "Seismic Resistance of Bridge Piers Based on Damage Avoidance Design," by J.B. Mander and C-T. Cheng, 12/10/97, (PB98-144223, A09, MF-A02).

NCEER-97-0015   "Seismic Response of Nominally Symmetric Systems with Strength Uncertainty," by S. Balopoulou and M. Grigoriu, 12/23/97, (PB98-153422, A11, MF-A03).

NCEER-97-0016   "Evaluation of Seismic Retrofit Methods for Reinforced Concrete Bridge Columns," by T.J. Wipf, F.W. Klaiber and F.M. Russo, 12/28/97, (PB98-144215, A12, MF-A03).

NCEER-97-0017   "Seismic Fragility of Existing Conventional Reinforced Concrete Highway Bridges," by C.L. Mullen and A.S. Cakmak, 12/30/97, (PB98-153406, A08, MF-A02).

NCEER-97-0018   "Loss Asssessment of Memphis Buildings," edited by D.P. Abrams and M. Shinozuka, 12/31/97, (PB98-144231, A13, MF-A03).

NCEER-97-0019   "Seismic Evaluation of Frames with Infill Walls Using Quasi-static Experiments," by K.M. Mosalam, R.N. White and P. Gergely, 12/31/97, (PB98-153455, A07, MF-A02).

NCEER-97-0020   "Seismic Evaluation of Frames with Infill Walls Using Pseudo-dynamic Experiments," by K.M. Mosalam, R.N. White and P. Gergely, 12/31/97, (PB98-153430, A07, MF-A02).

NCEER-97-0021   "Computational Strategies for Frames with Infill Walls: Discrete and Smeared Crack Analyses and Seismic Fragility," by K.M. Mosalam, R.N. White and P. Gergely, 12/31/97, (PB98-153414, A10, MF-A02).

NCEER-97-0022 "Proceedings of the NCEER Workshop on Evaluation of Liquefaction Resistance of Soils," edited by T.L. Youd and I.M. Idriss, 12/31/97, (PB98-155617, A15, MF-A03).

MCEER-98-0001 "Extraction of Nonlinear Hysteretic Properties of Seismically Isolated Bridges from Quick-Release Field Tests," by Q. Chen, B.M. Douglas, E.M. Maragakis and I.G. Buckle, 5/26/98, (PB99-118838, A06, MF-A01).

MCEER-98-0002 "Methodologies for Evaluating the Importance of Highway Bridges," by A. Thomas, S. Eshenaur and J. Kulicki, 5/29/98, (PB99-118846, A10, MF-A02).

MCEER-98-0003 "Capacity Design of Bridge Piers and the Analysis of Overstrength," by J.B. Mander, A. Dutta and P. Goel, 6/1/98, (PB99-118853, A09, MF-A02).

MCEER-98-0004 "Evaluation of Bridge Damage Data from the Loma Prieta and Northridge, California Earthquakes," by N. Basoz and A. Kiremidjian, 6/2/98, (PB99-118861, A15, MF-A03).

MCEER-98-0005 "Screening Guide for Rapid Assessment of Liquefaction Hazard at Highway Bridge Sites," by T. L. Youd, 6/16/98, (PB99-118879, A06, not available on microfiche).

MCEER-98-0006 "Structural Steel and Steel/Concrete Interface Details for Bridges," by P. Ritchie, N. Kauhl and J. Kulicki, 7/13/98, (PB99-118945, A06, MF-A01).

MCEER-98-0007 "Capacity Design and Fatigue Analysis of Confined Concrete Columns," by A. Dutta and J.B. Mander, 7/14/98, (PB99-118960, A14, MF-A03).

MCEER-98-0008 "Proceedings of the Workshop on Performance Criteria for Telecommunication Services Under Earthquake Conditions," edited by A.J. Schiff, 7/15/98, (PB99-118952, A08, MF-A02).

MCEER-98-0009 "Fatigue Analysis of Unconfined Concrete Columns," by J.B. Mander, A. Dutta and J.H. Kim, 9/12/98, (PB99-123655, A10, MF-A02).

MCEER-98-0010 "Centrifuge Modeling of Cyclic Lateral Response of Pile-Cap Systems and Seat-Type Abutments in Dry Sands," by A.D. Gadre and R. Dobry, 10/2/98, (PB99-123606, A13, MF-A03).

MCEER-98-0011 "IDARC-BRIDGE: A Computational Platform for Seismic Damage Assessment of Bridge Structures," by A.M. Reinhorn, V. Simeonov, G. Mylonakis and Y. Reichman, 10/2/98, (PB99-162919, A15, MF-A03).

MCEER-98-0012 "Experimental Investigation of the Dynamic Response of Two Bridges Before and After Retrofitting with Elastomeric Bearings," by D.A. Wendichansky, S.S. Chen and J.B. Mander, 10/2/98, (PB99-162927, A15, MF-A03).

MCEER-98-0013 "Design Procedures for Hinge Restrainers and Hinge Sear Width for Multiple-Frame Bridges," by R. Des Roches and G.L. Fenves, 11/3/98, (PB99-140477, A13, MF-A03).

MCEER-98-0014 "Response Modification Factors for Seismically Isolated Bridges," by M.C. Constantinou and J.K. Quarshie, 11/3/98, (PB99-140485, A14, MF-A03).

MCEER-98-0015 "Proceedings of the U.S.-Italy Workshop on Seismic Protective Systems for Bridges," edited by I.M. Friedland and M.C. Constantinou, 11/3/98, (PB2000-101711, A22, MF-A04).

MCEER-98-0016 "Appropriate Seismic Reliability for Critical Equipment Systems: Recommendations Based on Regional Analysis of Financial and Life Loss," by K. Porter, C. Scawthorn, C. Taylor and N. Blais, 11/10/98, (PB99-157265, A08, MF-A02).

MCEER-98-0017 "Proceedings of the U.S. Japan Joint Seminar on Civil Infrastructure Systems Research," edited by M. Shinozuka and A. Rose, 11/12/98, (PB99-156713, A16, MF-A03).

MCEER-98-0018 "Modeling of Pile Footings and Drilled Shafts for Seismic Design," by I. PoLam, M. Kapuskar and D. Chaudhuri, 12/21/98, (PB99-157257, A09, MF-A02).

MCEER-99-0001 "Seismic Evaluation of a Masonry Infilled Reinforced Concrete Frame by Pseudodynamic Testing," by S.G. Buonopane and R.N. White, 2/16/99, (PB99-162851, A09, MF-A02).

MCEER-99-0002 "Response History Analysis of Structures with Seismic Isolation and Energy Dissipation Systems: Verification Examples for Program SAP2000," by J. Scheller and M.C. Constantinou, 2/22/99, (PB99-162869, A08, MF-A02).

MCEER-99-0003 "Experimental Study on the Seismic Design and Retrofit of Bridge Columns Including Axial Load Effects," by A. Dutta, T. Kokorina and J.B. Mander, 2/22/99, (PB99-162877, A09, MF-A02).

MCEER-99-0004 "Experimental Study of Bridge Elastomeric and Other Isolation and Energy Dissipation Systems with Emphasis on Uplift Prevention and High Velocity Near-source Seismic Excitation," by A. Kasalanati and M. C. Constantinou, 2/26/99, (PB99-162885, A12, MF-A03).

MCEER-99-0005 "Truss Modeling of Reinforced Concrete Shear-flexure Behavior," by J.H. Kim and J.B. Mander, 3/8/99, (PB99-163693, A12, MF-A03).

MCEER-99-0006 "Experimental Investigation and Computational Modeling of Seismic Response of a 1:4 Scale Model Steel Structure with a Load Balancing Supplemental Damping System," by G. Pekcan, J.B. Mander and S.S. Chen, 4/2/99, (PB99-162893, A11, MF-A03).

MCEER-99-0007 "Effect of Vertical Ground Motions on the Structural Response of Highway Bridges," by M.R. Button, C.J. Cronin and R.L. Mayes, 4/10/99, (PB2000-101411, A10, MF-A03).

MCEER-99-0008 "Seismic Reliability Assessment of Critical Facilities: A Handbook, Supporting Documentation, and Model Code Provisions," by G.S. Johnson, R.E. Sheppard, M.D. Quilici, S.J. Eder and C.R. Scawthorn, 4/12/99, (PB2000-101701, A18, MF-A04).

MCEER-99-0009 "Impact Assessment of Selected MCEER Highway Project Research on the Seismic Design of Highway Structures," by C. Rojahn, R. Mayes, D.G. Anderson, J.H. Clark, D'Appolonia Engineering, S. Gloyd and R.V. Nutt, 4/14/99, (PB99-162901, A10, MF-A02).

MCEER-99-0010 "Site Factors and Site Categories in Seismic Codes," by R. Dobry, R. Ramos and M.S. Power, 7/19/99, (PB2000-101705, A08, MF-A02).

MCEER-99-0011 "Restrainer Design Procedures for Multi-Span Simply-Supported Bridges," by M.J. Randall, M. Saiidi, E. Maragakis and T. Isakovic, 7/20/99, (PB2000-101702, A10, MF-A02).

MCEER-99-0012 "Property Modification Factors for Seismic Isolation Bearings," by M.C. Constantinou, P. Tsopelas, A. Kasalanati and E. Wolff, 7/20/99, (PB2000-103387, A11, MF-A03).

MCEER-99-0013 "Critical Seismic Issues for Existing Steel Bridges," by P. Ritchie, N. Kauhl and J. Kulicki, 7/20/99, (PB2000-101697, A09, MF-A02).

MCEER-99-0014 "Nonstructural Damage Database," by A. Kao, T.T. Soong and A. Vender, 7/24/99, (PB2000-101407, A06, MF-A01).

MCEER-99-0015 "Guide to Remedial Measures for Liquefaction Mitigation at Existing Highway Bridge Sites," by H.G. Cooke and J. K. Mitchell, 7/26/99, (PB2000-101703, A11, MF-A03).

MCEER-99-0016 "Proceedings of the MCEER Workshop on Ground Motion Methodologies for the Eastern United States," edited by N. Abrahamson and A. Becker, 8/11/99, (PB2000-103385, A07, MF-A02).

MCEER-99-0017 "Quindío, Colombia Earthquake of January 25, 1999: Reconnaissance Report," by A.P. Asfura and P.J. Flores, 10/4/99, (PB2000-106893, A06, MF-A01).

MCEER-99-0018 "Hysteretic Models for Cyclic Behavior of Deteriorating Inelastic Structures," by M.V. Sivaselvan and A.M. Reinhorn, 11/5/99, (PB2000-103386, A08, MF-A02).

MCEER-99-0019   "Proceedings of the 7th U.S.- Japan Workshop on Earthquake Resistant Design of Lifeline Facilities and Countermeasures Against Soil Liquefaction," edited by T.D. O'Rourke, J.P. Bardet and M. Hamada, 11/19/99, (PB2000-103354, A99, MF-A06).

MCEER-99-0020   "Development of Measurement Capability for Micro-Vibration Evaluations with Application to Chip Fabrication Facilities," by G.C. Lee, Z. Liang, J.W. Song, J.D. Shen and W.C. Liu, 12/1/99, (PB2000-105993, A08, MF-A02).

MCEER-99-0021   "Design and Retrofit Methodology for Building Structures with Supplemental Energy Dissipating Systems," by G. Pekcan, J.B. Mander and S.S. Chen, 12/31/99, (PB2000-105994, A11, MF-A03).

MCEER-00-0001   "The Marmara, Turkey Earthquake of August 17, 1999: Reconnaissance Report," edited by C. Scawthorn; with major contributions by M. Bruneau, R. Eguchi, T. Holzer, G. Johnson, J. Mander, J. Mitchell, W. Mitchell, A. Papageorgiou, C. Scaethorn, and G. Webb, 3/23/00, (PB2000-106200, A11, MF-A03).

MCEER-00-0002   "Proceedings of the MCEER Workshop for Seismic Hazard Mitigation of Health Care Facilities," edited by G.C. Lee, M. Ettouney, M. Grigoriu, J. Hauer and J. Nigg, 3/29/00, (PB2000-106892, A08, MF-A02).

MCEER-00-0003   "The Chi-Chi, Taiwan Earthquake of September 21, 1999: Reconnaissance Report," edited by G.C. Lee and C.H. Loh, with major contributions by G.C. Lee, M. Bruneau, I.G. Buckle, S.E. Chang, P.J. Flores, T.D. O'Rourke, M. Shinozuka, T.T. Soong, C-H. Loh, K-C. Chang, Z-J. Chen, J-S. Hwang, M-L. Lin, G-Y. Liu, K-C. Tsai, G.C. Yao and C-L. Yen, 4/30/00, (PB2001-100980, A10, MF-A02).

MCEER-00-0004   "Seismic Retrofit of End-Sway Frames of Steel Deck-Truss Bridges with a Supplemental Tendon System: Experimental and Analytical Investigation," by G. Pekcan, J.B. Mander and S.S. Chen, 7/1/00, (PB2001-100982, A10, MF-A02).

MCEER-00-0005   "Sliding Fragility of Unrestrained Equipment in Critical Facilities," by W.H. Chong and T.T. Soong, 7/5/00, (PB2001-100983, A08, MF-A02).

MCEER-00-0006   "Seismic Response of Reinforced Concrete Bridge Pier Walls in the Weak Direction," by N. Abo-Shadi, M. Saiidi and D. Sanders, 7/17/00, (PB2001-100981, A17, MF-A03).

MCEER-00-0007   "Low-Cycle Fatigue Behavior of Longitudinal Reinforcement in Reinforced Concrete Bridge Columns," by J. Brown and S.K. Kunnath, 7/23/00, (PB2001-104392, A08, MF-A02).

MCEER-00-0008   "Soil Structure Interaction of Bridges for Seismic Analysis," I. PoLam and H. Law, 9/25/00, (PB2001-105397, A08, MF-A02).

MCEER-00-0009   "Proceedings of the First MCEER Workshop on Mitigation of Earthquake Disaster by Advanced Technologies (MEDAT-1), edited by M. Shinozuka, D.J. Inman and T.D. O'Rourke, 11/10/00, (PB2001-105399, A14, MF-A03).

MCEER-00-0010   "Development and Evaluation of Simplified Procedures for Analysis and Design of Buildings with Passive Energy Dissipation Systems, Revision 01," by O.M. Ramirez, M.C. Constantinou, C.A. Kircher, A.S. Whittaker, M.W. Johnson, J.D. Gomez and C. Chrysostomou, 11/16/01, (PB2001-105523, A23, MF-A04).

MCEER-00-0011   "Dynamic Soil-Foundation-Structure Interaction Analyses of Large Caissons," by C-Y. Chang, C-M. Mok, Z-L. Wang, R. Settgast, F. Waggoner, M.A. Ketchum, H.M. Gonnermann and C-C. Chin, 12/30/00, (PB2001-104373, A07, MF-A02).

MCEER-00-0012   "Experimental Evaluation of Seismic Performance of Bridge Restrainers," by A.G. Vlassis, E.M. Maragakis and M. Saiid Saiidi, 12/30/00, (PB2001-104354, A09, MF-A02).

MCEER-00-0013   "Effect of Spatial Variation of Ground Motion on Highway Structures," by M. Shinozuka, V. Saxena and G. Deodatis, 12/31/00, (PB2001-108755, A13, MF-A03).

MCEER-00-0014   "A Risk-Based Methodology for Assessing the Seismic Performance of Highway Systems," by S.D. Werner, C.E. Taylor, J.E. Moore, II, J.S. Walton and S. Cho, 12/31/00, (PB2001-108756, A14, MF-A03).

MCEER-01-0001 "Experimental Investigation of P-Delta Effects to Collapse During Earthquakes," by D. Vian and M. Bruneau, 6/25/01, (PB2002-100534, A17, MF-A03).

MCEER-01-0002 "Proceedings of the Second MCEER Workshop on Mitigation of Earthquake Disaster by Advanced Technologies (MEDAT-2)," edited by M. Bruneau and D.J. Inman, 7/23/01, (PB2002-100434, A16, MF-A03).

MCEER-01-0003 "Sensitivity Analysis of Dynamic Systems Subjected to Seismic Loads," by C. Roth and M. Grigoriu, 9/18/01, (PB2003-100884, A12, MF-A03).

MCEER-01-0004 "Overcoming Obstacles to Implementing Earthquake Hazard Mitigation Policies: Stage 1 Report," by D.J. Alesch and W.J. Petak, 12/17/01, (PB2002-107949, A07, MF-A02).

MCEER-01-0005 "Updating Real-Time Earthquake Loss Estimates: Methods, Problems and Insights," by C.E. Taylor, S.E. Chang and R.T. Eguchi, 12/17/01, (PB2002-107948, A05, MF-A01).

MCEER-01-0006 "Experimental Investigation and Retrofit of Steel Pile Foundations and Pile Bents Under Cyclic Lateral Loadings," by A. Shama, J. Mander, B. Blabac and S. Chen, 12/31/01, (PB2002-107950, A13, MF-A03).

MCEER-02-0001 "Assessment of Performance of Bolu Viaduct in the 1999 Duzce Earthquake in Turkey" by P.C. Roussis, M.C. Constantinou, M. Erdik, E. Durukal and M. Dicleli, 5/8/02, (PB2003-100883, A08, MF-A02).

MCEER-02-0002 "Seismic Behavior of Rail Counterweight Systems of Elevators in Buildings," by M.P. Singh, Rildova and L.E. Suarez, 5/27/02. (PB2003-100882, A11, MF-A03).

MCEER-02-0003 "Development of Analysis and Design Procedures for Spread Footings," by G. Mylonakis, G. Gazetas, S. Nikolaou and A. Chauncey, 10/02/02, (PB2004-101636, A13, MF-A03, CD-A13).

MCEER-02-0004 "Bare-Earth Algorithms for Use with SAR and LIDAR Digital Elevation Models," by C.K. Huyck, R.T. Eguchi and B. Houshmand, 10/16/02, (PB2004-101637, A07, CD-A07).

MCEER-02-0005 "Review of Energy Dissipation of Compression Members in Concentrically Braced Frames," by K.Lee and M. Bruneau, 10/18/02, (PB2004-101638, A10, CD-A10).

MCEER-03-0001 "Experimental Investigation of Light-Gauge Steel Plate Shear Walls for the Seismic Retrofit of Buildings" by J. Berman and M. Bruneau, 5/2/03, (PB2004-101622, A10, MF-A03, CD-A10).

MCEER-03-0002 "Statistical Analysis of Fragility Curves," by M. Shinozuka, M.Q. Feng, H. Kim, T. Uzawa and T. Ueda, 6/16/03, (PB2004-101849, A09, CD-A09).

MCEER-03-0003 "Proceedings of the Eighth U.S.-Japan Workshop on Earthquake Resistant Design f Lifeline Facilities and Countermeasures Against Liquefaction," edited by M. Hamada, J.P. Bardet and T.D. O'Rourke, 6/30/03, (PB2004-104386, A99, CD-A99).

MCEER-03-0004 "Proceedings of the PRC-US Workshop on Seismic Analysis and Design of Special Bridges," edited by L.C. Fan and G.C. Lee, 7/15/03, (PB2004-104387, A14, CD-A14).

MCEER-03-0005 "Urban Disaster Recovery: A Framework and Simulation Model," by S.B. Miles and S.E. Chang, 7/25/03, (PB2004-104388, A07, CD-A07).

MCEER-03-0006 "Behavior of Underground Piping Joints Due to Static and Dynamic Loading," by R.D. Meis, M. Maragakis and R. Siddharthan, 11/17/03, (PB2005-102194, A13, MF-A03, CD-A00).

MCEER-04-0001 "Experimental Study of Seismic Isolation Systems with Emphasis on Secondary System Response and Verification of Accuracy of Dynamic Response History Analysis Methods," by E. Wolff and M. Constantinou, 1/16/04 (PB2005-102195, A99, MF-E08, CD-A00).

MCEER-04-0002 "Tension, Compression and Cyclic Testing of Engineered Cementitious Composite Materials," by K. Kesner and S.L. Billington, 3/1/04, (PB2005-102196, A08, CD-A08).

MCEER-04-0003 "Cyclic Testing of Braces Laterally Restrained by Steel Studs to Enhance Performance During Earthquakes," by O.C. Celik, J.W. Berman and M. Bruneau, 3/16/04, (PB2005-102197, A13, MF-A03, CD-A00).

MCEER-04-0004 "Methodologies for Post Earthquake Building Damage Detection Using SAR and Optical Remote Sensing: Application to the August 17, 1999 Marmara, Turkey Earthquake," by C.K. Huyck, B.J. Adams, S. Cho, R.T. Eguchi, B. Mansouri and B. Houshmand, 6/15/04, (PB2005-104888, A10, CD-A00).

MCEER-04-0005 "Nonlinear Structural Analysis Towards Collapse Simulation: A Dynamical Systems Approach," by M.V. Sivaselvan and A.M. Reinhorn, 6/16/04, (PB2005-104889, A11, MF-A03, CD-A00).

MCEER-04-0006 "Proceedings of the Second PRC-US Workshop on Seismic Analysis and Design of Special Bridges," edited by G.C. Lee and L.C. Fan, 6/25/04, (PB2005-104890, A16, CD-A00).

MCEER-04-0007 "Seismic Vulnerability Evaluation of Axially Loaded Steel Built-up Laced Members," by K. Lee and M. Bruneau, 6/30/04, (PB2005-104891, A16, CD-A00).

MCEER-04-0008 "Evaluation of Accuracy of Simplified Methods of Analysis and Design of Buildings with Damping Systems for Near-Fault and for Soft-Soil Seismic Motions," by E.A. Pavlou and M.C. Constantinou, 8/16/04, (PB2005-104892, A08, MF-A02, CD-A00).

MCEER-04-0009 "Assessment of Geotechnical Issues in Acute Care Facilities in California," by M. Lew, T.D. O'Rourke, R. Dobry and M. Koch, 9/15/04, (PB2005-104893, A08, CD-A00).

MCEER-04-0010 "Scissor-Jack-Damper Energy Dissipation System," by A.N. Sigaher-Boyle and M.C. Constantinou, 12/1/04 (PB2005-108221).

MCEER-04-0011 "Seismic Retrofit of Bridge Steel Truss Piers Using a Controlled Rocking Approach," by M. Pollino and M. Bruneau, 12/20/04 (PB2006-105795).

MCEER-05-0001 "Experimental and Analytical Studies of Structures Seismically Isolated with an Uplift-Restraint Isolation System," by P.C. Roussis and M.C. Constantinou, 1/10/05 (PB2005-108222).

MCEER-05-0002 "A Versatile Experimentation Model for Study of Structures Near Collapse Applied to Seismic Evaluation of Irregular Structures," by D. Kusumastuti, A.M. Reinhorn and A. Rutenberg, 3/31/05 (PB2006-101523).

MCEER-05-0003 "Proceedings of the Third PRC-US Workshop on Seismic Analysis and Design of Special Bridges," edited by L.C. Fan and G.C. Lee, 4/20/05, (PB2006-105796).

MCEER-05-0004 "Approaches for the Seismic Retrofit of Braced Steel Bridge Piers and Proof-of-Concept Testing of an Eccentrically Braced Frame with Tubular Link," by J.W. Berman and M. Bruneau, 4/21/05 (PB2006-101524).

MCEER-05-0005 "Simulation of Strong Ground Motions for Seismic Fragility Evaluation of Nonstructural Components in Hospitals," by A. Wanitkorkul and A. Filiatrault, 5/26/05 (PB2006-500027).

MCEER-05-0006 "Seismic Safety in California Hospitals: Assessing an Attempt to Accelerate the Replacement or Seismic Retrofit of Older Hospital Facilities," by D.J. Alesch, L.A. Arendt and W.J. Petak, 6/6/05 (PB2006-105794).

MCEER-05-0007 "Development of Seismic Strengthening and Retrofit Strategies for Critical Facilities Using Engineered Cementitious Composite Materials," by K. Kesner and S.L. Billington, 8/29/05 (PB2006-111701).

MCEER-05-0008 "Experimental and Analytical Studies of Base Isolation Systems for Seismic Protection of Power Transformers," by N. Murota, M.Q. Feng and G-Y. Liu, 9/30/05 (PB2006-111702).

MCEER-05-0009 "3D-BASIS-ME-MB: Computer Program for Nonlinear Dynamic Analysis of Seismically Isolated Structures," by P.C. Tsopelas, P.C. Roussis, M.C. Constantinou, R. Buchanan and A.M. Reinhorn, 10/3/05 (PB2006-111703).

MCEER-05-0010 "Steel Plate Shear Walls for Seismic Design and Retrofit of Building Structures," by D. Vian and M. Bruneau, 12/15/05 (PB2006-111704).

MCEER-05-0011 "The Performance-Based Design Paradigm," by M.J. Astrella and A. Whittaker, 12/15/05 (PB2006-111705).

MCEER-06-0001 "Seismic Fragility of Suspended Ceiling Systems," H. Badillo-Almaraz, A.S. Whittaker, A.M. Reinhorn and G.P. Cimellaro, 2/4/06 (PB2006-111706).

MCEER-06-0002 "Multi-Dimensional Fragility of Structures," by G.P. Cimellaro, A.M. Reinhorn and M. Bruneau, 3/1/06 (PB2007-106974, A09, MF-A02, CD A00).

MCEER-06-0003 "Built-Up Shear Links as Energy Dissipators for Seismic Protection of Bridges," by P. Dusicka, A.M. Itani and I.G. Buckle, 3/15/06 (PB2006-111708).

MCEER-06-0004 "Analytical Investigation of the Structural Fuse Concept," by R.E. Vargas and M. Bruneau, 3/16/06 (PB2006-111709).

MCEER-06-0005 "Experimental Investigation of the Structural Fuse Concept," by R.E. Vargas and M. Bruneau, 3/17/06 (PB2006-111710).

MCEER-06-0006 "Further Development of Tubular Eccentrically Braced Frame Links for the Seismic Retrofit of Braced Steel Truss Bridge Piers," by J.W. Berman and M. Bruneau, 3/27/06 (PB2007-105147).

MCEER-06-0007 "REDARS Validation Report," by S. Cho, C.K. Huyck, S. Ghosh and R.T. Eguchi, 8/8/06 (PB2007-106983).

MCEER-06-0008 "Review of Current NDE Technologies for Post-Earthquake Assessment of Retrofitted Bridge Columns," by J.W. Song, Z. Liang and G.C. Lee, 8/21/06 (PB2007-106984).

MCEER-06-0009 "Liquefaction Remediation in Silty Soils Using Dynamic Compaction and Stone Columns," by S. Thevanayagam, G.R. Martin, R. Nashed, T. Shenthan, T. Kanagalingam and N. Ecemis, 8/28/06 (PB2007-106985).

MCEER-06-0010 "Conceptual Design and Experimental Investigation of Polymer Matrix Composite Infill Panels for Seismic Retrofitting," by W. Jung, M. Chiewanichakorn and A.J. Aref, 9/21/06 (PB2007-106986).

MCEER-06-0011 "A Study of the Coupled Horizontal-Vertical Behavior of Elastomeric and Lead-Rubber Seismic Isolation Bearings," by G.P. Warn and A.S. Whittaker, 9/22/06 (PB2007-108679).

MCEER-06-0012 "Proceedings of the Fourth PRC-US Workshop on Seismic Analysis and Design of Special Bridges: Advancing Bridge Technologies in Research, Design, Construction and Preservation," Edited by L.C. Fan, G.C. Lee and L. Ziang, 10/12/06 (PB2007-109042).

MCEER-06-0013 "Cyclic Response and Low Cycle Fatigue Characteristics of Plate Steels," by P. Dusicka, A.M. Itani and I.G. Buckle, 11/1/06 06 (PB2007-106987).

MCEER-06-0014 "Proceedings of the Second US-Taiwan Bridge Engineering Workshop," edited by W.P. Yen, J. Shen, J-Y. Chen and M. Wang, 11/15/06 (PB2008-500041).

MCEER-06-0015 "User Manual and Technical Documentation for the REDARS^{TM} Import Wizard," by S. Cho, S. Ghosh, C.K. Huyck and S.D. Werner, 11/30/06 (PB2007-114766).

MCEER-06-0016 "Hazard Mitigation Strategy and Monitoring Technologies for Urban and Infrastructure Public Buildings: Proceedings of the China-US Workshops," edited by X.Y. Zhou, A.L. Zhang, G.C. Lee and M. Tong, 12/12/06 (PB2008-500018).

MCEER-07-0001 "Static and Kinetic Coefficients of Friction for Rigid Blocks," by C. Kafali, S. Fathali, M. Grigoriu and A.S. Whittaker, 3/20/07 (PB2007-114767).

MCEER-07-0002 "Hazard Mitigation Investment Decision Making: Organizational Response to Legislative Mandate," by L.A. Arendt, D.J. Alesch and W.J. Petak, 4/9/07 (PB2007-114768).

MCEER-07-0003 "Seismic Behavior of Bidirectional-Resistant Ductile End Diaphragms with Unbonded Braces in Straight or Skewed Steel Bridges," by O. Celik and M. Bruneau, 4/11/07 (PB2008-105141).

MCEER-07-0004   "Modeling Pile Behavior in Large Pile Groups Under Lateral Loading," by A.M. Dodds and G.R. Martin, 4/16/07(PB2008-105142).

MCEER-07-0005   "Experimental Investigation of Blast Performance of Seismically Resistant Concrete-Filled Steel Tube Bridge Piers," by S. Fujikura, M. Bruneau and D. Lopez-Garcia, 4/20/07 (PB2008-105143).

MCEER-07-0006   "Seismic Analysis of Conventional and Isolated Liquefied Natural Gas Tanks Using Mechanical Analogs," by I.P. Christovasilis and A.S. Whittaker, 5/1/07.

MCEER-07-0007   "Experimental Seismic Performance Evaluation of Isolation/Restraint Systems for Mechanical Equipment – Part 1: Heavy Equipment Study," by S. Fathali and A. Filiatrault, 6/6/07 (PB2008-105144).

MCEER-07-0008   "Seismic Vulnerability of Timber Bridges and Timber Substructures," by A.A. Sharma, J.B. Mander, I.M. Friedland and D.R. Allicock, 6/7/07 (PB2008-105145).

MCEER-07-0009   "Experimental and Analytical Study of the XY-Friction Pendulum (XY-FP) Bearing for Bridge Applications," by C.C. Marin-Artieda, A.S. Whittaker and M.C. Constantinou, 6/7/07 (PB2008-105191).

MCEER-07-0010   "Proceedings of the PRC-US Earthquake Engineering Forum for Young Researchers," Edited by G.C. Lee and X.Z. Qi, 6/8/07.

MCEER-07-0011   "Design Recommendations for Perforated Steel Plate Shear Walls," by R. Purba and M. Bruneau, 6/18/07, (PB2008-105192).

MCEER-07-0012   "Performance of Seismic Isolation Hardware Under Service and Seismic Loading," by M.C. Constantinou, A.S. Whittaker, Y. Kalpakidis, D.M. Fenz and G.P. Warn, 8/27/07, (PB2008-105193).

MCEER-07-0013   "Experimental Evaluation of the Seismic Performance of Hospital Piping Subassemblies," by E.R. Goodwin, E. Maragakis and A.M. Itani, 9/4/07, (PB2008-105194).

MCEER-07-0014   "A Simulation Model of Urban Disaster Recovery and Resilience: Implementation for the 1994 Northridge Earthquake," by S. Miles and S.E. Chang, 9/7/07, (PB2008-106426).

MCEER-07-0015   "Statistical and Mechanistic Fragility Analysis of Concrete Bridges," by M. Shinozuka, S. Banerjee and S-H. Kim, 9/10/07, (PB2008-106427).

MCEER-07-0016   "Three-Dimensional Modeling of Inelastic Buckling in Frame Structures," by M. Schachter and AM. Reinhorn, 9/13/07, (PB2008-108125).

MCEER-07-0017   "Modeling of Seismic Wave Scattering on Pile Groups and Caissons," by I. Po Lam, H. Law and C.T. Yang, 9/17/07 (PB2008-108150).

MCEER-07-0018   "Bridge Foundations: Modeling Large Pile Groups and Caissons for Seismic Design," by I. Po Lam, H. Law and G.R. Martin (Coordinating Author), 12/1/07 (PB2008-111190).

MCEER-07-0019   "Principles and Performance of Roller Seismic Isolation Bearings for Highway Bridges," by G.C. Lee, Y.C. Ou, Z. Liang, T.C. Niu and J. Song, 12/10/07.

MCEER-07-0020   "Centrifuge Modeling of Permeability and Pinning Reinforcement Effects on Pile Response to Lateral Spreading," by L.L Gonzalez-Lagos, T. Abdoun and R. Dobry, 12/10/07 (PB2008-111191).

MCEER-07-0021   "Damage to the Highway System from the Pisco, Perú Earthquake of August 15, 2007," by J.S. O'Connor, L. Mesa and M. Nykamp, 12/10/07, (PB2008-108126).

MCEER-07-0022   "Experimental Seismic Performance Evaluation of Isolation/Restraint Systems for Mechanical Equipment – Part 2: Light Equipment Study," by S. Fathali and A. Filiatrault, 12/13/07 (PB2008-111192).

MCEER-07-0023   "Fragility Considerations in Highway Bridge Design," by M. Shinozuka, S. Banerjee and S.H. Kim, 12/14/07 (PB2008-111193).

MCEER-07-0024 "Performance Estimates for Seismically Isolated Bridges," by G.P. Warn and A.S. Whittaker, 12/30/07 (PB2008-112230).

MCEER-08-0001 "Seismic Performance of Steel Girder Bridge Superstructures with Conventional Cross Frames," by L.P. Carden, A.M. Itani and I.G. Buckle, 1/7/08, (PB2008-112231).

MCEER-08-0002 "Seismic Performance of Steel Girder Bridge Superstructures with Ductile End Cross Frames with Seismic Isolators," by L.P. Carden, A.M. Itani and I.G. Buckle, 1/7/08 (PB2008-112232).

MCEER-08-0003 "Analytical and Experimental Investigation of a Controlled Rocking Approach for Seismic Protection of Bridge Steel Truss Piers," by M. Pollino and M. Bruneau, 1/21/08 (PB2008-112233).

MCEER-08-0004 "Linking Lifeline Infrastructure Performance and Community Disaster Resilience: Models and Multi-Stakeholder Processes," by S.E. Chang, C. Pasion, K. Tatebe and R. Ahmad, 3/3/08 (PB2008-112234).

MCEER-08-0005 "Modal Analysis of Generally Damped Linear Structures Subjected to Seismic Excitations," by J. Song, Y-L. Chu, Z. Liang and G.C. Lee, 3/4/08.

MCEER-08-0006 "System Performance Under Multi-Hazard Environments," by C. Kafali and M. Grigoriu, 3/4/08 (PB2008-112235).

MCEER-08-0007 "Mechanical Behavior of Multi-Spherical Sliding Bearings," by D.M. Fenz and M.C. Constantinou, 3/6/08 (PB2008-112236).

MCEER-08-0008 "Post-Earthquake Restoration of the Los Angeles Water Supply System," by T.H.P. Tabucchi and R.A. Davidson, 3/7/08 (PB2008-112237).

MCEER-08-0009 "Fragility Analysis of Water Supply Systems," by A. Jacobson and M. Grigoriu, 3/10/08.

MCEER-08-0010 "Experimental Investigation of Full-Scale Two-Story Steel Plate Shear Walls with Reduced Beam Section Connections," by B. Qu and M. Bruneau, 3/17/08, MCEER-08-0010.

MCEER-08-0011 "Seismic Evaluation and Rehabilitation of Critical Components of Electrical Power Systems," S. Ersoy, B. Feizi, A. Ashrafi and M. Ala Saadeghvaziri, 3/17/08.

MCEER-08-0012 "Seismic Behavior and Design of Boundary Frame Members of Steel Plate Shear Walls," by B. Qu and M. Bruneau, 4/26/08.